THE DEVELOPMENT OF THE 5,5-DIMETHYLPHLORIN AND 10,10-DIMETHYLBILADIENE TETRAPYRROLE PLATFORMS

by

Allen J. Pistner

A dissertation submitted to the Faculty of the University of Delaware in partial fulfillment of the requirements for the degree of Doctor of Philosophy in Chemistry and Biochemistry

Spring 2015

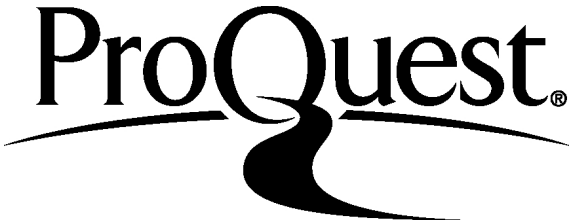

THE DEVELOPMENT OF THE 5,5-DIMETHYLPHLORIN

AND 10,10-DIMETHYLBILADIENE TETRAPYRROLE PLATFORMS

by

Allen J. Pistner

Approved: _____

Murray V. Johnston, Ph.D.
Chair of the Department of Chemistry and Biochemistry

Approved: _____

George H. Watson, Ph.D.
Dean of the College of Arts and Sciences

Approved: _____

James G. Richards, Ph.D.
Vice Provost for Graduate and Professional Education

I certify that I have read this dissertation and that in my opinion it meets the academic and professional standard required by the University as a dissertation for the degree of Doctor of Philosophy.

Signed: _____

Joel Rosenthal, Ph.D.
Professor in charge of dissertation

I certify that I have read this dissertation and that in my opinion it meets the academic and professional standard required by the University as a dissertation for the degree of Doctor of Philosophy.

Signed: _____

Joseph M. Fox, Ph.D.
Member of dissertation committee

I certify that I have read this dissertation and that in my opinion it meets the academic and professional standard required by the University as a dissertation for the degree of Doctor of Philosophy.

Signed: _____

Mary P. Watson, Ph.D.
Member of dissertation committee

I certify that I have read this dissertation and that in my opinion it meets the academic and professional standard required by the University as a dissertation for the degree of Doctor of Philosophy.

Signed: _____

Matthew F. Doty, Ph.D.
Member of dissertation committee

ACKNOWLEDGMENTS

I would like to first and foremost thank my Mom and Dad, Tina and Steve for their continued love and support throughout my long journey of schooling. I would also like to thank my family for their support throughout my education process.

I would like to thank my advisor Dr. Joel Rosenthal for the opportunity to join and help set up his lab. I have enjoyed working for you as your passion for science is unmistakable and contagious. I would also like to thank my committee members Dr. Joseph Fox, Dr. Mary Watson and Dr. Matthew Doty for their guidance and for taking the time out of their schedules to serve on my doctoral committee.

I would like to thank the members of the Rosenthal research lab both past and present for not only your insightful discussions but also your friendship. Having the opportunity to work alongside fun and intelligent people has made my time in graduate school unforgettable. Furthermore, I would like to thank my friends at UD and value the time we spent together both in and out of the lab.

Finally, I would like to thank my wife Jessica for her never ending love, support and companionship as this could not be possible without you.

TABLE OF CONTENTS

Appendix

LIST OF TABLES

LIST OF FIGURES

LIST OF SCHEMES

ABSTRACT

Tetrapyrrole scaffolds containing a dimethyl sp^3-meso center were explored. The 5,5-dimethylphlorin was explored as X-ray crystallography and NMR spectroscopy were used to determine that the phlorin, unlike the common porphyrin is nonaromatic. Several phlorin derivatives were synthesized through variation of the aromatic group at the 15-meso-position including pentafluorophenyl (3H(Phl^{F})), mesityl (3H(Phl^{Mes})), 4-nitrophenyl (3H(Phl^{NO2})), 4-tert-butylcarboxyphenyl (3H(Phl^{CO2tBu})), 2,6-bismethoxyphenyl (3H(Phl^{OMe})), 3,5-bistrifluoromethylphenyl (3H(Phl^{CF3})), and 3,5-bis-tert-butylphenyl (3H(Phl$^{3,5\text{-}tBu}$)).

The phlorin macrocycles were found to display unusual multielectron redox chemistry and photophysical properties. The phlorins were able to be oxidized up to three times at modest potentials and reduced two times. The substitution at the 15-meso-position was found to have the ability to attenuate the redox potentials of the phlorins. The electron donating substituents were easier to oxidize and more difficult to reduce as the electron withdrawing groups were easier to reduce and required more positive potentials to be oxidized. The photophysics of the phlorins were also influenced through the substitution at the 15-meso-position with the electron rich derivatives having higher quantum yields and longer fluorescence lifetimes. The phlorin also displays solvatochroism in the Soret absorption, where the polarized LUMO+1 state observed from the DFT calculations is involved.

The phlorin macrocycle also displays unique supramolecular activity with the ability to cooperatively bind two equivalents of F^- anions but not bind any other

halogens such as Cl^- and Br^-. Carboxylate anions were also found to form hydrogen bonding assemblies, but in a 1:1 ratio with the phlorin. The binding of anions was found to significantly attenuate both the redox and photophysical properties of the phlorin. The formation of the hydrogen binding assemblies was probed using carboxylates of different size and basicity.

The addition of a transition metal to the center of the phlorin core was also explored and two novel gold(III) phlorin derivatives were synthesized. The coordination of the gold(III) to the phlorin core was found to have a significant impact on the redox and photophysical properties. The crystal structure obtained for the gold(III) phlorin displays significant flattening of the macrocycle and the absorption profile in the Q band region red shifts by approximately 100 nm. The gold(III) phlorin derivatives that were synthesized were found to display solvatochroism, similar to that observed with the free base phlorin. The redox properties from the metalated derivative were significantly different from the free base. The gold(III) phlorins displayed two oxidations and two reductions, all of which were fully reversible. Both the gold(III) and free base phlorin derivatives show the ability to react with (dichloroiodo)benzene to chlorinate the phlorin backbone at β-pyrrole positions.

Another tetrapyrrole scaffold containing a dimethyl sp^3-meso center, the 10,10-dimethylbiladiene was investigated for its use as a ligand system. The dimethylbiladiene (DMBil) is a non-macrocyclic system that is able to bind Zn^{2+} and Cu^{2+} centers. X-ray crystallography shows that the open ligand design of the DMBil binds a single metal center at the core. The DMBil, Zn(DMBil) and Cu(DMBil) all display interesting redox chemistry with the ability to be both oxidized and reduced by two electrons. The biladiene derivatives also display strong absorption in the UV-vis

region and are weakly emissive. The sensitization of $^1O_2$ was investigated using the free base DMBil and the Zn(DMBil) as photosensitizers with 500 nm wavelength light. Both DMBil and Zn(DMBil) were found to sensitize $^1O_2$ with modest efficiencies and may provide a potential platform for the use in photodynamic therapy.

Chapter 1

INTRODUCTION

1.1 Porphyrins in Nature

Porphyrin structures are used throughout nature as protein cofactors. The most common form of a porphyrin in nature as well as one of the most studied cofactors is heme cofactor that consists of the iron complex of protoporhyrin IX, displayed in Figure 1.1.[1] This scaffold allows for nature to tune the electronic and redox properties of the cofactor through noncovalent interactions of the periphery of the porphyrin along with hydrogen bonding and control of the axial coordination at the iron center.[2] The ability to modify the electronics of the porphyrin creates the opportunity for these platforms to be used for wide range of natural processes including dioxygen coordination and transportation by globins,[3] activation of the O–O bind by cytochrome P-450,[4] the removal of peroxide and superoxide by peroxidases and catalases,[5] and single electron transfer by cytochromes.[6]

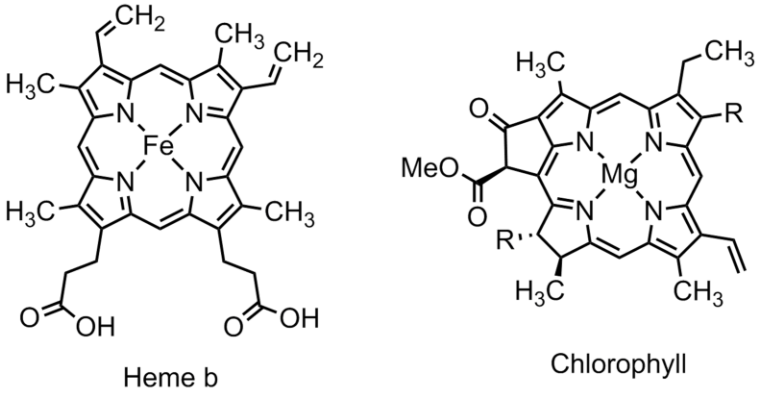

Figure 1.1 Structure of naturally occurring porphyrinoids heme and chlorophyll.

The use of the porphyrin platforms by nature is not limited to catalytic transformations as they are also used for light harvesting. Chlorophylls and other porphyrinoids are employed by plants[7,8] and cyanobacteria[9] to harvest sunlight throughout the UV-vis region, making the porphyrin platform one of the most utilized ligand systems. With the widespread use of porphyrins in nature, researchers have looked to develop synthetic porphyrin systems for a variety of applications.

1.2 Applications of Porphyrin in Catalysis

With nature serving as inspiration, porphyrins have been investigated as ligand platforms for several applications in catalysis. The planar tetrapyrrole macrocycle has shown the ability to easily coordinate a wide variety of different transition metals into the central core for use in catalysis.

The porphyrin ligand itself has shown the ability to be modified to enhance the activity in many different applications. One such application is in hydrogen evolution reactions,[10-13] where cobalt porphyrins have been shown to be effective catalysts for the production of hydrogen gas from acidic solutions. The activity has been enhanced through synthetic design. For example, Nocera and coworkers have developed cobalt porphyrins in which a pendant carboxylate group has been placed in the proximity of the metal center.[13] This functionality can act as a proton shuttle, similar to the environment surrounding hydrogenases where pendant proton shuttles are held near metal centers for enzymatic catalysis.[14-18]

Cobalt and iron porphyrins have been shown to be effective catalysis for the activation of dioxygen. Through modification of the porphyrin, either through the construction of a bimetallic catalyst, as in the case of the pacman porphyrins, or again

through the use of a pendant carboxylate group the activity for the reduction of dioxygen has been greatly enhanced.[19-21]

Iron porphyrins have also been used as catalysts for the formation of epoxides from olefins. The activity and the selectivity of the formation of the epoxide can be controlled through the design of the porphyrin ligand, creating versatile catalytic systems.[22-25] Iron porphyrins have also served as effective molecular electrocatalysts for the reduction of carbon dioxide to carbon monoxide. Much like other catalytic systems that use porphyrins as ligands, modifications of the porphyrin core has allowed for great enhancement of the activity. The use of proton transfer groups near the iron center has a substantial effect of the overall efficiency of the iron porphyrin catalyst.[26-29]

1.3 Limitation of Porphyrin Redox Chemistry

Although porphyrins have been vigorously studied, there are shortcomings to the use of the porphyrin as a ligand. The redox chemistry of the porphyrin is limited to single electron oxidation chemistry, as removing electrons from the fully conjugated porphyrin ring is difficult as judged by the electrochemistry of simple electron deficient free base porphyrin, 2H(TpFPP) (1.61 V).[30] This redox chemistry displayed by the porphyrin can have a limiting effect on the conditions in which porphyrins can be used for chemical transformations. The chemistry is typically linked to the metal center of the porphyrin in a M^n to M^{n+1} type fashion, with the porphyrin typically remaining as an innocent ligand system.[31-36]

Multielectron redox chemistry has long been studied as a function of bimetallic systems, with redox cooperativity between the metal centers allowing for two- and

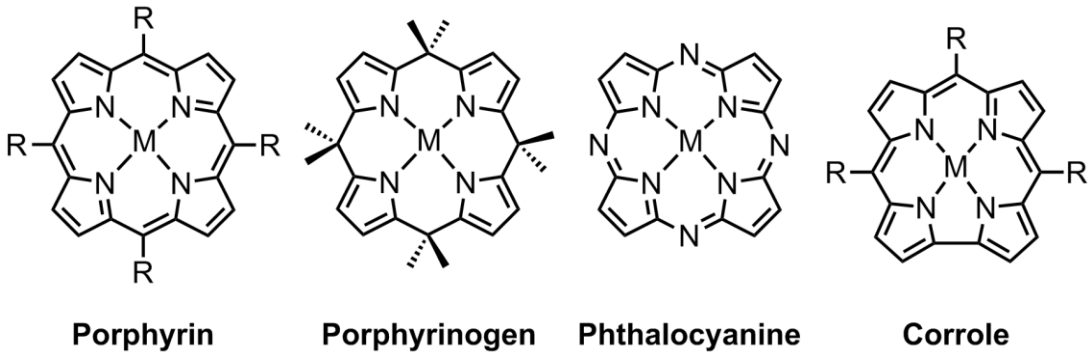

Figure 1.2 Structures of common tetrapyrrole macrocycles.

four-electron transformations.[37-40] However, bimetallic systems are limited by the ligand framework needed to ensure the metal to metal charge transfer.[37,39,41,42] The ligand design for multielectron chemistry plays a critical role in bimetallic systems, however is not directly involved in the electron transfer.

1.4 Porphyrinogens

While porphyrins are often thought of as ligands that support single electron redox chemistry, it has been shown that other tetrapyrrole ligands are able to participate in multielectron redox chemistry. Porphyrinogens, which are tetrapyrrole ligand scaffolds containing sp^3-hybridized *meso*-carbon centers as shown in Figure 1.2, are one such example where the ligand can undergo two distinct two-electron oxidations.[43,44] Scheme 1.1 displays the transformations in which the porphyrinogen forms a spiro-cyclopropane after the first two-electron oxidation event at one of the sp^3-hybridized *meso*-carbon centers. The porphyrinogen is able to undergo a second two-electron oxidation, in which a second spiro-cyclopropane forms

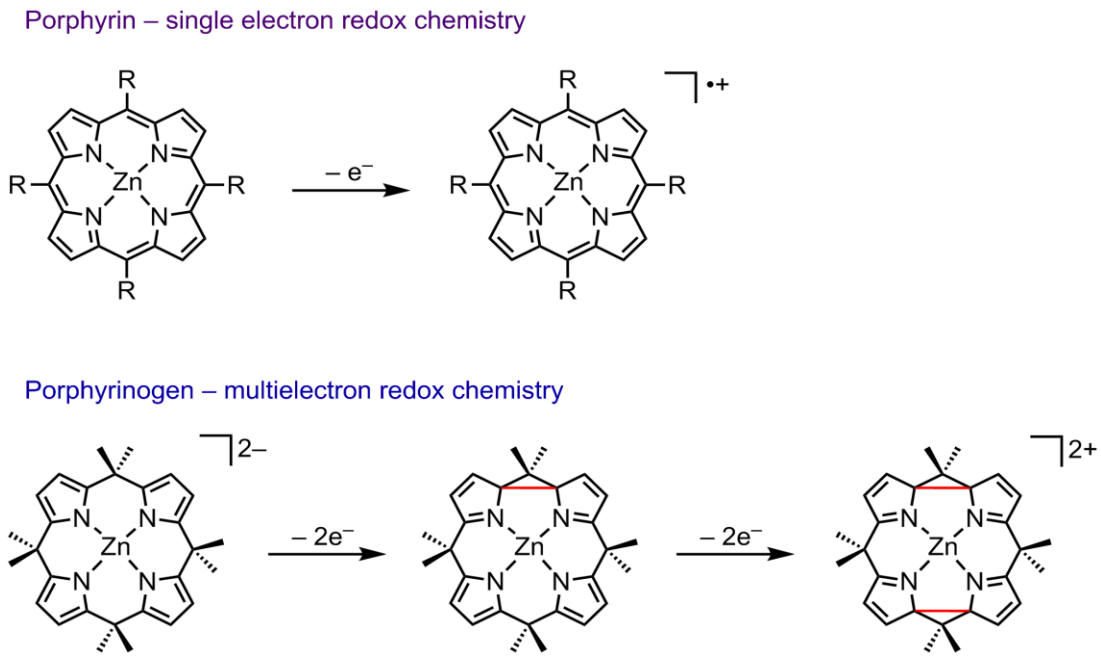

Scheme 1.1 Comparison of the redox chemistry between porphyrins and porphyrinogens

at the sp^3-hybridized *meso*-carbon center directly opposite of the first spiro-cyclopropane.

This incredible and unique property of the porphyrinoid clearly shows that the implementation of sp^3-hybridized *meso*-carbon centers allows for the ligand to participate in multielectron redox chemistry. There are however, disadvantages to the porphyrinogen system which include the instability and the limited absorption profile. The introduction of the four sp^3-hybridized *meso*-carbon centers creates the opportunity for multielectron redox chemistry, however the conjugation observed for the porphyrin is disrupted, making the individual pyrrole groups electronically isolated and severely limiting the absorption profile to the UV wavelength region.

1.5 Porphyrins for Light Harvesting

Tetrapyrrole macrocycles like that of chlorophyll play a critical role in the light harvesting for photosynthesis in nature. Researchers have long looked to mimic photosynthesis to develop efficient solar harvesting devices to be used as a source of alternative energy, as a result porphyrin based devices have been explored, mainly with use as light harvesting dyes in dye sensitized solar cells (DSCs).

Dye sensitized solar cells (DSCs), one of the emerging solar harvesting technologies, have employed porphyrins but have typically suffered from light to current conversion efficiencies below 7%.[45,46] The low efficiencies that are typically obtained using simple porphyrin derivatives are partially due to the limitations of the porphyrin to harvest light from the solar power spectrum (SPS). The absorption profile of a simple porphyrin consists of a strong narrow absorption in the Soret region from 375-425 nm and an absorption in the Q band region from 500-600 nm. While the porphyrin can effectively harvest photons from the UV and high energy visible regions, the longer wavelength photons are wasted, lowering the efficiency of the DSC. The need to harvest the longer wavelength photons is critical to be able to develop DSCs that are efficient enough to be used for wide spread applications.

The inefficiency of light harvesting in nature by the chlorophyll porphyrinoids is overcome through the use of carotenoids, which can harvest photons at the low energy end of the visible spectrum.[47-49] Advances in the development of synthetic porphyrins have enabled the increase in the light harvesting abilities of the porphyrin dyes. This can be accomplished through the extension of π-conjugation along with the incorporation of electron donating moieties. The tailoring of the electronics of the porphyrin periphery shifts the absorption maxima to the red and broadens the absorption profile to better match the solar power spectrum. Implementing these

enhancements to the electronic structure of the porphyrin has shown to be an effective way to increase the efficiency of DSCs. To date the most efficient DSCs have been achieved through the use of these electronically tailored porphyrins, giving light to current conversion efficiencies greater than 12%.[50,51]

The construction of these modified porphyrins is a very intensive process that relies heavily on chromatographic separation of challenging and low yielding intermediates. The challenging synthesis of these particular porphyrin dyes will likely prohibit there widespread use in DSCs. Although higher efficiencies can be obtained using the porphyrin platform, other light harvesting dyes have been investigated.

1.6 Other Porphyrinoids for Light Harvesting

Other tetrapyrrole macrocycles have been investigated for use as light harvesters in DSCs. Phthalocyanines are similar to porphyrins, but contain nitrogen atoms at the *meso*-positions as shown in Figure 1.2. These non-natural macrocycles have been investigated due to the increased conjugation that allows the phthalocyanine to naturally absorb longer wavelength photons. The absorption profile of a typical metalophtalocyanine has an absorption in the Soret region (300-400 nm) and an absorption maxima in the Q band region (600-700 nm).[52,53] Although phtalocyanines are able to harvest light in the near-IR region of the SPS, there is essential no light absorption between 400 and 600 nm. This limitation is a contributing factor to the lower light conversion efficiencies that have been observed for phtalocyanines, with the highest to date reaching 6.4%.[54,55]

Corroles are another subset of tetrapyrrole macrocycles with one of the *meso*-positions being eliminated, forming a direct pyrrole-pyrrole linkage. While there is a very limited amount of research that has been reported with the incorporation of

corroles in DSCs, the efficiencies are far below both the phthalocyanine and the porphyrin derivatives, with the highest reported to date being 1.6%.[56]

For the continued development of DSCs, new light harvesting dyes are needed to be able to produce devices that not only have high light to current conversion efficiencies but are able to be easily synthesized. Chapter 3 and Chapter 4 will investigate the synthesis, redox and photophysical properties of a new potential dye for use in DSCs. The unique properties of the tetrapyrrole macrocycle, the phlorin will be unveiled. Chapter 5 will detail the synthesis and properties of gold(III) metalated phlorin complexes and investigate the potential of the multielectron redox properties of the phlorin ligand.

1.7 Photodynamic Therapy

Photodynamic therapy (PDT) is a treatment that utilizes three components light, photosensitizer and tissue oxygen to target cells for death. PDT has proven to be an effective treatment for diseases such as cancer and age-related macular degeneration. PDT works by the use of light to excite the photosensitizer, which will then react with oxygen, forming a reactive oxygen species, such as free radicals or singlet oxygen that is toxic to the nearby cells. The photosensitizer is given to a patient as either an injection or applied topically, depending on the targeted type of cells or tissue, after which the photosensitizer tends to accumulate within the tumor cells making PDT a more targeted approach. PDT has been used to treat different types of cancer such as esophageal and lung cancer in the United States.

Although PDT has been a useful treatment for some cancers there are some limitations. The penetration of the light used to activate the photosensitizer is limited to approximately 1 cm. This restricts the type of cancers that can be irradiated with

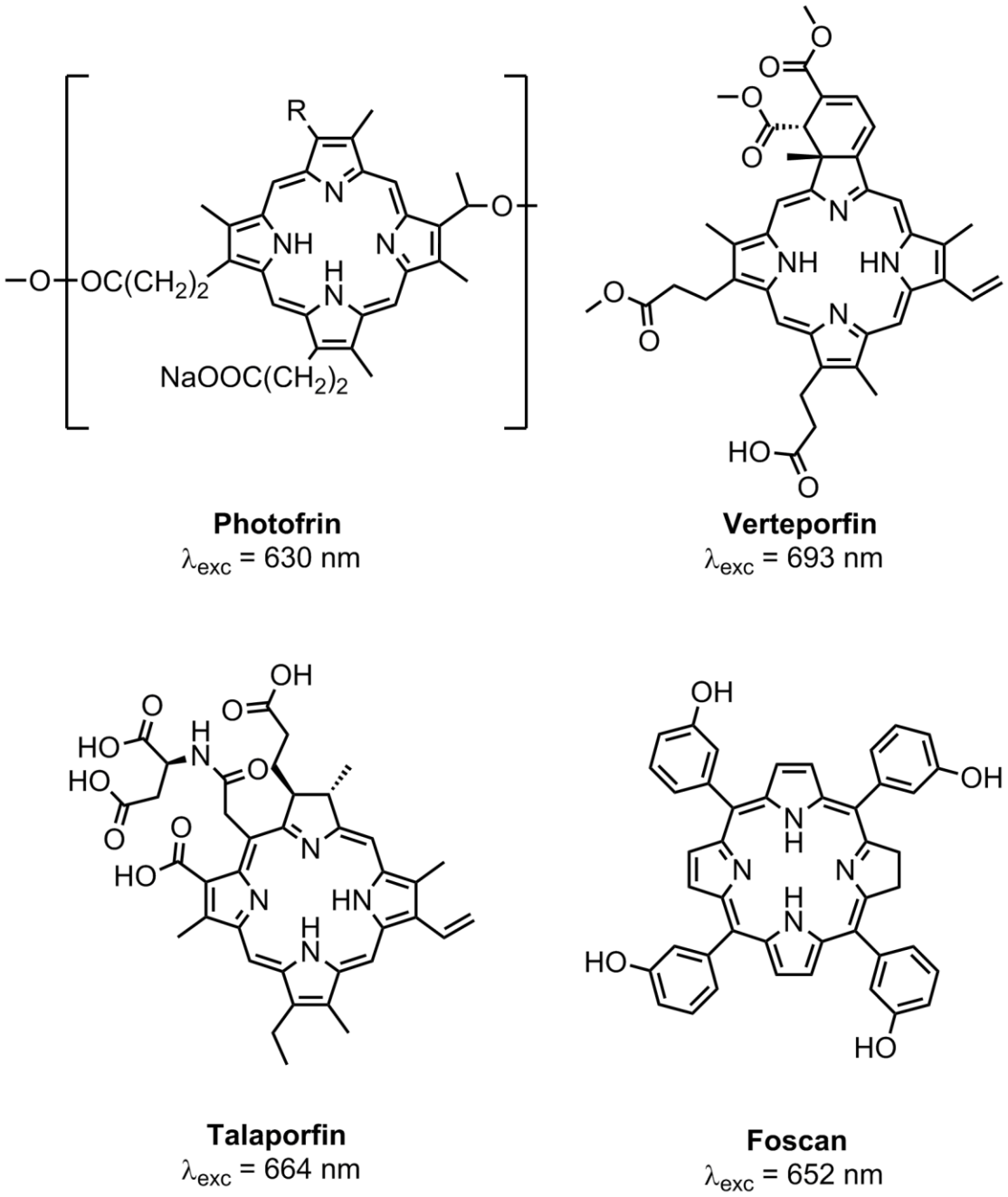

Figure 1.3 Photosensitizers that have been successfully used in PDT.

light to those either just under the skin or on the lining of the organs. PDT can also only be used for cancers that have localized tumors and have not metastasized throughout the body.

There are significant limitations with the photosensitizers that have been developed for the use in PDT due to the longer wavelengths of light required for excitation. The range of wavelengths used in PDT fall within 600 nm to 800 nm, with the longer wavelengths being preferred due to the enhanced depth of penetration by the light. The need for the photosensitizer to not only have the ability to harvest light at these longer wavelengths but also become photo-active with respect to oxygen has proven to be difficult.

Photofrin shown in Figure 1.3 has been approved by the FDA since 1998, and is the most widely used photosensitizer in PDT. One of the limitations associated with Photofrin is the synthesis and purification because it contains close to 60 compounds causing the reproduction of the composition to be difficult. Photofrin is activated using light at 630 nm, which is within the range of wavelengths used in PDT, but Photofrin has a low molar absorptivity at this wavelength. This creates a need for increasing the concentrations used for treatment leading to undesirable effects including photosensitivity where the patient has to avoid direct sunlight and bright indoor light for 4-6 weeks.[57]

As a result, other photosensitizers have been actively pursued for use in PDT. Like Photofrin, many are porphyrinoid derivatives as shown in Figure 1.3.One such photosensitizer is Foscan, which is a chlorin based dye. Foscan has been used to treat cancer in the head and neck region and has some advantages over the more commonly used Photofrin including increased reactivity and activation by longer wavelength

light (652 nm). Foscan has been approved by European Medicines Evaluation Agency for use as cancer treatment; it was not approved by the FDA. Other chlorin derivatives such as Taloporfin have been well studied and have been approved for cancer treatments in Japan. Verteporfin has been a successful photosensitizer for PDT, although not for cancer treatment but, but is widely used for age-related macular degeneration.[58]

Although there has been significant research in the development of photosensitizers there is still a need for new dyes that have the ability to be photo-activated at longer wavelengths, as to increase the depth of light penetration. One such approach is to use dyes that naturally absorb light in the desired range (600-800 nm) and have high molar absorptivities. Phthalocyanines are natural candidates for use in PDT due to their strong absorption in the Q band region and a silicon phthalocyanine, Pc4, is currently under clinical trials.[59,60]

While there has been a great amount of research devoted to some porphyrinoid derivatives, there are still other tetrapyrrole systems that have yet to be explored for PDT. One such class is the dimethyl biladiene (DMBil). In Chapter 6 a detailed synthesis and investigation of the redox and photophysical properties of the free base DMBil as well as the zinc and copper complexes is presented. These tetrapyrrole systems were also be investigated for the production of singlet oxygen for use in PDT.

Chapter 2

EXPERIMENTAL SECTION

2.1 General Procedure

Reactions were performed in oven-dried round-bottomed flasks unless otherwise noted. Reactions that required an inert atmosphere were conducted under a positive pressure of N_2 using flasks fitted with Suba-Seal rubber septa or in a nitrogen filled glove box. Air and moisture sensitive reagents were transferred using standard syringe or cannula techniques.

2.1.1 Materials

Reagents and solvents were purchased from Sigma Aldrich, Acros, Fisher, Strem, or Cambridge Isotopes Laboratories. Solvents for synthesis were of reagent grade or better and were dried by passage through activated alumina and then stored over 4 Å molecular sieves prior to use.[61] Column chromatography was performed with 40-63 μm silica gel with the eluent reported in parentheses. Analytical thin-layer chromatography (TLC) was performed on precoated glass plates and visualized by UV or by staining with Ninhydrin. 3,5-Di-tert-butylbenzaldehyde,[62] 5-(4-nitrophenyl)dipyrromethane and 5-mesityldipyrromethane[63,64] were synthesized according to previously reported procedures.

2.1.2 Compound Characterization

^{1}H NMR and ^{13}C NMR spectra were recorded at 25 °C on a Bruker 400 MHz or 600 MHz spectrometer. Proton spectra are referenced to the residual proton resonance of the deuterated solvent ($CDCl_3$ = δ 7.26) or (CD_3CN = δ 1.94) and carbon spectra are referenced to the carbon resonances of the solvent ($CDCl_3$ = δ 77.16). All chemical shifts are reported using the standard δ rotation in parts-per-million; positive chemical shifts are to higher frequency from the given reference. LR-GCMS data were obtained using an Agilent gas chromatograph consisting of a 6850 Series GC System equipped with a 5973 Network Mass Selective Detector. Low resolution MS data was obtained using either a LCQ Advantage from Thermofinnigan or a Shimadzu LC/MS-2020 single quadrupole MS coupled with an HPLC system, with dual ESI/APCI source. High-resolution mass spectrometry analyses were either performed by the Mass Spectrometry Laboratory in the Department of Chemistry and Biochemistry at the University of Delaware or at the University of Illinois at Urbana-Champaign.

2.1.3 UV-vis Absorption Experiments

UV/visible absorbance spectra were acquired on a StellarNet CCD array UV-vis spectrometer using screw cap quartz cuvettes (6q or 7q) of 1 cm pathlength from Starna. All absorbance spectra were recorded at room temperature. All samples for spectroscopic analysis were prepared in dry solvent within a N_2 filled glovebox.

2.1.4 Anion Titrations

TBAF titrations were conducted by placing 2.5 mL of a 10 μM solutions of $3H(Phl^R)$ in CH_2Cl_2 into a screw cap quartz cuvette. Following the recording of an initial UV-vis absorbance spectrum, 10 – 50 μL aliquots of a 0.25 mM solution of TBAF and phlorin (10 μM) in CH_2Cl_2 were added to the cuvette and changes in the

UV-vis profile were monitored. Since the aliquots were all 10 μM in 3H(Phl^R), the concentration of phlorin did not change over the course of the experiment, which significantly simplifies analysis of the titration data. Job analysis for fluoride binding to each phlorin was carried out using solutions containing 10 μM of total analyte (TBAF + 3H(Phl^R)) in CH_2Cl_2. The ratio of phlorin to fluoride was systematically varied by combining the appropriately sized aliquots of 10 μM stock solutions of TBAF and 3H(Phl^R) in CH_2Cl_2. Titrations and Job analyses conducted for binding of 3H(Phl^{CF3}) to carboxylate salts were carried out using analogous methods.

2.1.5 Steady-State Fluorescence Measurements

Spectra were recorded on an automated Photon Technology International (PTI) QuantaMaster 40 fluorometer equipped with a 75-W Xenon arc lamp, a LPS-220B lamp power supply, and a Hamamatsu R2658 photomultiplier tube. Samples for fluorescence analysis were prepared in an analogous method to that described above for the preparation of samples for UV−vis spectroscopy. Samples were excited at λ_{ex} = 500 nm and emission was monitored with a step size of 1 nm or 0.5 nm and integration time of 0.5 s or 0.25 s. Reported spectra are the average of at least three individual acquisitions. Emission quantum yields were calculated using [$Ru(bpy)_3Cl_2$] in acetonitrile (Φ_{ref} = 0.06)[65] or Nile Blue in ethanol (Φ_{ref} = 0.27)[66] as the reference actinometer using the expression below,[67]

$$\Phi_{em} = \Phi_{ref}\left(\frac{A_{ref}}{A_{em}}\right)\left(\frac{I_{em}}{I_{ref}}\right)\left(\frac{\eta_{em}}{\eta_{ref}}\right)^2$$

where Φ_{em} and Φ_{ref} are the emission quantum yields of the sample and the reference, respectively, A_{ref} and A_{em} are the measured absorbances of the reference and sample at

the excitation wavelength, respectively, I_{ref} and I_{em} are the integrated emission intensities of the reference and sample, respectively, and η_{ref} and η_{em} are the refractive indices of the solvents of the reference and sample, respectively.

2.1.6 Time-Resolved Fluorescence Measurements

The experimental setup for picosecond timecorrelated single-photon-counting (TCSPC) measurements has been described in detail previously[68] and only a brief account will be given here. The detection system includes an actively quenched single photon avalanche photodiode (PDM 50CT module, Micro Photon Devices) and a TCSPC module (PicoHarp 300, PicoQuant). The light source was an optical parametric amplifier pumped by a 250 kHz Ti:Sapphire regenerative amplifier. Excitation was at 650 nm with typically 50 fs (full width at half maximum, fwhm) pulse duration and < 10 nJ pulse energy. Fluorescence emission was selected by using a 10 nm (fwhm) bandpass filter centered at 750 nm (CVI, F10-750.0-4-1.00), which were chosen according to the peak wavelength of the fluorescence emission spectra. The instrument response function (IRF) showed a fwhm of ~40 ps as recorded at the excitation wavelength using a dilute water suspension of coffee creamer. A 4.0-ps channel time was chosen and typically more than 10,000 counts were collected in the peak channel in order to obtain an acceptable signal-to-noise ratio. The polarization of the excitation beam was set to the magic angle (54.7°) with respect to an emission linear polarizer, which enables us to eliminate any depolarization contribution. Quantitative analysis of the time-resolved fluorescence data were performed by employing a least squares deconvolution fitting algorithm with explicit consideration of the finite IRF (FluoFit, PicoQuant) and a reduced chi-squares ($\chi 2$) value is used to judge the quality of each fit.

2.1.7 Electrochemical Measurements

All electrochemistry was performed using either a CHI-620D potentiostat/galvanostat or a CHI CHI-760D bipotentiostat. Cyclic voltammetry and differential pulse voltammetry were performed in a N_2 filled glove box using a standard three-electrode configuration. CV and DPV scans were recorded for quiescent solutions using a glassy carbon working disk electrode (3.0 mm diameter) or a platinum working disk electrode (2.0 mm), a platinum wire auxiliary electrode and a silver wire quasi-reference electrode. CV experiments were performed in a dry degassed solvent with a 0.1 M tetrabutylammonium hexafluorophosphate ($TBAPF_6$) as the supporting electrolyte. Concentrations of analytes were 1 mM and a scan rate of 50 mV/s and Sensitivity of 10 μA/V were maintained during data acquisition. All potentials are referenced to Ag/AgCl using a decamethylferrocenium-decamethylferrocene internal standard of 12 mV (CH_2Cl_2) or 1 mV (CH_3CN) vs Ag/AgCl.[69]

2.1.8 Singlet Oxygen Sensitization

Quantification of singlet oxygen sensitization was carried out using the fluorescent probe 1,3-diphenyl-isobenzofuran as a trapping agent for $^1O_2$.[70] Fluorescence measurements were recorded for CH_3OH solutions that were 10 μM in sensitizer and 1,3-diphenylisobenzofuran. The solutions (2.0 mL total volume) were contained in screw cap quartz cuvettes (7q) of 1 cm pathlength and were irradiated with light passed through either a 500 nm bandpass filter. The rate of $^1O_2$ production was determined by monitoring consumption of the 1,3-diphenylisobenzofuran. This was accomplished by determining the decrease in integrated emission intensity from unreacted furan every five minutes for a total of 30 minutes. $^1O_2$ sensitization quantum

yields were determined using $[Ru(bpy)_3]Cl_2$ (Φ_{ref} = 0.81 in CH_3OH)[71] as a reference sensitizer and the expression below, where Φ_{1O2} and Φ_{ref} are the singlet oxygen sensitization quantum yields for the sample and reference, respectively, m_{sample} and m_{ref} are the slopes of the decrease in furan fluorescence for the sample and the reference, respectively, and ε_{sample} and ε_{ref} are the molar absorptivities at the irradiation wavelength (500 nm) for the sample and reference, respectively.

$$\Phi_{1O2} = \Phi_{ref}\left(\frac{m_{sample}}{m_{ref}}\right)\left(\frac{\varepsilon_{ref}}{\varepsilon_{sample}}\right)$$

2.1.9 Computations

2.1.9.1 3H(Phl^{CF3})

All density functional calculations were performed using the Gaussian 09 (G09) program package,[72] with the Becke three-parameter hybrid exchange and Lee−Yang−Parr correlation functional (B3LYP).[73-75] A 6-31G* basis set was used for all atoms. All geometry optimizations were performed in C1 symmetry with subsequent vibrational frequency analysis to confirm that each stationary point was a minimum on the potential energy surface. A polarizable continuum model was utilized in the geometry optimization to model the solvent effects of the system.[76-80] The vertical singlet transition energies of the complexes were computed at the time-dependent density functional theory (TDDFT) level in CH_2Cl_2 within G09 by using the optimized ground state structure.

2.1.9.2 Au(Phl$^{3,5\text{-}tBu}$)

All density functional calculations were performed using the Gaussian 09 (G09) program package,[72] with the Becke three-parameter hybrid exchange and Lee−Yang−Parr correlation functional (B3LYP).[73-75]The 6-31G(d) basis set was used for C, N, and F atoms. The LANL2DZ[81] pseudopotential was used for Au. All calculations used the SMD universal continuum model[82] with CH_2Cl_2 as the solvent (ε =8.93). All geometry optimizations were performed in C1symmetry with subsequent vibrational frequency analysis to confirm that each stationary point was a minimum on the potential energy surface. The vertical singlet transition energies of the complexes were computed at the time-dependent density functional theory (TD-DFT) level in CH_2Cl_2 within G09 by using the optimized ground-state structure.

2.1.9.3 DMBil and Zn(DMBil)

All density functional calculations were performed using the Gaussian 09 (G09) program package,[72] with the Becke three-parameter hybrid exchange and Lee−Yang−Parr correlation functional (B3LYP).[73-75]The 6-31G* basis set was used for C, N, and F atoms. The LANL2DZ[83] pseudopotential was used for Zn. All calculations used the SMD universal continuum model[84] with CH_2Cl_2 as the solvent (ε =8.93). All geometry optimizations were performed in C1symmetry with subsequent vibrational frequency analysis to confirm that each stationary point was a minimum on the potential energy surface. The vertical singlet transition energies of the complexes were computed at the time-dependent density functional theory (TD-DFT) level in CH_2Cl_2 within G09 by using the optimized ground-state structure.

2.2 Preparation of Dipyrromethane Starting Materials

2.2.1 5,5-Dimethyldipyrromethane

This compound was prepared using a literature method.[63] Pyrrole (87.0 mL, 1.25 mol) and acetone (3.7 mL, 50.0 mmol) were combined in a round bottom flask and the resulting mixture was sparged with N_2 for 10 minutes. To the degassed solution was added trifluoroacetic acid (380 μL, 5 mmol) and the mixture was stirred for 5 min, following which time, the reaction was quenched with 100 mL of 0.1 M NaOH. The product was then extracted into ethyl acetate and this organic layer was washed with water and dried over sodium sulfate. Following removal of the solvent by rotary evaporation, the desired product was purified via vacuum distillation to give 4.15 g of the title compound as a white solid (47% based on acetone starting material). ^{1}H NMR (400 MHz, $CDCl_3$, 25 °C) δ/ppm: 7.71 (br s, 2H), 6.61 (m, 2H), 6.14 (m, 2H), 6.10 (m, 2H), 1.64 (s, 6H). ^{13}C NMR (101 MHz, $CDCl_3$, 25 °C) δ/ppm: 139.22, 117.21, 107.82, 103.83, 77.16, 35.46, 29.43. GCMS: $[M]^+$ m/z: calcd for $C_{11}H_{14}N_2$, 174.12; found, 174.

2.2.2 5-(Pentafluorophenyl)dipyrromethane

This compound was prepared using a literature method.[63] Pyrrole (25 mL, 360 mmol) and pentafluorobenzaldehyde (1.76 mL, 14.4 mmol) were combined in a round bottom flask and the resulting mixture was sparged with N_2 for 10 minutes. To the degassed solution was added trifluoroacetic acid (110 μL, 1.4 mmol) and the mixture was stirred for 5 min, following which time, the reaction was quenched with 100 mL of 0.1 M NaOH. The product was then extracted into ethyl acetate and this organic layer was washed with water and dried over Na_2SO_4. Following removal of the solvent by rotary evaporation, the desired product was purified via vacuum distillation to give

3.1 g of the title compound as a white solid (69%). ^{1}H NMR (400 MHz, $CDCl_3$, 25 °C) δ/ppm: 8.14 (br s, 2H), 6.73 (m, *J* = 2.7, 1.6 Hz, 2H), 6.17 (q, *J* = 6.1, 2.7 Hz, 2H), 6.03 (m, 2H), 5.90 (s, 1H). ^{13}C NMR (101 MHz, $CDCl_3$, 25 °C) δ/ppm: 128.23, 118.26, 108.81, 107.77, 77.16, 33.18. GCMS: $[M]^+$ m/z: calcd for $C_{15}H_9F_5N_2$, 312.17; found, 312.

2.2.3 5-(2,6-Dimethoxyphenyl)dipyrromethane

Pyrrole (10.5 mL, 150 mmol) and 2,6-dimethoxybenzaldehyde (1 g, 6 mmol) were combined in a round bottom flask and the resulting mixture was sparged with N_2 for 10 minutes. To the degassed solution was added trifluoroacetic acid (50 μL, 650 μmol) and the mixture was stirred for 5 min, following which time, the reaction was quenched with 100 mL of 0.1 M NaOH. The product was then extracted into ethyl acetate and this organic layer was washed with water and dried over Na_2SO_4. Following removal of the solvent by rotary evaporation, the desired product was purified via column chromatography on silica (10% ethyl acetate in hexanes) to give 1.3 g of the title compound as a grey solid (33%). ^{1}H NMR (400 MHz, $CDCl_3$, 25 °C) δ/ppm: 8.54 (br s, 2H), 7.22 (t, *J* = 8.4 Hz, 1H), 6.65-6.63 (m, 4H), 6.20 (s, 1H), 6.13-6.11 (m, 2H), 5.94 (m, 2H), 3.76 (s, 6H). ^{13}C NMR (101 MHz, $CDCl_3$, 25 °C) δ/ppm: 158.30, 133.11, 128.30, 119.62, 116.27, 107.83, 105.96, 56.57, 32.69. HR-EI-MS: $[M]^+$ m/z: calcd for $C_{17}H_{18}N_2NaO_2$, 282.1368; found, 282.1375.

2.2.4 5-(4-tert-butylcarboxyphenyl)dipyrromethane

Pyrrole (4.9 mL, 70 mmol) and tert-butyl 4-formylbenzoate (580 mg, 2.8 mmol) were combined in a round bottom flask and the resulting mixture was sparged with N_2 for 10 min. To the degassed solution was added trifluoroacetic acid (20 μL,

280 μmol) and the mixture was stirred for 5 min, following which time, the reaction was quenched with 100 mL of 0.1 M NaOH. The product was then extracted into ethyl acetate and this organic layer was washed with water and dried over Na_2SO_4. Following removal of the solvent by rotary evaporation, the desired product was purified via column chromatography (15% ethyl acetate in hexanes) to give 500 mg of the title compound as a grey solid (55%). ^{1}H NMR (400 MHz, $CDCl_3$, 25 °C) δ/ppm: 7.95 (d, *J* = 8.24 Hz, 2H), 7.28 (d, *J* = 8.28 Hz, 2H), 6.72 (s, 2H), 6.18 (q, *J* = 2.8 Hz, 2H), 5.92 (s, 2H), 5.53 (s, 1H), 1.62 (s, 9H). ^{13}C NMR (101 MHz, $CDCl_3$, 25 °C) δ/ppm: 165.75, 146.92, 131.88, 130.85, 129.89, 128.39, 117.63, 108.67, 107.60, 81.15, 44.06, 28.32. HR-CI-MS: $[M]^+$ m/z: calcd for $C_{20}H_{23}N_2O_2$, 322.1681; found, 322.1690.

2.2.5 5-(3,5-bis(tertbutyl)phenyl)dipyrromethane

This compound was prepared by adapting a literature procedure.[85] Pyrrole (36 mL, 520 mmol) and 3,5-Di-tert-butylbenzaldehyde (4.5 g, 20.6 mmol) were combined in a round bottom flask and the resulting mixture was sparged with N_2 for 10 minutes. To the degassed solution was added BF_3•OEt_2 (1.54 mL, XX mmol) and the mixture was stirred for 2 hours under an atmosphere of N_2. The dark brown solution was then evaporated in vaccu. The residue was dissolved in CH_2Cl_2 and washed twice with 1 M NaOH and dried over Na_2SO_4. Following removal of solvent, the desired product was purified via silica column chromatography with hexane, ethyl acetate and TEA (85:14:1) as the eleuent. A second basic alumina column was needed to remove remaining impurities using CH_2Cl_2 as the eleuent to give 5 g of the title compound as a light brown solid (72 %). ^{1}H NMR (400 MHz, $CDCl_3$) δ 7.93 (s, 2H), 7.31 (s, 1H), 7.06 (d, *J* = 1.8 Hz, 2H), 6.70 (d, *J* = 1.8 Hz, 2H), 6.16 (d, *J* = 3.0 Hz, 2H), 5.93 (s,

2H), 5.45 (s, 1H), 1.28 (s, 18H). ^{13}C NMR (101 MHz, $CDCl_3$) δ 151.06, 140.95, 133.04, 122.85, 121.03, 117.11, 108.44, 107.23, 44.62, 34.96, 31.61.

2.2.6 5-(3,5-bis(trifluoromethyl)phenyl)dipyrromethane

This compound was prepared by adapting a literature method.[63] Pyrrole (25 mL, 360 mmol) and 3,5-bis(trifluoromethyl)benzaldehyde (1.76 mL, 14.4 mmol) were combined in a round bottom flask and the resulting mixture was sparged with N_2 for 10 minutes. To the degassed solution was added trifluoroacetic acid (110 μL, 1.4 mmol) and the mixture was stirred for 5 min, following which time, the reaction was quenched with 100 mL of 0.1 M NaOH. The product was then extracted into ethyl acetate and this organic layer was washed with water and dried over sodium sulfate. Following removal of the solvent by rotary evaporation, the desired product was purified via vacuum distillation to give 3.1 g of the title compound as a white solid (69%). ^{1}H NMR (400 MHz, $CDCl_3$, 25 °C) δ/ppm: 8.14 (br s, 2H), 6.73 (m, J = 2.7, 1.6 Hz, 2H), 6.17 (q, J = 6.1, 2.7 Hz, 2H), 6.03 (m, 2H), 5.90 (s, 1H). ^{13}C NMR (101 MHz, $CDCl_3$, 25°C) δ/ppm: 128.23, 118.26, 108.81, 107.77, 77.16, 33.18. GCMS: $[M]^+$ m/z: calcd for $C_{17}H_{12}F_6N_2$, 358.09; found, 358. HR-EI-MS: m/z: calcd for $C_{17}H_{12}F_6N_2$, 358.0905; found, 358.0895.

2.2.7 5,5-Dimethyl-1,9-bis(pentafluorobenzoyly)dipyrromethane

This compound was prepared by amending a previously described method.[86] To 5,5- dipyrromethane (0.871 g, 5.00 mmol) was added 100 mL of dry toluene under an atmosphere of N_2. To the resulting solution was added ethyl magnesium bromide (25 mL, 25.0 mmol, 1 M in THF) in dropwise fashion and the resulting mixture was stirred for 30 min at room temperature. A solution of 1.80 mL of pentafluorobenzoyl

chloride (12.5 mmol) in 12.5 mL of dry toluene was then added to the stirred reaction in dropwise fashion and the resulting solution was stirred for an additional 30 min. The reaction was quenched with 75 mL of saturated NH_4Cl and the organic layer was then separated, washed sequentially with water and brine, and then dried over Na_2SO_4. Following solvent removal under reduced pressure, the crude product was purified by flash chromatography on silica (33% ethyl acetate in hexanes). Recrystallization of the product at –35 °C from CH_2Cl_2/hexanes delivered 843 mg of the title compound as a white solid (30%). ^{1}H NMR (400 MHz, $CDCl_3$, 25 °C) δ/ppm: 9.77 (br s, 2H), 6.66 (d, 2H), 6.24 (d, *J* = 4.0 Hz, 2H), 1.81 (s, 6H). ^{13}C NMR (101 MHz, $CDCl_3$, 25 °C) δ/ppm: 172.4, 148.3, 144.1, 142.5, 137.7, 131.6, 122.6, 113.9, 109.8, 36.5, 28.4. ESI-MS: $[M+H]^+$ m/z: calcd for $C_{25}H_{13}F_{10}N_2O_2$, 563.08; found, 563.

2.3 Preparation of 3H(Phl^R) (R = F, OMe, NO_2, Mes, CO_2tBu, CF_3, 3,5-tBu)

2.3.1 5,5-Dimethyl-10,15,20-tris(pentafluorophenyl)phlorin (3H(Phl^F))

This compound was prepared by amending a previously described method. To a solution of 5,5-Dimethyl-1,9-bis(pentafluorobenzoyly)dipyrromethane (281 mg, 0.50 mmol) dissolved in 40 mL of THF and MeOH (3:1) was added 946 mg of $NaBH_4$ (25.0 mmol). The resulting mixture was stirred at room temperature for 2 hrs, following which time, the reaction was quenched with H_2O and extracted with CH_2Cl_2. The organic layer was washed sequentially with H_2O and brine and then dried over Na_2SO_4. The solvent was then removed via rotary evaporation and the resulting residue was dissolved in 200 mL of dichloromethane and combined with 156 mg of 5-(pentafluorophenyl)dipyrromethane (0.50 mmol) and 1.54 mL of trifluoroacetic acid (20.0 mmol). The resulting solution was stirred at room temperature for 15 min, after

which time 167 mg of DDQ (0.730 mmol) was added to the reaction. After stirring the reaction for an additional 5 min, 14 mL of triethylamine (100 mmol) was added. After stirring the solution for an additional 30 min, the reaction was filtered through a pad of silica and eluted with CH_2Cl_2 until the mobile phase was no longer green. Following removal of the solvent under reduced pressure, the crude green colored material was purified by flash chromatography on silica using hexanes and CH_2Cl_2 (3:1) as the eluent to deliver 200 mg of the title compound as an deep green powder (48%). ^{1}H NMR (400 MHz, $CDCl_3$, 25 °C) δ/ppm: 7.37 (d, *J* = 5.0 Hz, 2H), 7.14 (d, *J* = 5.0 Hz, 2H), 6.94 (d, *J* = 3.9 Hz, 2H), 6.78 (d, *J* = 3.9 Hz, 2H), 5.16 (br s, 3H), 1.42 (s, 6H). HR-ESI-MS: $[M+H]^+$ m/z: calcd for $C_{40}H_{18}F_{15}N_4$, 839.1292; found, 839.1286.

2.3.2 5,5-Dimethyl-10,20-bis(pentafluorophenyl)-15-(2,6-dimethoxyphenyl)phlorin (3H(Phl^{OMe}))

To a solution of 5,5-Dimethyl-1,9-bis(pentafluorobenzoyly)dipyrromethane (281 mg, 0.50 mmol) dissolved in 40 mL of THF and MeOH (3:1) was added 946 mg of $NaBH_4$ (25.0 mmol). The resulting mixture was stirred at room temperature for 2 hrs, following which time, the reaction was quenched with H_2O and extracted with CH_2Cl_2. The organic layer was washed sequentially with H_2O and brine and then dried over Na_2SO_4. The solvent was then removed via rotary evaporation and the resulting residue was dissolved in 200 mL of CH_2Cl_2 and combined with 144 mg of 5-(2,6-dimethoxyphenyl)dipyrromethane (0.50 mmol) and 1.54 mL of trifluoroacetic acid (20.0 mmol). The resulting solution was stirred at room temperature for 15 min, after which time 167 mg of DDQ (0.730 mmol) was added to the reaction. After stirring the reaction for an additional 5 min, 14 mL of triethylamine (100 mmol) was added. After stirring the solution for an additional 30 min, the reaction was filtered through a pad of

silica and eluted with CH_2Cl_2 until the mobile phase was no longer green. Following removal of the solvent under reduced pressure, the crude green colored material was purified by flash chromatography on silica using hexanes and CH_2Cl_2 (3:1) as the eluent to deliver 148 mg of the title compound as an deep green powder (36%). ^{1}H NMR (400 MHz, $CDCl_3$, 25 °C) δ/ppm: 7.47 (t, *J* = 8.0 Hz, 1H), 7.16 (d, *J* = 8.0 Hz, 2H), 7.06 (d, *J* = 8.0 Hz, 2H), 6.83 (d, *J* = 4.0 Hz, 2H), 6.77 (d, *J* = 8.0 Hz, 2H), 6.72 (d, *J* = 4.0 Hz, 2H), 5.46 (br s, 3H), 3.68 (s, 6H), 1.51 (s, 6H). HR-ESI-MS: $[M+H]^+$ m/z: calcd for $C_{42}H_{27}F_{16}N_4$, 808.1896; found, 809.1965.

2.3.3 5,5-Dimethyl-10,20-bis(pentafluorophenyl)-15-(4-nitrophenyl)phlorin (3H(Phl^{NO2}))

To a solution of 5,5-Dimethyl-1,9-bis(pentafluorobenzoyly)dipyrromethane (281 mg, 0.50 mmol) dissolved in 40 mL of THF and MeOH (3:1) was added 946 mg of $NaBH_4$ (25.0 mmol). The resulting mixture was stirred at room temperature for 2 hrs, following which time, the reaction was quenched with H_2O and extracted with CH_2Cl_2. The organic layer was washed sequentially with H_2O and brine and then dried over Na_2SO_4. The solvent was then removed via rotary evaporation and the resulting residue was dissolved in 200 mL of CH_2Cl_2 and combined with 134 mg of 5-(4-nitrophenyl)dipyrromethane (0.50 mmol) and 1.54 mL of trifluoroacetic acid (20.0 mmol). The resulting solution was stirred at room temperature for 15 min, after which time 167 mg of DDQ (0.730 mmol) was added to the reaction. After stirring the reaction for an additional 5 min, 14 mL of triethylamine (100 mmol) was added. After stirring the solution for an additional 30 min, the reaction was filtered through a pad of silica and eluted with CH_2Cl_2 until the mobile phase was no longer green. Following removal of the solvent under reduced pressure, the crude green colored material was

purified by flash chromatography on silica using hexanes and CH_2Cl_2 (3:1) as the eluent to deliver 166 mg of the title compound as an deep green powder (42%). ^{1}H NMR (400 MHz, $CDCl_3$, 25 °C) δ/ppm: 8.42 (d, *J* = 8.0 Hz, 2H), 7.87 (d, *J* = 8.0 Hz, 2H), 7.36 (d, *J* = 8.0 Hz, 2H), 7.23 (d, *J* = 5.2 Hz, 2H), 6.98 (d, *J* = 3.9 Hz, 2H), 6.84 (d, *J* = 3.9 Hz, 2H), 5.05 (br s, 3H), 1.46 (s, 6H). HR-ESI-MS: $[M+H]^+$ m/z: calcd for $C_{40}H_{22}F_{10}N_5O_2$, 794.1614; found, 794.1606.

2.3.4 5,5-Dimethyl-10,20-bis(pentafluorophenyl)-15-(mesityl)phlorin (3H(Phl^{Mes}))

To a solution of 5,5-Dimethyl-1,9-bis(pentafluorobenzoyly)dipyrromethane (281 mg, 0.50 mmol) dissolved in 40 mL of THF and MeOH (3:1) was added 946 mg of $NaBH_4$ (25.0 mmol). The resulting mixture was stirred at room temperature for 2 hrs, following which time, the reaction was quenched with H_2O and extracted with CH_2Cl_2. The organic layer was washed sequentially with H_2O and brine and then dried over Na_2SO_4. The solvent was then removed via rotary evaporation and the resulting residue was dissolved in 200 mL of CH_2Cl_2 and combined with 132 mg of 5-mesityldipyrromethane (0.50 mmol) and 1.54 mL of trifluoroacetic acid (20.0 mmol). The resulting solution was stirred at room temperature for 15 min, after which time 167 mg of DDQ (0.730 mmol) was added to the reaction. After stirring the reaction for an additional 5 min, 14 mL of triethylamine (100 mmol) was added. After stirring the solution for an additional 30 min, the reaction was filtered through a pad of silica and eluted with CH_2Cl_2 until the mobile phase was no longer green. Following removal of the solvent under reduced pressure, the crude green colored material was purified by flash chromatography on silica using hexanes and CH_2Cl_2 (4:1) as the eluent to deliver 182 mg of the title compound as an deep green powder (46%). ^{1}H NMR (400 MHz,

$CDCl_3$, 25 °C) δ/ppm: 7.21 (d, *J* = 4.0 Hz, 2H), 7.06 (s, 2H), 7.01 (d, *J* = 4.0 Hz, 2H), 6.90 (d, *J* = 4.0 Hz, 2H), 6.77 (d, *J* = 4.0 Hz, 2H), 5.27 (br s, 3H), 2.43 (s, 3H), 2.03 (s, 6H), 1.51 (s, 6H). HR-ESI-MS: $[M+H]^+$ m/z: calcd for $C_{43}H_{28}F_{10}N_4$, 790.2154; found, 791.2221.

2.3.5 5,5-Dimethyl-10,20-bis(pentafluorophenyl)-15-(4-tert-butylcarboxy)phenyl)phlorin (3H(Phl^{CO2tBu}))

To a solution of 5,5-Dimethyl-1,9-bis(pentafluorobenzoyly)dipyrromethane (281 mg, 0.50 mmol) dissolved in 40 mL of THF and MeOH (3:1) was added 946 mg of $NaBH_4$ (25.0 mmol). The resulting mixture was stirred at room temperature for 2 hrs, following which time, the reaction was quenched with H_2O and extracted with CH_2Cl_2. The organic layer was washed sequentially with H2O and brine and then dried over Na_2SO_4. The solvent was then removed via rotary evaporation and the resulting residue was dissolved in 200 mL of CH_2Cl_2 and combined with 161 mg of 5-(4-tbutylcarboxyphenyl) dipyrromethane (0.50 mmol) and 1.54 mL of trifluoroacetic acid (20.0 mmol). The resulting solution was stirred at room temperature for 15 min, after which time 167 mg of DDQ (0.730 mmol) was added to the reaction. After stirring the reaction for an additional 5 min, 14 mL of triethylamine (100 mmol) was added. After stirring the solution for an additional 30 min, the reaction was filtered through a pad of silica and eluted with CH_2Cl_2 until the mobile phase was no longer green. Following removal of the solvent under reduced pressure, the crude green colored material was purified by flash chromatography on silica using hexanes and CH_2Cl_2 (3:1) as the eluent to deliver 194 mg of the title compound as an deep green powder (48%). ^{1}H NMR (400 MHz, CD_3CN 25 °C) /ppm: 8.13 (d, *J* = 8.0 Hz, 2H), 7.76 (d, *J* = 8.0 Hz, 2H), 7.44 (d, *J* = 5.0 Hz, 2H), 7.27 (d, *J* = 5.0 Hz, 2H), 6.99 (d, *J* =

3.8 Hz, 2H), 6.80 (d, *J* = 3.8 Hz, 2H), 5.67 (br s, 2H), 1.67 (s, 9H), 1.64 (s, 9H), 1.49 (s, 6H). HR-ESI-MS: $[M+H]^+$ m/z: calcd for $C_{45}H_{31}F_{10}N_4O_2$, 849.2287; found, 849.2309.

2.3.6 5,5-Dimethyl-10,20-bis(pentafluorophenyl)-15-(bis-3,5-trifluoromethylphenyl)phlorin (3H(Phl^{CF3}))

To a solution of 5,5-Dimethyl-1,9-bis(pentafluorobenzoyly)dipyrromethane (281 mg, 0.50 mmol) dissolved in 40 mL of THF and MeOH (3:1) was added 946 mg of $NaBH_4$ (25.0 mmol). The resulting mixture was stirred at room temperature for 2 hrs, following which time, the reaction was quenched with H_2O and extracted with dichloromethane. The organic layer was washed sequentially with H_2O and brine and then dried over Na_2SO_4. The solvent was then removed via rotary evaporation and the resulting residue was dissolved in 200 mL of dichloromethane and combined with 173 mg (0.50 mmol) of 5,5-dimethyl-1,9-bis(pentafluorobenzoyly)dipyrromethane and 1.54 mL (20.0 mmol) of trifluoroacetic acid. The resulting solution was stirred at room temperature for 15 min, after which time 167 mg of DDQ (0.730 mmol) was added to the reaction. After stirring the reaction for an additional 5 min, 14 mL (100 mmol) of triethylamine was added. After stirring the solution for an additional 30 min, the reaction was filtered through a pad of silica and eluted with CH_2Cl_2 until the mobile phase was no longer green. Following removal of the solvent under reduced pressure, the crude green colored material was purified by flash chromatography on silica using hexanes and CH_2Cl_2 (2:1) as the eluent to deliver 183 mg of the title compound as an deep green powder (41%). ^{1}H NMR (400 MHz, $CDCl_3$, 25 °C) δ/ppm: 8.17 (s, 2H), 8.05 (s, 1H), 7.38 (d, *J* = 5.0 Hz, 2H), 7.18 (d, *J* = 5.0 Hz, 2H), 6.99 (d, *J* = 3.8 Hz, 2H), 6.84 (d, *J* = 3.9 Hz, 2H), 4.98 (s, 3H), 1.44 (s, 6H). ^{19}F NMR (376 MHz, $CDCl_3$,

25 °C) δ/ppm: –63.49 (s), –139.09 to –139.60 (m), –153.73 (t, *J* = 21.0 Hz), –162.35 (td, *J* = 23.3, 8.0 Hz). HR-ESI-MS: $[M + H]^+$ m/z: calcd for $C_{42}H_{21}F_{16}N_4$, 885.1511; found, 885.1496.

2.3.7 5,5-Dimethyl-10,20-bis(pentafluorophenyl)-15-(bis-3,5-tert-butylphenyl)phlorin (3H(Phl$^{3,5\text{-}tBu}$))

To a solution of 5,5-Dimethyl-1,9-bis(pentafluorobenzoyly)dipyrromethane (281 mg, 0.50 mmol) dissolved in 40 mL of THF and MeOH (3:1) was added 946 mg of $NaBH_4$ (25.0 mmol). The resulting mixture was stirred at room temperature for 2 hrs, following which time, the reaction was quenched with H_2O and extracted with CH_2Cl_2. The organic layer was washed sequentially with H_2O and brine and then dried over Na_2SO_4. The solvent was then removed via rotary evaporation and the resulting residue was dissolved in 200 mL of CH_2Cl_2 and combined with 167 mg of 5-(3,5-bis(tertbutyl)phenyl)dipyrromethane (0.50 mmol) and 1.54 mL of trifluoroacetic acid (20.0 mmol). The resulting solution was stirred at room temperature for 15 min, after which time 167 mg of DDQ (0.730 mmol) was added to the reaction. After stirring the reaction for an additional 5 min, 14 mL of triethylamine (100 mmol) was added. After stirring the solution for an additional 30 min, the reaction was filtered through a pad of silica and eluted with CH_2Cl_2 until the mobile phase was no longer green. Following removal of the solvent under reduced pressure, the crude green colored material was purified by flash chromatography on silica using hexanes and CH_2Cl_2 (3:1) as the eluent to deliver 200 mg of the title compound as an deep green powder (46%). ^{1}H NMR (400 MHz, CD_3CN) δ/ppm: 7.62 (s, 1H), 7.53 (s, 2H), 7.43 (d, *J* = 4.0 Hz, 2H), 7.26 (d, *J* = 4.8 Hz, 2H), 6.98 (d, *J* = 3.0 Hz, 2H), 6.80 (d, *J* = 3.0 Hz, 2H), 1.50 (s, 6H), 1.40 (s, 19H). ^{19}F NMR (565 MHz, CD_3CN, 25 °C) δ/ppm: -141.95 (dd, *J* = 22.2,

5.8 Hz), -157.02 (t, *J* = 20.2 Hz), -164.52 (td, *J* = 22.9, 6.7 Hz). HR-LIFDI-MS: $[M-H]^+$ m/z: calcd for $C_{48}H_{37}F_{10}N_4$, 859.2855; found, 859.2859.

2.4 Preparation of Au(Phl^R) (R = F, 3,5-tBu)

2.4.1 Gold(5,5-Dimethyl-10,15,20-tris(pentafluorophenyl)phlorin) (Au(Phl^F))

3H(Phl^F) (200 mg, 0.24 mmol) was dissolved in 10 mL in THF and 60 mL of toluene and was placed in a –35 °C freezer in a nitrogen filled glovebox for 1 hour. KO^{t}Bu (80 mg, 0.71 mmol) was dissolved in 2 mL of THF and added to the phlorin solution. The reaction stirred for 4 hours followed by the addition of $AuBr_3$ (104 mg, 0.24 mmol) dissolved in 2 mL of THF. The reaction stirred for 15 hours followed by the removal of the solvent under reduced pressure. The product was purified with column chromatography on silica with hexanes and CH_2Cl_2 (3:1) as the eluent to give 34 mg as a brown solid (14 %). ^{1}H NMR (400 MHz, $CDCl_3$) δ/ppm: 7.39 (d, *J* = 5.3 Hz, 2H), 7.34 (d, *J* = 4.3 Hz, 2H), 7.17 (t, *J* = 4.5 Hz, 4H), 1.53 (s, 6H). ^{19}F NMR (565 MHz, $CDCl_3$) δ/ppm: -137.35 (dd, *J* = 24.5, 7.9 Hz), -138.00 (dd, *J* = 23.5, 7.2 Hz), -152.35 (t, *J* = 20.8 Hz), -152.60 (t, *J* = 20.8 Hz), -161.01 (t, *J* = 18.4 Hz). HR-LIFDI-MS $[M]^+$ m/z: calc for $C_{40}H_{14}N_4F_{15}Au$, 1032.0645; found, 1032.0636.

2.4.2 Gold(5,5-Dimethyl-10,20-bis(pentafluorophenyl)-15-(bis-3,5-tert-butylphenyl)phlorin) (Au(Phl$^{3,5\text{-}tBu}$))

3H(Phl$^{3,5\text{-}tBu}$) (200 mg, 0.23 mmol) was dissolved in 10 mL in THF and 60 mL of toluene and was placed in a –35 °C freezer in a nitrogen filled glovebox for 1 hour. KO^{t}Bu (71 mg, 0.70 mmol) was dissolved in 2 mL of THF and added to the phlorin solution. The reaction stirred for 4 hours followed by the addition of $AuBr_3$ (100 mg,

0.23 mmol) dissolved in 2 mL of THF. The reaction stirred for 15 hours followed by the removal of the solvent under reduced pressure. The product was purified with column chromatography on silica with hexanes and CH_2Cl_2 (3:1) as the eluent to give 23 mg as a brown solid (9 %). ^{1}H NMR (400 MHz, CD_3CN) δ/ppm: 7.66 (s, 1H), 7.55 (d, *J* = 1.8 Hz, 2H), 7.51 (d, *J* = 5.1 Hz, 2H), 7.46 (d, *J* = 4.0 Hz, 2H), 7.36 (d, *J* = 5.3 Hz, 2H), 7.23 (d, *J* = 4.0 Hz, 2H), 1.46 (s, 6H), 1.40 (s, 21H). ^{19}F NMR (565 MHz, CD_3CN) δ/ppm: -141.56 (dd, *J* = 23.6, 7.4 Hz), -156.33 (t, *J* = 20.1 Hz), -163.94 (td, *J* = 22.2, 7.6 Hz). HR-LIFDI-MS $[M]^+$ m/z: calc for $C_{48}H_{35}N_4F_{10}Au$, 1054.2368; found, 1054.2397.

2.5 Preparation of R(Phl$^{3,5\text{-}tBu}$Cl$_x$) (R = 3H, Au) (X = 1,2)

2.5.1 Au(Phl$^{3,5\text{-}tBu}$Cl$_2$)

To a solution of 38 mg of Au(Phl^{3,5tBu}) (36 μmol) dissolved in 15 mL of degassed CH_2Cl_2 10 mg of (dichloroiodo)benzene (36 μmol) was added and reaction was stirred at room temperature for 36 hours under a nitrogen atmosphere. The solvent was removed via rotary evaporation and purified by chromatography on silica with hexanes and CH_2Cl_2 (15:1) as the eluent to give 21 mg as a brown solid (52 %). ^{1}H NMR (600 MHz, CD_3CN) δ/ppm: 7.68 (s, 1H), 7.54 (s, 2H), 7.49 (d, *J* = 5.3 Hz, 2H), 7.38 (d, *J* = 5.3 Hz, 2H), 7.27 (s, 2H), 1.44 (s, 3H), 1.40 (s, 24H). ^{19}F NMR (565 MHz, Acetonitrile-d_3) δ/ppm: -141.93 (d, *J* = 16.4 Hz), -155.32 (t, *J* = 19.9 Hz), -164.51 (td, *J* = 23.3, 7.1 Hz). HR-LIFDI-MS $[M]^+$ m/z: calc for $C_{48}H_{33}N_4F_{10}Cl_2Au$, 1122.1588; found, 1122.1570.

2.5.2 Au(Phl3,5-tBuCl)

The title compound was isolated as byproduct for the reaction of $PhICl_2$ with $Au(Phl^{3,5\text{-}tBu})$ as described above and purified by chromatography on silica with hexanes and CH_2Cl_2 (12:1) as the eluent to give 15 mg as a brown solid (14 %). ^1H NMR (600 MHz, CD_3CN) δ/ppm: 7.66 (s, 1H), 7.54 (s, 2H), 7.53 (d, *J* = 5.5 Hz, 1H), 7.47 (s, 1H), 7.45 (d, *J* = 5.5 Hz, 1H), 7.38 (d, *J* = 5.1 Hz, 1H), 7.35 (d, *J* = 5.3 Hz, 1H), 7.24 (s, 1H), 7.21 (s, 1H), 1.41 (s, 6H), 1.39 (s, 18H). ^{19}F NMR (565 MHz, CD_3CN) δ/ppm: -141.51 (d, *J* = 16.4 Hz), -141.87 – -142.03 (m), -155.60 (t, *J* = 20.0 Hz), -156.07 (t, *J* = 20.2 Hz), -163.66 – -163.93 (m), -164.67 (td, *J* = 23.0, 22.3, 6.8 Hz). HR-LIFDI-MS $[M]^+$ m/z: calc for $C_{48}H_{34}N_4F_{10}ClAu$, 1088.1978; found, 1088.1958.

2.5.3 3H(Phl$^{3,5\text{-}tBu}$Cl)

To a solution of 50 mg of $3H(Phl^{3,5tBu})$ (58 μmol) dissolved in 15 mL of degassed $C_2H_4Cl_2$ 10 mg of (dichloroiodo)benzene (58 μmol) was added and the reaction was heated to 60 °C for four days under an atmosphere of nitrogen. The solvent was removed via rotary evaporation and purified by chromatography on silica with hexanes and CH_2Cl_2 (6:1) as the eluent to give 17 mg as a green solid (33 %). ^1H NMR (600 MHz, CD_3CN) δ/ppm: 7.62 (s, 1H), 7.49 (s, 2H), 7.42 (d, *J* = 5.3 Hz, 1H), 7.36 – 7.29 (m, 2H), 7.07 (d, *J* = 3.9 Hz, 1H), 7.02 (d, *J* = 4.6 Hz, 1H), 6.90 (d, *J* = 3.9 Hz, 1H), 6.51 (s, 1H), 1.50 (s, 6H), 1.40 (s, 18H). ^{19}F NMR (565 MHz, CD_3CN) δ/ppm: -141.98 (d, *J* = 16.8 Hz), -142.26 (dd, *J* = 22.2, 5.9 Hz), -156.59 (t, *J* = 19.9 Hz), -157.06 (t, *J* = 19.3 Hz), -164.16 – -164.32 (m), -165.00 (t, *J* = 18.0 Hz). HR-LIFDI-MS $[M]^+$ m/z: calc for $C_{48}H_{37}N_4F_{10}Cl$, 894.2547; found, 894.2549.

2.6 Preparation of M(DMBil) (M = Zn, Cu)

2.6.1 10,10-Dimethyl-5,15-dipentflurophenylbiladiene (DMBil)

To a solution of 5,5-Dimethyl-1,9-bis(pentafluorobenzoyly)-dipyrromethane (281 mg, 0.50 mmol) dissolved in 40 mL of THF and MeOH (3:1) was added 946 mg of $NaBH_4$ (25.0 mmol). The resulting mixture was stirred at room temperature for 2 hrs, following which time, the reaction was quenched with H_2O and extracted with dichloromethane. The organic layer was washed sequentially with H_2O and brine and then dried over Na_2SO_4. The solvent was then removed via rotary evaporation and the resulting residue was dissolved in 200 mL of dichloromethane and combined with $InCl_3$ (15 mg, 68 μmol) and pyrrole (100 μL, 1.44 mmol). The reaction was stirred at room temperature under air for 30 minutes, after which time, 180 mg of DDQ (0.8 mmol) was added to the stirred solution. After stirring the reaction for an additional 5 minutes, 14 mL of triethylamine (100 mmol) was added and the mixture was stirred for an additional 2 hours. Following removal of the solvent under reduced pressure, the crude product was purified by chromatography on silica using a mixture of hexanes and CH_2Cl_2 (2:1) as the eluent to give 160 mg of the title compound in 53% yield. ^{1}H NMR (400 MHz, $CDCl_3$, 25 °C) δ/ppm: 12.43 (s, 2H), 7.18 (s, 2H), 6.63 (d, *J* = 4.6 Hz, 2H), 6.57 (d, *J* = 4.6 Hz, 2H), 6.29 – 6.24 (m, 2H), 6.22 (d, *J* = 3.7 Hz, 2H), 1.81 (s, 6H). ^{13}C NMR (101 MHz, $CDCl_3$, 25 °C) δ/ppm: 177.54, 148.12, 145.05 (d, *J* = 248 Hz), 141.65 (d, *J* = 254 Hz), 137.62 (d, *J* = 252 Hz), 133.09, 132.34, 130.52, 124.68, 122.07, 120.31, 112.69, 111.75, 42.23, 26.07. HR-LIFDI-MS $[M]^+$ m/z: calc for $C_{33}H_{18}N_4F_{10}$, 660.1372; found, 660.1372. Anal. Calc for $C_{33}H_{18}F_{10}N_4$: C, 60.01; H, 2.75; N, 8.48. Found: C, 59.60; H, 3.04; N, 8.17.

2.6.2 Zn(DMBil)

To a solution of 100 mg of DMBil (0.15 mmol) dissolved in 30 mL of DMF was added 665 mg of $Zn(OAc)_2$ (3 mmol). This solution was heated at 60 °C for 4 hours. Following removal of solvent under reduced pressure, the resulting residue was dissolved in CH_2Cl_2 and filtered through celite. The filtrate was washed with brine, dried over Na_2SO_4 the solvent was removed by rotary evaporation. Recrystallization of the resulting material delivered 76 mg of the title compound in 70% yield. ^{1}H NMR (400 MHz, $CDCl_3$, 25 °C) δ/ppm: 7.12 (s, 2H), 6.58 (d, *J* = 4.1 Hz, 2H), 6.54 (d, *J* = 3.9 Hz, 2H), 6.50 (d, *J* = 4.2 Hz, 2H), 6.38 (d, *J* = 3.7 Hz, 2H), 1.74 (s, 6H). ^{13}C NMR (101 MHz, $CDCl_3$) δ/ppm: 170.62, 150.79, 144.92 (d, *J* = 248.7 Hz), 141.29 (d, *J* = 248.7 Hz), 141.14, 139.82, 137.27 (d, *J* = 253.1 Hz), 131.51, 129.30, 128.22, 116.97, 116.61, 39.50, 30.26. HR-EI-MS $[M]^+$ m/z: calc for $C_{33}H_{16}N_4F_{10}Zn$, 722.05064; found, 722.04983. Anal. Calc for $C_{33}H_{16}F_{10}N_4Zn$ + ½ CH_3OH + DMF: C, 54.42; H, 2.89; N, 8.05. Found: C, 54.23; H, 2.57; N, 7.94.

2.6.3 Cu(DMBil)

To a solution of 100 mg of DMBil (0.15 mmol) dissolved in 40 mL of CH_3CN was added 45 mg of $Cu(OAc)_2$ (0.225 mmol). This solution was heated to 60 °C for 4 hours. Following removal of solvent under reduced pressure the crude material was purified by chromatography on silica using hexane and CH_2Cl_2 (2:1) as the eluent to give 100 mg of the title compound in 92% yield. HR-ESI-MS $[M+H]^+$ m/z: calc for $C_{33}H_{17}N_4F_{10}Cu$, 722.0590; found, 722.0595. Anal. Calc for $C_{33}H_{16}F_{10}N_4Cu$: C, 54.89; H, 2.23; N, 7.76. Found: C, 54.90; H, 2.01; N, 7.48.

2.7 X-ray Crystallography

2.7.1 X-ray Structure Solution and Refinement

2.7.1.1 3H(Phl^F)

Crystals of 3H(Phl^F) were mounted using viscous oil onto a plastic mesh and cooled to the data collection temperature. Data were collected on a Bruker-AXS APEX 2 DUO CCD diffractometer with Cu Kα radiation (λ = 1.54178 Å) collimated and monochromated using Goebel mirrors. Unit cell parameters were obtained from 60 data frames, 0.5° ω, from three different sections of the Ewald sphere. The systematic absences in the diffraction data are consistent with P21 and P21/m, but the observed occupancy and the absence of a molecular mirror are consistent with the noncentrosymmetric P21 which yielded chemically reasonable and computationally stable results of refinement. The absolute structure parameter was refined to 0.06(2), indicating that the true hand of the data has been determined and an inspection of the packing diagram suggests no overlooked symmetry. The data set was treated with numerical absorption corrections based on indexed crystal faces and dimensions (Apex2 software suite, Madison, WI, 2005). The structure was solved using direct methods and refined with full-matrix, least-squares procedures on F2.[87] A disordered, cocrystallized molecule of chloroform solvent was located in the asymmetric unit with a refined site occupancy ratio of 56/44. The 1,1 and 1,2 interatomic distances were restrained to be equal in the disordered solvent molecule and treated with rigid bond restraints and with the carbon atom disordered contributions constrained to have equal anisotropic parameters. All non-hydrogen atoms were refined with anisotropic displacement parameters. All hydrogen atoms were treated as idealized contributions. Atomic scattering factors are contained in the SHELXTL 6.12 program library. The

CIFs are available from the Cambridge Crystallographic Data Centre under the depository number CCDC 878742.

2.7.1.2 3H(Phl^{CF3})

Crystals of 3H(Phl^{CF3}) were mounted using viscous oil onto a plastic mesh and cooled to the data collection temperature. Data were collected on a Bruker-AXS APEX CCD diffractometer with graphite-monochromated Mo−Kα radiation (λ = 0.71073 Å). Unit cell parameters were obtained from 36 data frames, 0.3° ω, from three different sections of the Ewald sphere. The systematic absences in the diffraction data are uniquely consistent with the reported space group. The data sets were treated with absorption corrections based on redundant multiscan data. The structures were solved using direct methods and refined with full-matrix, least-squares procedures on F2. All nonhydrogen atoms were refined with anisotropic displacement parameters. All hydrogen atoms were treated as idealized contributions. Structure factors are contained in the SHELXTL 6.12 program library. The CIF has been deposited under CCDC 960702.

2.7.1.3 Au($Phl^{3,5\text{-}tBu}$), Au($Phl^{3,5\text{-}tBu}Cl_2$), and Au($Phl^{3,5\text{-}tBu}Cl$)

X-ray structural analysis for Au($Phl^{3,5\text{-}tBu}$), Au($Phl^{3,5\text{-}tBu}Cl_2$), and Au($Phl^{3,5\text{-}tBu}Cl$): Crystals were mounted using viscous oil onto a plastic mesh and cooled to the data collection temperature. Data were collected on a Bruker-AXS APEX CCD diffractometer with graphite-monochromated Mo-Kα radiation (λ=0.71073 Å). Unit cell parameters were obtained from 36 data frames, 0.3º ω, from

three different sections of the Ewald sphere. The systematic absences in the diffraction data are uniquely consistent with the reported space group, *Pbca*, for Au(Phl$^{3,5\text{-}tBu}$Cl$_2$) and Au(Phl$^{3,5\text{-}tBu}$Cl). No symmetry higher than triclinic was observed for Au(Phl$^{3,5\text{-}tBu}$) and solution in the centrosymmetric space group option, *P*-1, yielded chemically reasonable and computationally stable results of refinement. The data-sets were treated with multi-scan absorption (Apex2 software suite, Madison, WI, 2005). The structures were solved using direct methods and refined with full-matrix, least-squares procedures on F^2. Two symmetry unique but chemically identical compound molecules were located in the asymmetric unit of Au(Phl$^{3,5\text{-}tBu}$) each located at inversion. The chlorine atom in Au(Phl$^{3,5\text{-}tBu}$Cl) is located disordered with a hydrogen atom at two chemically equivalent molecular positions with refined site occupancy of 77/23. The two perfluorophenyl and a chloropyrrole ring are found disordered in two positions in Au(Phl$^{3,5\text{-}tBu}$Cl$_2$) with refined site occupancies of 66/34, 53/47 and 55/45. The disordered rings in Au(Phl$^{3,5\text{-}tBu}$Cl$_2$) were treated with geometrical restraints, rigid-bond constraints and equal atomic displacement restraints for chemically equivalent atoms. All atoms were treated with rigid-bond constraints in Au(Phl$^{3,5\text{-}tBu}$) and Au(Phl$^{3,5\text{-}tBu}$Cl). All three structures displayed solvent accessible voids and were treated with Platon Squeeze to model the bulk solvent effects.[88] In Au(Phl$^{3,5\text{-}tBu}$Cl$_2$), the void space analysis was consistent with three molecules of water per gold complex and the formula was amended as the trihydrate. No chemically reasonable solvent could be assigned for Au(Phl$^{3,5\text{-}tBu}$) and Au(Phl$^{3,5\text{-}tBu}$Cl) although the crystals were grown in a mixture of methanol, chloroform, acetonitrile and dichloromethane. All non-hydrogen atoms were refined with anisotropic displacement parameters. All

hydrogen atoms were treated as idealized contributions. Scattering factors are contained in the SHELXTL 6.12 program library.[87]

2.7.1.4 DMBil, Zn(DMBil), and Cu(DMBil)

X-ray structural analysis for DMBil, Zn(DMBil), and Cu(DMBil): Crystals were mounted using viscous oil onto a plastic mesh and cooled to the data collection temperature. Data were collected on a Bruker-AXS APEX 2 DUO CCD diffractometer with Cu Kα radiation (λ = 1.54178 Å) collimated and monochromated using Goebel mirrors or with Mo Kα radiation (λ = 0.71073 Å) monochromated with a graphite crystal. Unit cell parameters were obtained from 36 data frames, 0.5° ω, from three different sections of the Ewald sphere. No higher symmetry than triclinic was observed for DMBil and Zn(DMBil). Solution in P-1 yielded chemically reasonable and computationally stable results of refinement. The unit cell parameters and systematic absences in the diffraction data for Cu(DMBil) are consistent with Pna21 and Pnam [Pnma]. However, the observed occupancy and the absence of either a molecular mirror or a molecular inversion center are consistent exclusively with the noncentrosymmetric space group, Pna21. The absolute structure parameter in Cu(DMBil) refined to nil, indicating the true hand of the data, has been determined. An inspection of the packing diagram suggests no overlooked symmetry. The data sets were treated with numerical absorption corrections based on indexed crystal faces and dimensions (Apex2 software suite, Madison, WI, 2005). The structures were solved using direct methods and refined with full-matrix, least-squares procedures on F2.[87] A P−M pseudohelical isomer pair, with a 3.4 Å π−π offset parallel intermolecular distance, and severely disordered solvent molecules (two ethanol molecules and two

chloroform molecules, one of which was located near the origin at halfoccupancy) were located in the asymmetric unit of Zn(DMBil). Co-crystallized, non-coordinated, solvent molecules in Zn(DMBil) were treated as diffused diffraction contributions using Squeeze.[88] All non-hydrogen atoms were refined with anisotropic displacement parameters. The amine hydrogen atoms in Zn(DMBil) were assigned to be consistent with surrounding non-hydrogen atom geometry and allowed to refine in position but with the anisotropic parameter restrained to 1.2 Ueq of the attached nitrogen atom. All other hydrogen atoms were treated as idealized contributions. Atomic scattering factors are contained in the SHELXTL 6.12 program library. The CIF has been deposited under CCDC 996931-996933.

2.7.2 Crystallographic Information Tables.

Table 2.1 Crystallographic data for 3H(Phl^{F}) and 3H(Phl^{CF3}).

Formula	3H(Phl^{F})	3H(Phl^{CF3})
Fw	957.94	884.62
Crystal System	Monoclinic	monoclinic
Space Group	P2(1)	P2(1)/n
a	15.2855(5) Å	15.454(8) Å
b	9.2994(3) Å	9.361(5) Å
c	15.5097(5) Å	27.907(14) Å
α	90°	90°
β	116.573(2) °	96.211(8) °
γ	90°	90°
V	1971.75(11) A^3	4014(3) A^3
Z	2	4
Temp	100(2) K	200(2) K
D_{calcd}	1.613 Mg/m^3	1.464 Mg/m^3
2θ range	6.38 to 141.06°	3.16 to 50.00°
μ (Mo Kα)	3.102 mm^{-1}	0.139 mm^{-1}
Reflections	31054	41796
Unique	6920	7066
R (int)	0.0476	0.0527
R_1	0.0556	0.0826
wR_2	0.1526	0.2360

Table 2.2 Crystallographic data for Au(Phl$^{3,5\text{-tBu}}$), Au(Phl$^{3,5\text{-tBu}}$Cl) and Au(Phl$^{3,5\text{-tBu}}$Cl$_2$)

Formula	**Au(Phl$^{3,5\text{-tBu}}$)**	**Au(Phl$^{3,5\text{-tBu}}$Cl)**	**Au(Phl$^{3,5\text{-tBu}}$Cl$_2$)**
Fw	973.49	1089.21	1177.70
Crystal System	Triclinic	Orthorhombic	Orthorhombic
Space Group	P-1	Pbca	Pbca
a	15.193(2)	9.8754(6)	10.022(2) Å
b	15.444(2)	29.2900(18)	30.046(6) Å
c	20.177(3)	32.955(2)	33.028(7) Å
α	96.997(2)°	90°	90°
β	91.030(2)°	90°	90°
γ	102.613(2)°	90°	90°
V	4580.8(10) A^3	9543.8(10) A^3	9945(3) A^3
Z	8	8	8
Temp	200(2) K	200(2) K	200(2) K
D_{calcd}	2.823 Mg/m^3	1.516 Mg/m^3	1.573 Mg/m^3
2θ range	2.036 to 55.162°	3.718 to 55.132°	4.934 to 55.77°
μ (Mo Kα)	6.615 mm^{-1}	3.214 mm^{-1}	3.147 mm^{-1}
Reflections	57485	120975	220315
Unique	21018	10995	11819
R (int)	0.0591	0.0494	0.0472
R_1	0.1124	0.0627	0.0731
wR_2	0.2624	0.1380	0.1812

Table 2.3 Crystallographic data for DMBil, Zn(DMBil) and Cu(DMBil).

Formula	DMBil	Zn(DMBil)	Cu(DMBil)
Fw	660.5	877.48	722.04
Crystal System	Triclinic	Triclinic	Orthorombic
Space Group	P-1	P-1	Pna2 (1)
a	9.762(2) Å	9.4815(3) Å	10.4143(3) Å
b	9.830(2) Å	14.8240(5) Å	19.3742(5) Å
c	15.163(4) Å	26.6756(10) Å	14.0031(4) Å
α	100.996(4)°	104.113(2)°	90°
β	93.420(4)°	98.585(2)°	90°
γ	96.674(4)°	91.238(2)°	90°
V	1414.7(6) A^3	3588.9(2) A^3	2825.39(14) A^3
Z	2	4	4
Temp	200(2) K	200(2) K	200(2) K
D_{calcd}	1.551 Mg/m^3	1.624 Mg/m^3	1.697 Mg/m^3
2θ range	4.22 to 54.92°	6.92 to 147.66°	7.78 to 136.46°
μ (Mo Kα)	0.139 mm^{-1}	3.326 mm^{-1}	1.999 mm^{-1}
Relections	18532	116052	15559
Unique	6426	13894	4610
R (int)	0.0235	0.0683	0.0182
R_1	0.0396	0.0424	0.237
wR_2	0.0924	0.1080	0.0659

Chapter 3

SYNTHESIS, PHOTOPHYSICS, ELECTROCHEMISTRY AND FLUORIDE BINDING OF A SUITE OF PHLORIN DERIVATIVES

3.1 Introduction

Phlorins have remained mostly unexplored compared to the other tetrapyrrole macrocycle systems. The phlorin was first described over five decades ago through the work of Woodard in 1962.[89] The introduction of the sp^3-hybridized *meso*-carbon causes a disruption in the conjugation within the macrocycle, leading to the phlorin being non-aromatic, unlike the homologous porphyrin, shown in Figure 3.1. Although similar in size to porphyrins, the phlorin maintain three N-H protons, while porphyrins contain two N-H protons. The presence of three N-H protons allows for the phlorin to be a trianionic ligand scaffold similar to that of the well-studied corrole macrocycle.

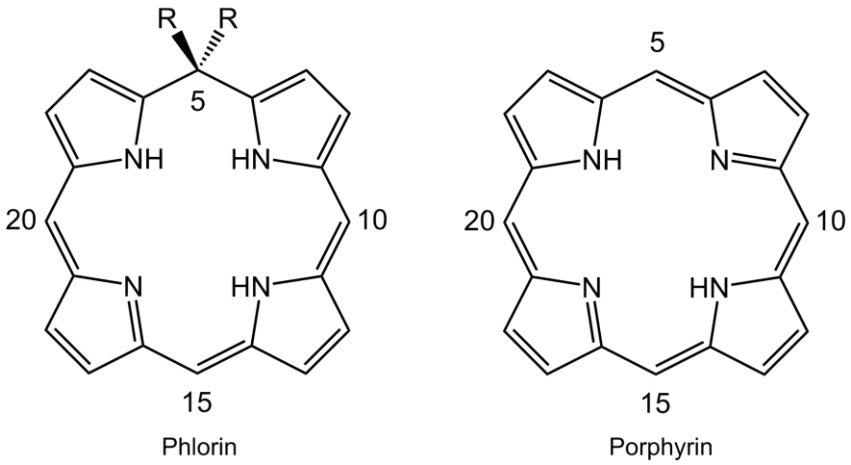

Figure 3.1 Phlorin and porphyrin macrocycles with common number scheme

Phlorin macrocycles have long been thought of as relatively unstable porphyrinoids, as those containing a hydrogen atom bound to the sp^3 *meso*-carbon are easily oxidized to the aromatic porphyrin. A ring opening oxidation product has also been observed for phlorins with substituted sp^3 centers preventing the formation of the porphyrin.[90] There are only a few reported examples of free base phlorins that were isolated with differing tethering groups such as phenyl or alkene groups are attached to the center nitrogen atoms, as shown in Figure 3.2.[91-99] This perturbs not only the geometry of the phlorin but also influences the electronic structure as well. The use of the tether groups makes the phlorins more stable; however this severally limits the chemistry available to the phlorin such as the insertion of a transition metal to the core. Woodward demonstrated that the introduction of steric bulk at the β-pyrrole position of the phlorin improved the stability of the macrocycle.[89] This was further demonstrated by the improvement of the stability through the incorporation of mesityl substituents at the sp^2 hybridized *meso*-carbon positions, although these phlorins were still prone to auto oxidation by air.[100]

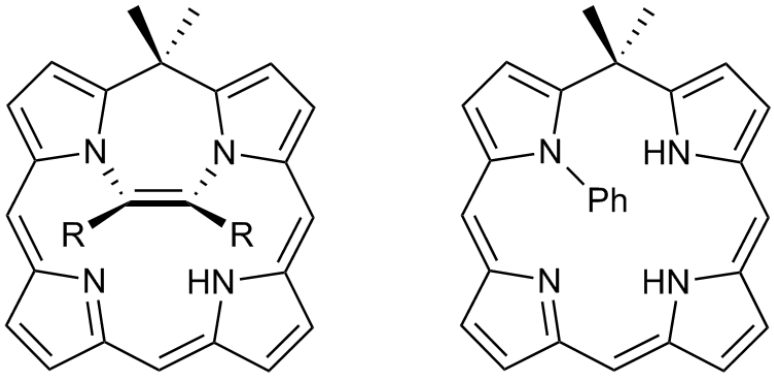

Figure 3.2 Phlorin derivatives with representative tethering groups bound to the core nitrogen atoms.

The increase in steric bulk around the phlorin resulted in improved stability; however the use of electron withdrawing groups at the sp^2 hybridized *meso*-carbon positions dramatically increased the overall tolerance of the phlorin to both light and oxygen.[101]

Although phlorins with improved stability had been developed, the synthetic routes available to obtain them were relatively limited. The general synthetic strategy used for phlorin synthesis was the nucleophilic attack at the sp^2 hybridized *meso*-carbons of porphyrin precursor as shown in Scheme 3.1.[99,102] This approach is limited by the inherently low yields due to the mixtures of products produced by this route and by the difficult separation of these products.

Shortly prior to our undertaking this project, Geier and co-workers reported a synthetic route that afforded the free base phlorins in good yield and did not require the tethering of groups to the core nitrogen atoms.[101] This created an opportunity to be able to synthesize several different free base phlorin derivatives in good yields. This chapter describes the initial studies that were undertaken by our lab to further reveal the interesting properties of the phlorin macrocycle including the synthesis of several novel phlorin macrocycles and a thorough study of their photophysical and redox properties.

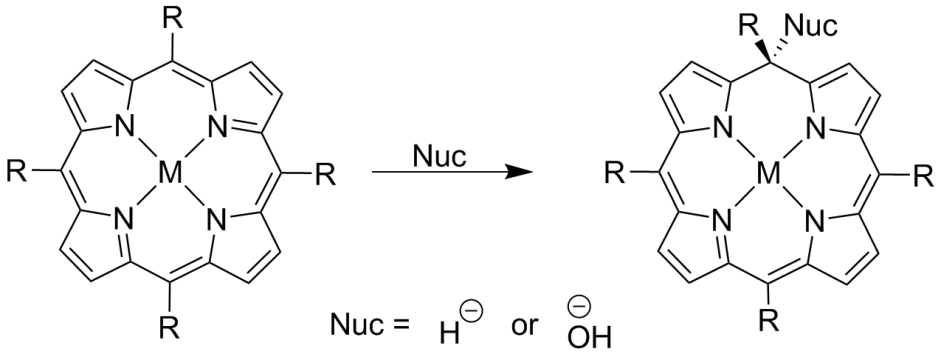

Scheme 3.1 Typical synthesis of phlorin macrocycles through the nucleophilic attack at the *meso*-carbon of porphyrin precursor.

3.2 3H(Phl^{R}) (R = F, OMe, NO_2, Mes, CO_2tBu)

Several phlorin macrocycles were developed through varying of the substitution at the 15-*meso*-position. The influence of this synthetic alteration on the electronic structure of the phlorin was probed through the incorporation of both electron donating groups such as mesityl, and 2,6-bismethoxyphenyl as well as electron withdrawing groups such as pentafluorophenyl, 4-nitrophenyl and 4-*tert*-butoxyphenyl.

3.2.1 Synthesis 3H(Phl^{R})

The synthesis of the family of phlorins began with the adaptation of a modular synthesis that was previously reported, Scheme 3.2.[101] The synthesis began with the condensation of pyrrole with acetone in the presence of TFA to afford the 5,5'-dimethyldipyrromethane (1).[63] EtMgBr was used to deprotonate the 5,5'-dimethyldipyrromethane derivative followed by the addition of pentafluorobenzoyl chloride to give the diacylated dipyrromethane derivative (2). This was a useful building block for the development of a suite of phlorin derivatives. The diacylated dipyrromethane was reduced using $NaBH_4$ in THF and methanol (3:1) to give the dicarbinol product, which was condensed with of several 5-aryldipyrromethane derivatives (3-7) with the presence of TFA. Following oxidation using DDQ and purification by chromatography, five phlorin derivatives were synthesized in good yield (35-50 %), with the mesityl (3H(Phl^{Mes})), 2,6-bismethoxyphenyl (3H(Phl^{OMe})), 4-nitrophenyl (3H(Phl^{NO2})), and 4-*tert*-butoxyphenyl (3H(Phl^{CO2tBu})) not having been previously reported. With the development of the synthesis of these derivatives we were able to greatly expand the library of the known phlorins reported in the literature.

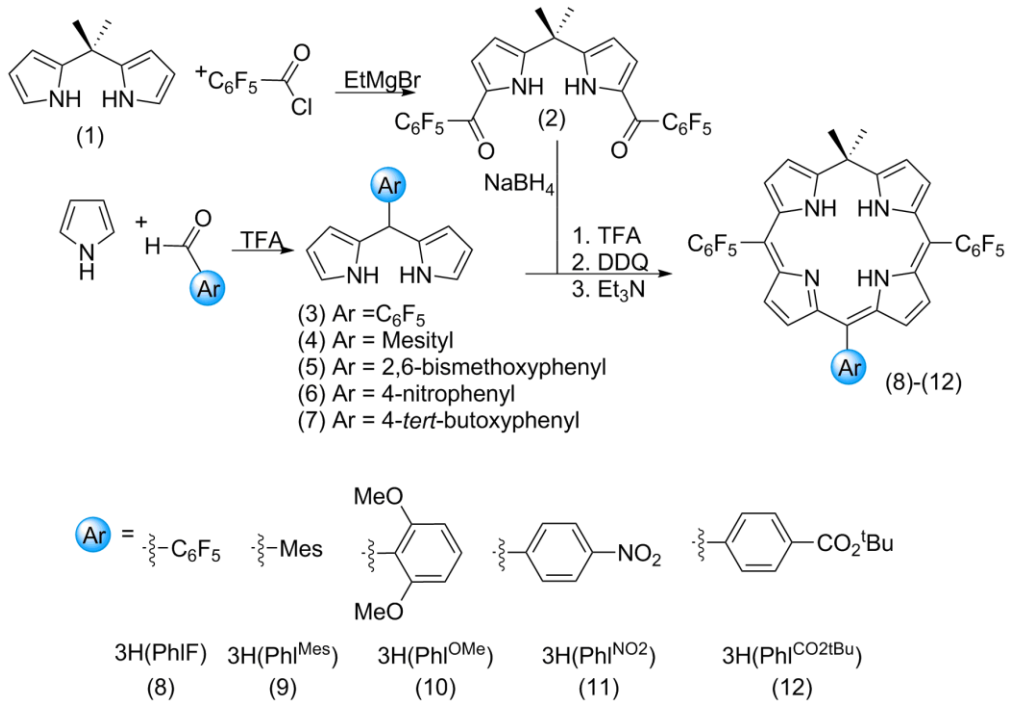

Scheme 3.2 Synthesis of a suite of phlorins with differing substitution at the 15-*meso*-position.

3.2.2 Molecular Structure of 3H(Phl^{F})

The solid state structure of 3H(Phl^{F}) shown in Figure 3.3, was the first crystallographically studied free base phlorin bearing a 5,5'-dimethyl substitution pattern at the sp^3-hybridized center. The introduction of the sp^3-hybridized center causes the phlorin macrocycle to lack the aromaticity that is seen in typical porphyrins. This is demonstrated by the puckering of the reduced half of the macrocycle containing the sp^3-center. This puckering can be seen through the approximation of a plane using the dipyrromethane unit that is directly across from the sp^3-center, where the reduced dipyrromethane group is approximately 0.6 Å out of plane.

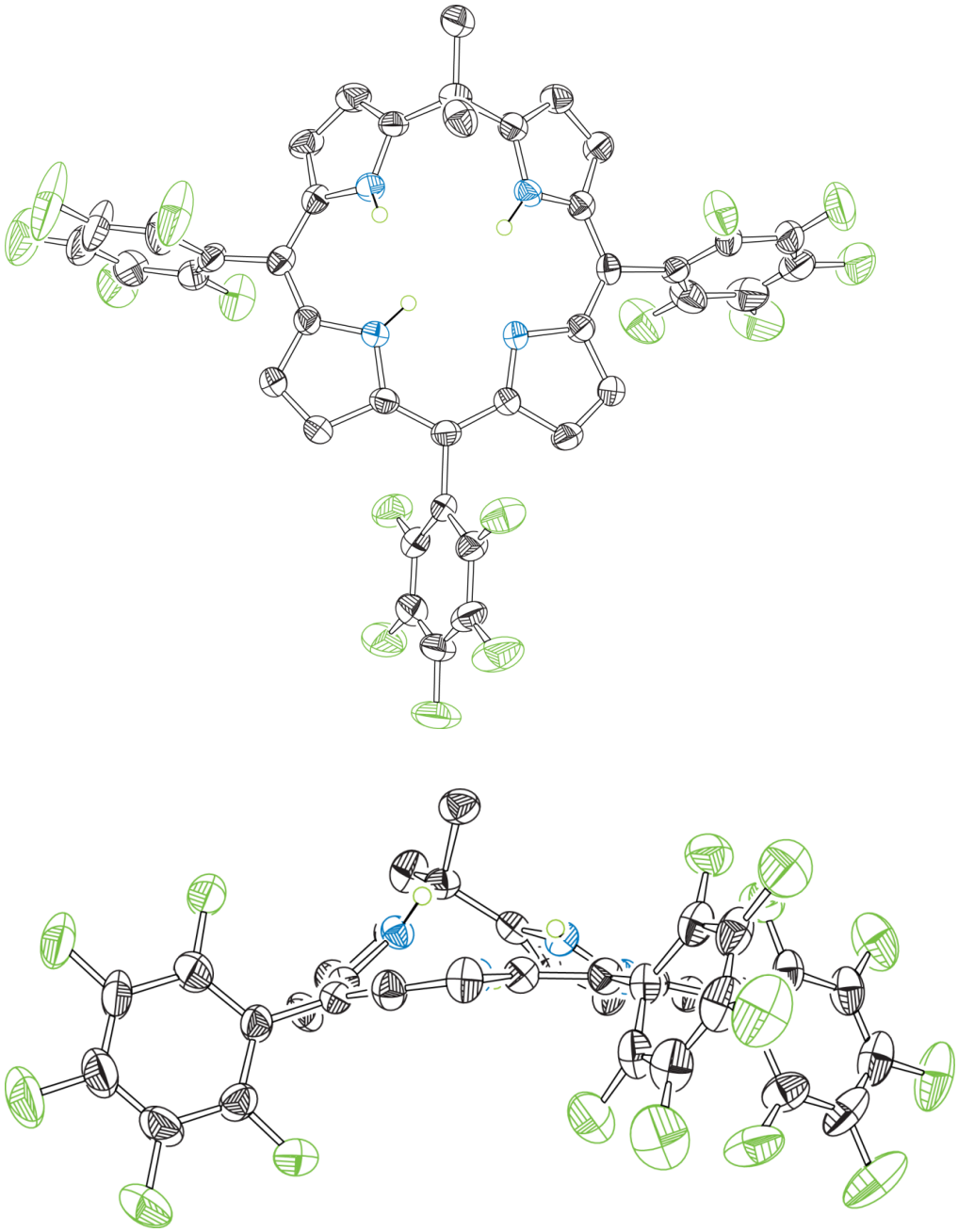

Figure 3.3 Solid state crystal structure of 3H(Phl^{F}) displaying a view from (a) the top of the macrocycle and (b) side on. A molecule of co-crystallized $CHCl_3$ and all non-nitrogen bound hydrogens were omitted for clarity. Thermal ellipsoids are shown at 50% probability.

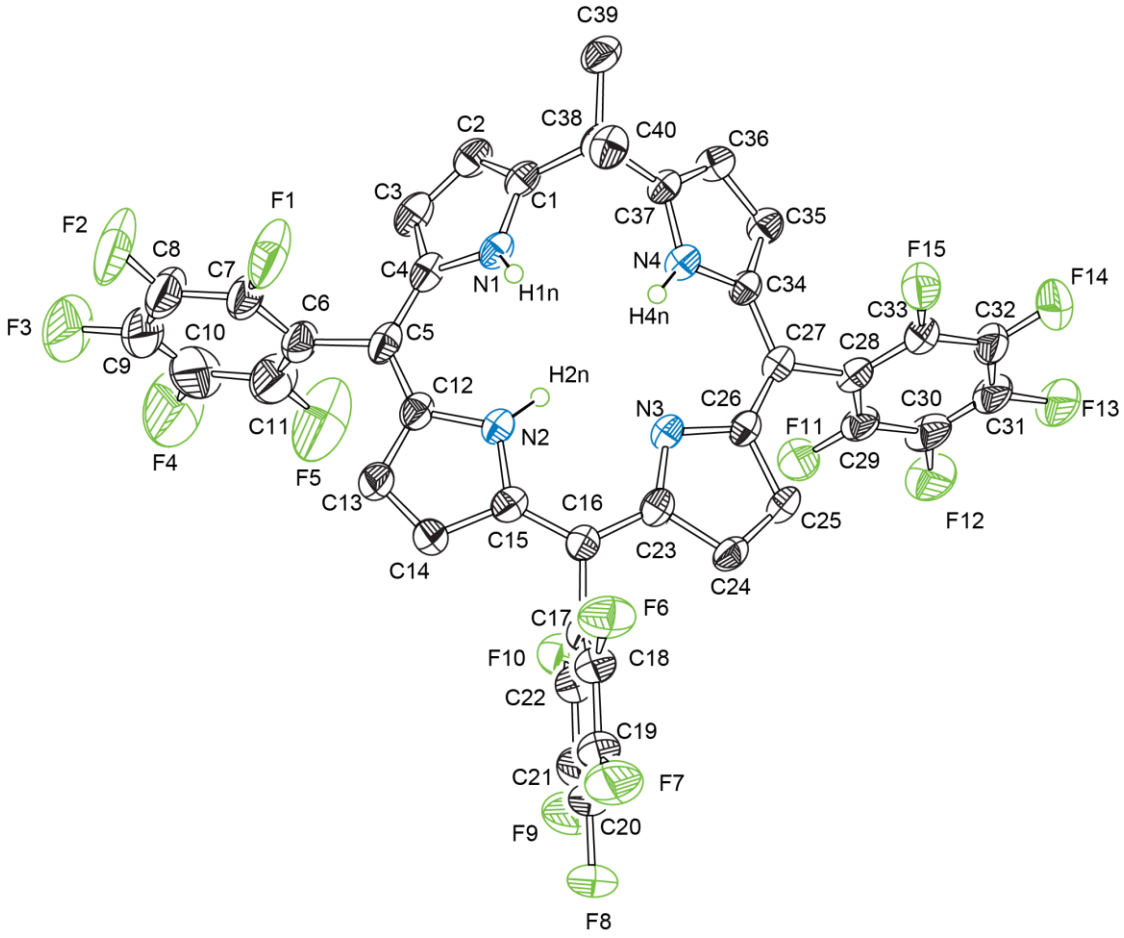

Figure 3.4 Numbered crystal structure of 3H(Phl^{F}) with all non-nitrogen bound hydrogens omitted for clarity and thermal ellipsoids are shown at 50% probability.

Table 3.1 Selected bond lengths and angles for 3H(Phl^{F}).

Atoms	Bond Lengths (Å)	Atoms	Bond Angles (°)
C(1)–C(38)	1.502(5)	**C(1)–C(38)–C(37)**	106.3(3)
C(38)–C(37)	1.518(5)	**C(12)–C(4)–C(5)**	125.7(3)
C(38)–C(39)	1.527(5)	**C(15)–C(16)–C(23)**	124.7(3)
C(38)–C(40)	1.521(6)	**C(26)–C(27)–C(34)**	125.9(3)

3.2.3 Proton NMR Spectroscopy of 3H(Phl^F)

The lack of aromaticity that is implied by the solid state structure shown in Figure 3.3 is also supported by the ^{1}H NMR spectrum of 3H(Phl^F). The N-H protons displayed a broad resonance at 5.15 ppm, as shown in Figure 3.5. This is very different compared to the N-H protons of typical aromatic porphyrins, which are strongly shielded and display resonances far upfield (-3.7 ppm for 2H(TPP))[103] because of the magnetically induced diatropic ring currents.[104-106] The break in aromaticity created by the introduction of the sp^3-*meso*-carbon causes the N-H protons to be more deshielded than the analogous 2H(TpFPP) that has a N-H resonance at -2.9 ppm.

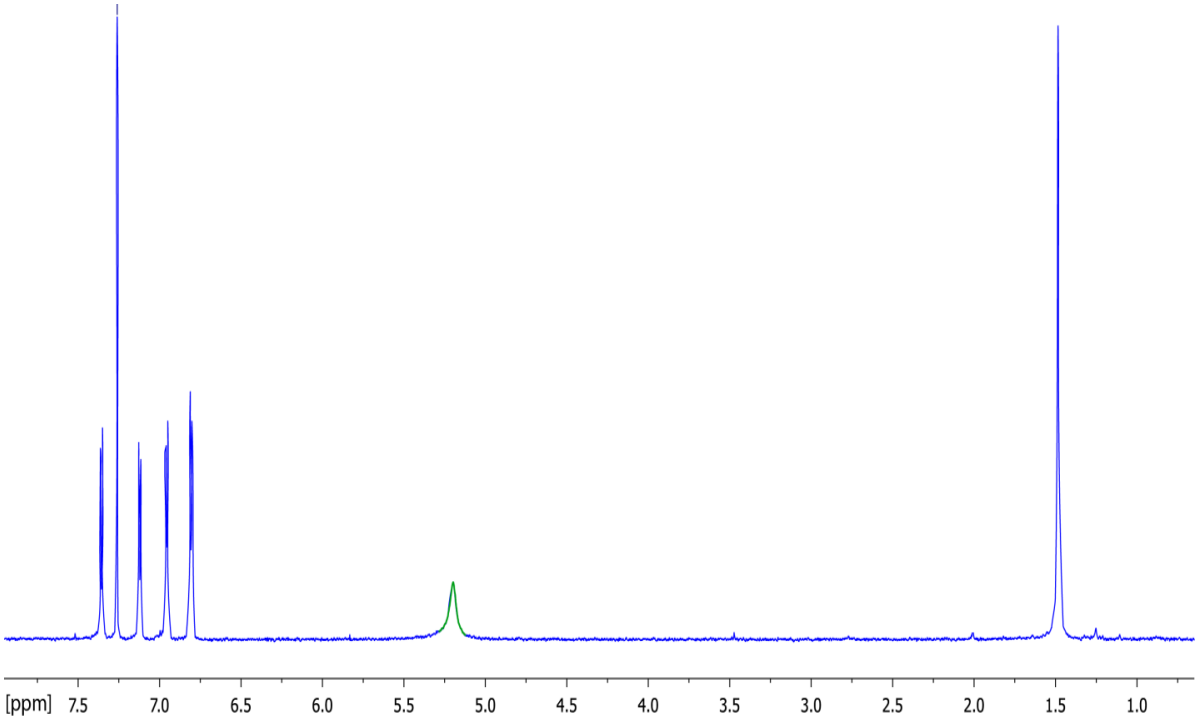

Figure 3.5 ^{1}H NMR spectrum of 3H(Phl^F) in $CDCl_3$. The N-H proton resonance at 5.15 ppm is highlighted in green.

3.2.4 Photophysics of Phlorin Macrocycles

After the completion of the synthesis of the phlorin derivatives, a systematic study of the photophysics of the macrocycles was performed. Solutions for each of the different phlorin derivatives were emerald green in color. All phlorins studied were found to be good chromophores with absorption profile ranging from 300 to 750 nm, with maxima near 415-435 nm and 655-670 nm. Variation of the substituent at the 15-*meso*-position of the phlorins did not significantly alter the shape of the absorption profile, as shown in Figure 3.6. There were subtle changes in the extinction coefficients of with the electron donating derivatives such as the 3H(Phl^{Mes}) and 3H(Phl^{OMe}) having slightly stronger absorption in both the Soret and Q band regions than the 3H(Phl^{F}). Although modifying the 15-*meso*-position of the phlorin did not have a great influence on the absorbance, the phlorin macrocycle is markedly different than the more studied tetrapyrrole macrocycles such as the porphyrin and corrole, as shown in Figure 3.7. The analogous fluorinated porphyrin displays narrow absorption in the Soret region (375-425 nm) and Q band (490-530 nm and 570-600 nm) regions. The phlorin macrocycle, having the sp^3 center is markedly different, as absorptions are broadened and shifted to longer wavelengths. The absorption profile of the fluorinated corrole is similar to that of the phlorin with absorption in the Soret region (375-450 nm) and Q band regions (535-630 nm); however, the phlorin has much broader absorption at the low energy wavelengths.

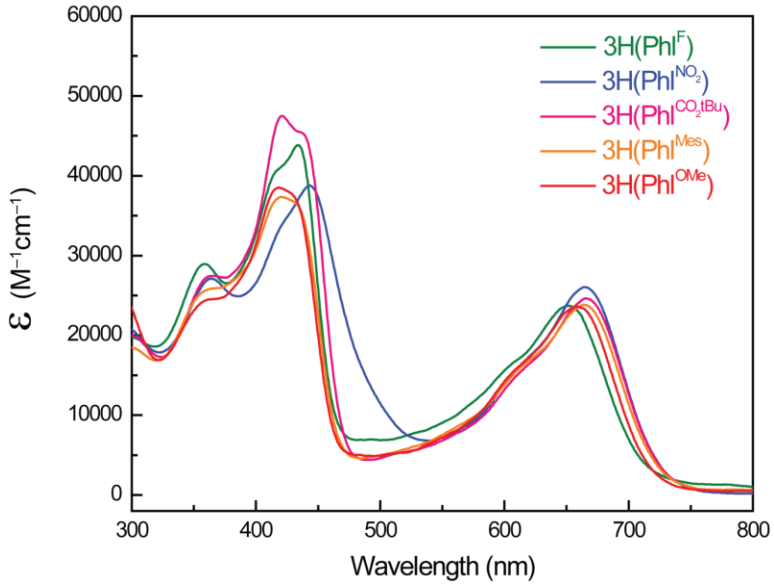

Figure 3.6 UV-vis absorption spectra for each of the 3H(Phl^{R}) derivatives studied in CH_2Cl_2.

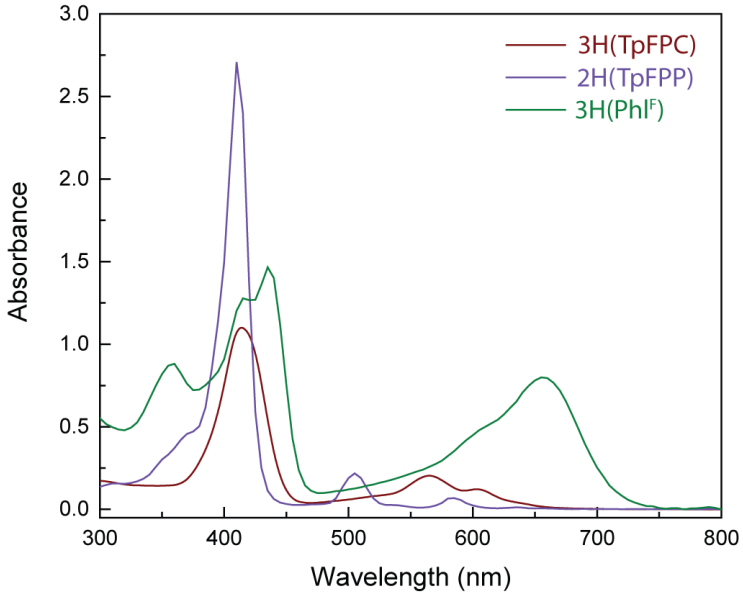

Figure 3.7 UV-vis absorption spectra overlay of a 50 μM solution of 3H(Phl^{F}) (green) and 10 μM solutions of 2H(TpFPP) (purple) and 3H(TpFPC) (maroon) in THF.

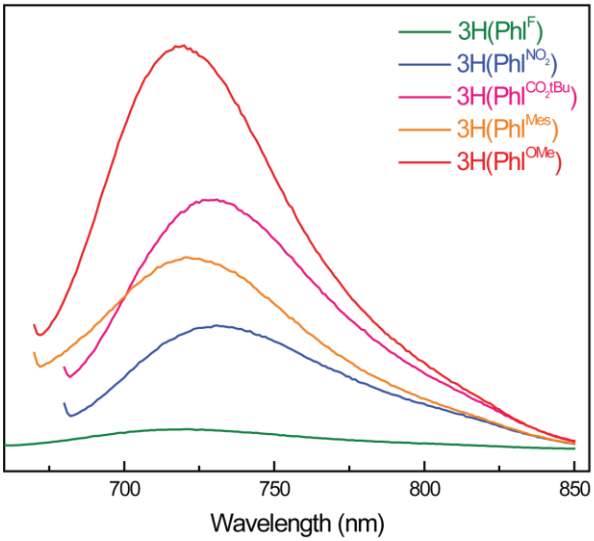

Figure 3.8 Fluorescence spectra for each of the 3H(Phl^{R}) macrocycles in deaerated CH_2Cl_2 (10 μM). Samples were excited at λ = 650 nm.

The phlorin macrocycles also displayed broad emission spectrum that were mirror images of the Q band absorption, with maxima centered between 720 and 732 nm when excited in the Q band region, shown in Figure 3.8. The quantum yield (Φ_{Fl}) revealed a general trend among the phlorins differing substitution at the 15-*meso*-position. The most electron withdrawing group, the pentafluorophenyl on the 3H(Phl^{F}) had the lowest quantum yield of 5.3 X 10^{-4} and the highest quantum yield of 17.6 X 10^{-4} was obtained by the electron donating methoxy substituted group (3H(Phl^{OMe})). The fluorescence lifetimes (τ_{Fl}) follow a similar trend with the electron deficient 3H(Phl^{F}) having the lowest emission lifetime of 37 ps and the more electron rich 3H(Phl^{OMe}) displaying the longest emission lifetime of 101 ps. The results are summarized in Table 3.2 for all phlorin derivatives, where the observable trend of the

more electron rich phlorins exhibit the larger quantum yields and longer lived excited state lifetimes.

Table 3.2 Summary of the photophysics of phlorin derivatives.

	absorption		emission		
	Soret λ_{max}, nm (ε, $cm^{-1}M^{-1}$)	Q band λ_{max}, nm (ε, $cm^{-1}M^{-1}$)	λ_{em} nm	τ_{Fl} ps	Φ_{Fl}
3H(Phl^{F})	435 (29300)	655 (16000)	722	37	5.34×10^{-4}
3H(Phl^{NO2})	445 (30800)	670 (21200)	732	37	6.35×10^{-4}
3H(Phl^{CO2tBu})	435 (45100)	665 (24700)	731	66	9.96×10^{-4}
3H(Phl^{Mes})	420 (36400)	669 (24200)	721	58	9.65×10^{-4}
3H(Phl^{OMe})	415 (38400)	665 (24900)	720	101	17.6×10^{-4}

3.2.5 Electrochemical Characterization

The redox properties of the phlorin macrocycles were probed using cyclic voltammetry (CV) and differential pulse voltammetry (DPV). Such experiments employed solutions containing 1 mM of a phlorin derivative in CH_2Cl_2, 0.1 M $TBAPF_6$, and an internal reference of decamethylferrocene. Cyclic voltammetry experiments began with the initial study of the 3H(Phl^{F}) derivative and the analogous perfluoronated porphyrin and corrole macrocycles with the results shown in Figure 3.9. The CVs recorded for 3H(Phl^{F}) displayed interesting redox properties with three quasi reversible oxidations at $E_{1/2}$ = 0.75 V, 0.99 V, 1.26 V and two largely irreversible reductions at $E_{1/2}$ = –0.93 V, –1.43 V. This is rather different compared to 2H(TpFPP) which displays two reversible oxidations at $E_{1/2}$ = 1.61 V, 1.82 and two reversible reductions at $E_{1/2}$ = –0.76 V, –1.17 V. The oxidations of 3H(Phl^{F}) are at a

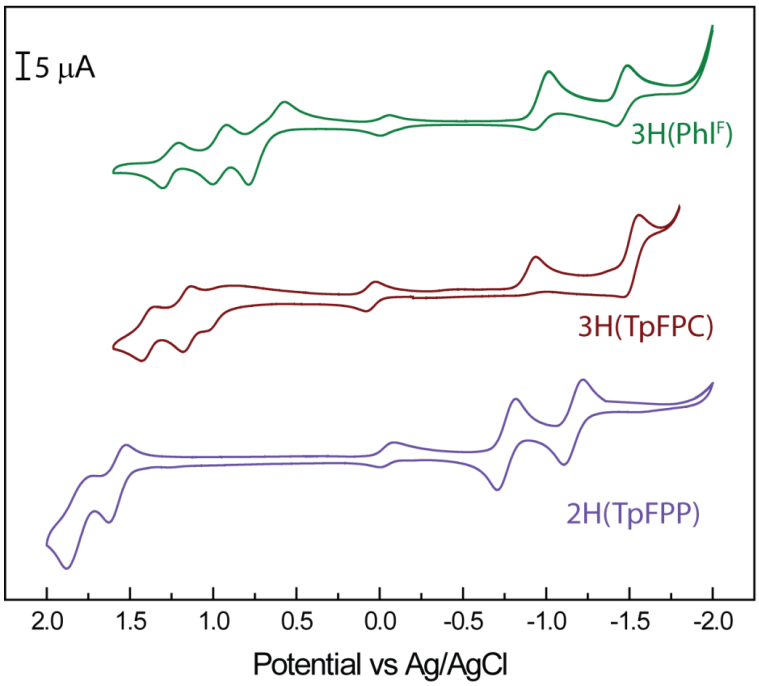

Figure 3.9 Cyclic voltammograms for 3H(Phl^F) (green), 3H(TpFPC) (maroon) and 2H(TpFPP) (purple) recorded in CH_2Cl_2 containing 0.1 M $TBAPF_6$, 1.0 mM analyte and an internal reference decamethylferrocene (Fc*). A standard three electrode set up was used with a glassy carbon disk electrode (working electrode) and platinum wire (auxiliary) and a silver wire as a quasi-reference. Scan rate of 50 mV/s.

much more accessible potentials with all three of the phlorin oxidations occurring before the first oxidation of the porphyrin. The redox chemistry of 3H(TpFPC) is similar to that of the phlorin displaying three oxidations at $E_{1/2}$ = 0.87 V, 1.16 V, 1.39 V and two irreversible reductions at $E_{1/2}$ = –0.97 V, and –1.51 V. The potentials for the corrole oxidations are slightly higher positive potentials (~12-16 mV) than that of the phlorin. The reductions for the corrole occur at very similar potentials, however the reductions are more reversible in the phlorin.

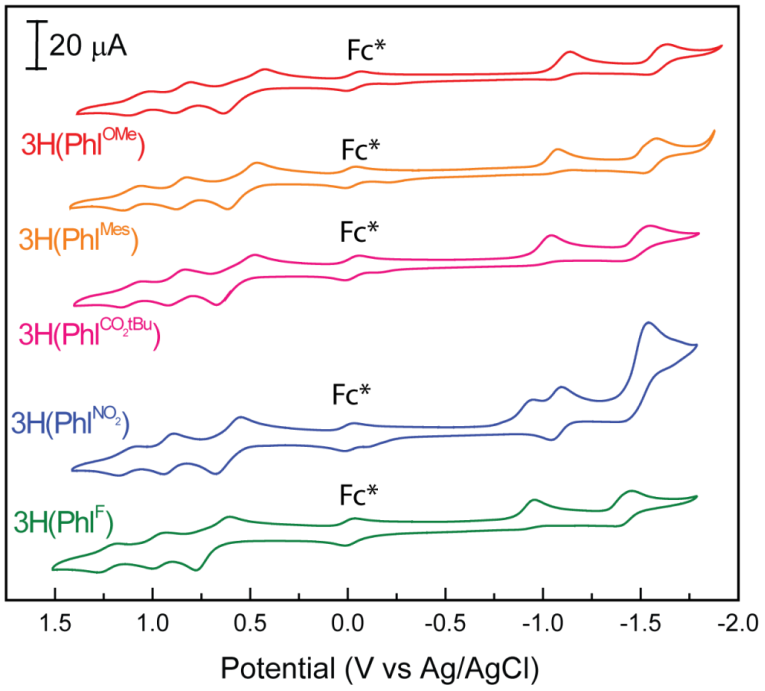

Figure 3.10 Cyclic voltammograms of the each of the phlorin derivatives (1.0 mM) studied in CH_2Cl_2 containing 0.1 M $TBAPF_6$ and an internal reference decamethylferrocene (Fc*). A standard three electrode set up was used with a glassy carbon disk electrode (working electrode) and platinum wire (auxiliary) and a silver wire as a quasi-reference. Scan rate of 50 mV/s.

The substitution at the 15-*meso*-position on the phlorin has a strong influence on the redox potentials, as shown in Figure 3.10. The inclusion of electron donating groups such as the methoxy groups on 3H(Phl^{OMe}) or the mesityl group 3H(Phl^{Mes}), significantly attenuates the redox events. The first oxidation occurs at $E_{1/2}$ = 0.6 V, and 0.61 V for 3H(Phl^{OMe}) and 3H(Phl^{Mes}), respectively, which is 150 mV less positive than that observed for the electron withdrawing perfluoronated phenyl derivative (3H(Phl^{F})). These oxidations occur at potentials that are not typical for many

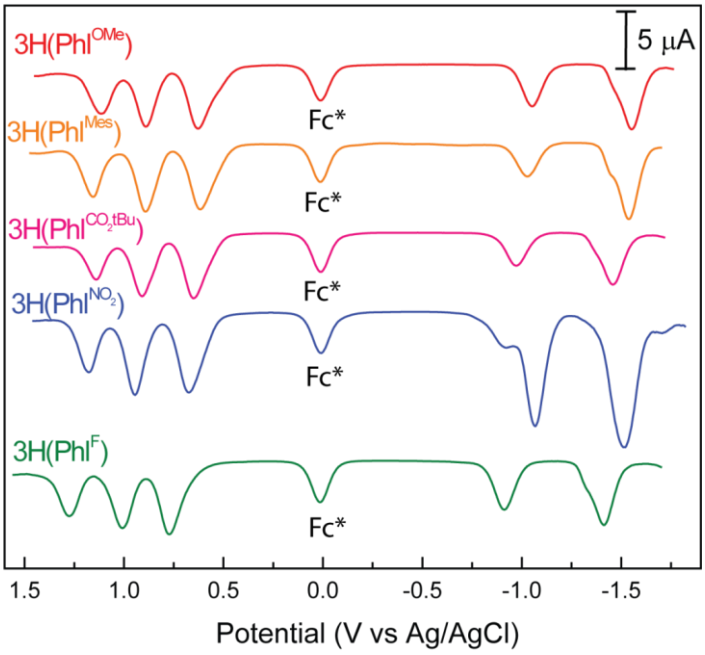

Figure 3.11 Differential pulse voltammograms of the each of the phlorin derivatives (1.0 mM) studied in CH_2Cl_2 containing 0.1 M $TBAPF_6$ and an internal reference decamethylferrocene (Fc*).

porphyrinoid systems (*vide supra*), with the first oxidation of 3H(Phl^{OMe}) occurring at a potential that is nearly 1 V less positive than the first oxidation of 2H(TpFPP). The oxidation of the electron rich phlorin derivatives is near the redox potential for a commonly used organometallic complex ferrocene.[107] The substitution at the 15-*meso*-position with electron withdrawing aryl groups like that of the 3H(Phl^{NO2}) and 3H(Phl^{CO2tBu}) modulates the potentials to fall between that observed for the electron poor 3H(Phl^{F}) and electron rich 3H(Phl^{OMe}). All phlorin electrochemistry metrics are compiled in Table 3.3.

The electrochemical HOMO-LUMO gap of the different phlorin derivatives is smaller compared typical porphyrin systems. The HOMO-LUMO gaps for the

phlorins investigated ranged from 1.62 eV to 1.75 eV, as judged from the DPV of each of the phlorin derivatives shown in Figure 3.11, which can be attributed to the low oxidation potentials. These lower values are consistent with the strong absorptions observed in the energies lower than 600 nm. The fluorinated porphyrin (2H(TpFPP)) and corrole (3H(TpFPC)) were found to have a HOMO-LUMO gaps of 2.4 eV and 1.8 eV, respectively, which are significantly higher than that of the phlorins.

Table 3.3 Summary of the redox properties of 2H(TpFPP), 3H(TpFPC) and a suite of phlorin derivatives.

	redox properties					
	$E_{ox}(1)$, V	$E_{ox}(2)$, V	$E_{ox}(3)$, V	$E_{red}(1)$, V	$E_{red}(2)$, V	E_{0-0}, V
2H(TpFPP)	1.61	1.82		–0.76	–1.17	2.40
3H(TpFPC)	0.87	1.16	1.39	–0.97	–1.51	1.80
3H(Phl^{F})	0.75	0.99	1.26	–0.93	–1.43	1.68
3H(Phl^{NO2})	0.65	0.93	1.16	–0.94	–1.53	1.73
3H(Phl^{CO2tBu})	0.63	0.89	1.12	–0.99	–1.49	1.62
3H(Phl^{Mes})	0.60	0.87	1.14	–1.05	–1.56	1.65
3H(Phl^{OMe})	0.61	0.87	1.10	–1.07	–1.58	1.68

3.2.6 Supramolecular Chemistry

The phlorin macrocycles also displayed an interesting supramolecular chemistry with fluoride anions. These systems are able to bind fluoride through hydrogen bonding of the N–H groups from the pyrroles that make up core of the phlorin. This intriguing chemistry has been shown for other calipyrroles[108-110] and

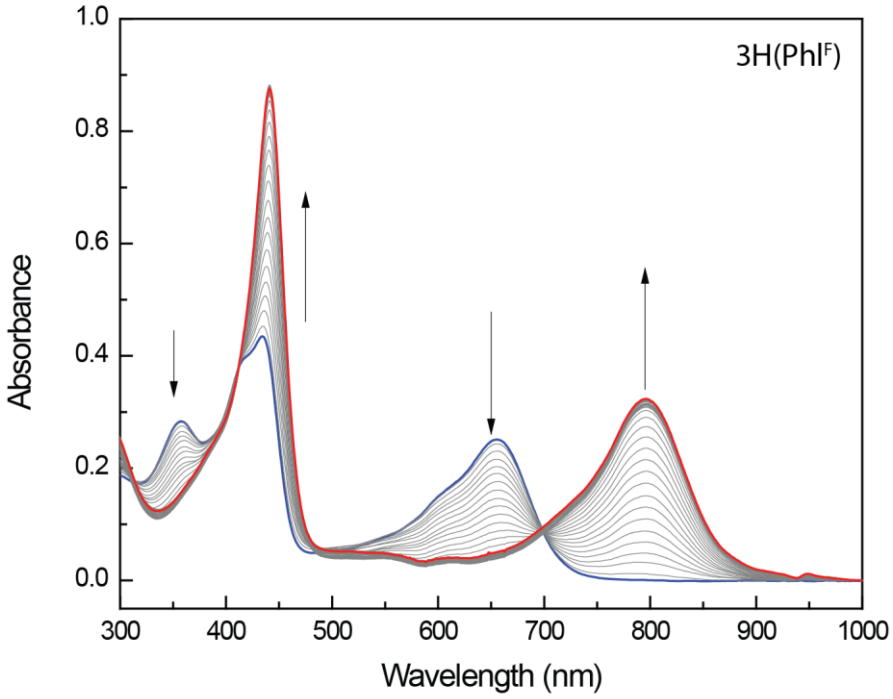

Figure 3.12 UV-vis absorption changes in 3H(Phl^F) with the addition of TBAF solution in CH_2Cl_2.

polypyrrolic systems,[111-114] where anions are able to form hydrogen bonds to the N–H groups.

The investigation of the fluoride binding was performed through titration of *n*-tetrabutylammonium fluoride (TBAF) into a 3H(Phl^F) solution with CH_2Cl_2 as the solvent. The typical emerald green phlorin solution underwent a distinct color change to light brown upon addition of fluoride. This absorbance change was monitored via UV-vis spectroscopy. The addition of fluoride caused dramatic changes in the absorption profile in both the visible and near-IR regions, as shown in Figure 3.12. There is a significant enhancement in molar absorptivity in the Soret region and a substantial shift in the Q band region from ~670 nm to 805 nm.

The binding of fluoride was also confirmed through the use of ^{1}H and ^{19}F NMR, as shown in Figure 3.13 and Figure 3.14, respectively. The ^{1}H NMR spectrum shown for the addition of 10 equivalents of TBAF to a 3H(Phl^{F}) solution in CD_3CN confirms the presence of the N–H protons and that the color change observed through the addition of fluoride is due to a hydrogen bonding interaction rather than deprotonation by the fluoride anion. The ^{19}F NMR spectrum displayed a broadened resonance at –150.21 ppm, which is shifted from unbound TBAF, which displayed a resonance at –115.25 ppm. The bound ^{19}F resonance integrates to approximately 2, when normalizing the integration to the pentafluoro phenyl groups of 3H(Phl^{F}).

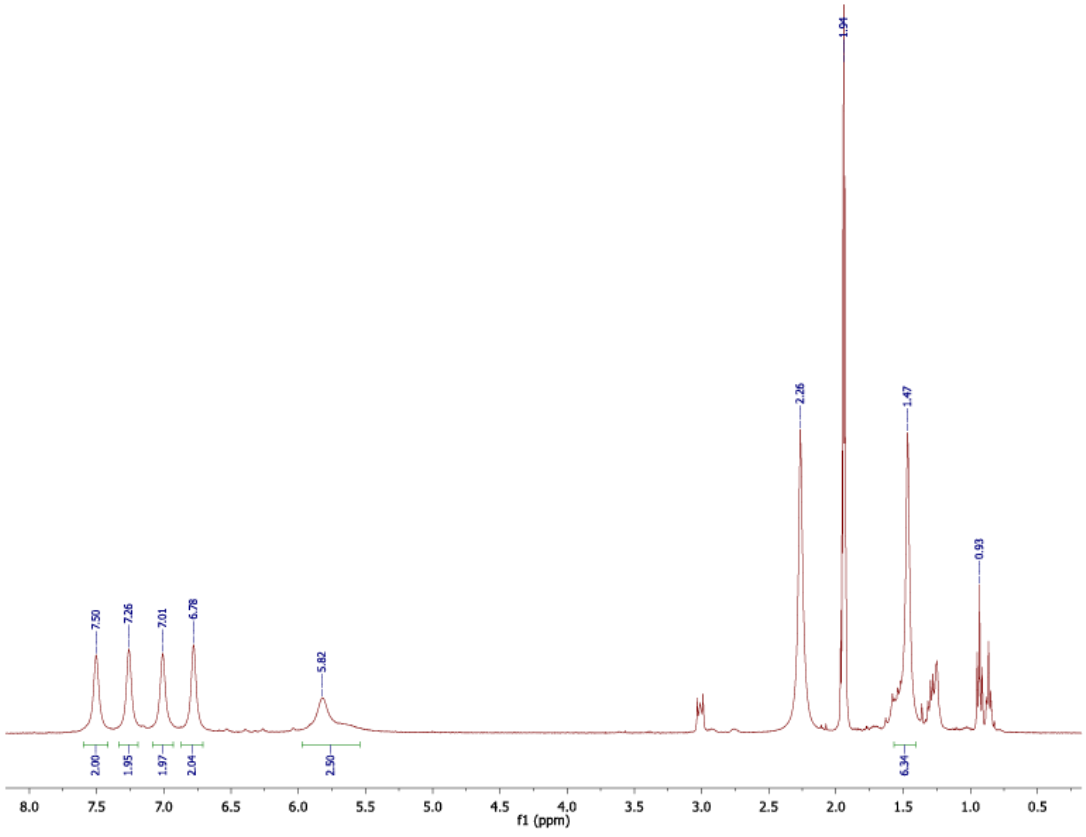

Figure 3.13 ^{1}H NMR spectrum of 3H(Phl^{F}) with 10 equivalents of TBAF in CD_3CN.

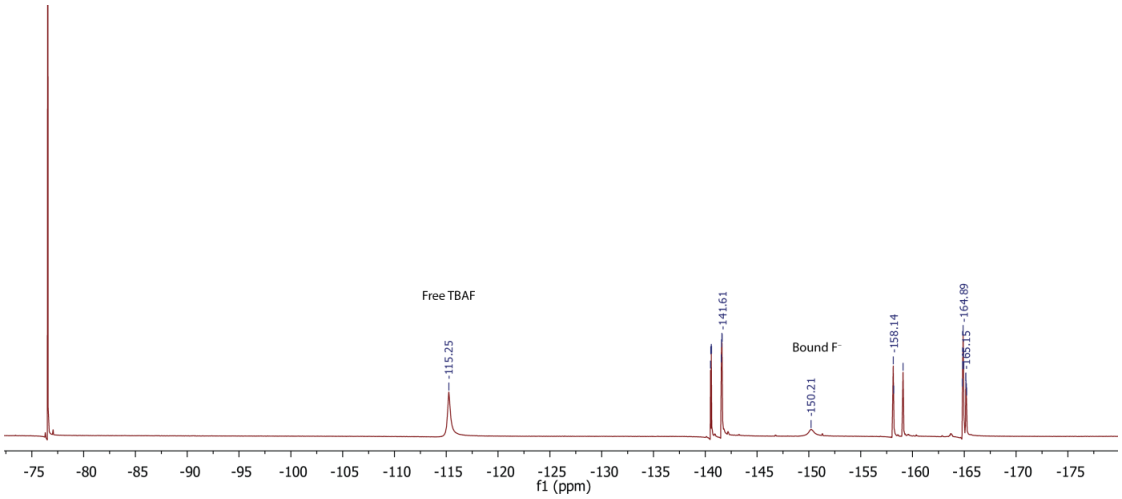

Figure 3.14 ^{19}F NMR spectrum of 3H(Phl^F) with 10 equivalents of TBAF in CD_3CN.

The titration data from the phlorin derivatives all reveal the presence of well anchored isosbestic points throughout the addition of fluoride, as displayed in Figure 3.15. Isosbestic points are typically observed within systems where there is clean conversion to product from the starting material without any appreciable buildup of an intermediate species. This is a typical hallmark of systems that display 1:1 binding, with no intermediates, and suggested that the binding of fluoride to the phlorin macrocycles occurs with 1:1 binding stoichiometry.

The stoichiometry of fluoride binding to the phlorin was investigated further by fitting the TBAF titration data obtained in Figure 3.12 to a Benesi-Hildebrand plot, where the linear plot would allow for the extraction of the binding constant. However, the plotting of the titration data revealed a non-linear fit of the data, as shown in Figure 3.16. This is suggestive of a binding event that was not in a 1:1 binding ratio as expected.

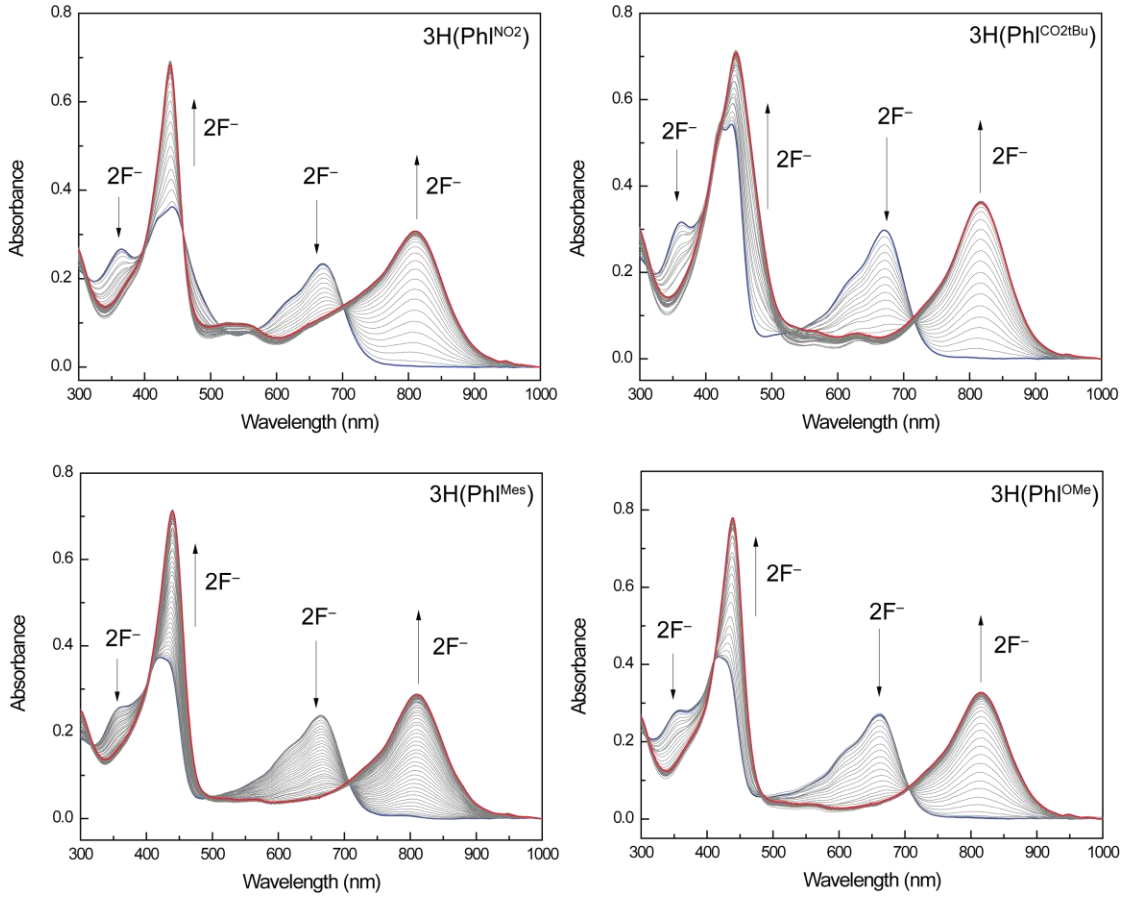

Figure 3.15 UV-vis absorption spectra changes with the addition of TBAF in CH_2Cl_2.

The exact stoichiometry of fluoride binding was revealed through Job plot analysis, as shown in Figure 3.17. These UV-vis experiments are performed by recording the absorption spectra of solutions with varying mole fraction ratios of fluoride and phlorin, while maintaining a total concentration of 10 μM analyte. The Job plots are constructed by plotting the mole fraction of phlorin versus the absorbance maxima near 800 nm. The maximized peak in the Job plot indicates the binding ratio of the guest host. The Job plots for the phlorin macrocycles had a

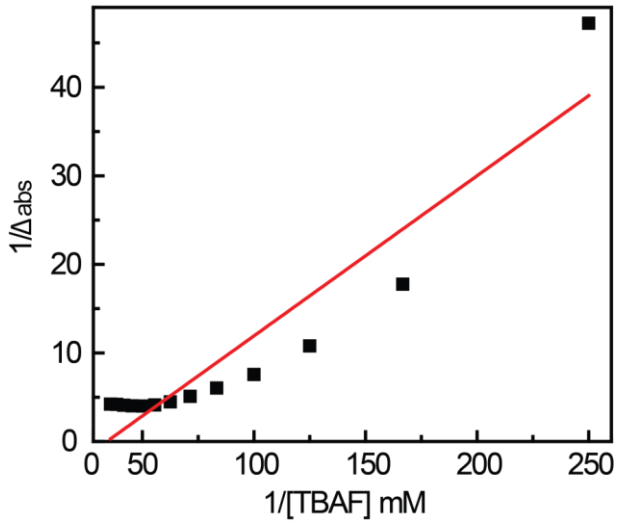

Figure 3.16 Benesi-Hildebrandt plot from the titration data of Figure 3.12. The non-linear fit shows that the binding model is not consistent with formation of a 1:1 supramolecular complex.

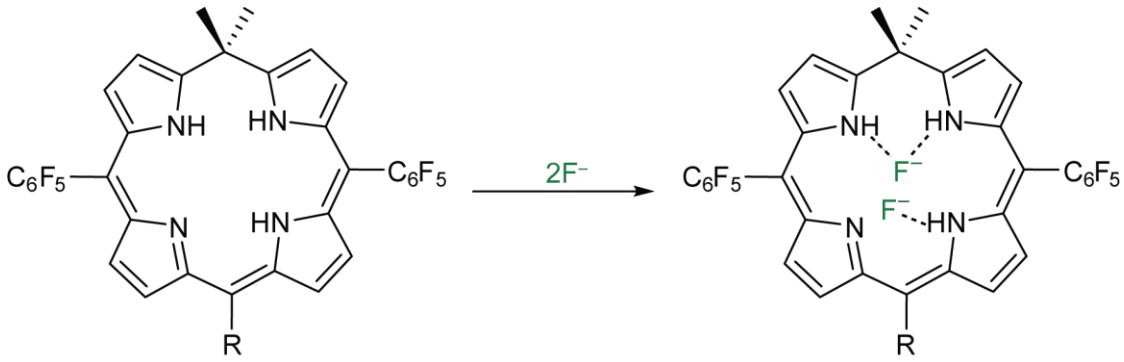

Scheme 3.3 Representation of the binding for the formation of a 2:1 fluoride to phlorin ternary complex.

maximum near 0.3 to 0.35 mole fraction of phlorin, which indicates the formation of a 2:1 fluoride to phlorin ternary complex represented as $3H(Phl^{R})\bullet 2F^{-}$. A Hill analysis was performed on the titration data to investigate the binding events of each of the fluoride anions to the phlorin macrocycle, which supports the 2:1 binding, shown in

Figure 3.18. The linear portion of the Hill analysis allows for the determination of the cooperativity constant (β_2) of the formation of the ternary complex, which relates to the strength of the fluoride binding. The determination of the individual equilibrium constants (K_1 and K_2) was not able to be obtained for the formation of the binary ($3H(Phl^R)\bullet F^-$) or the ternary ($3H(Phl^R)\bullet 2F^-$) complexes. However, the titration data suggests that the equilibrium constant K_2 is much larger than that of K_1 and that the formation of ($3H(Phl^R)\bullet F^-$) may undergo a conformational change upon the binding of the first fluoride anion. This could potentially lead to a destabilization of the singly bound species, leading to cooperativity in binding the second fluoride anion species.

The substitution at the 15-*meso*-position of the phlorin macrocycles has a distinct effect on the binding of fluoride anions, with the results shown in Table 3.4. The cooperative binding or β_2 values for the electron withdrawing groups were significantly higher than those of the electron donating groups, with the highest being observed for the pentafluorophenyl derivative ($3H(Phl^F)$) ($\beta_2 = 1.6 \times 10^{15}$) and the smallest for the mesityl derivative ($3H(Phl^{Mes})$) ($\beta_2 = 4.5 \times 10^8$). This trend can be rationalized by the hard fluoride anion being more attracted to the hydrogens with the most electropositive character, which is the case for the electron withdrawing groups.

The Hill coefficient (η) is a measure of the cooperativity of the binding of the fluoride to the phlorin macrocycles, with larger values of η corresponding to greater levels of cooperativity. The trend within the Hill coefficients (η) follows that of the β_2 values with the more electron deficient phlorins displaying a higher propensity for cooperative binding of fluoride. With the results shown in Table 3.4, the electron

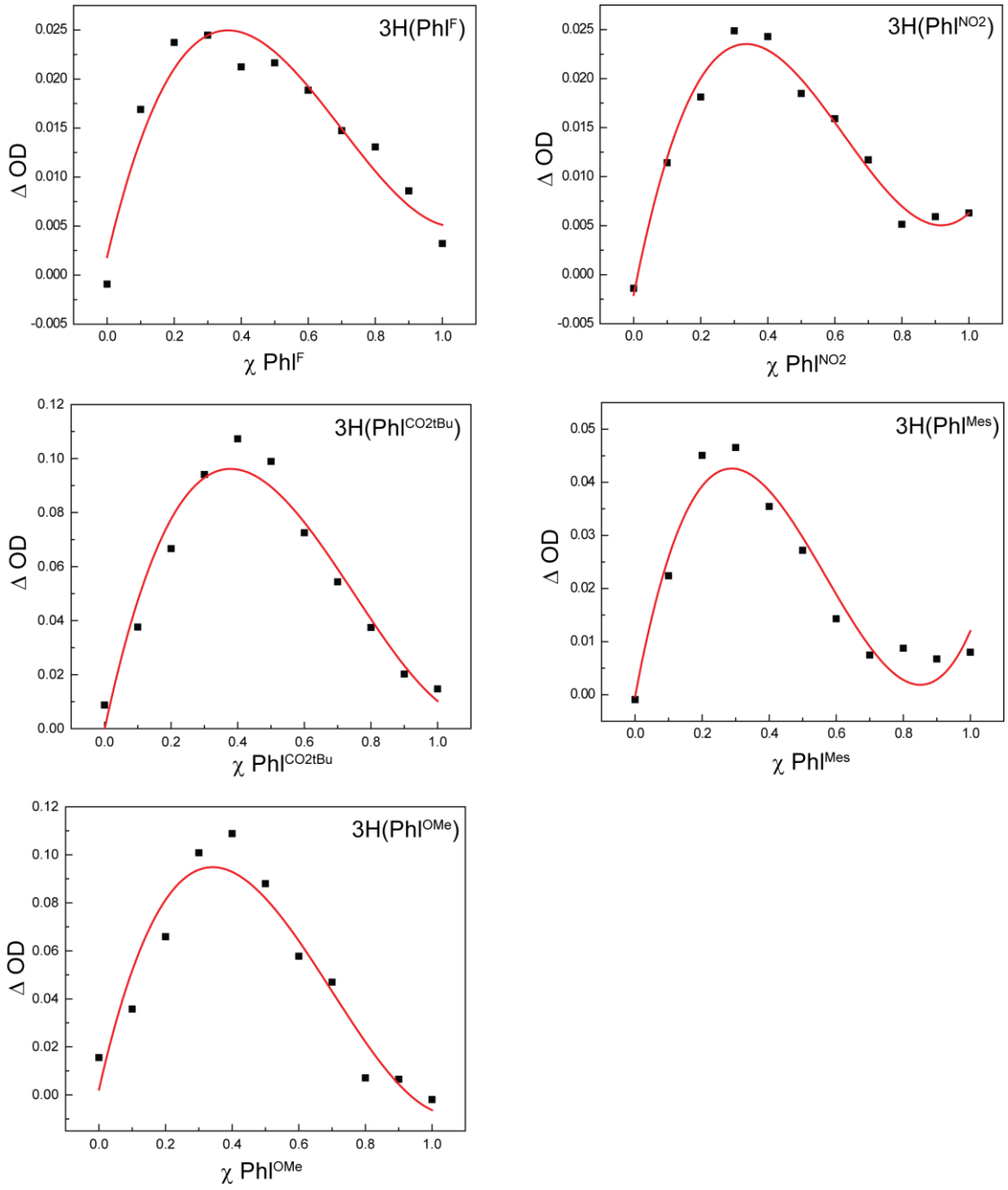

Figure 3.17 Job plots constructed for each of the phlorin derivatives in CH_2Cl_2.

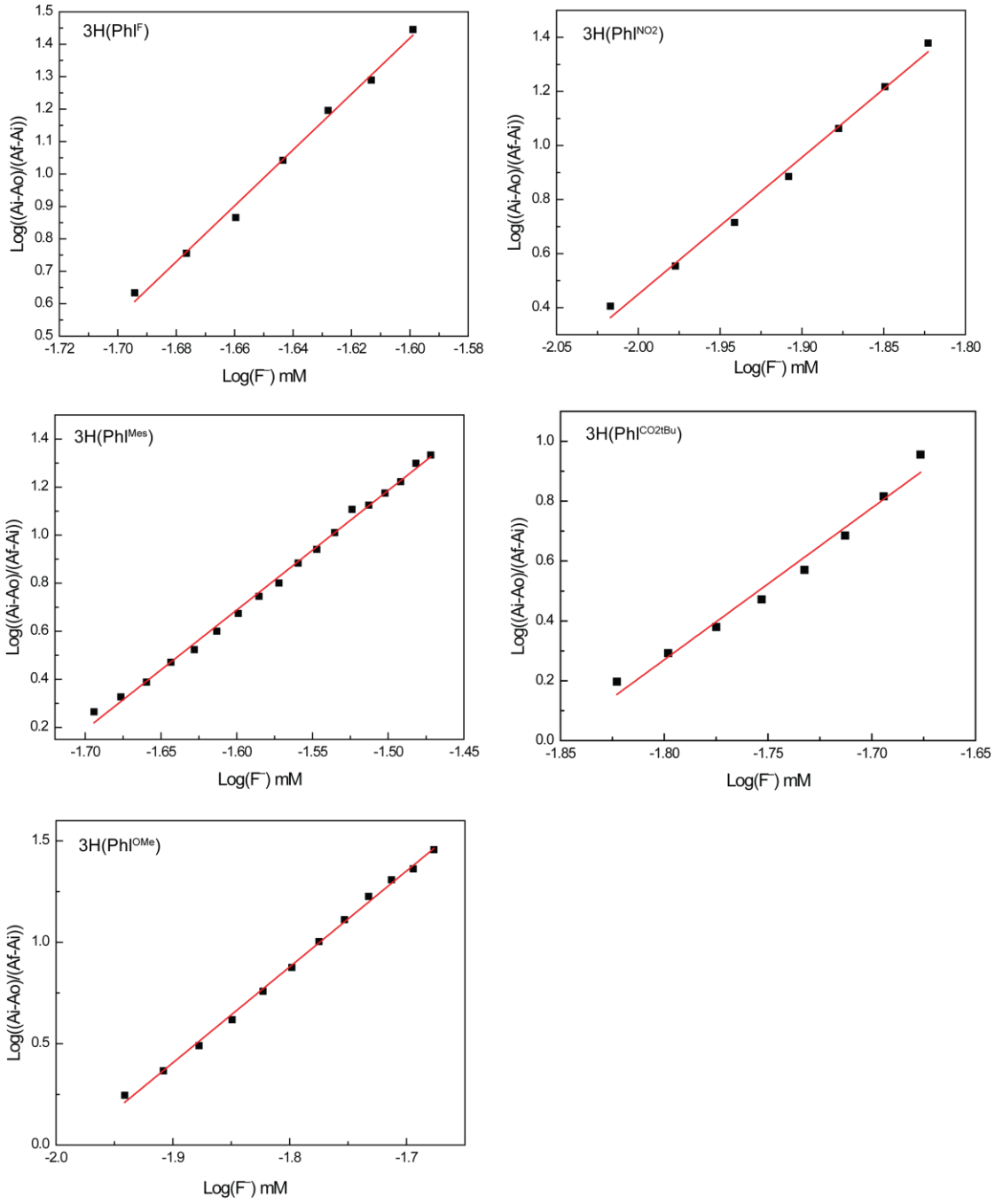

Figure 3.18 Hill plots constructed from the titration data of Figure 3.12 and Figure 3.15 for each of the phlorin derivatives.

	β_2, M^{-2}	Hill Constant (η)
3H(Phl^{F})	1.6 X 10^{15}	8.6
3H(Phl^{NO2})	2.5 X 10^{12}	7.4
3H(Phl^{CO2tBu})	2.4 X 10^{10}	5.1
3H(Phl^{Mes})	4.5 X 10^{8}	5.0
3H(Phl^{OMe})	6.3 X 10^{9}	5.4

Table 3.4 Cooperativity constants (β_2) and Hill coefficients (η) for each of the phlorin derivatives.

donating mesityl derivative (3H(Phl^{Mes})) had the smallest Hill coefficient (η) being determined as 5.0 and the electron withdrawing pentafluorophenyl derivative (3H(Phl^{F})) was determined to have the largest Hill coefficient (η) of 8.6.

The substitution at the 15-*meso*-position of the phlorin macrocycle has been shown to have several influences in the macrocycles properties, such as the supramolecular and redox properties. Figure 3.19 displays the correlation between the Hill coefficient (η) and first oxidation potential of the different phlorins. This near linear relationship shows that the easily oxidized (electron rich) phlorins display less cooperative fluoride binding while the less easily oxidized (electron poor) phlorins display more pronounced cooperativity. Similarly, the same trend can be followed through plotting the log(β_2) against the first oxidation potentials of the phlorins, shown in Figure 3.19. The strength of the binding of fluoride to the phlorins increases with the ability of the group at the 15-*meso*-position to remove electron density from the phlorin core. This general trend shown between the oxidation potentials, strength and cooperativity of

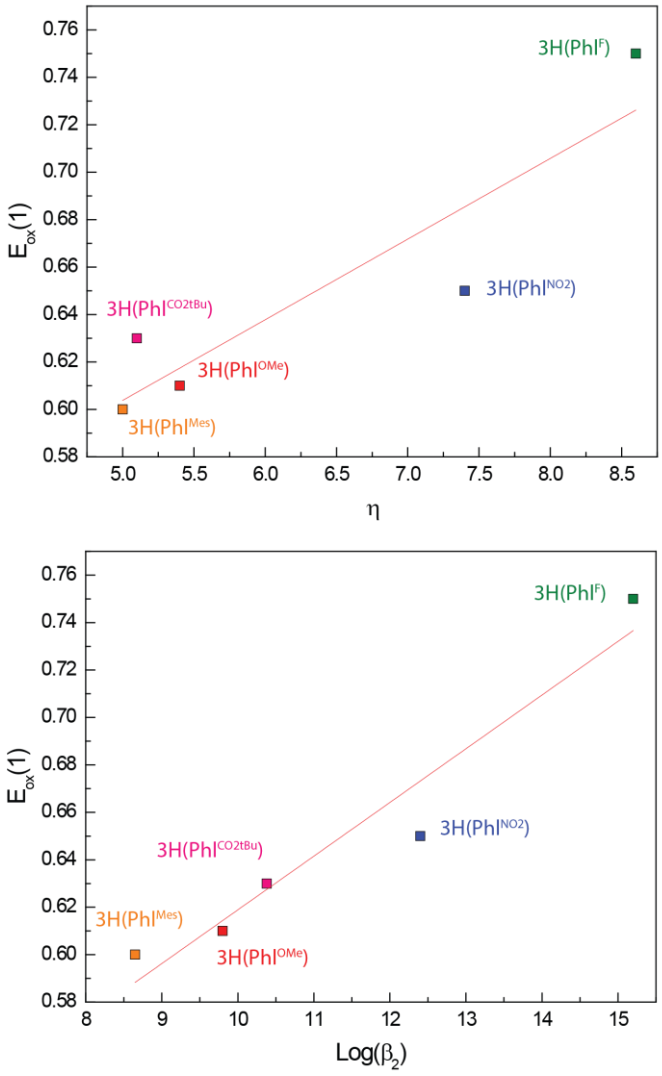

Figure 3.19 The correlation between the first oxidation potential of the phlorins versus Hill Coefficient (η) and the log of fluoride binding strength ($Log(\beta_2)$) .

the fluoride binding is a direct result of the electronic structure of the phlorin macrocycle.

The binding of fluoride anions not only perturbs the electronics of the phlorin macrocycle, as judged by UV-vis spectroscopy but the redox potentials are also influenced. As summarized in Table 3.5, the addition of fluoride has a profound effect on the redox potentials of the phlorins. As shown in the DPVs in Figure 3.20, 3H(Phl^{F}) had a shift to a less positive potential in the first oxidation by 210 mV, while other derivatives displayed shifts of up to 540 mV (3H(Phl^{NO2})) less positive oxidation potentials. Similar trends have been reported with the binding of fluoride to oxoporphyrinogen complexes.[115]

Table 3.5 The changes in the redox potentials for the family of phlorin derivatives, upon binding two equivalents of fluoride.

	$\Delta E_{ox}(1)$, mV	**$\Delta E_{red}(1)$, mV**
3H(Phl^{F})	210	450
3H(Phl^{NO2})	540	420
3H(Phl^{CO2tBu})	470	320
3H(Phl^{Mes})	400	280
3H(Phl^{OMe})	410	260

The reduction potentials of the phlorin derivatives are also influenced through the binding of fluoride, with the potential shifting to more negative values as shown in Figure 3.21. The first reduction potential for 3H(Phl^{F}) is shifted by 450 mV more negative, and the same trend is seen in the other derivatives as well, with shifts ranging from 260 to 450 mV more negative.

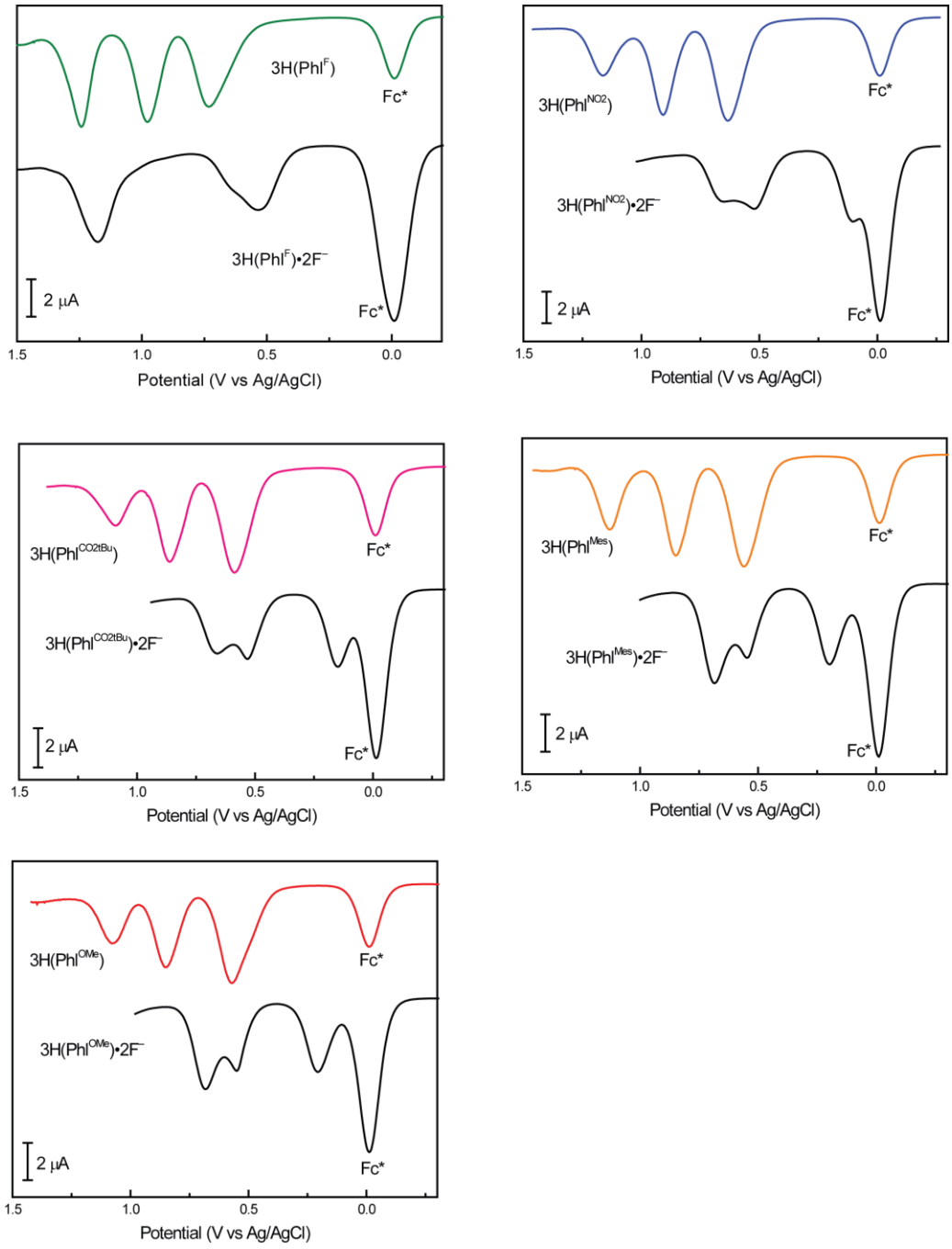

Figure 3.20 DPV traces of the phlorin oxidation waves versus Ag/AgCl for the free base and fluoride bound phlorin derivatives. DPVs were obtained with 1 mM of analyte, 0.1 M $TBAPF_6$ and an internal reference of decamethylferrocene in CH_2Cl_2.

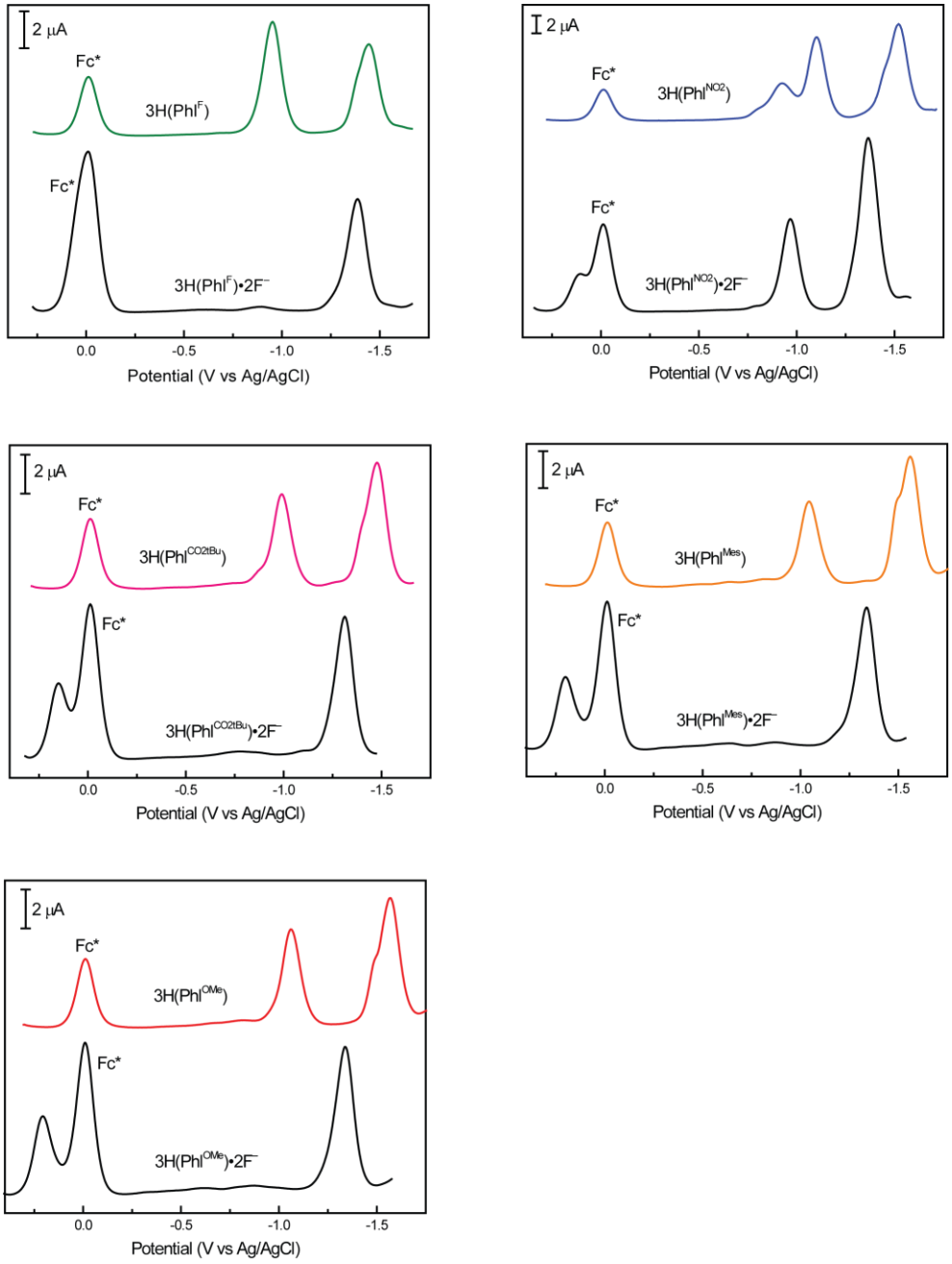

Figure 3.21 DPV traces of the phlorin reduction waves versus Ag/AgCl for the free base and fluoride bound phlorin derivatives. DPVs were obtained with 1 mM of analyte, 0.1 M $TBAPF_6$ and an internal reference of decamethylferrocene in CH_2Cl_2.

The interesting properties of the phlorin macrocycles such as the multielectron redox chemistry and the photophysics make this an intriguing chromophore for use in solar light harvesting. Figure 3.22 displays the solar power spectrum (SPS) along with the absorption profiles of 2H(TpFPP) and 3H(Phl^{F}). The 2H(TpFPP) absorption profile represents that of a typical porphyrin, with strong absorption at ~325-425 nm and 500-550 nm. This clearly shows that there are large areas of the SPS that are not able to be harvested by porphyrin based chromophores, in particular at longer wavelengths (>550 nm). Nature employs the use of carotenoids to harvest longer wavelength photons that are not able to be accessed by the porphyrinoid, chlorophyll.[116,117]

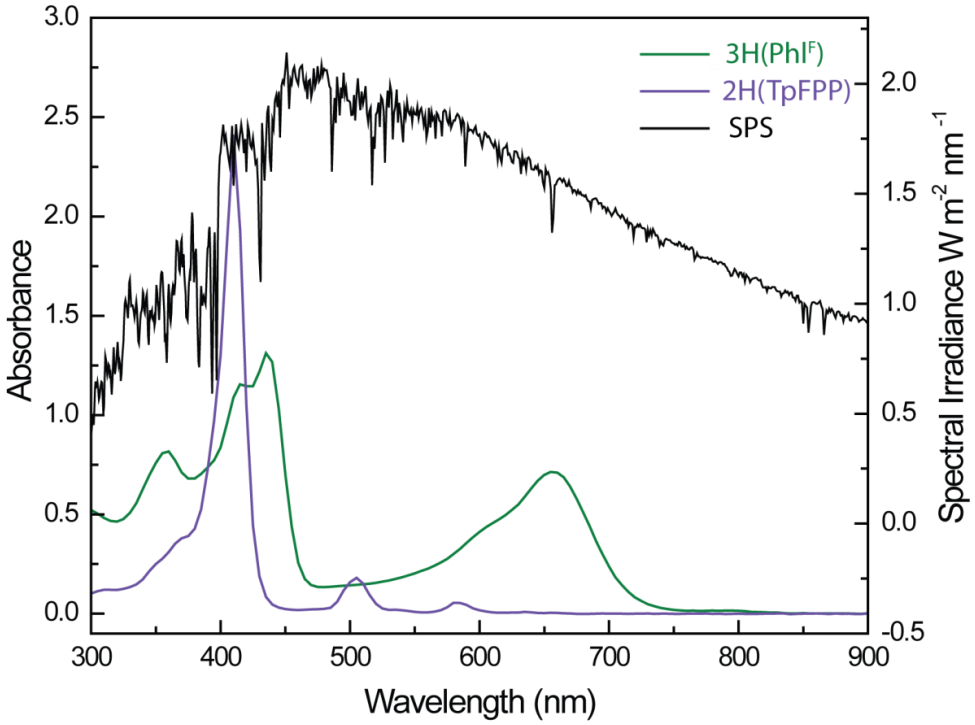

Figure 3.22 Overlay of the solar power spectrum (SPS) (black) and the absorption profiles of 3H(Phl^{F}) (green) and 2H(TpFPP) (purple).

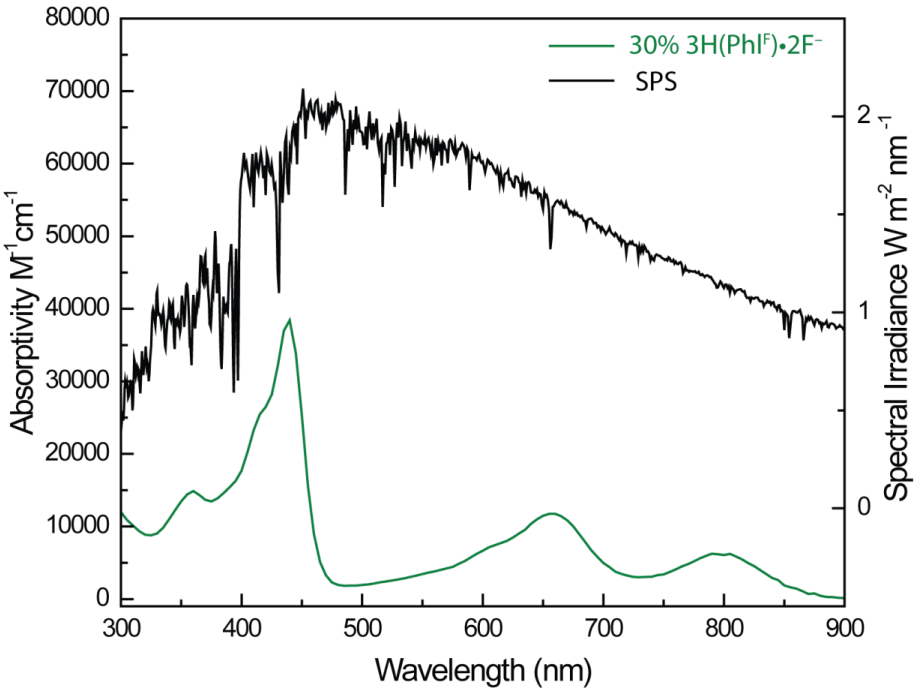

Figure 3.23 Overlay of the SPS and the absorption profile for a solution containing 10 uM 3H(Phl^{F}) and 0.6 equivalents of TBAF. The resulting spectrum is that of a solution containing 70% 3H(Phl^{F}) and 30% 3H(Phl^{F})•2F^{-}.

The absorption profile of the porphyrin can also be modified through synthesis. Several synthetically modified porphyrinoids have been developed to increase the absorption at longer wavelengths and have been used to create the most efficient dye-sensitized solar cells (DSCs) to date.[50,51] However, these porphyrin derivatives are challenging synthetic targets and suffer from intense use of chromatography and low yields which may limit their use for wide scale applications. In comparison, the phlorin macrocycles are easily constructed and are naturally able to harvest the longer wavelengths of sunlight, as seen by the overlay with the SPS in Figure 3.22.

The unique ability of the phlorin to bind fluoride also creates an opportunity to modify the absorption profile without any further synthetic processes. Shown in Figure 3.23 is the absorption spectrum of a mixture of 70 % 3H(Phl^F) and 30 % (3H(Phl^F)•$2F^-$) formed upon the simple addition of 0.6 equivalents of TBAF. The absorption spectrum now displays the ability of the phlorin macrocycle to harvest an even greater portion of the SPS, with strong absorption from 300-475 nm and 550-850 nm. This ability to harvest large portions of the SPS combined with the multielectron redox chemistry make the phlorin macrocycle an intriguing candidate for use as a chromophore in light harvesting applications.

The ability of the phlorin to bind to colloidal TiO_2 and the study of the excited state dynamics in both solution and solid state has recently been described. Investigation into the practical use of the phlorin macrocycle in light harvesting devices is currently underway.[118]

3.3 Summary

Our studies of the phlorin macrocycles have revealed that the geometric and electronic structures differ from more commonly studied porphyrins and corroles. By systematically varying the substitution at the 15-*meso*-position, several novel macrocycles with differing electronic properties have been synthesized. The novel phlorin derivatives described here nearly tripled the number of previously reported 5,5-dimethylphlorins. The ^{1}H NMR N-H resonances along with the crystal structure clearly show that the phlorin is non-aromatic due to the introduction of the dimethyl sp^3 hybridized *meso*-carbon. The phlorin macrocycles also display rich redox chemistry, with the ability to be oxidized three times at modest potentials as well as two largely irreversible reductions. The phlorin has interesting photophysical

properties including a broad absorption profile. The photophysics including the quantum yield and fluorescence lifetimes and the redox potentials are able to be attenuated through the substitution at the 15-*meso*-position.

The phlorin macrocycles have shown unique supramolecular chemistry that is uncommon for tetrapyrrole macrocycles. Phlorins are able to bind fluoride anions in a 2:1 binding ratio as judged by both UV-vis and NMR studies. Through Hill analysis, the fluoride binding has been shown to be a highly cooperative binding process with both the strength and cooperativity correlating to the electronic structure of the phlorin. The binding of fluoride causes a change in the electronic structure of the phlorin as observed by both the increase in the molar absorptivity and shift in the absorption to the near-IR region. The ternary complexes ($3H(Phl^{R})\bullet 2F^{-}$) are more easily oxidized by several hundred millivolts compared to the free base phlorins. These macrocycles have displayed interesting properties that make them suitable platforms for potential applications in photocatalysis, electrocatalysis, anion sensing and solar light capture.

Chapter 4

INSIGHT IN TO THE SUPRAMOLECULAR ACTIVITY OF PHLORIN MACROCYCLES

4.1 Introduction

Tetrapyrrole macrocycles can have varying properties that depend upon the hybridization of the carbon atoms that connect each of the pyrrole groups. Porphyrins have four sp^2-hybridized *meso*-carbons that maintain π-conjugation throughout the macrocycle, giving it intriguing photophysical properties that have applications that range from light harvesting[50,51,119-124] to photocatalysis.[125-130] Porphyrinogens contain four sp^3 hybridized carbons that disrupt the π-conjugation, which eliminates the ability of the macrocycle to absorb light in the visible region. However, this connectivity between the pyrrole groups has been shown to support multielectron redox chemistry[43,44] along with interesting supramolecular chemistry.[131,132]

Phlorin macrocycles contain a single sp^3-hybridized *meso*-carbon and have also been shown to support multielectron redox chemistry. But unlike the porphyrinogen, the phlorin maintains π-conjugation throughout the periphery of the macrocycle allowing for an absorption profile that covers a large portion of the UV-vis spectrum. The unique non-planar geometry of the phlorin allows for hydrogen bonding assemblies to be formed with fluoride anions. This supramolecular activity creates the opportunity for both the photophysical and redox properties to be attenuated through the addition of fluoride anions.

Further insight in to the electronic structure of the macrocycle and the ability to bind fluoride anions was needed to determine the fundamental factors that influence these unique properties. In the previous chapter it was demonstrated that phlorins have been shown to bind fluoride cooperatively in a 2:1 binding ratio, while neither Cl^- or Br^- have shown the ability to hydrogen bond to the N-H protons of the phlorin. This selectivity may be useful for colorimetric fluoride sensing, although the selectivity had not yet been explained.

To gain a greater understanding, this chapter will describe additional studies, which probe the fundamental properties of the phlorin. Density functional theory (DFT) calculations and a complete study of the photophysics of the phlorin were used to investigate the electronic structure of the phlorin. The ability of the phlorin to form hydrogen bonding assemblies with carboxylate anions was also studied.

4.2 Synthesis of 3H(Phl^{CF3})

The 3H(Phl^{CF3}) derivative was synthesized by modifying the synthetic route used in Chapter 3, which is shown in Scheme 4.1. The diacylated dipyrromethane derivative (2) was reduced using $NaBH_4$ in tetrahydrofuran and methanol (3:1) as the solvent. Following the reduction, the corresponding diol was then dissolved in CH_2Cl_2 and 5-(3,5-bis(trifluoromethyl)phenyl)dipyrromethane (1) was added. Following the condensation in the presence of TFA, DDQ was added to oxidize the newly formed macrocycle. After the addition of triethylamine, the reaction was purified through column chromatography, giving 3H(Phl^{CF3}) in 41% yield.

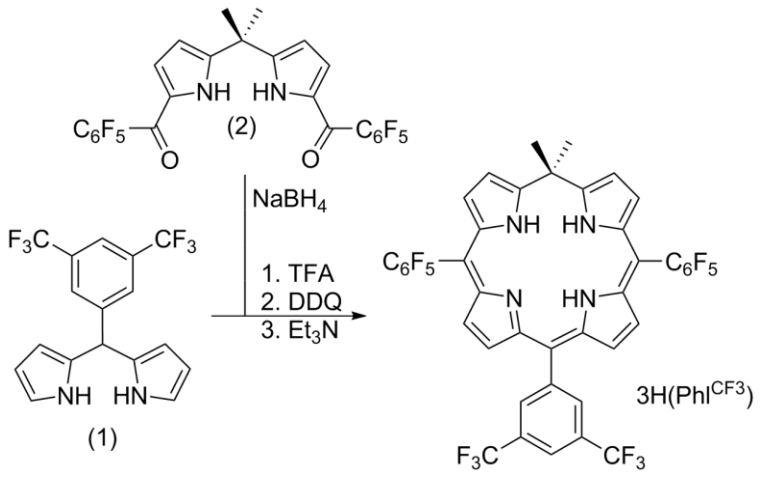

Scheme 4.1 Synthetic route for the synthesis of 3H(Phl^{CF3}).

4.2.1 Molecular structure of 3H(Phl^{CF3})

The solid state structure of 3H(Phl^{CF3}) was only the second 5,5-dimethyl phlorin scaffold reported in the literature.[133] The macrocycle is severely puckered in the reduced half of the phlorin containing the sp^3 hybridized *meso*-carbon, as shown in Figure 4.1. The carbon of the dimethyl group is positioned approximately 1.3 Å above the plane containing both the pyrrole groups on the bottom of the macrocycle, opposite of the sp^3-hybridized *meso*-carbon. The structure is similar to that of 3H(Phl^{F}) displayed in Chapter 3.

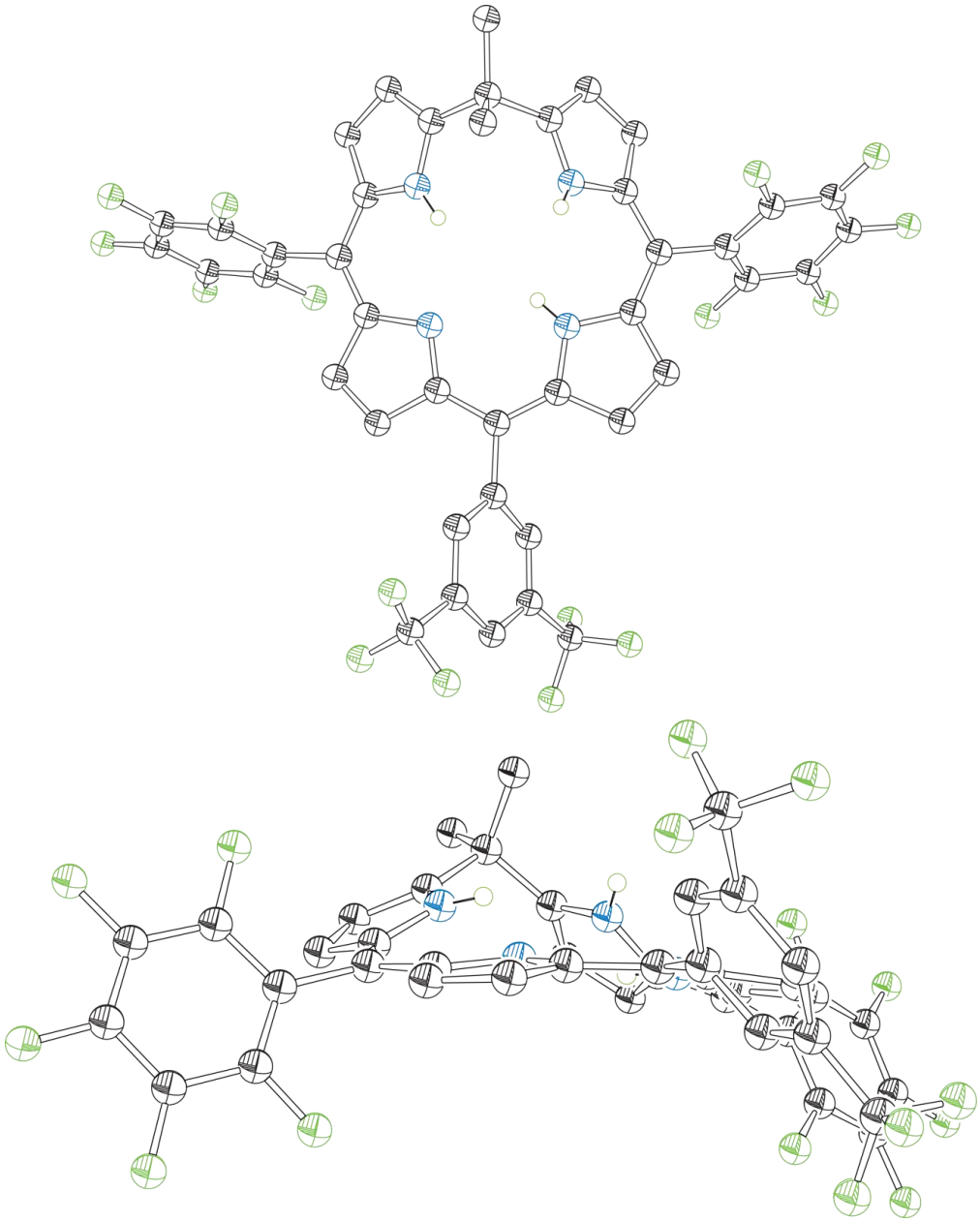

Figure 4.1 Solid state structure of 3H(Phl^{CF3}) with top and side-on view. All non-nitrogen bound hydrogens were omitted for clarity. Thermal ellipsoids are shown at 50% probability.

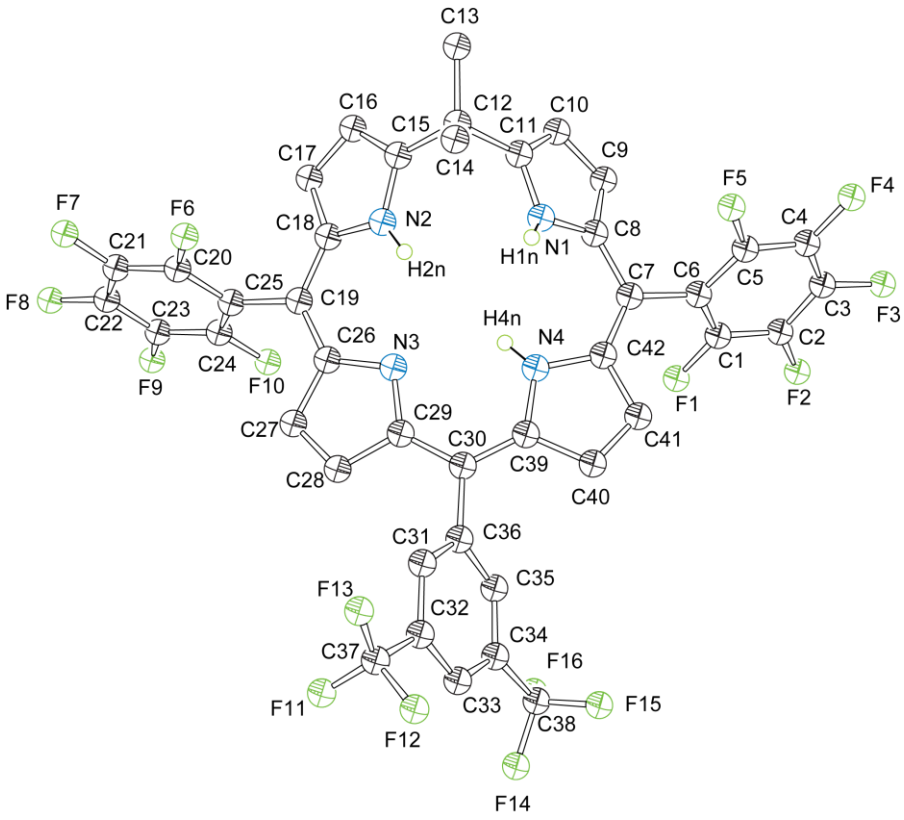

Figure 4.2 Number crystal structure of 3H(Phl^{CF3}) with all non-nitrogen bound hydrogens omitted for clarity and thermal ellipsoids shown at 50% probability.

Table 4.1 Selected bond lengths and angles for 3H(Phl^{CF3}).

Atoms	Bond Lengths (Å)	Atoms	Bond Angles (°)
C(12)–C(15)	1.511(6)	**C(15)–C(12)–C(11)**	105.6(3)
C(11)–C(12)	1.513(6)	**C(26)–C(19)–C(18)**	126.0(4)
C(12)–C(13)	1.529(6)	**C(39)–C(30)–C(29)**	124.0(4)
C(12)–C(14)	1.538(7)	**C(42)–C(7)–C(8)**	124.6(4)

4.2.2 Calculated electronic structure of 3H(Phl^{CF3})

Density functional theory (DFT) and time-dependent DFT (TD-DFT) calculation were used to investigate the electronic transitions of the phlorin displayed in Figure 4.3. The results show that there is considerable electron density spread across all four of the pyrroles in the macrocycle. The major transitions contain frontier molecular orbitals that similar to those described by Gouterman, for his standard four orbital model used to describe the electronic structure of porphyrins, with some distortion because of the reduction in symmetry.[134-137] The calculations for the LUMO +1 state display orbital density that is not equally distributed throughout the macrocycle. The orbital density is localized on the half of the macrocycle opposite to the side containing the sp^3 hybridized *meso*-carbon.

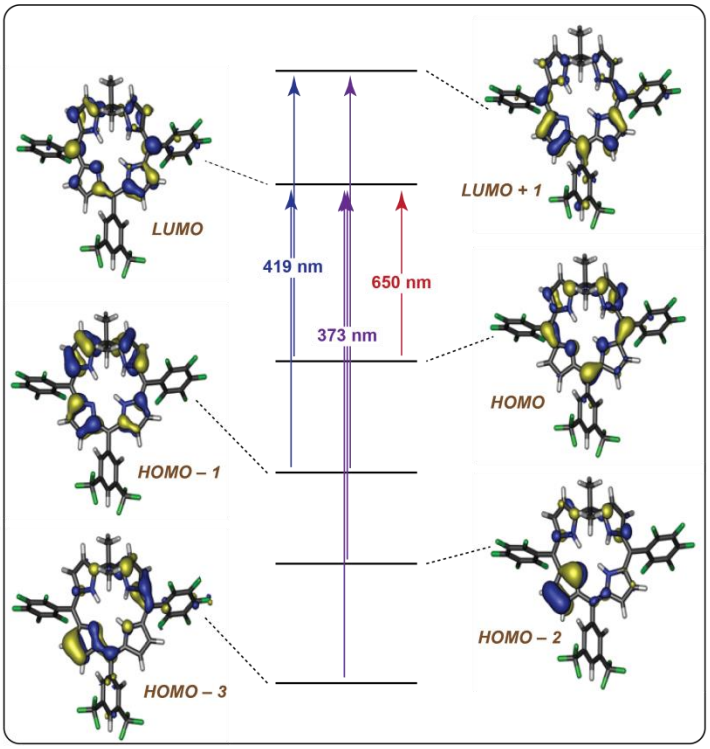

Figure 4.3 Depiction of the molecular orbitals involved with the Soret and Q-band transitions for 3H(Phl^{CF3}).

4.2.3 Absorption Profile of 3H(Phl^{CF3})

The absorption profile for 3H(Phl^{CF3}) is similar to that of the other phlorin derivatives described in Chapter 3, with a strong absorption in the Soret region at ~440 nm and the Q band region at ~665 nm. The electronic transitions calculated for the phlorin describe the LUMO +1 state as containing considerable localization of orbital density on one half of the macrocycle, suggesting that transitions involving this molecular orbital should display charge transfer character. As such, the transitions containing the excited state associated with the LUMO +1 state should be influenced by the polarity of the environment around the macrocycle. This was probed by investigating the absorption profile of 3H(Phl^{CF3}) in a several solvents with differing polarities, with the results shown in Figure 4.4. There is a shift in the absorption maxima near ~440 nm that was dependent on the polarity of the solvent. The Soret maxima in benzene ($\varepsilon = 2.3$) was found to be at 442 nm, while the maxima shifted to 435 nm in polar acetonitrile ($\varepsilon = 36.6$). There was a linear trend in the correlation between the polarity of the solvents used (ε, dielectric constant) and the Soret maxima for the 3H(Phl^{CF3}) derivative, shown in Figure 4.5. This shift clearly shows that the 3H(Phl^{CF3}) displays solvatochromism for the Soret maxima and there was no appreciable shift in the Q band maxima at ~665 nm, as the corresponding HOMO to LUMO transition maintains orbital density throughout the macrocycle.

4.2.4 Photophysics of 3H(Phl^{CF3})

The 3H(Phl^{CF3}) is weakly emissive with a quantum yield of $\Phi_{Fl} = 5.7 \times 10^{-4}$ in deaerated CH_2Cl_2. The fluorescence lifetime for the phlorin derivative was measured and found to be $\tau_{Fl} = 45$ ps. The results of these fluorescence measurements are similar to the results obtained for the other electron poor phlorin macrocycles.[138]

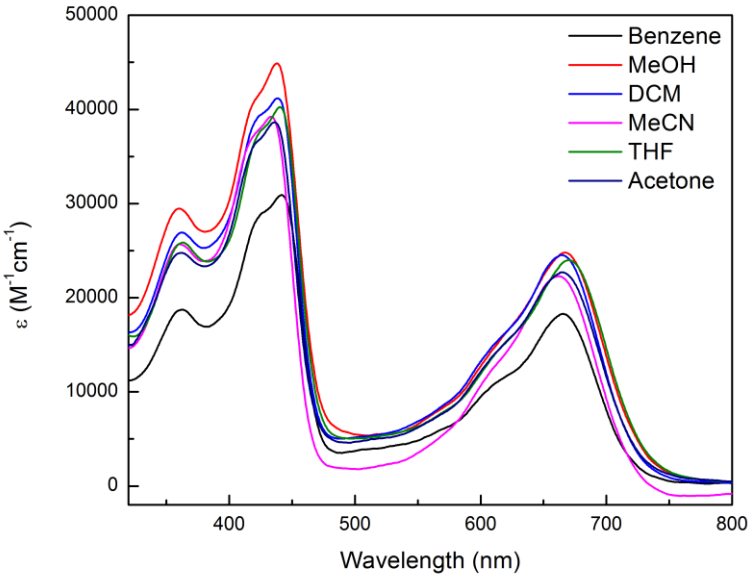

Figure 4.4 Absorption profile of 3H(Phl^{CF3}) taken in solvents with differing polarity.

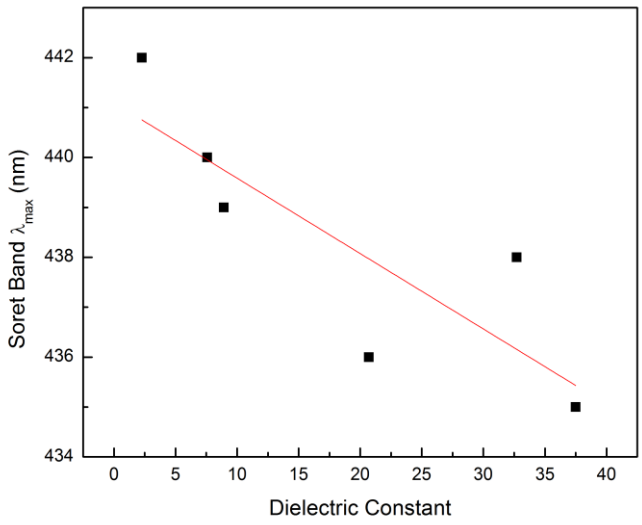

Figure 4.5 Depiction of the change of the λ_{max} of the Soret band corresponding to the polarity of the solvent.

4.3 Supramolecular Chemistry

4.3.1 Fluoride Binding

The fluoride binding for 3H(Phl^{CF3}) was investigated by the titration of TBAF in to a 10 μM solution of phlorin in CH_2Cl_2. The changes in the absorption profile were similar to those seen for the other phlorin derivatives, with the increase in the absorption at ~440 nm and a shifting of the absorption from ~665 nm to ~800 nm displayed in Figure 4.6. The UV-vis titration data revealed the presence of well-anchored isosbestic points that were maintained, suggesting a lack of intermediates being detected. Job plot analysis in Figure 4.7 confirmed a 2:1 fluoride to phlorin binding ratio and the subsequent Hill analysis shown in Figure 4.8 of the titration data gave a cooperativity coefficient $\beta_2 = 1.6 \text{ X } 10^{13} \text{ M}^{-2}$ and a Hill coefficient of $\eta = 7.8$, which are consistent with the other electron poor phlorins previously studied.[138]

This strong fluoride binding was also investigated in acetonitrile, which is significantly more polar than CH_2Cl_2. A UV-vis monitored TBAF titration was performed using a 10 μM solution of phlorin in MeCN, displayed in Figure 4.9. The changes in the absorption profile were the same as titrations performed in CH_2Cl_2. The Job plot analysis in Figure 4.10 again revealed a 2:1 binding ratio. The titration data was used for the Hill analysis plotted in Figure 4.11 and found a Hill coefficient of $\eta = 3.3$ and a cooperativity constant of $\beta_2 = 6.4 \text{ X } 10^5 \text{ M}^{-2}$. This demonstrates that the fluoride binding although weakened in polar solvent is still able to maintain not only the unique 2:1 binding ratio but also strong coordination.

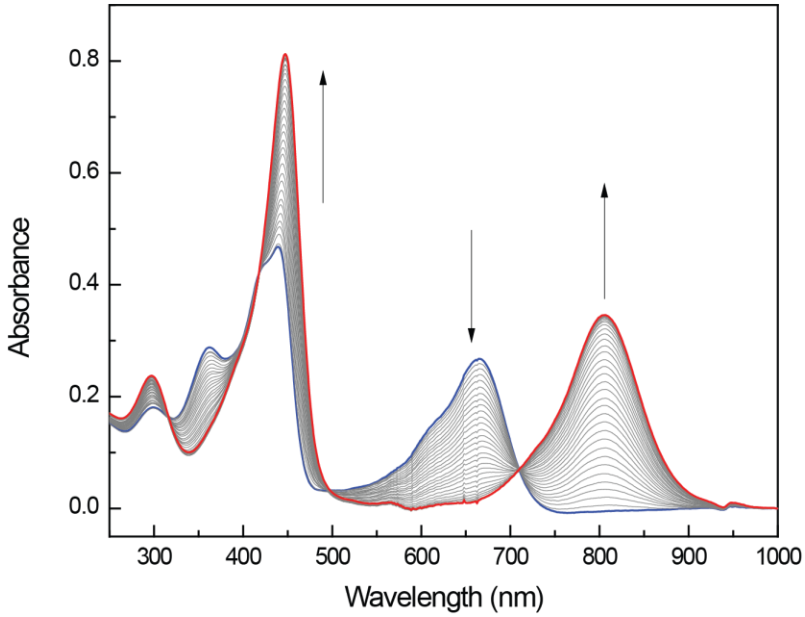

Figure 4.6 Change in the absorption profile of 3H(Phl^{CF3}) with the addition of TBAF in CH_2Cl_2.

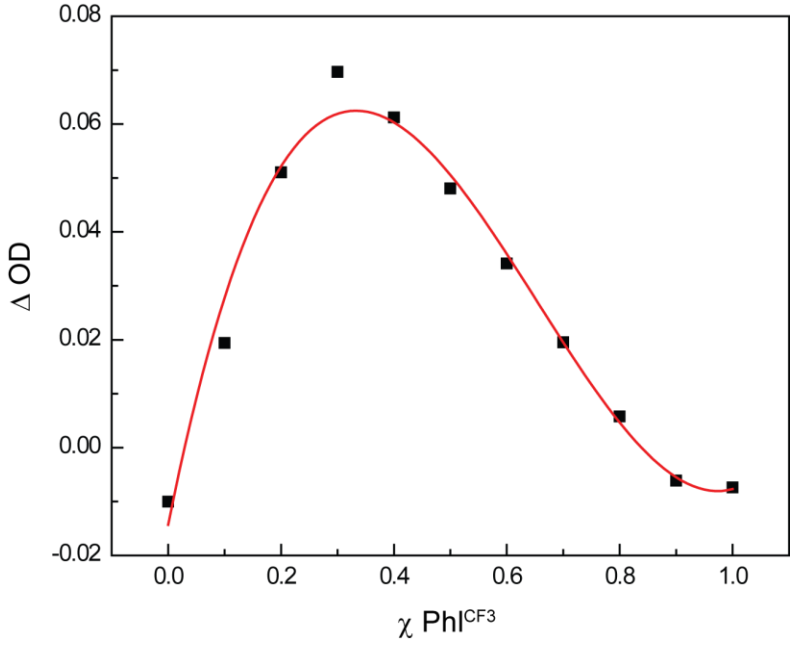

Figure 4.7 Job plot for the addition of TBAF to 3H(Phl^{CF3}) in CH_2Cl_2.

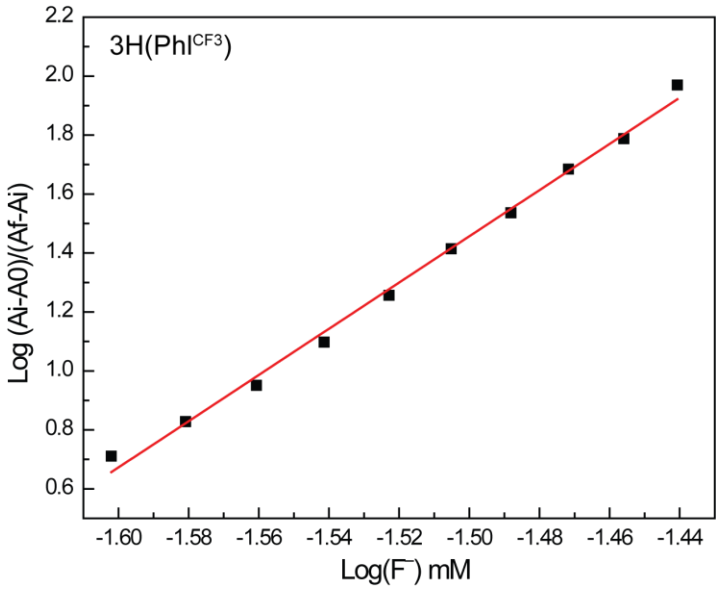

Figure 4.8 Hill plot constructed from the titration of TBAF in to a 3H(Phl^{CF3}) in CH_2Cl_2.

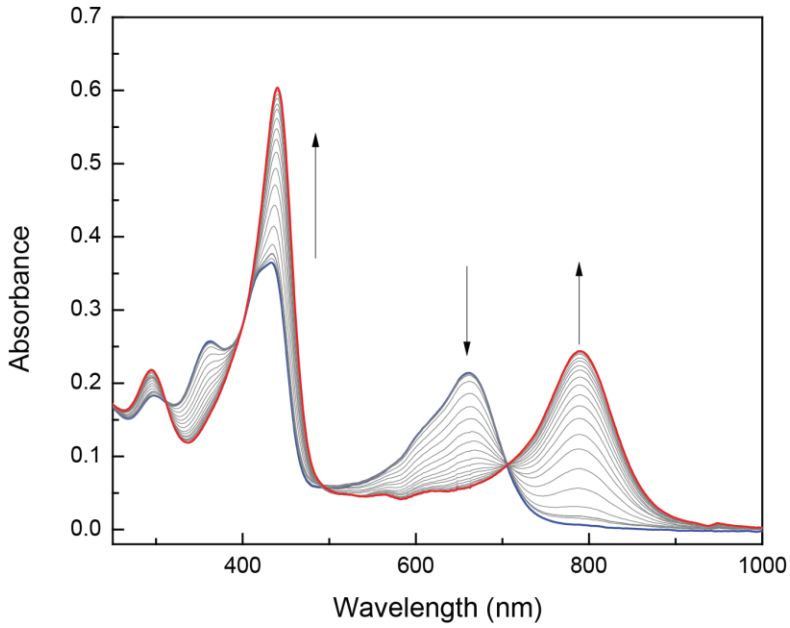

Figure 4.9 Changes in the absorption profile of 3H(Phl^{CF3}) with the addition of TBAF in MeCN.

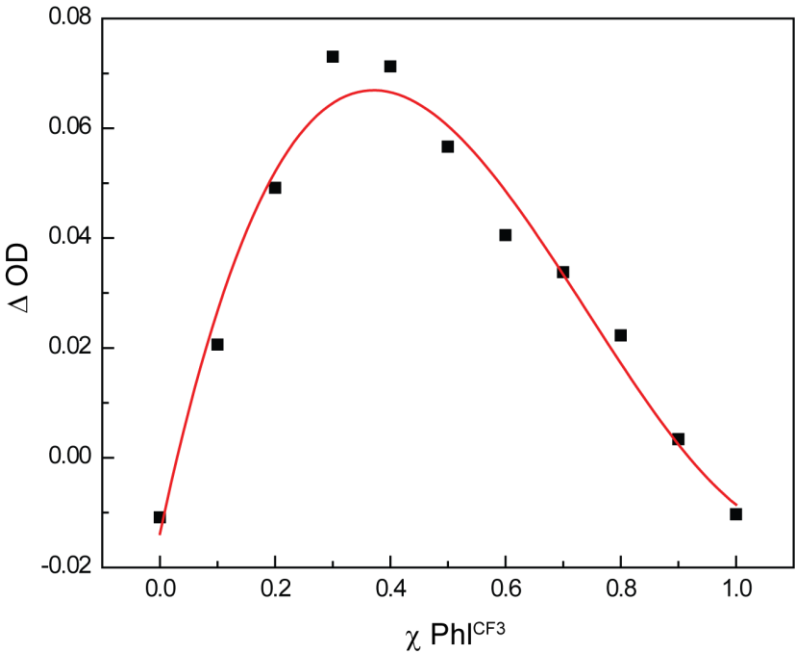

Figure 4.10 Job plot constructed for the addition of TBAF to 3H(Phl^{CF3}) in MeCN.

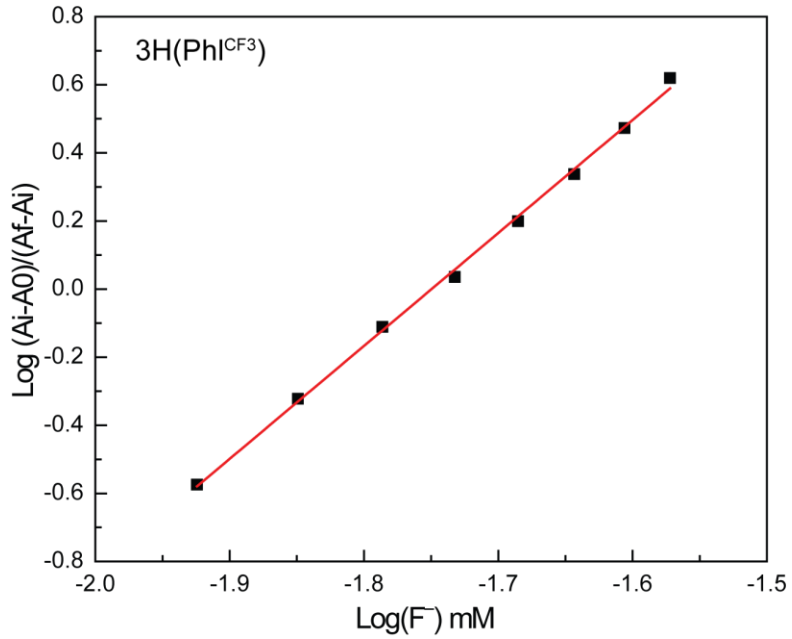

Figure 4.11 Hill plot constructed from the titration of TBAF in to a solution of 3H(Phl^{CF3}) in MeCN.

4.3.2 Carboxylate Binding

To gain further insight into the properties required of an anion for binding to the phlorin, we needed to select an anion that allows for control of both sterics and acidity is required. There have been previously reported examples in the literature of polypyrrole systems that have shown the ability to bind oxygen anions.[139,140] Carboxylate groups are intriguing anions due to the ability to control both the acidity and the steric properties. Carboxylates also have the potential to form a two point hydrogen bond with the phlorin core.

The investigation of carboxylate binding began with the titration of tetrabutylammonium acetate (TBAOAc) in to a 10 μM 3H(Phl^{CF3}) solution with

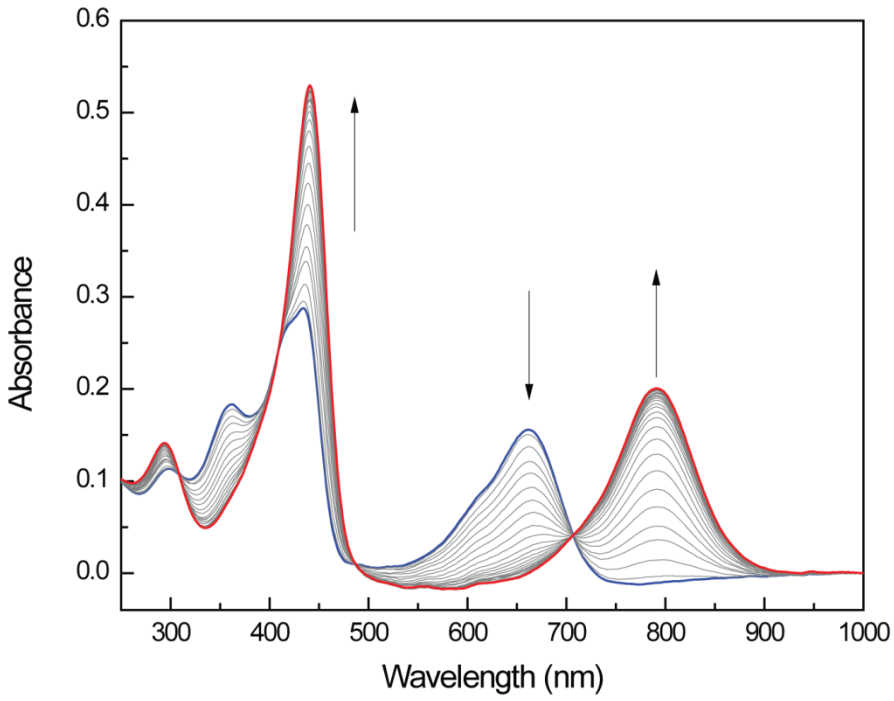

Figure 4.12 Changes in the absorption profile of a 10 μM solution of 3H(Phl^{CF3}) upon the addition of TBAOAc in MeCN.

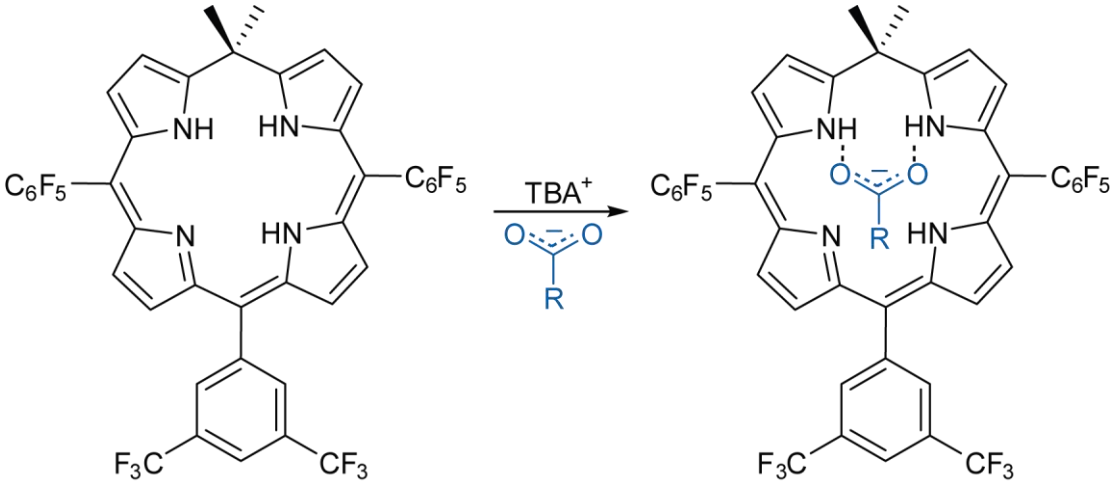

Scheme 4.2 Representation of the carboxylate anion hydrogen bonding to the inner core of the phlorin macrocycle.

MeCN as the solvent. The solution was monitored by changes in the UV-vis absorbance with slow addition of TBAOAc. The absorption profile changed as before with the addition of fluoride with well anchored isosbestic points, as shown in Figure 4.12. However, unlike the fluoride binding the Job plot analysis in Figure 4.13 suggested that the acetate binds in a 1:1 ratio. Benesi-Hildebrandt analysis of the titration data revealed a linear fit of the data that is also consistent with a 1:1 binding process (Figure 4.14). The formation constant (K_f) for the binding of acetate was found to be K_f = 440, which is similar in magnitude to that observed for amidinium-carboxylate hydrogen bonding scaffolds.[141-143] This binding process is also fully reversible, as displayed in Figure 4.15, as the addition of a protic solvent such as methanol disrupts the hydrogen bonding and the absorption profile is returned to that of the free base 3H(Phl^{CF3}).

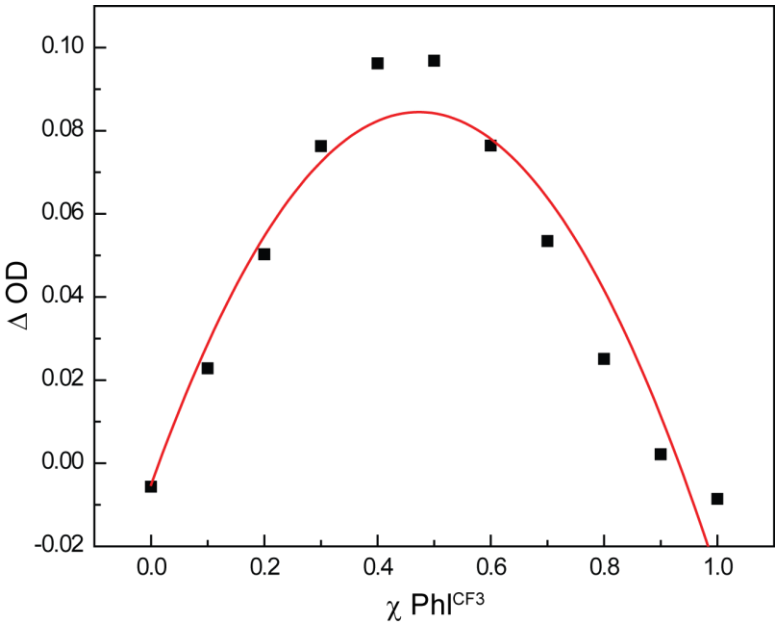

Figure 4.13 Job plot constructed for the addition of TBAOAc to 3H(Phl^{CF3}) in MeCN.

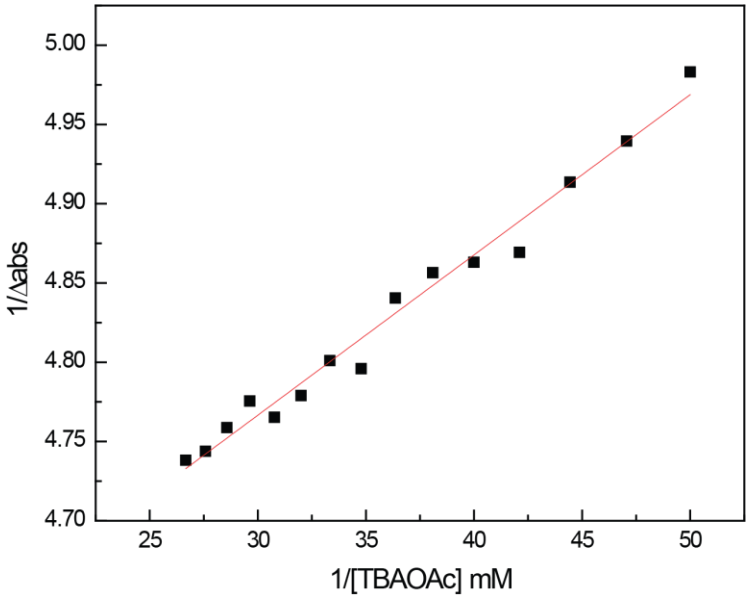

Figure 4.14 Benesi-Hildebrandt analysis constructed from the titration of TBAOAc into a solution of 10 μM 3H(Phl^{CF3}) in MeCN.

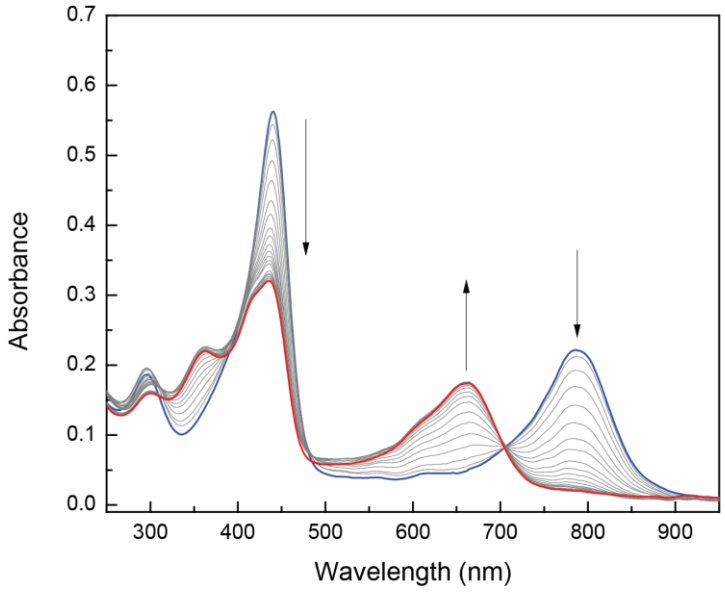

Figure 4.15 Changes in the absorption profile of 3H(Phl^{CF3})•OAc^{-} with the addition of MeOH.

With the ability of the phlorin macrocycle to bind carboxylate anions being clearly demonstrated, further insight into the factors that limit the binding could now be garnered. The effect of anion size was first tested using tetrabutylammonium 4-dimethylaminobenzoate salt (TBA($^{-}$O$_2$C-Φ-4-Me$_2$N)), which is much larger than that of acetate. The pK_a of the conjugate acid in MeCN (pK_a = 23)[144] is similar to that of acetate (pK_a = 22.3)[144] shown in Table 4.2, making 4-dimethylaminobenzoate a good candidate to investigate the effect of anion size on the binding.

A titration was performed with 4-dimethylaminobenzoate, as shown in Figure 4.16 and the absorption profile changes were the same as the acetate titration, as judged by UV-vis. Benesi-Hildebrandt analysis (Figure 4.17) of the titration data gave K_f = 435, which is very similar to the formation constant of acetate. This result

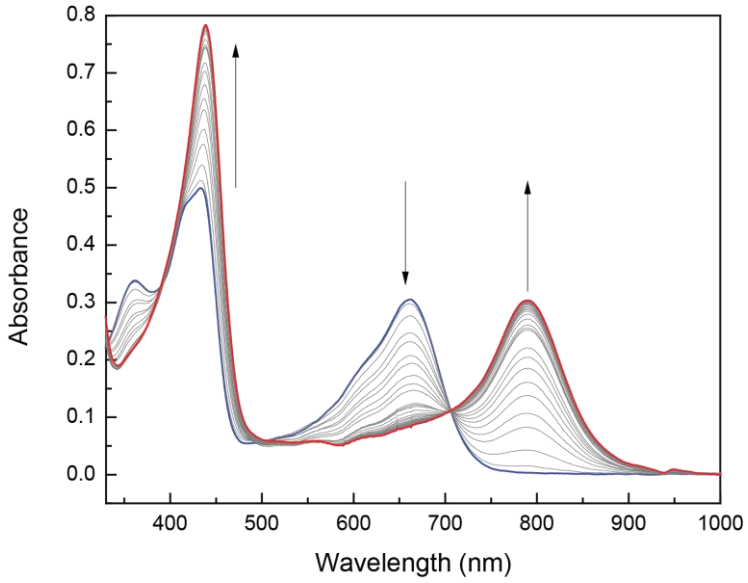

Figure 4.16 Absorption profile changes for 3H(Phl^{CF3}) with the addition of TBA($^{-}O_2C$-Φ-4-Me_2N) in MeCN.

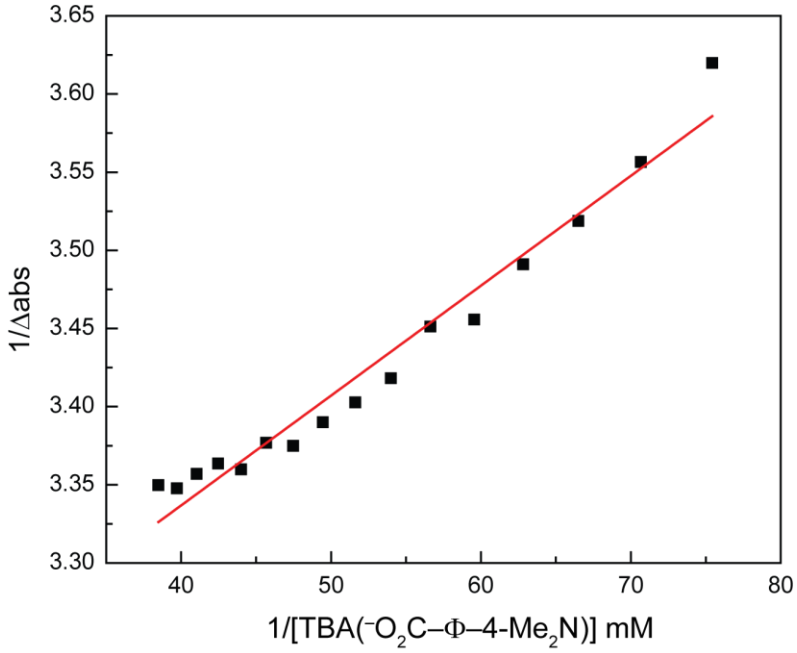

Figure 4.17 Benesi-Hildebrandt analysis for the titration of TBA($^{-}O_2C$-Φ-4-Me_2N) into a 10 μM MeCN solution of 3H(Phl^{CF3}).

suggests that the size of the anion is not the limiting factor for binding to the phlorin macrocycle.

The effect of the basicity of the anion was further probed using several different carboxylate anions. The TBA salts of benzoate ($PhCO_2^-$), 4-bromo-benzoate (4-Br- Φ -CO_2^-) and 4-nitro-benzoate (4-O_2N- Φ -CO_2^-), shown in Figure 4.18 provided a reasonable range of basicity to determine the effect of anion pK_a on the strength of binding to the phlorin macrocycle. Figure 4.19 shows the UV-vis titrations performed in MeCN with each of the carboxylate anions displaying the characteristic absorption profile changes noted for anion binding to 3H(Phl^{CF3}). The titration data was used for the Benesi-Hildebrandt analysis shown in Figure 4.20 and allowed for the extraction of the formation constants in MeCN for each of the carboxylates. These results displayed in Table 4.2 show that the basicity has a strong influence on the formation constants. The 4-nitro-benzoate anion only weakly binds to the phlorin and its conjugate acid (pK_a of 18.7 in MeCN)[144] appears to be close to the limit as anions

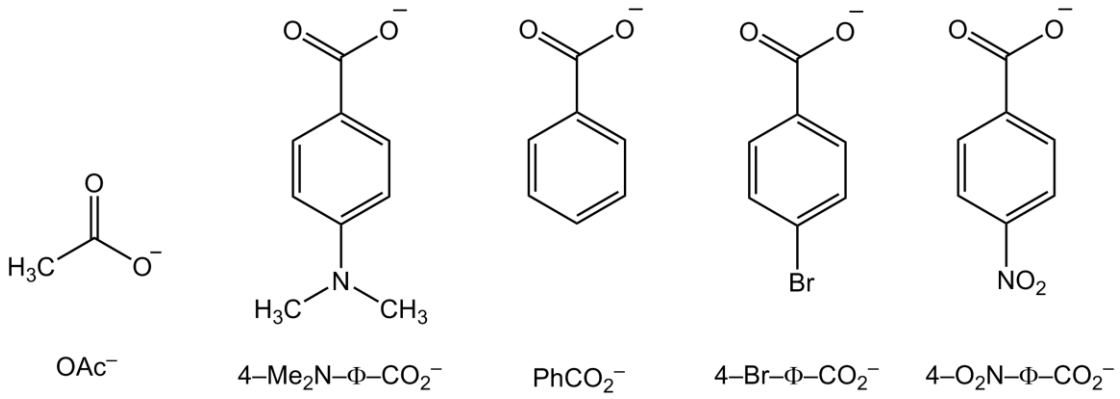

Figure 4.18 Carboxylate anions used for the binding studies with 3H(Phl^{CF3}). All carboxylates were prepared as TBA salts.

Table 4.2 Carboxylate binding parameters for the formation of hydrogen-bonding assemblies with 3H(Phl^{CF3}).

anion	pK_a [a]	K_f
OAc^-	22.3	440
4-Me_2N- Φ -CO_2^-	23.0	435
$PhCO_2^-$	20.7	27.0
4-Br- Φ -CO_2^-	20.3	8.21
4-O_2N- Φ -CO_2^-	18.7	1.79

[a] pK_a values correspond to the conjugate acid in MeCN as reproduced from ref 143.

that are more acidic do not bind. One such example is that of 3,5-dinitro-benzoate (pK_a = 17 in MeCN),[144] where even after the addition of 3500 equivalents there was no binding to the phlorin as judged by UV-vis.

Although a steric interaction limiting the anion binding cannot be completely ruled out, smaller oxygen based anions such as nitrate, methanesulfonate and perchlorate did not display any binding interactions with 3H(Phl^{CF3}). This further demonstrates that the basicity of the anion plays a critical role in the formation of the hydrogen bonds with the N-H protons of the phlorin core. This can also help explain the selectivity for fluoride from the rest of the halogens. The comparison of the pK_a values for the halogens (HF, HCl, HBr; pK_a values in a polar nonprotic solvent are 15, 1.8, and 0.9 respectively)[145] shows that the decrease in the basicity of the anion is likely the cause for the lack of hydrogen bonding for the Cl^- and Br^- anions.

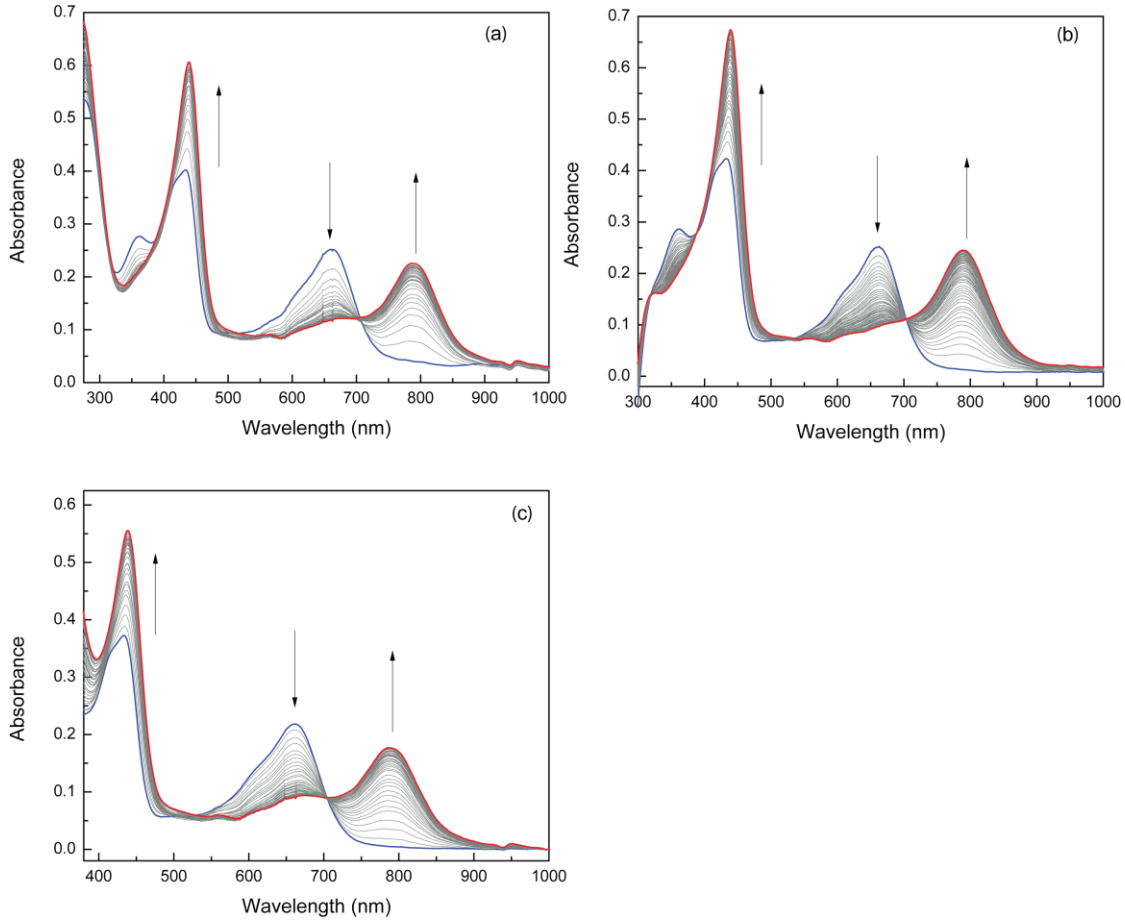

Figure 4.19 Absorption profile changes with the addition of (a) TBA($^{-}CO_2$-Ph), (b) TBA($^{-}O_2C$-Φ-4-Br) and (c) TBA($^{-}O_2C$-Φ-4-NO_2) to a MeCN solution of 3H(Phl^{CF3}).

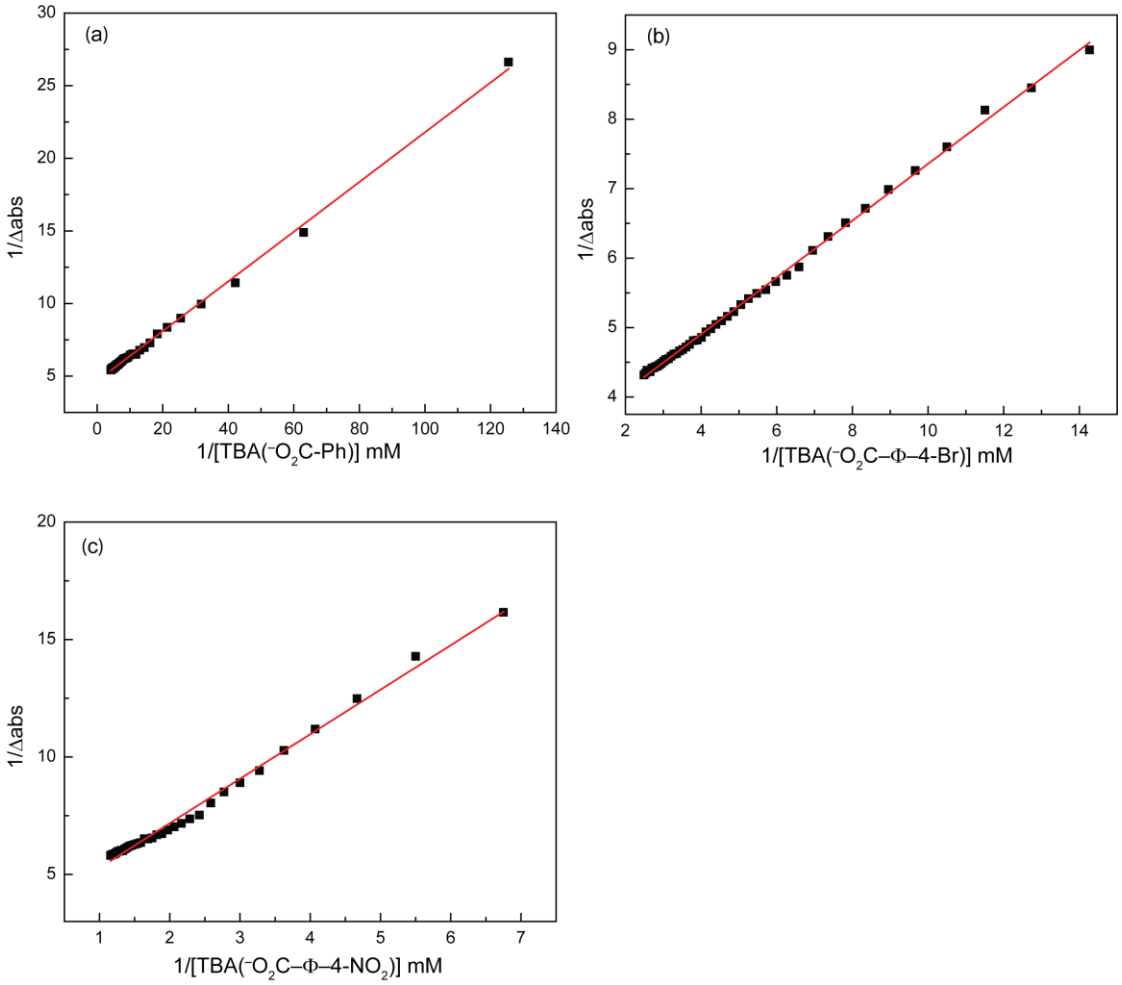

Figure 4.20 Benesi-Hildebrandt plots for the titrations of (a) TBA($^{-}CO_2$-Ph), (b) TBA($^{-}O_2$C-Φ-4-Br) and (c) TBA($^{-}O_2$C-Φ-4-NO_2).

4.3.3 Electrochemical Study of Carboxylate Binding

Like the phlorins described in preceeding chapters, 3H(PhlCF3) also displays a rich redox chemistry. The redox potentials also have the ability to be attenuated following the addition of anions that can form hydrogen bonds to the phlorin core. With the discovery of the binding of carboxylates to the phlorin, the effects on the

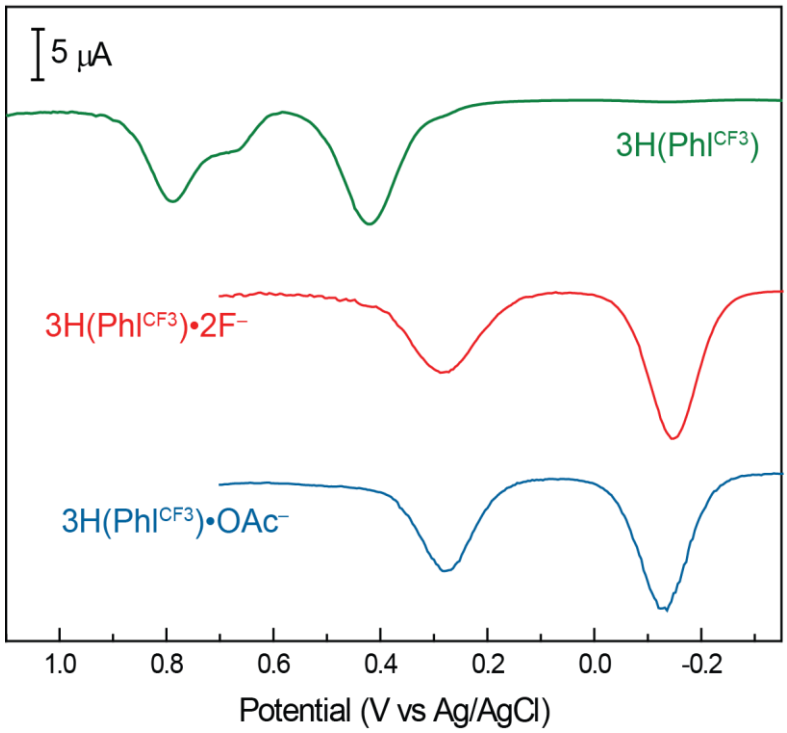

Figure 4.21 DPV traces of the phlorin oxidation waves versus Ag/AgCl for 3H(Phl^{CF3}) (green), 3H(Phl^{CF3})•2F^{-} (red) and 3H(Phl^{CF3})•OAc^{-} (blue) in MeCN containing 1 mM of analyte, 0.1 M $TBAPF_6$. A standard three electrode set up was used with a glassy carbon disk electrode (working electrode), platinum wire (auxiliary) and Ag/AgCl reference electrode.

redox chemistry were probed through the use of differential pulse voltammetry (DPV). The DPV trace recorded for 3H(Phl^{CF3}) in MeCN shown in Figure 4.21, displays three oxidations at modest potentials of E_{ox} (1) = 0.42 V, E_{ox} (2) = 0.67 V and E_{ox} (3) = 0.79 V versus Ag/AgCl. The addition of both F^- and OAc^- cause a dramatic shift in the oxidative potentials of 3H(Phl^{CF3}) with the DPV traces displayed in Figure 4.21. The formation of 3H(Phl^{CF3})•2F^- and 3H(Phl^{CF3})•OAc^- through the addition of F^- and OAc^-, respectively cause the potentials to shift to less positive potentials, which can be

justified with the neutral phlorin now becoming negatively charged. The DPV traces in Figure 4.21 differ from those displayed for $3H(Phl^{R})•2F^{-}$ in Chapter 3 that were recorded in CH_2Cl_2, with the first and second oxidations coalescing into a two electron wave at E_{ox} = –0.14 V and E_{ox} = –0.13 V for $3H(Phl^{CF3})•OAc^{-}$ and $3H(Phl^{R})•2F^{-}$, respectively. The third oxidation occurs at ~0.28 V for each of the hydrogen-bonding assemblies. The addition of anions with the appropriate basicity can perturb the electronics of the phlorin allowing for the attenuation of the redox potentials.

4.4 Summary

A new phlorin macrocycle, $3H(Phl^{CF3})$, was synthesized, adding to the suite of 5,5-dimethyl phlorin scaffolds that we have developed. The solid state structure of $3H(Phl^{CF3})$ was illuminated, which marks making only the second free base phlorin structure containing dimethyl substituents at the sp^3-hybridized *meso*-carbon. The phlorin construct is non-aromatic and is distorted from the planarity seen in most porphyrinoids. $3H(Phl^{CF3})$ displays solvatochromism due to the polarization on one half of the macrocycle in the LUMO+1 state, which is a major contributor to the transitions near ~370-420 nm. The supramolecular chemistry of the phlorin has been investigated. The phlorin is able to cooperatively bind fluoride in a 2:1 ratio in MeCN, a polar non-protic solvent and CH_2Cl_2. The ability to also bind carboxylate anions in a 1:1 ratio was also shown for the first time. Several different carboxylate anions were selected based on size and the basicity of the anion. The binding results showed that the formation of hydrogen bonding moieties is not limited by the size of the anion but rather is influenced by the basicity. Carboxylate anions that are more electron rich than 4-nitro-benzoate are able to form strong hydrogen bonds even in a polar solvent environment. This observation can help rationalize the lack of hydrogen bond

formation for other oxygen based anions such as nitrate, methanesulfonate and perchlorate, where the anions are too electron deficient to form bonding interactions.

Chapter 5

DEVELOPMENT OF THE PHLORIN AS A LIGAND

5.1 Introduction

Metalloporphyrinoids are ubiquitous throughout nature, with some of the most studied biological examples being heme, chlorophyll and vitamin B12.[146] Porphyrinoids can not only stabilize metal centers in varying redox states, but can act as a light harvester in the case of the chlorophyll complexes. The intriguing properties and uses that have been discovered for porphyrins in nature have led to porphyrin being one of the most heavily investigated ligand systems.

Porphyrins have also been extensively studied in several research areas including for light harvesting in dye sensitized solar cells. Indeed, dye-sensitized solar cells containing modified porphyrin derivatives have been the most efficient cells developed to date displaying solar to electric current efficiencies that approach 13%.[50,51] Porphyrins have also been investigated for performing many catalytic reactions including hydrogen evolution reactions,[10-13] epoxidations,[22-25] reduction of CO_2 to CO[26-29] and dioxygen activation.[19-21]

While porphyrins have been shown to be employed throughout nature, other tetrapyrrole macrocycles such as the phlorin are not as commonly observed. Phlorins are not, however, completely absent in nature, as they have been discovered in orange peels,[147] are thought to be involved in the heme P460 catalytic cycle of hydroxylamine oxidoreductase,[148] and have served as models for the study of coenzyme F430.[149,150]

Phlorins have also been proposed to be intermediates in hydrogen evolution reactions under acidic conditions using porphyrins as the active catalyst.[151,152]

With the slow development of the phlorin, there is very limited amount of literature on their use as a ligand. The first metalated phlorin was reported in 1963 by Closs *et. al*. where zinc is coordinated in the center of the phlorin core and was studied using UV-vis and ^{1}H NMR characterization.[153] However, it was noted that the zinc metalated phlorin was not stable and would undergo a rearrangement to form the corresponding chlorin. It was proposed in 1982 by Sugimoto that the rearrangement of the metal coordinated phlorin could be prevented through the formation of a neutral metalated phlorin species rather than the ionic nature of the zinc phlorin.[154] In his pursuit of studying a neutral metal coordinated phlorin, gold was proposed to be an excellent candidate for the metalation of the phlorin core. This was reasoned because the gold could remain in the trivalent state maintaining a neutral complex, as gold(III) porphyrins had shown that their electrochemical reductions were ligand based and the oxidation state of the central gold remained as gold(III).[155] The gold(III) phlorin was able to be synthesized starting with the gold(III) porphyrin followed by nucleophilic attack of hydride or hydroxide at the *meso*-carbon, as shown in Scheme 5.1. This was the first gold(III) phlorin to be isolated and was able to be studied through UV-vis, IR and ^{1}H NMR spectroscopy. Other examples of gold(III) phlorins have been reported in the literature, but are only detected through UV-vis spectroscopy as a byproduct of photoreduction reaction of gold(III) porphyrins at low pH.[151,156] The only other example of an isolated gold(III) porphyrin was reported in 1992 by Shimidzu and coworkers, where they were able to isolate a hydroxyphlorin, again through the nucleophilic attack at the *meso*-carbon.[157] The characterization of the gold(III)

hydroxyphlorin was consistent with the previously reported gold(III) phlorin,[154] making these the rare examples of gold(III) phlorins described in some detail.

With the limited reports of metalated phlorins in the literature, we endeavored to further investigate these intriguing complexes. In this chapter we describe the development of a synthetic pathway for the formation of a gold(III) phlorin that does not use the parent porphyrin, but rather utilize the free base phlorin directly. We have shown the ability to synthesize a variety of free base phlorin macrocycles with varying electronic configurations that can now be used to investigate the influence on the electronic structure of the phlorin through the coordination of a metal center. This chapter will describe the synthesis and characterization of the first gold(III) phlorins bearing geminal dimethyl substituents at the sp^3-hybridized *meso*-carbon. The crystal structure and redox chemistry of isolated gold(III) phlorins were examined along with the investigation into the reactivity of the metalated phlorin complex.

Scheme 5.1 Synthetic pathway used for the formation of metalated phlorin derivatives.

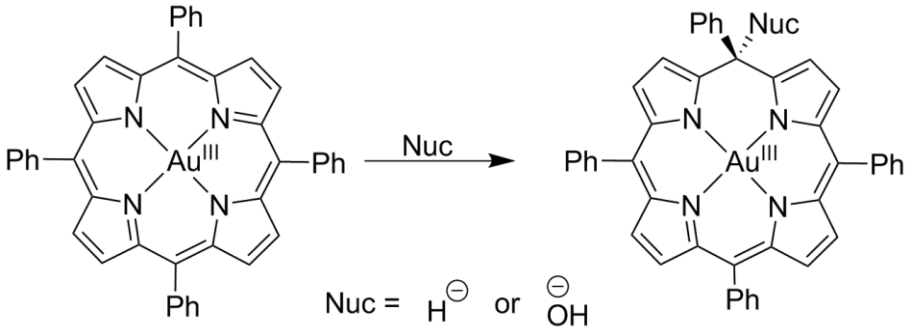

5.2 Synthesis of M(Phl)

Prior to our work in this area, a general synthetic route for the formation of metalated phlorin macrocycles had yet to be developed. The previous examples reported within the literature begin from the porphyrin macrocycle that is already coordinated to a metal center which is then subjected to nucleophilic attack at one of the four *meso*-carbons along the backbone.[151,153,154,156,157] This approach for the synthesis of metal coordinated phlorins is limited due to the ability of the nucleophile to substitute at any of the four *meso*-carbons. The substituents at the sp^3-center are also limited by their potential nucleophilicity to break the aromaticity of the porphyrin macrocycle.

Our attempt to use the freebase phlorin macrocycle as a ligand began with the use of typical procedures for the formation of metalated porphyrinoid complexes. The coordination of the metal atoms to the core of macrocycles such corroles has been well established and served as a guide in the development of the synthetic pathway to form metalated phlorin complexes.

Zinc was one of the first targeted metals for the insertion in to the center of the phlorin because of the redox inactivity. Synthesis of a zinc-phlorin complex would provide an opportunity for the study of the electronic communication between the phlorin and the metal center. Diethyl zinc ($ZnEt_2$) was added to a phlorin solution with an additional equivalent of n-butyl lithium (n-BuLi) to deprotonate the core pyrrole groups and coordinate the Zn^{2+} center. However, this did not result in the isolation of the $[Zn(Phl)]^-$ but rather in the decomposition of the phlorin ligand. Other attempts using $ZnEt_2$ were investigated but continued to give decomposition as the major product. Zinc dichloride ($ZnCl_2$) was investigated with the use of several different bases including triethylamine (Et_3N), methyl lithium (MeLi), sodium hydride (NaH),

and potassium *tert*-butoxide (KO^tBu), however all failed to deliver the desired product leading to a mixture of recovered free base phlorin and decomposition products. With the attempts at making the zinc coordinated phlorin proving unsuccessful, other redox inactive metals were investigated. Aluminum, indium, and gallium were selected for the insertion to the phlorin core as the trivalent state of these metals would be appropriate for the trianionic phlorin, forming a neutral complex. Modifying reported synthetic preparations of corroles containing each of these metals was used in attempts in making metalated phlorins. Aluminum corroles have been synthesized using trimethyl aluminum ($AlMe_3$) to both deprotonated and insert aluminum in to the central core of the corrole.[158,159] Utilizing this established route, $AlMe_3$ was added to a phlorin solution in pyridine. However, after several attempts the desired Al(Phl) was never isolated, with the results similar to that obtained for the $ZnEt_2$ efforts, where decomposition seemed to be the major pathway. Indium corroles, although limited in the reported literature have been shown to form through simply heating a corrole solution in the presence of $InCl_3$.[160] The phlorin was unreactive under these conditions and bases were used in an attempt facilitate the coordination of indium to the phlorin center. However, these attempts remained unsuccessful and we shifted out focus to gallium. Much like the attempts made with $InCl_3$, $GaCl_3$ was used while heating, with pyridine being used as both the solvent and a mild base. The phlorin remained unreacted under these conditions, and the addition of a stronger base did not yield any traceable products. The conditions used for these metalation attempts are summarized in Table 5.1, where unfortunately none of the conditions used led to the formation of the desired metalated phlorin products.

Table 5.1 Attempted metalations for the phlorin macrocycle.

Metal	Reagent	Base	Conditions
Zn	$ZnEt_2$	BuLi	rt, N_2
	$ZnEt_2$	MeLi	rt, N_2
	$ZnCl_2$	Et_3N	rt, N_2
	$ZnCl_2$	MeLi	rt, N_2
	$ZnCl_2$	NaH	rt, N_2
	$ZnCl_2$	KO^tBu	rt, N_2
Al	$AlMe_3$	pyridine	N_2
In	$InCl_3$	NaH	rt, N_2
	$InCl_3$	MeLi	rt, N_2
Ga	$GaCl_3$	pyridine	heat
	$GaCl_3$	NaH	rt, N_2
Sn	$SnPh_4$		rt, N_2
	Ph_3SnCl		rt, N_2
	$PhSnCl_3$		DMF, 100 °C
	$SnCl_4$	KO^tBu	rt, N_2
	$SnCl_2$		rt, N_2
Fe	$FeCl_2$	pyridine	Heated w/ MeOH
Bi	$Bi(OAc)_3$	pyridine	rt, N_2
	$Bi(OTf)_3$	KO^tBu	rt, N_2
Cr	$CrCl_3$	KO^tBu	rt, N_2
Cu	$Cu(OAc)_2$	pyridine	rt, N_2
Pd	$Pd(OAc)_2$		heat
	$PdCl_2$	KO^tBu	rt, N_2
Ni	$NiCl_2$	KO^tBu	rt, N_2
	$Ni(OAc)_2$	pyridine	rt, N_2

With the mounting number of unsuccessful attempts for the metalation of the phlorin macrocycle with redox inactive metals, we expanded our investigation to other metal ions such as Sn^{4+},[161,162] Bi^{3+},[163,164] Cr^{3+},[165-167] Fe^{2+},[168] and Cu^{2+} [169,170] that are commonly observed in the corrole literature. Tin corroles have frequently been

reported with the coordination of Sn(IV) with either chloride or C_6H_5 serving as an axial ligand. The synthesis of these Sn(IV) corrole complexes typically begin with the use of $SnCl_2$,which is oxidized under air to form the final complex. The application of this method to the phlorin macrocycle yielded no reaction when performed under an atmosphere of nitrogen and when heated under air, the phlorin macrocycle decomposed, which was not unexpected.[90] With the inability to form the Sn(IV) product beginning from $SnCl_2$, we proposed the use of Sn(IV) reagents directly to avoid the need for the oxidation. Several Sn(IV) reagents were investigated as shown in Table 5.1, however none resulted in the formation of $[Sn^{(IV)}(Phl)]^+$. These reagents were unreactive towards the phlorin, with almost quantitative recovery of the phlorin macrocycle. The use of additional base only resulted in the decomposition of some of the macrocycle and did not provide the desired product. The synthesis of iron corroles is very similar to that of the tin derivatives, with the use of $FeCl_2$ followed oxidation in air, typically giving the Fe(IV) corrole.[168] The attempts made in the formation of iron phlorins gave results similar to that observed with tin, with no reactivity under an atmosphere of nitrogen and decomposition upon heating the reaction solution under air.

The coordination of Bi(III) and Cr(III) were investigated using similar approaches. $CrCl_3$ and $Bi(OTf)_3$ were used with KO^tBu serving as the base. Neither of these reactions led to the formation of the metalated phlorin however. Additional attempts made with bismuth included the use of $Bi(OAc)_3$ in pyridine which proved to be unproductive and led to the recovery of the phlorin macrocycle. Similar attempts were made with Cu(II),[169,170] however, the use of $Cu(OAc)_2$ in pyridine did not afford

the desired product, illustrating that the metalation of the phlorin is not as facile as the insertion of a metal center into a corrole.

With many unsuccessful attempts made for the coordination of the metal to the phlorin core displayed in Table 5.1, Ni(II)[171,172] and Pd(II),[173,174] which are less commonly used metals in the corrole literature, were used in an attempt to coordinate to the phlorin. $Ni(OAc)_2$ and $Pd(OAc)_2$ were used with the phlorin, however as seen before there was no metalation observed. A more aggressive approach was used with deprotonation using KO^tBu followed by the addition of either $PdCl_2$ or $NiCl_2$ which again did not yield the desired products.

The insertion of a metal into the core of the phlorin had proven rather difficult compared to the more commonly studied porphyrins and corroles. Unlike these other porphyrinoids, there exists only a limited number of reported phlorins containing metal centers,[153] with the majority describing gold(III) as the central atom.[154,156,157] Knowing that gold(III) phlorins have been demonstrated to be stable, our pursuit of investigating phlorins as ligands now focused upon the use of gold(III) as the metal center. Applying the same $Au(OAc)_3$ in pyridine synthetic route that has been used for corrole metallation[175-177] to the phlorin free base led to the first promising result in the formation of a metalated phlorin. Purification of the reaction containing $3H(Phl^F)$ and $Au(OAc)_3$ in pyridine led to the isolation of a brown band that eluted before the free base phlorin on a silica column. The ^1H NMR and ^{19}F NMR spectra displayed in Figure 5.1 and Figure 5.2, respectively for the isolated fraction along with mass spectrometry suggested the formation of $Au(Phl^F)$ in 10% yield (Scheme 5.2). The four doublets observed for the pyrrole backbone of the free base phlorin now give way

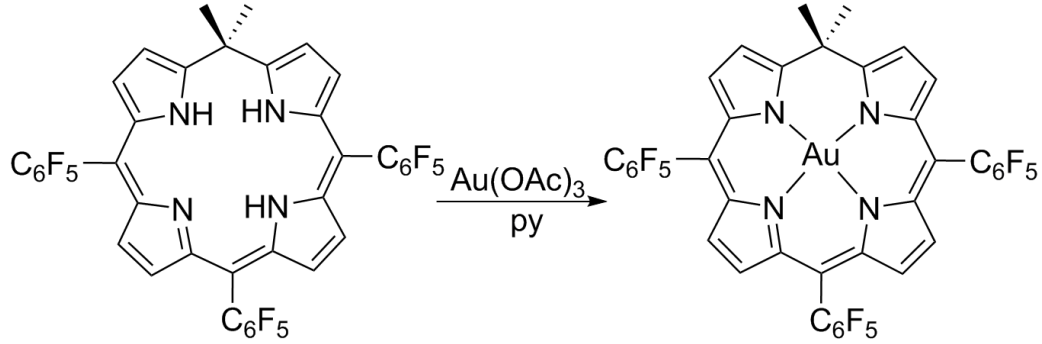

Scheme 5.2 Synthetic route for the formation of Au(Phl^{F}) in 10 % yield.

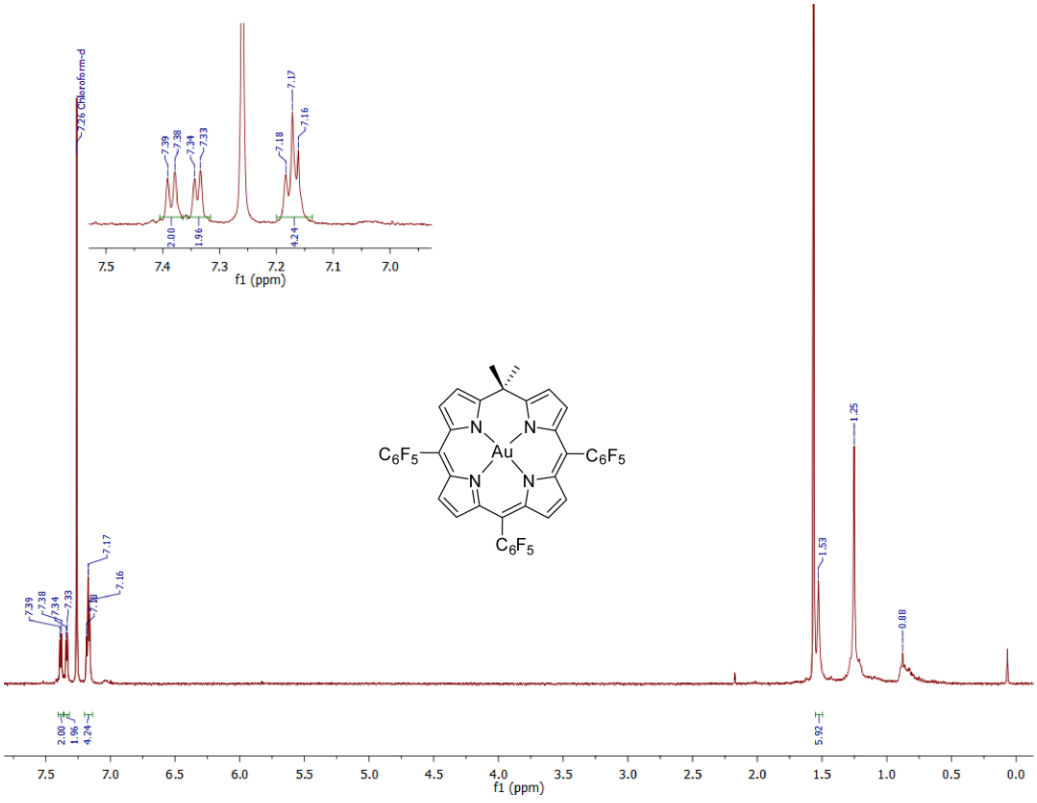

Figure 5.1 ^{1}H NMR of Au(Phl^{F}) in $CDCl_3$, with the aromatic region enlarged in the inset.

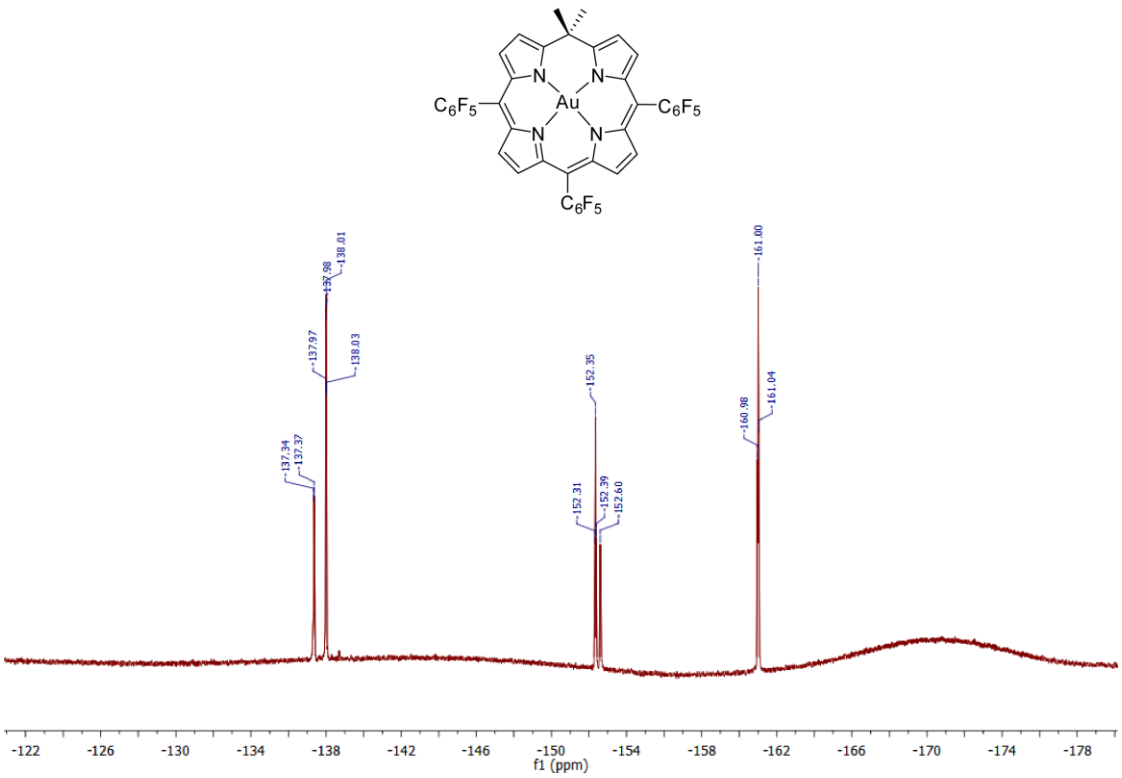

Figure 5.2 ^{19}F NMR of Au(Phl^{F}) in $CDCl_3$.

to two sets of doublets and a multiplet. This shift indicated that the electronic structure of the phlorin has changed indicative of the insertion of the gold to the core of the phlorin. This is the first example of a metalted phlorin without having to first synthesize the parent porphyrin, but proceed through the free base of the phlorin macrocycle. Having shown that the Au(Phl^{F}) can be made, improvement of the yield of the reaction now became the focus. The addition of heat to the reaction did not have a substantial effect upon the yield of the metalation reaction. DMF was chosen as a

replacement solvent for pyridine, however no reactivity was observed. The addition of NaH to the reaction failed to give the desired product.

The moderate yield for Au(Phl^F) was thought to be partially attributed to the poor solubility of the $Au(OAc)_3$, so the use of a more soluble gold(III) salt, $AuBr_3$ was explored. However, under similar conditions with pyridine, the $AuBr_3$ was unreactive and did not form Au(Phl^F). The addition of different bases was explored as summarized in Table 5.2 with MeLi, NaH and KO^{t}Bu being some of the first to be investigated. The only conditions that were found to yield product was the use of KO^{t}Bu, which provided Au(Phl^F) in 14% yield, which offered a slight improvement on the yield of the Au(Phl^F), as displayed in Scheme 5.3.

Continued efforts to increase the yield of the metalation reaction led us to explore other gold(III) sources. The first being $AuCl_3$, which was added after the deprotonation of the phlorin with KO^{t}Bu gave similar yields to that of the $AuBr_3$, (~10%). Attempts were made using potassium tetrabromoaurate(III) (K[$AuBr_4$]), however no product was isolated from the reaction.

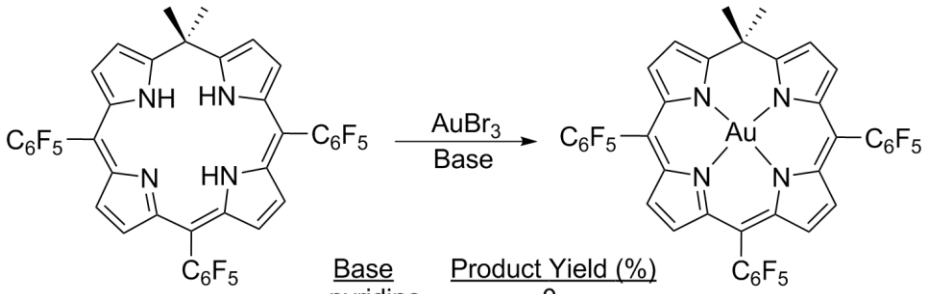

Base	Product Yield (%)
pyridine	0
MeLi	0
NaH	0
KO^{t}Bu	14
K[N(SiMe$_3$)$_2$]	0

Scheme 5.3 Synthetic route for the formation of Au(Phl^F) using $AuBr_3$ and base.

Table 5.2 Metalation conditions investigated for the formation of Au(Phl).

Metal	Reagent	Base	Conditions
Au^{I}	(THT)AuCl	pyridine	rt, N_2
	(THT)AuCl	pyridine	DDQ
	$(PEt_3)AuCl$		rt, N_2
	$(PEt_3)AuCl$	KO^tBu	rt, N_2
	(Imes)AuCl		rt, N_2
Au^{III}	$Au(OAc)_3$	pyridine	rt and heated
	$Au(OAc)_3$		rt, N_2
	$Au(OAc)_3$	NaH	rt, N_2
	$AuBr_3$	pyrindine	rt and reflux
	$AuBr_3$		DMF rt and reflux
	$AuBr_3$	MeLi	rt, N_2
	$AuBr_3$	NaH	rt, N_2
	$AuBr_3$		rt, N_2
	$AuBr_3$	KO^tBu	rt, N_2
	$AuBr_3$	$K[N(SiMe_3)_2]$	rt, N_2
	$AuBr_3$	TlOEt	rt, N_2
	$AuBr_3$	TlOAc	rt, N_2
	$AuCl_3$	KO^tBu	rt, N_2
	$Au[N(SiMe_3)_2]_3$		rt, N_2
	$K[AuBr_4]$	NaOAc	AcOH, reflux

Corroles have also shown the intriguing ability to form gold(I) complexes through bonding of one of the nitrogens in the core of the corrole.[178] Not only have these been able to be isolated, but they can also be oxidized using N-iodosuccinomide to form the gold(III) corrole. Gold(I) complexes such as $(PEt_3)Au^{I}Cl$ and $IMesAu^{I}Cl$ were examined for the ability to bind gold through one of the pyrroles of the phlorin core, however none of the Au(I) complexes that were tested showed any sign of

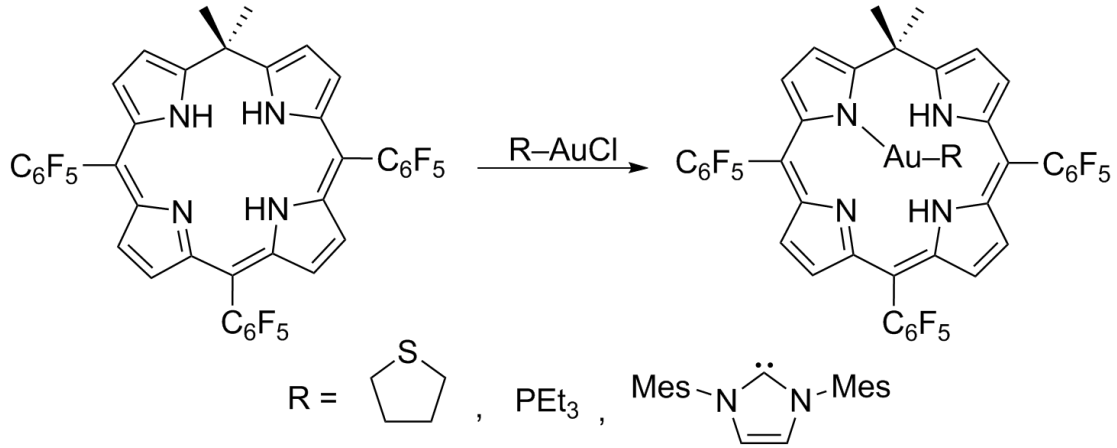

Scheme 5.4 Attempted metalation of 3H(Phl^{F}) with Au^{I} reagents.

reactivity with the phlorin (Scheme 5.4). Attempts to deprotonate one of the pyrroles to help facilitate the binding of the Au(I) did not result in the formation of product.

Therefore the most successful route for the formation of Au(Phl^{F}) was found to be the deprotonation of phlorin using KO^{t}Bu followed by the addition of $AuBr_3$, however the product is formed in only modest yield along with recovery of about 20-25% of the starting phlorin ligand. In order to investigate the low yield of the reaction the deprotonation step was evaluated further. When the phlorin is deprotonated with the KO^{t}Bu followed by the addition of ammonium chloride in aqueous workup and purification, only 56% of the starting phlorin was recovered. This is a significant loss of the phlorin and can be considered a significant contributor for the lower yield obtained for Au(Phl^{F}).

5.2.1 Synthesis of 5,5-Dimethyl-10,20-bis(pentafluorophenyl)-15-(bis-3,5-*tert*-butylphenyl)phlorin (3H(Phl$^{3,5\text{-}tBu}$))

After the synthesis of Au(Phl^{F}), several attempts were made to crystalize the compound with no success. It was hypothesized that the addition of a bulky

substituent at the 15-position would improve the crystalinity of the metalated phlorin complex, allowing us the opportunity to study the coordination geometry. The addition of a 3,5-*tert*-butylphenyl substituent at the 15-position was expected to provide the necessary steric bulk needed for quality crystal growth.

The 3H(Phl$^{3,5\text{-}tBu}$) derivative was synthesized by modifying the synthetic route used in Chapter 3, shown in Scheme 5.5. The diacylated dipyrromethane derivative (2) was reduced using $NaBH_4$ in tetrahydrofuran and methanol (3:1) as the solvent. Following the reduction, the corresponding diol was then dissolved in CH_2Cl_2 and 5-(3,5-bis(*tert*-butylphenyl)dipyrromethane (3) was added. Following the condensation in the presence of TFA, DDQ was added to oxidize the newly formed macrocycle.

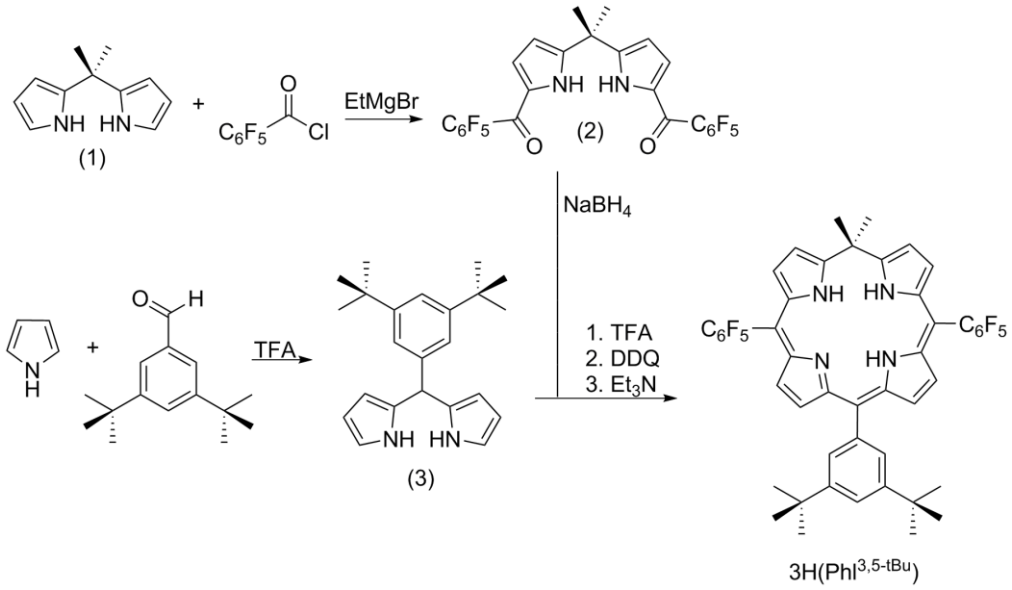

Scheme 5.5 Synthesis of 3H(Phl$^{3,5\text{-}tBu}$).

After the addition of triethylamine, the reaction was purified by column chromatography, giving the 3H(Phl$^{3,5\text{-}tBu}$) derivative in 43% yield with the ^{1}H NMR and ^{19}F NMR spectra shown in Figure 5.3 and Figure 5.4, respectively.

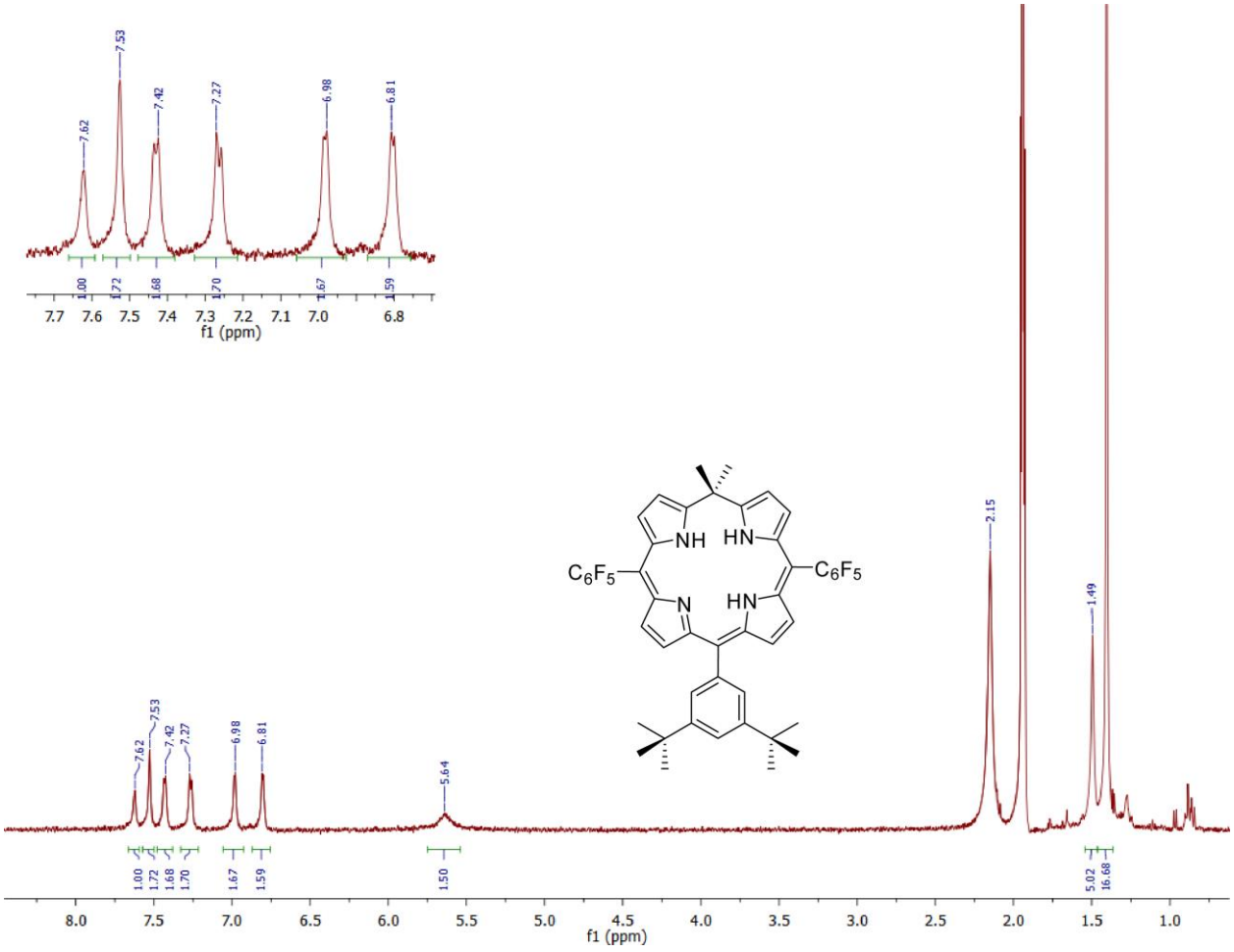

Figure 5.3 ^{1}H NMR of 3H(Phl$^{3,5\text{-}tBu}$) in CD_3CN, with the aromatic region enlarged in the inset.

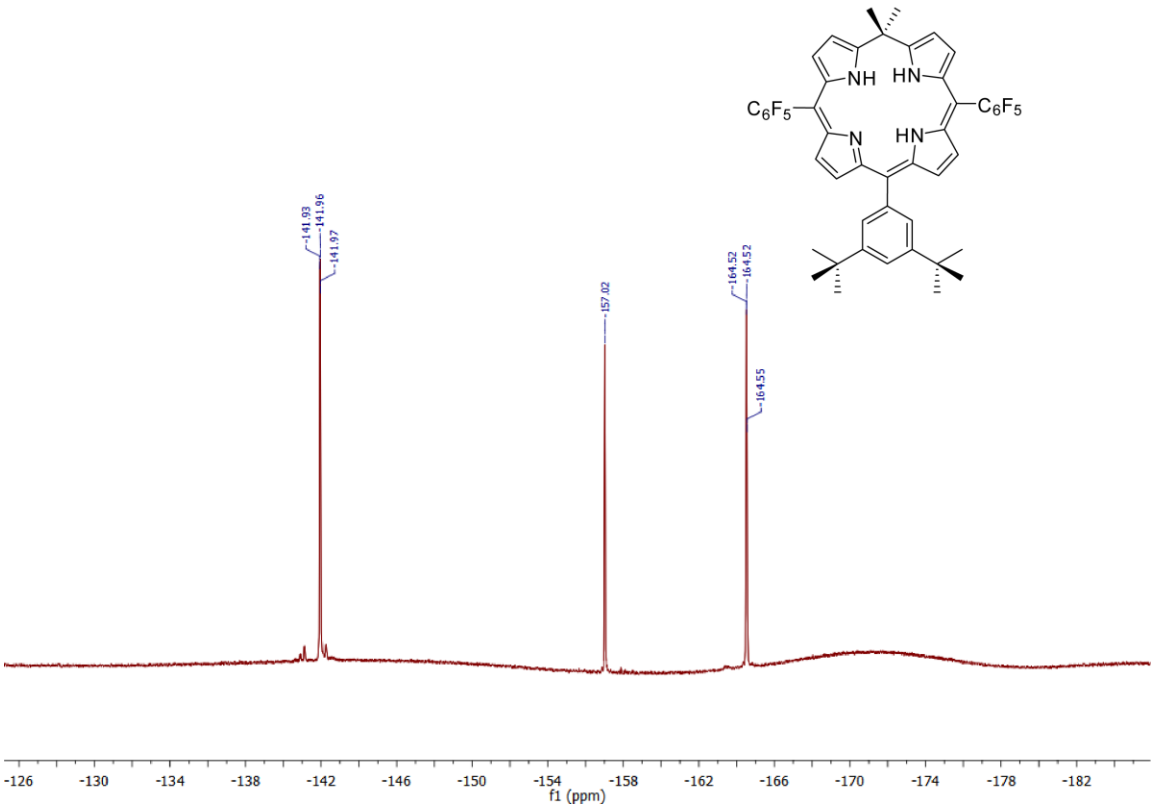

Figure 5.4 ^{19}F NMR of 3H(Phl$^{3,5\text{-tBu}}$) in CD_3CN.

5.2.2 Synthesis of gold(III) (5,5-Dimethyl-10,20-bis(pentafluorophenyl)-15-(bis-3,5-*tert*-butylphenyl)phlorin) (Au(Phl$^{3,5\text{-tBu}}$))

Au(Phl$^{3,5\text{-tBu}}$) was synthesized using the same procedure described as before for the formation of Au(Phl^{F}) as depicted in Scheme 5.6. 3H(Phl$^{3,5\text{-tBu}}$) was dissolved in a THF and toluene (1:30) mixture and cooled to –35 °C followed by the addition of KO^{t}Bu and $AuBr_3$. Following column chromatography, the formation of Au(Phl$^{3,5\text{-tBu}}$) was confirmed by NMR and mass spectrometry as a brown solid in 9% yield, with the ^{1}H and ^{19}F NMR spectra shown in Figure 5.5 and Figure 5.6, respectively.

Scheme 5.6 Synthetic pathway for the formation of Au(Phl).

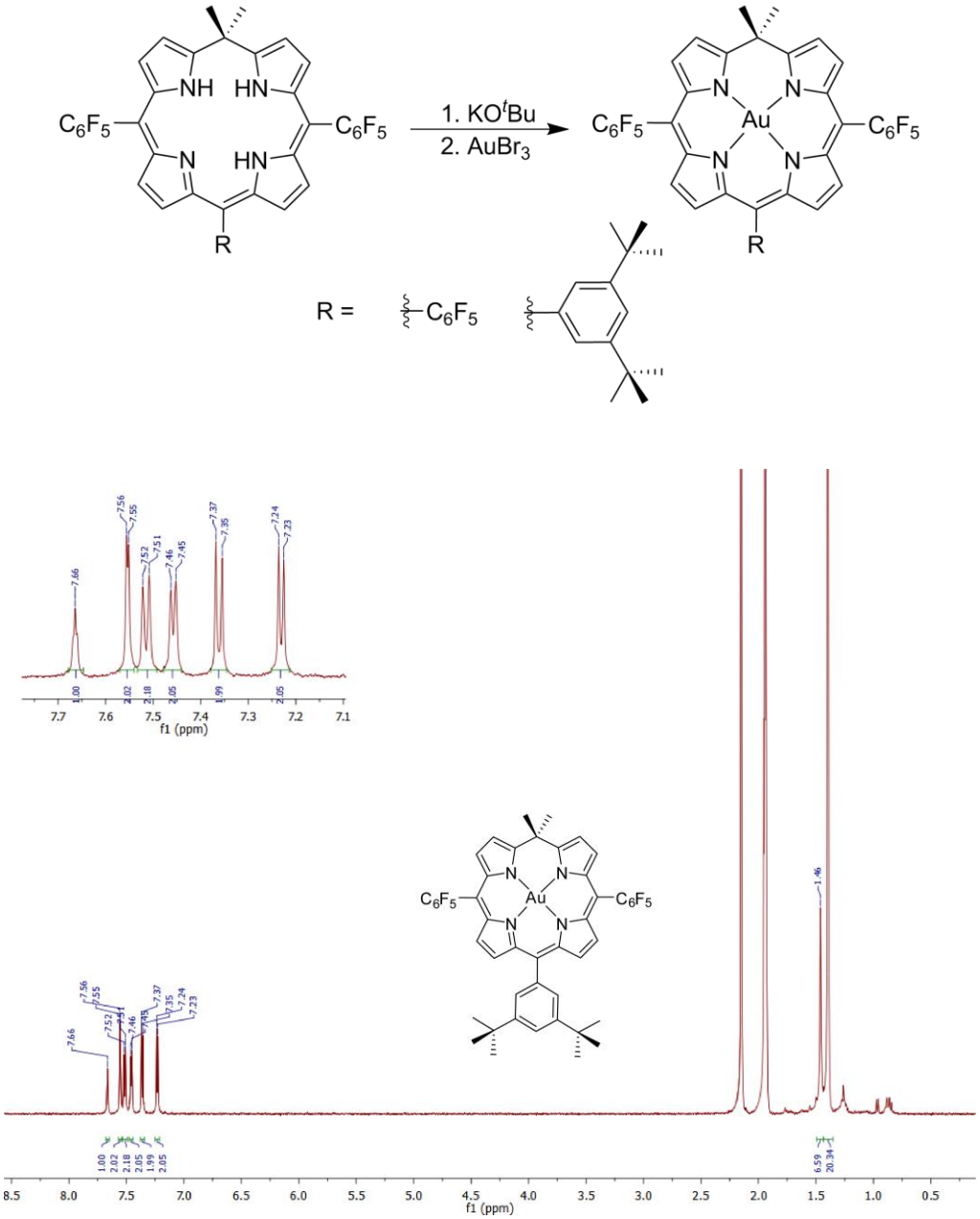

Figure 5.5 ^{1}H NMR of Au(Phl$^{3,5\text{-}tBu}$) in CD_3CN, with the aromatic region enlarged in the inset.

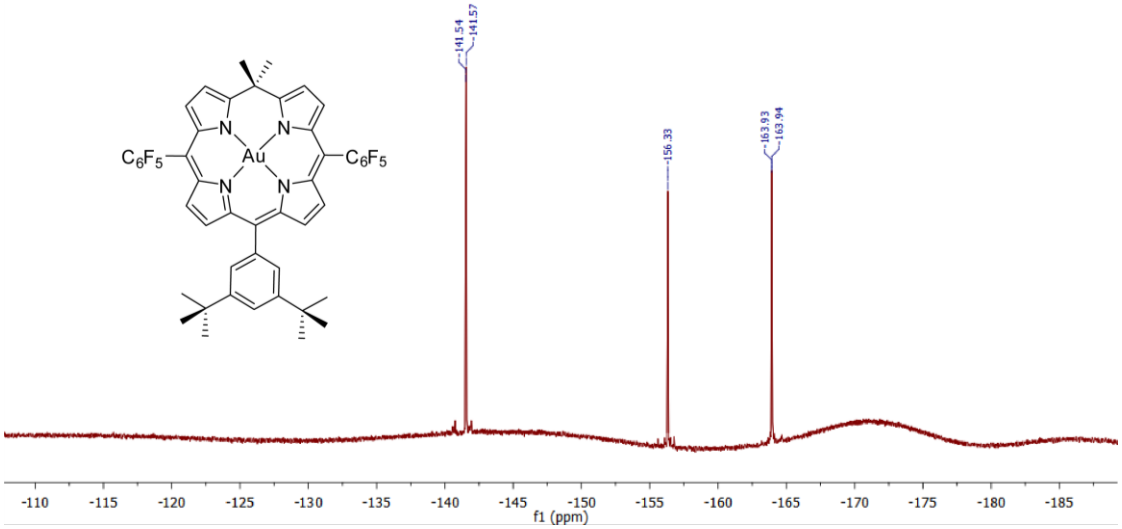

Figure 5.6 ^{19}F NMR of Au(Phl$^{3,5\text{-}tBu}$) in CD_3CN.

5.2.3 Crystal Structure of Au(Phl$^{3,5\text{-}tBu}$)

The solid state structure of Au(Phl$^{3,5\text{-}tBu}$) was obtained from the slow evaporation of 1:1 solvent mixture of dichloromethane and acetonitrile and marks the first crystallographically studied gold(III) phlorin with geminal 5,5'-dimethyl substitution. The coordination of the central gold(III) atom causes a very distinct change in the overall geometry of the phlorin macrocycle. The puckering that was observed for the free base structures described in Chapters 3 and 4 is greatly reduced. The coordination around the central gold atom is square planar with respect to the nitrogens of the pyrrole groups. The increase in the planar nature of the Au(Phl$^{3,5\text{-}tBu}$) is easily seen in the side view of Figure 5.7.

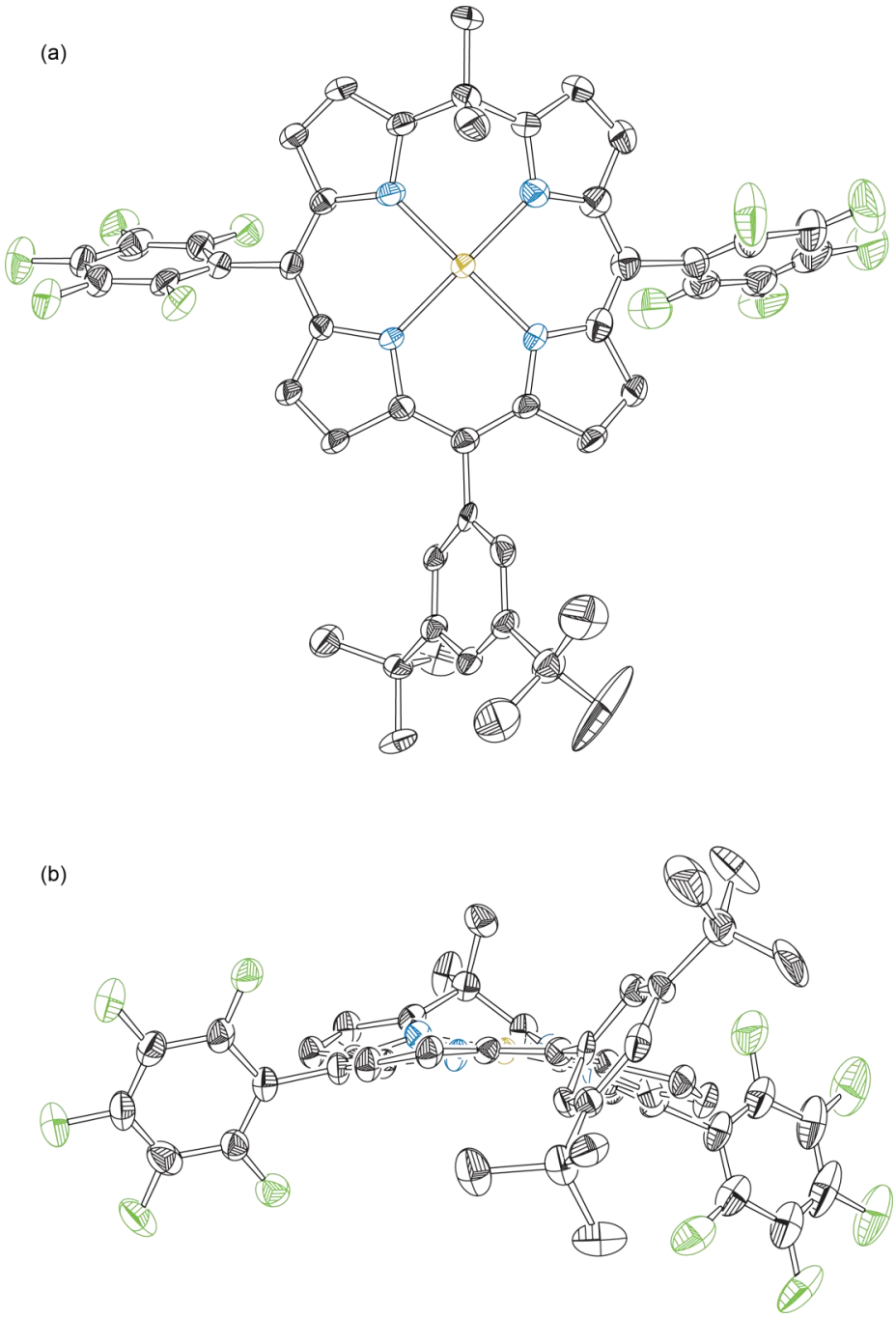

Figure 5.7 Crystal structure of Au(Phl$^{3,5\text{-}tBu}$) with view from (a) top and (b) side on. All hydrogen atoms were omitted for clarity and thermal ellipsoids are shown at 50% probability.

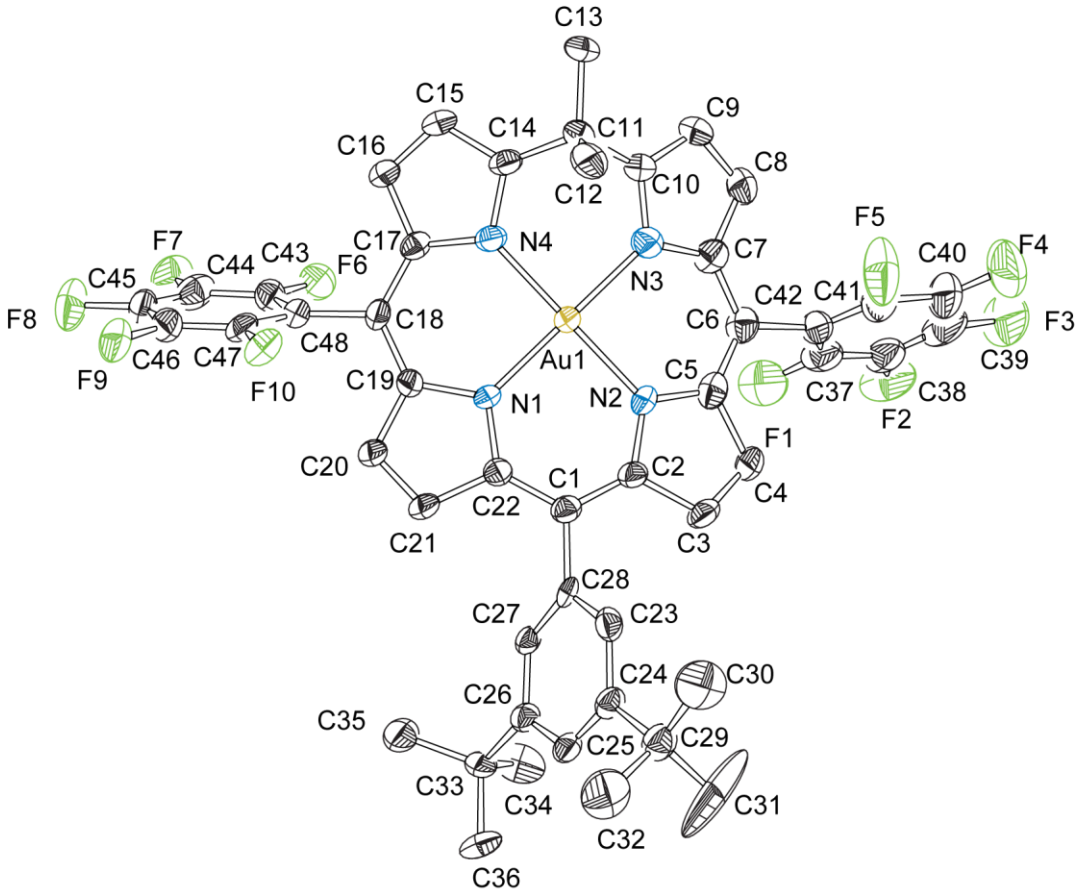

Figure 5.8 Numbered crystal structure of Au(Phl$^{3,5\text{-}tBu}$) with all hydrogen atoms omitted for clarity and thermal ellipsoids shown at 50% probability.

Table 5.3 Selected bond lengths and angles for Au(Phl$^{3,5\text{-}tBu}$).

Atoms	Bond Lengths (Å)	Atoms	Bond Angles (°)
Au(1)-N(1)	1.997(10)	**N(4)-Au-N(1)**	90.2(4)
Au(1)-N(2)	2.006(10)	**N(4)-Au-N(3)**	90.0(5)
Au(1)-N(3)	2.005(11)	**N(1)-Au-N(3)**	178.5(5)
Au(1)-N(4)	1.994(10)	**N(4)-Au-N(2)**	178.8(5)
		N(1)-Au-N(2)	90.1(4)
		N(3)-Au-N(2)	89.7(5)

5.2.4 Absorption Profile of Metaled Phlorins

The coordination of a central gold atom causes distinct changes in both the electronic and geometric structure of the phlorin. This can be seen in part through the changes in the absorption profile for the metalated derivatives compared to the free base phlorins. Au(Phl^{F}) has an absorption profile that differs significantly from the free base 3H(Phl^{F}) as shown in Figure 5.9, where the free base has a Soret maximum at 435 nm (ε = 29300) and Q band maximum at 655 nm (ε = 16000). Au(Phl^{F}) has a Soret maximum at 449 nm (ε = 52970) and a Q band maximum at 774 nm (ε = 16530). The Soret maxima occur at similar wavelengths for both the gold and free base phlorins, however the molar absorptivity for the gold phlorin is almost twice that of the free base. The longer wavelength absorptions differ considerably, as the coordination of gold causes the Q band absorption to red-shift by almost 120 nm. It is of note that the coordination of gold causes a shift in the absorption profile reminiscent of the binding of anions discussed in previous chapters.

The absorption profile for 3H(Phl$^{3,5\text{-}tBu}$) resembles those seen for the other phlorin derivatives discussed in Chapter 3 with electron donating substituents at the 15-position. 3H(Phl$^{3,5\text{-}tBu}$) has a Soret maximum at 426 nm (ε = 37210) along with a Q band maximum at 671 nm (ε = 23990)as displayed in Figure 5.10. As with the pentafluorophenyl substituted phlorin derivative there are significant changes in the absorption profile with the coordination of gold. Au(Phl$^{3,5\text{-}tBu}$) has a Soret maximum at 452 nm (ε = 46770) and long wavelength absorption maximum at 781 nm (ε = 16200). There is an enhancement in the molar absorptivity in the Soret region upon the addition of gold along with the red shifting longer wavelength absorption that is consistent with the results from the pentafluorophenyl derivatives as well as those previously reported.[154,156,157]

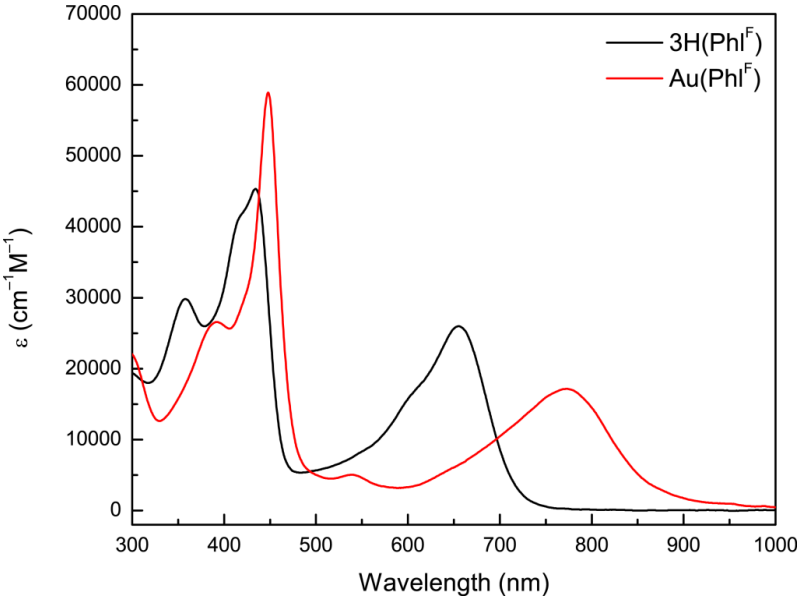

Figure 5.9 Absorption profiles of 3H(Phl^{F}) and Au(Phl^{F}) obtained from solutions made from CH_2Cl_2.

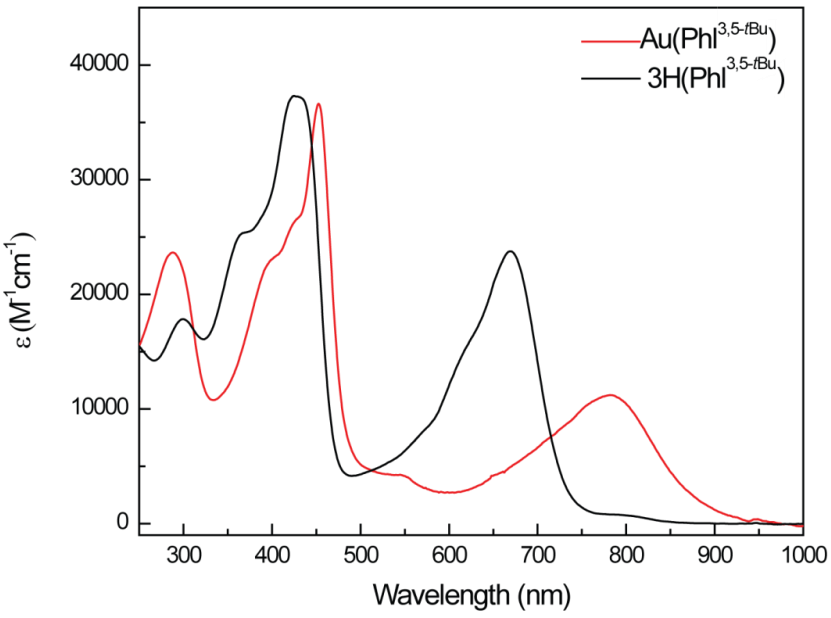

Figure 5.10 Absorption profiles of 3H(Phl$^{3,5\text{-tBu}}$) and Au(Phl$^{3,5\text{-tBu}}$) obtained from solutions made from CH_2Cl_2.

The emission profiles for each of the gold phlorin derivatives were also investigated. However, not surprisingly, there was no fluorescence detected for either of the gold phlorin derivatives in deaerated CH_2Cl_2 at room temperature as the central gold atom likely quenches the phlorin fluorescence via the heavy atom effect.

5.2.5 TD-DFT Calculated Transitions

Density functional theory (DFT) and time-dependent DFT (TD-DFT) were used to further ellucidate the electronic structure of Au($Phl^{3,5\text{-}tBu}$). These calculations showed that the frontier molecular orbitals that are involved in the major transitions display electron density distributed throughout the phlorin ligand, with the HOMO–2, LUMO and LUMO+1 also containing electron density at the gold metal center. The TD-DFT calculations revealed that the major transition in the Soret region (~450 nm) is comprised of several different electronic states from HOMO–2 to LUMO+2, as represented in Figure 5.11. The longer wavelength absorption that occurs at ~770 nm appears to arise from transitions between HOMO to LUMO and HOMO to LUMO+1, with the LUMO and LUMO+1 being relatively close in energy. This is reminiscent of the transitions calculated for the free base phlorin macrocycle, as discussed in Chapter 4. The introduction of gold(III) to the center of the phlorin macrocycle does have an impact upon the frontier molecular orbitals that are involved in the transitions, however it is clear that the majority of the electron density remains on the phlorin macrocycle.

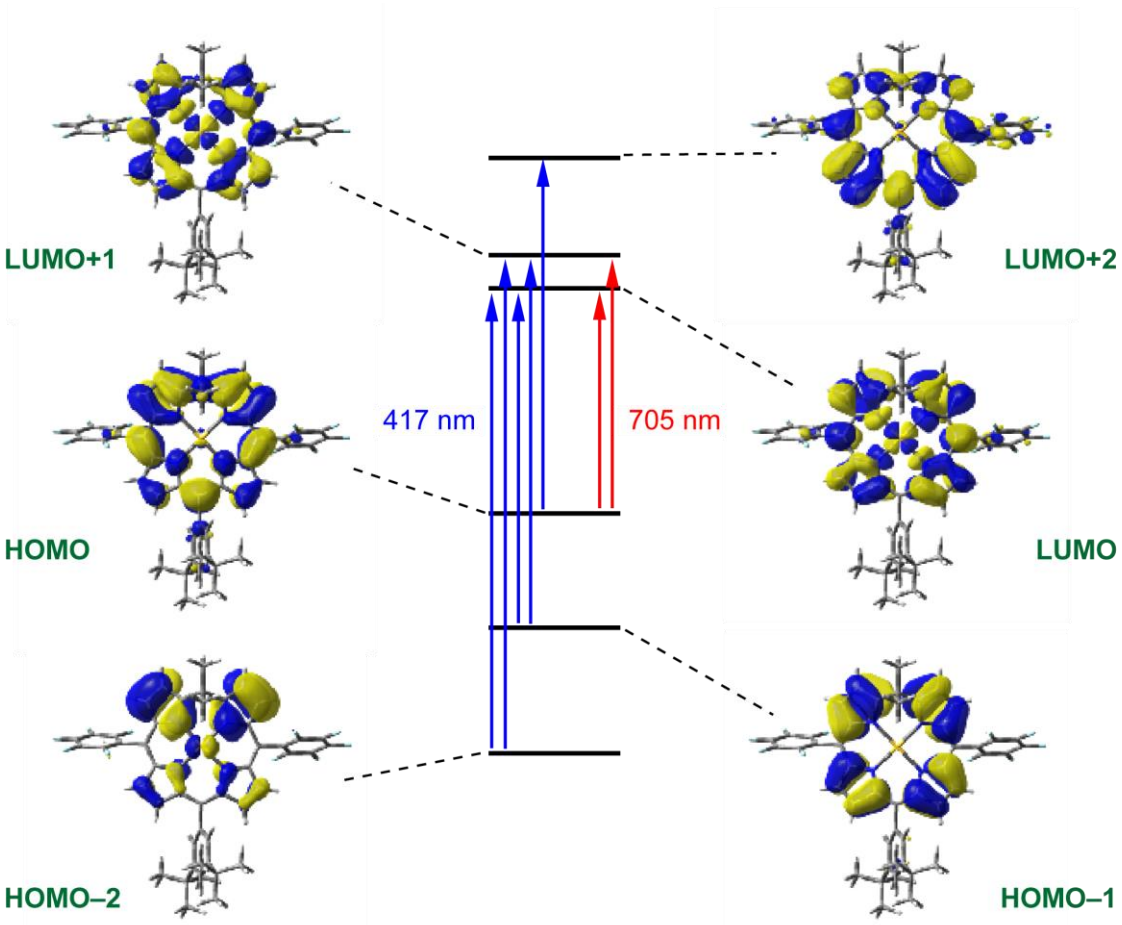

Figure 5.11 Representation of the molecular orbitals involved in the major Soret and Q-band transitions of Au(Phl$^{3,5\text{-}tBu}$).

5.2.6 Solvatochroism of Au(Phl^{F}) and Au(Phl$^{3,5\text{-}tBu}$)

Like the calculations of the free base 3H(Phl^{CF3}), one of the calculated unoccupied molecular orbitals of Au(Phl) (i.e. LUMO+2) displays asymmetry with respect to the electron density on the macrocycle. This polarized molecular orbital state would be expected to display charge transfer character that would be sensitive to the polarity of the surrounding solvent. The solvatochroic behavior of Au(Phl) was

probed by measuring the absorption profile of the gold(III) phlorin complexes in a variety of solvents of differing polarities.

The absorption profiles for Au(Phl^{F}) and Au($Phl^{3,5\text{-}tBu}$) were measured in several different solvents, as displayed in Figure 5.12 and Figure 5.13, respectively. The Soret maxima for both of the gold(III) phlorins were influenced by the polarity of the solvents tested. Au(Phl^{F}) was found to have a Soret maximum at 455 nm in the non-polar benzene ($\varepsilon = 2.27$), while the maximum was shifted to 449 nm in the polar acetonitrile ($\varepsilon = 37.5$). This shift in the maximum wavelengths indicates the surrounding solvent can influence the energy of the molecule's LUMO+2. Analyzing the maxima obtained from the other solvents and plotting them with the corresponding dielectric constant from solvent reveals a linear trend displayed in Figure 5.14a.

Au($Phl^{3,5\text{-}tBu}$) was found to have a similar trend in the Soret region of the absorption profile, with the maximum of 455 nm in benzene and 444 nm in acetonitrile. Figure 5.14b is the plot of the Soret maxima in several solvents versus the dielectric constants of the solvents, which again reveals a linear trend. The results of the gold(III) phlorin complexes displaying solvatochroism for the transitions involved with the Soret absorption is similar to that of the free base phlorin (3H(Phl^{CF3})) discussed in Chapter 4. However, one noticeable difference with the gold(III) phlorins is the shifts in the maxima of the long wave absorption. Figure 5.15 shows that both Au(Phl^{F}) and Au($Phl^{3,5\text{-}tBu}$), respectively, display solvatochroism for the maxima in the Q-band region. This cannot be readily explained with the current TD-DFT calculations displayed in Figure 5.11, as the LUMO and LUMO+1 associated with this transition appear to have rather symmetric electron density distribution throughout the phlorin macrocycle.

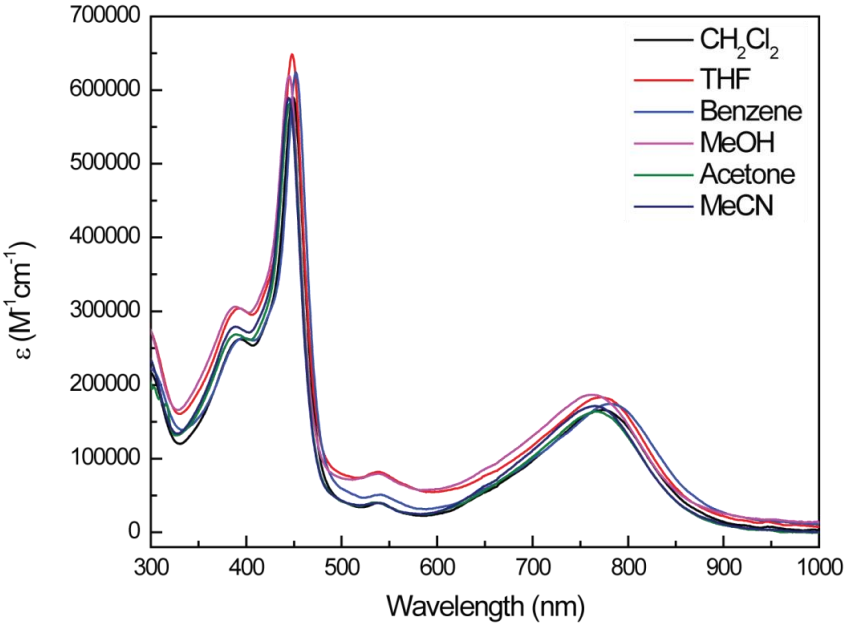

Figure 5.12 Absorbance spectra of Au(Phl^{F}) taken in solvents of differing polarity.

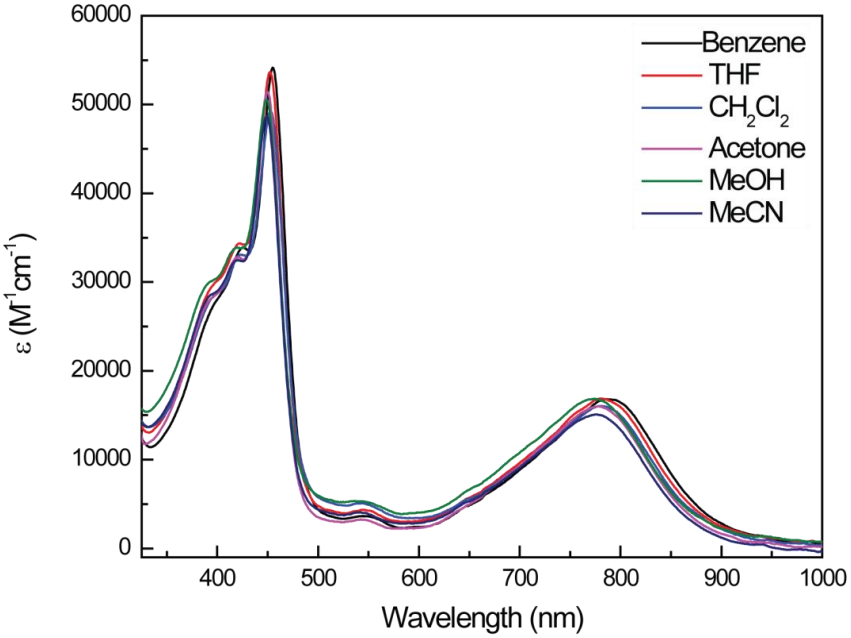

Figure 5.13 Absorbance spectra of Au(Phl^{F}) taken in solvents of differing polarity.

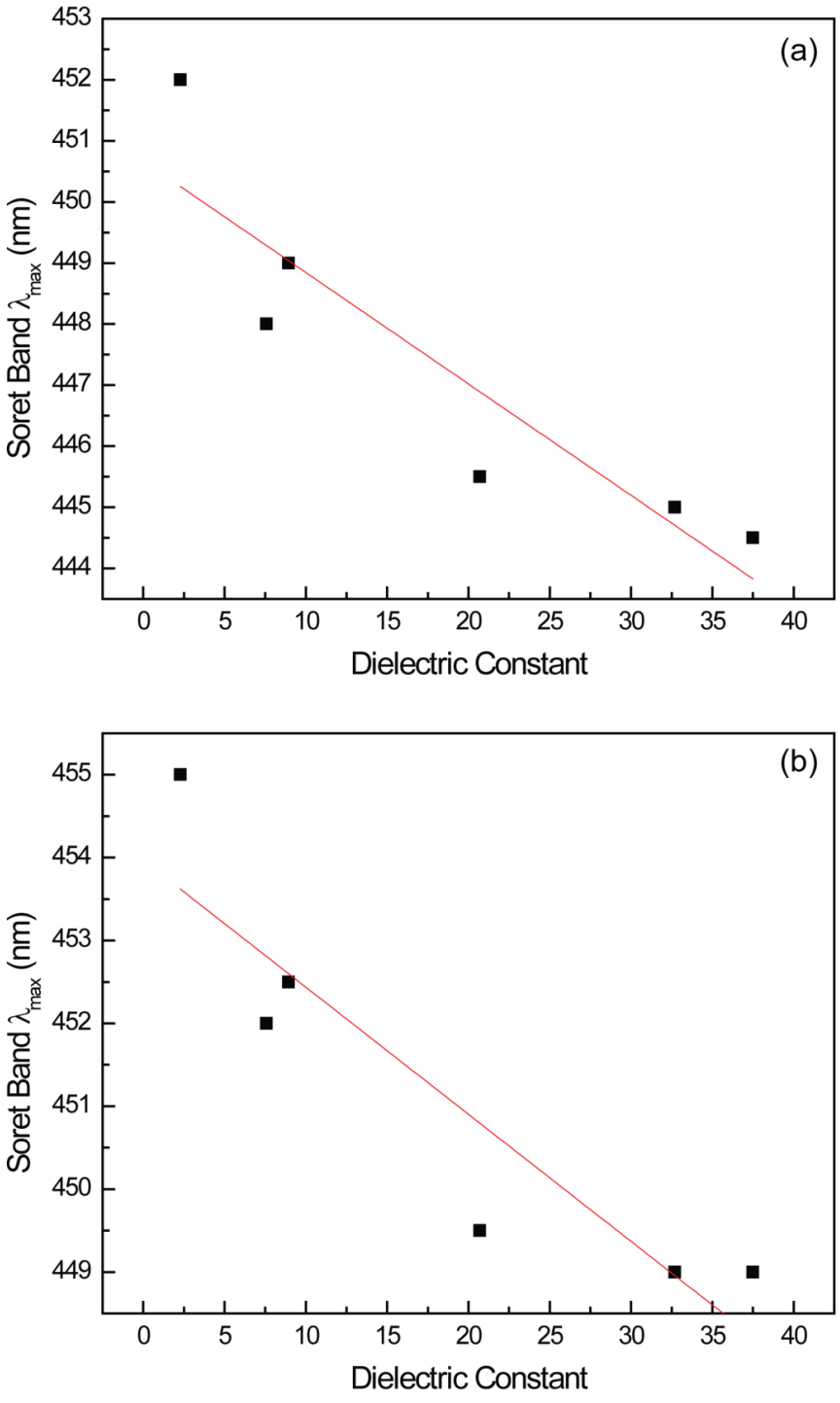

Figure 5.14 Plots displaying the effect of the solvent polarity on the λ_{max} of the Soret band for (a) Au(Phl^{F}) and (b) Au(Phl$^{3,5\text{-}tBu}$).

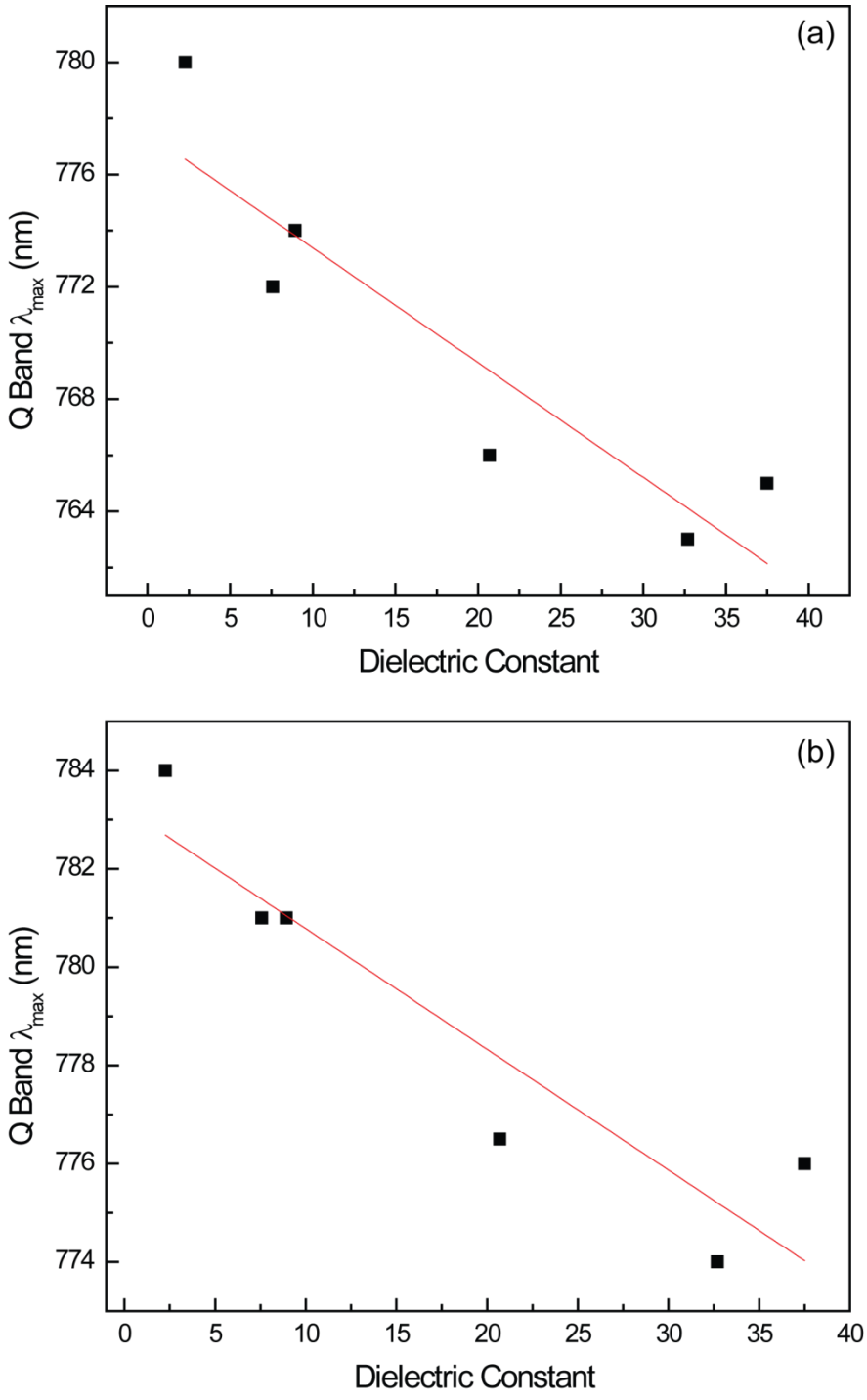

Figure 5.15 Plots displaying the effect of the solvent polarity on the λ_{max} of the Q-band for (a) Au(Phl^{F}) and (b) Au(Phl$^{3,5\text{-}tBu}$).

5.2.7 Redox Chemistry of Au(Phl^{F}) and Au(Phl$^{3,5\text{-}tBu}$)

The redox chemistry for each of the phlorin derivatives was probed through cyclic voltammetry (CV) and differential pulse voltammetry (DPV) and the resulting traces are displayed in Figure 5.16 and Figure 5.17, respectively. The redox chemistry of 3H(Phl^{F}) has previously been demonstrated to have three quasi reversible oxidations ($E_{ox}(1)$ = 0.75 V, $E_{ox}(2)$ = 0.99 V, $E_{ox}(3)$ = 1.26 V) and two irreversible reductions ($E_{red}(1)$ = –0.93 V, $E_{red}(2)$ = –1.43 V). The CV trace observed for 3H(Phl$^{3,5\text{-}tBu}$) is similar to that of 3H(Phl^{F}) where that are three quasi reversible oxidations and two largely irreversible reductions. In keeping with the trend that was previously observed, the electronics of the phlorin systems can be modified through substitution at the 15-position. The electron donating group of the 3,5-*tert*-butylphenyl causes a shift in the redox potentials. The first oxidation of 3H(Phl$^{3,5\text{-}tBu}$) occurs at $E_{ox}(1)$ = 0.59 V, with the second and third oxidations occurring at $E_{ox}(2)$ = 0.84 V, and $E_{ox}(3)$ = 1.04 V, respectively. The irreversible reductions occur at $E_{red}(1)$ = –1.03 V and $E_{ox}(1)$ = –1.56 V, which are consistent with the other electron rich phlorins, 3H(Phl^{Mes}) and 3H(Phl^{OMe}) studied in Chapter 3.

With the redox chemistry of the free base phlorins established, the effect on the electronic structure of the phlorin through the addition of gold could now be investigated. The redox chemistry of Au(Phl^{F}) is quite different compared to that of the free base phlorin. In the oxidative region there are only two fully reversible oxidations at $E_{ox}(1)$ = 0.73 V and $E_{ox}(2)$ = 1.16 V. The first oxidation for both the free base and gold derivatives occur at almost the same potential, differing by only 20 mV, while the second oxidation potential for Au(Phl^{F}) occurs between the second and third oxidations of the corresponding free base, 3H(Phl^{F}). There are two reductions observed for Au(Phl^{F}) at $E_{red}(1)$ = –0.88 V and $E_{red}(2)$ = –1.46 V that are fully

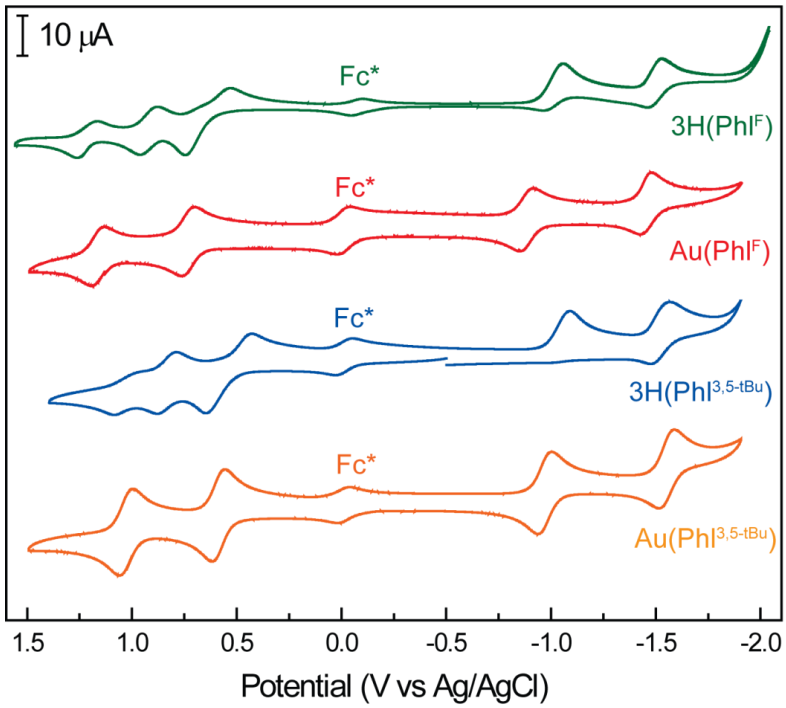

Figure 5.16 Cyclic voltammograms recorded for gold(III) and free base phlorins (1 mM) at a scan rate of 50 mv/s in CH_2Cl_2 containing $TBAPF_6$ with an internal decamethylferrocene standard (Fc*).

reversible, which is in contrast to the largely irreversible reductions of the free base phlorin. The potentials at which the reductions occur are very similar between the free base 3H(Phl^F) and Au(Phl^F).

The redox chemistry observed for Au(Phl$^{3,5\text{-}tBu}$) is very similar to that observed for the Au(Phl^F) derivative. There are two reversible oxidations at $E_{ox}(1) = 0.59$ V and $E_{ox}(2) = 1.04$ V and two reversible reductions that occur at $E_{red}(1) = –0.97$ V and $E_{red}(2) = –1.56$ V. The ability to attenuate the redox potentials through the substitution at the 15-position observed for the free base phlorins is maintained with the coordination of gold to the center. The more electron rich Au(Phl$^{3,5\text{-}tBu}$) is more easily

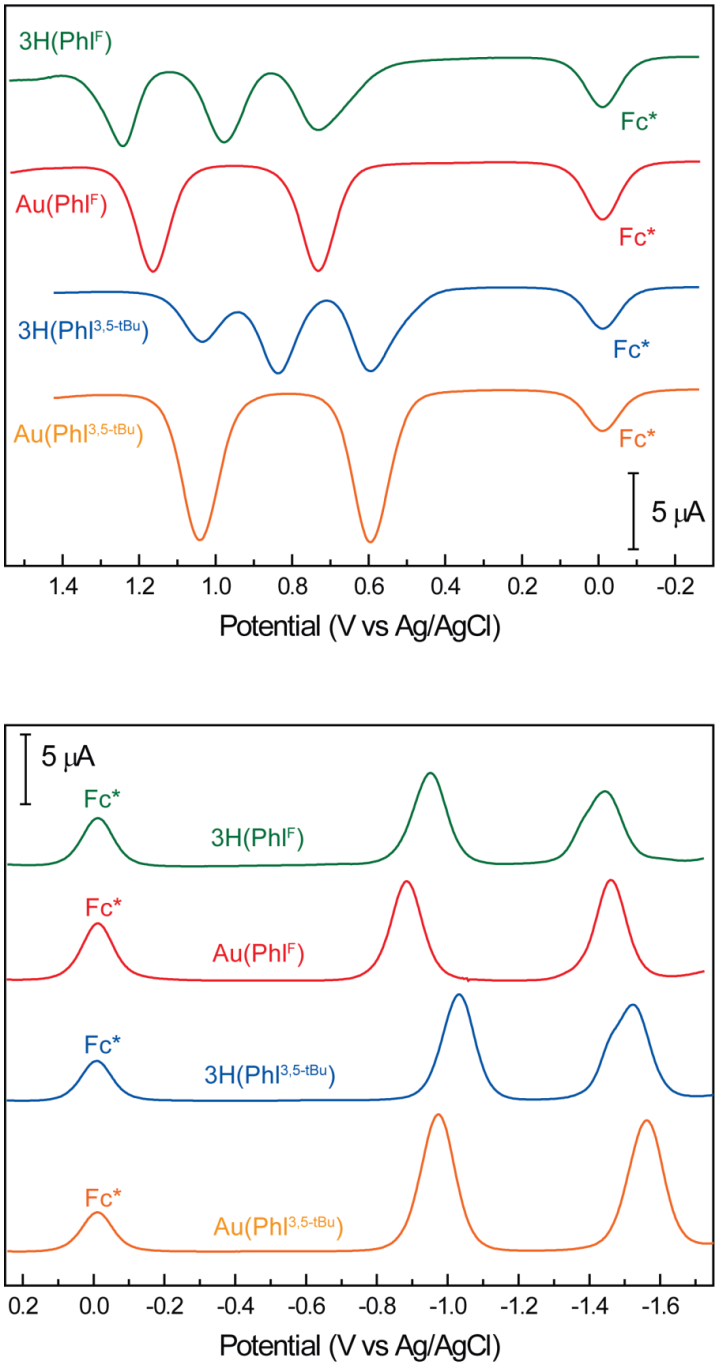

Figure 5.17 Differential pulse voltammograms recorded for gold(III) and free base phlorin derivatives (1 mM) in CH_2Cl_2 containing $TBAPF_6$ and internal decamethylferrocene standard (Fc*).

oxidized than the electron poor Au(Phl^{F}), with both the gold(III) phlorins able to undergo the first oxidation at essentially the same potential as their respective free base phlorin scaffolds. A similar trend is observed with the reduction potentials, where the electron poor gold and free base pentafluorophenyl derivatives are reduced at less negative potentials than the electron rich 3,5-*tert*-butylphenyl derivatives.

Table 5.4 Redox potentials recorded for the gold(III) and free base phlorins.

	redox properties					
	$E_{ox}(1)$, V	$E_{ox}(2)$, V	$E_{ox}(3)$, V	$E_{red}(1)$, V	$E_{red}(2)$, V	E_{0-0}, V
3H(Phl^{F})	0.75	0.99	1.26	–0.93	–1.43	1.68
3H(Phl$^{3,5\text{-}tBu}$)	0.59	0.84	1.04	–1.03	–1.52	1.62
Au(Phl^{F})	0.73	1.16		–0.88	–1.46	1.61
Au(Phl$^{3,5\text{-}tBu}$)	0.59	1.04		–0.97	–1.56	1.56

5.3 Au(Phl) as a Catalyst for Hydrogen Production

The photochemical production of hydrogen gas from water has been a long standing goal in the field of molecular energy conversion. There have been several different molecular catalysts that have been developed for the formation of H_2 under photochemical conditions.[179] Some of the most successfully studied systems are binuclear catalysts developed in the Nocera group shown in Scheme 5.7, which began with the study of a binuclear rhodium catalyst.[180] These bimetallic rhodium complexes led to the photochemical release of H_2 from homogeneous H-X solutions, however it was determined that the reactivity of the these catalysts was hindered by the slow release of the dihalogen product. This system was further improved by the formation

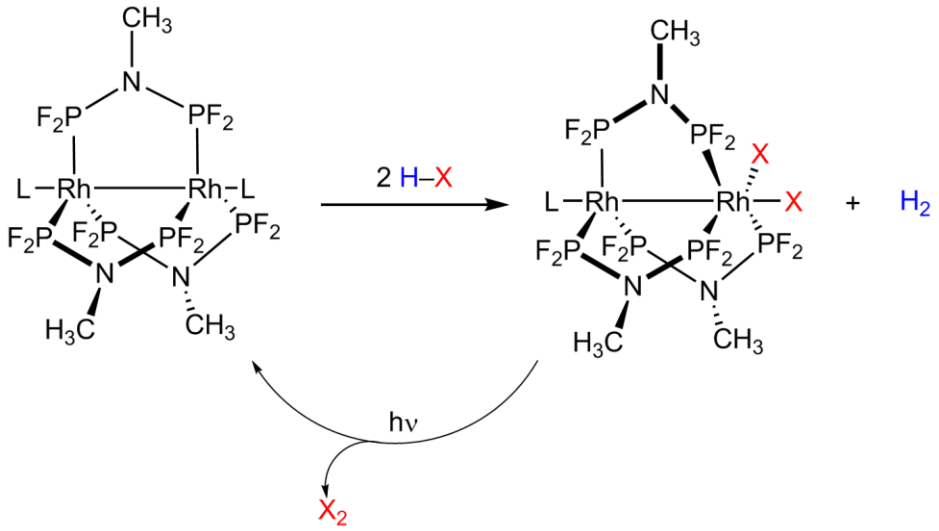

Scheme 5.7 The photochemical production of H_2 from a bimetallic rhodium complex.

of mixed heterobimetallic complexs containing either a rhodium or platinum center and one gold center.[181,182] Gold halogen complexes have shown to be light-sensitive,[183] allowing for easier release of the dihalogen product improving the overall reactivity.

With the use of these bimetallic systems as photocatalysts for the production of H_2 well established, we looked to implement the gold(III) phlorin as a potential catalysts for this process. Scheme 5.8 displays the potential route in which these gold phlorin systems could have a viable impact of the study of energy storing catalysis. The addition of an acid, such as hydrochloric acid, could allow for the formation of hydrogen gas and oxidized gold phlorin species, $Au(Cl)_2(Phl^{3,5\text{-}tBu})$. Following the use of light and the subsequent reductive elimination of an equivalent chlorine gas the gold phlorin would return to the initial state to re-enter the catalytic cycle. The unique properties of the phlorin macrocycle such as broadened absorption spectra and

multielectron redox chemistry make the phlorin an intriguing ligand for this transformation. The ability to be oxidized and reduced at modest potentials creates an opportunity to use these non-innocent ligands to help drive the formation of a useful product such as hydrogen gas.

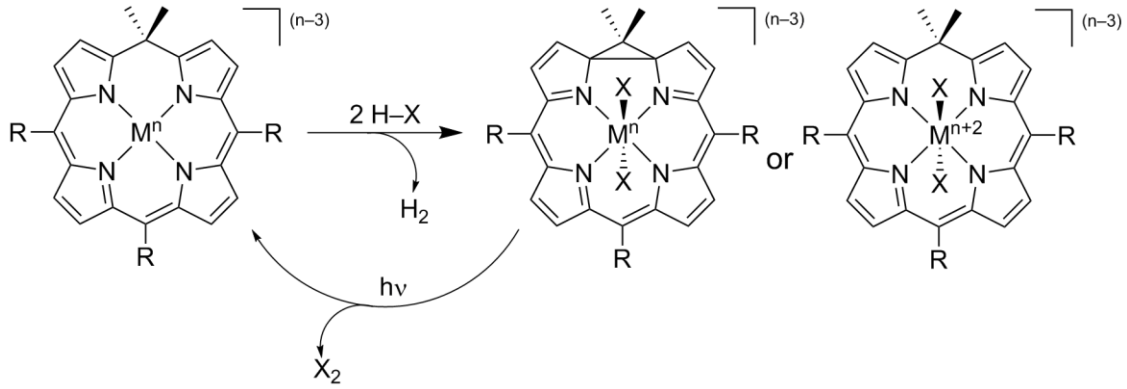

Scheme 5.8 Potential scheme for the use of the metalated phlorin macrocycle as a photocatalyst for the production of H_2 from acidic solutions.

5.3.1 Reactivity of (Dichloroiodo)benzene with Au(Phl$^{3,5\text{-}tBu}$)

In order to gain insight in to the validity of the use of gold phlorins for this transformation, the formation of the $Au(Cl)_2(Phl^{3,5\text{-}tBu})$ intermediate was first investigated. (Dichloroiodo)benzene ($PhICl_2$), which is a convenient source of Cl_2, provided the opportunity to oxidize the $Au(Phl^{3,5\text{-}tBu})$ and supply the needed chloride anions to provide a direct route to the formation of $Au(Cl)_2(Phl^{3,5\text{-}tBu})$ as shown in Scheme 5.9.

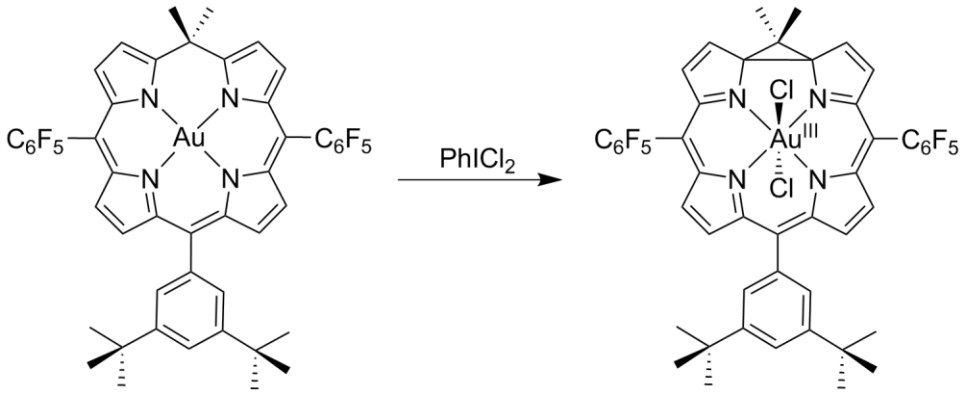

Scheme 5.9 Proposed reaction of Au(Phl$^{3,5\text{-}tBu}$) with $PhICl_2$.

The attempted synthesis of Au(Cl)$_2$(Phl$^{3,5\text{-}tBu}$) began with the addition of one equivalent of $PhICl_2$ to a solution of Au(Phl$^{3,5\text{-}tBu}$) in CH_2Cl_2 . After stirring at room temperature for 36 hours, the reaction was purified by column chromatography. Two major fraction giving brown solids were isolated and characterized. The ^{1}H NMR of the first brown fraction shown in Figure 5.18 was consistent with that of a symmetric gold phlorin macrocycle with the disappearance of two protons from the aromatic region. The ^{19}F NMR spectrum in Figure 5.19 also confirmed the retention of symmetry of the phlorin macrocycle, with the three resonances for the pentafluorophenyl groups at the 10 and 20 positions. Mass spectrometry began to shed light upon the explanation of the loss of the two aromatic protons from the phlorin scaffold. The results from the mass spectrometry data suggested that the chlorine anions did add to Au(Phl$^{3,5\text{-}tBu}$), however they did not coordinate to the gold center, but had substituted on the pyrrole backbone of the phlorin. This was confirmed by obtaining a crystal structure of the product (Figure 5.20), revealing the chlorination at the 2- and 8-positions of the phlorin scaffold.

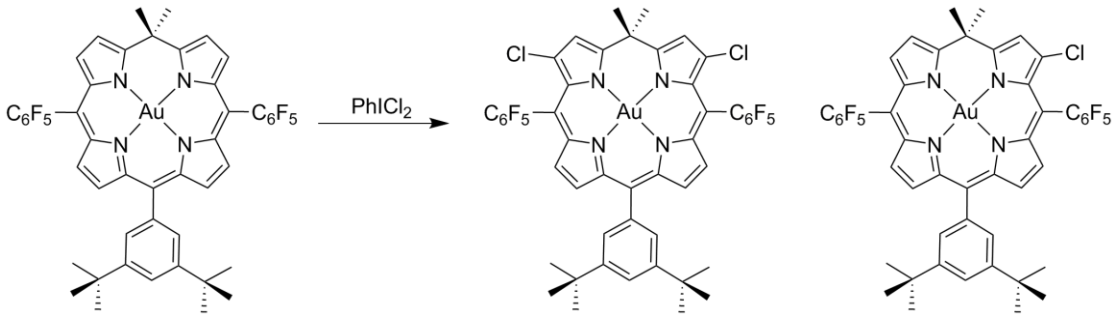

Scheme 5.10 Reaction products isolated from the reactivity of $PhICl_2$ with $Au(Phl^{3,5\text{-}tBu})$.

The second fraction that was isolated from the reaction of $PhICl_2$ and $Au(Phl^{3,5\text{-}tBu})$ gave a ^{1}H NMR spectrum shown in Figure 5.22 that resembled an asymmetric phlorin structure, unlike the data obtained for the first fraction. ^{19}F NMR spectrum in Figure 5.23 confirmed the asymmetric phlorin, with the six resonances observed in the spectrum, indicating the pentafluorophenyl rings at the 10 and 20 position are different. The use of mass spectrometry indicated that the product was the result of the addition of a single chloride anion to the pyrrole back bone. The crystal structure in Figure 5.24 revealed the site of chlorination was at the 2-position.

The results from the reaction of $PhICl_2$ and $Au(Phl^{3,5\text{-}tBu})$ suggests that the addition of chlorine to the phlorin back bone is regionally selective for the 2- and 8-positions as shown in Scheme 5.10 and does not display the desired dichlorinated gold species shown in Scheme 5.5. This positioning can be rationalized using the calculated electronic structures of the gold(III) phlorin displayed in Figure 5.6 where there is significant electron density displayed near the 2- and 8-positions of the HOMO-2 molecular orbital representation, which would be the result of the two electron oxidation product.

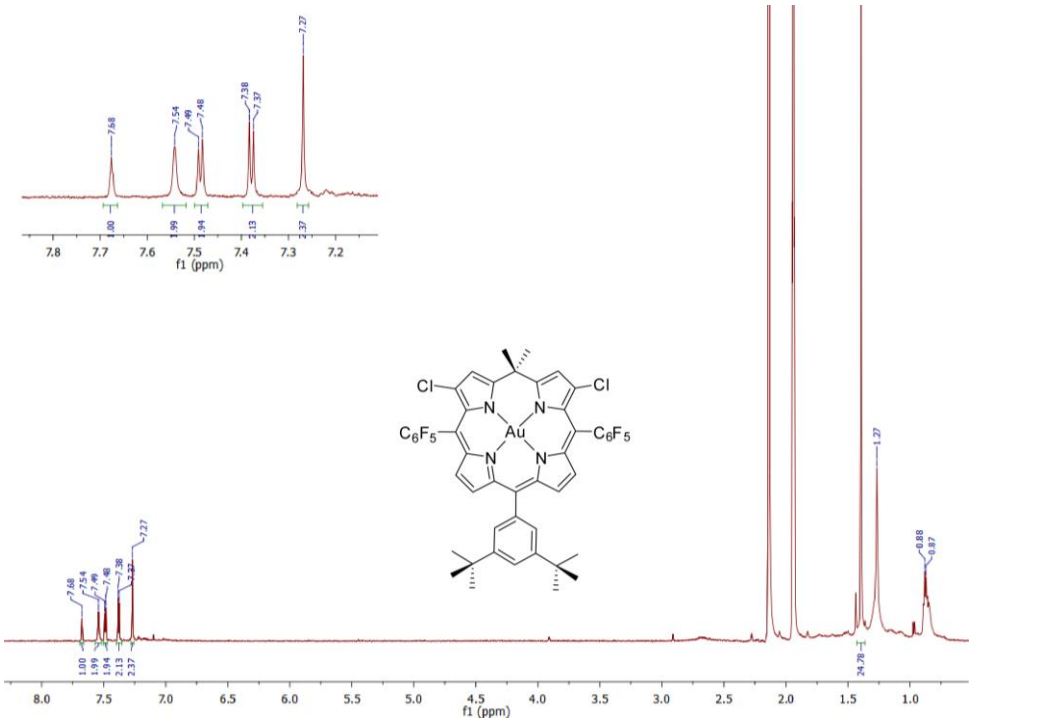

Figure 5.18 ^{1}H NMR of Au(Phl$^{3,5\text{-}tBu}$Cl$_2$) in CD_3CN displaying the binding of chloride to the β-positions of the pyrrole backbone of the phlorin macrocycle at the 2- and 8-positions.

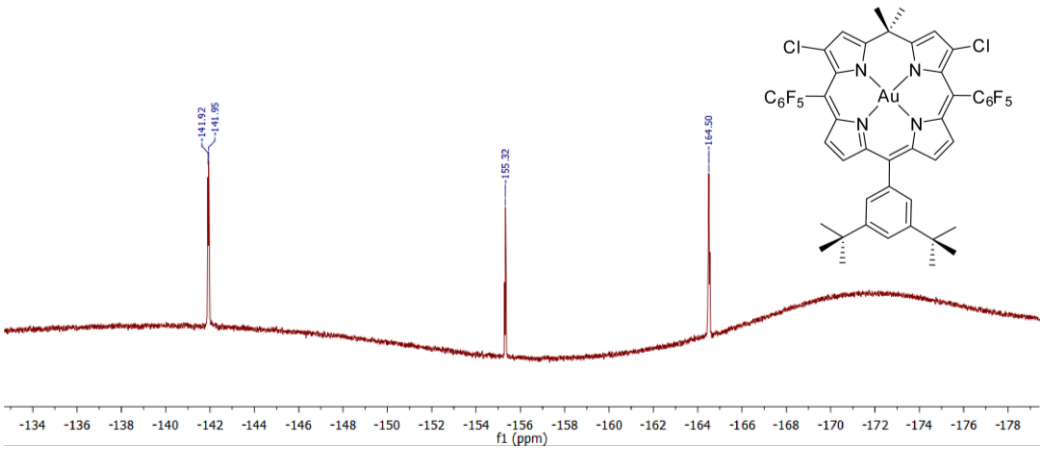

Figure 5.19 ^{19}F NMR of Au(Phl$^{3,5\text{-}tBu}$Cl$_2$) in CD_3CN shows that the pentafluorophenyl groups remain equivalent that is consistent with preservation of symmetry throughout the macrocycle.

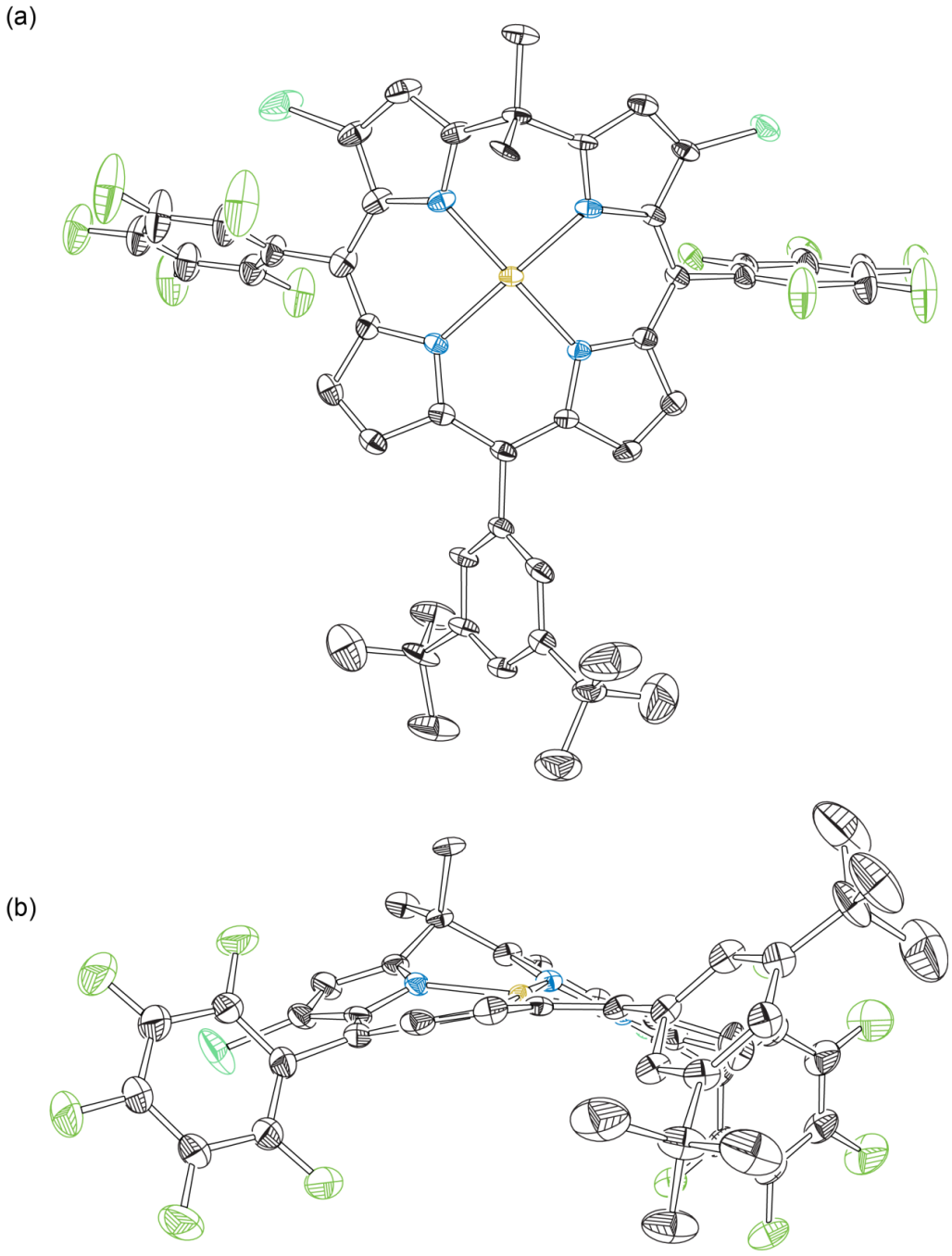

Figure 5.20 Crystal structure of Au(Phl$^{3,5\text{-}tBu}$Cl$_2$) with view from (a) top and (b) side on. All hydrogen atoms were omitted for clarity and thermal ellipsoids are shown at 50% probability.

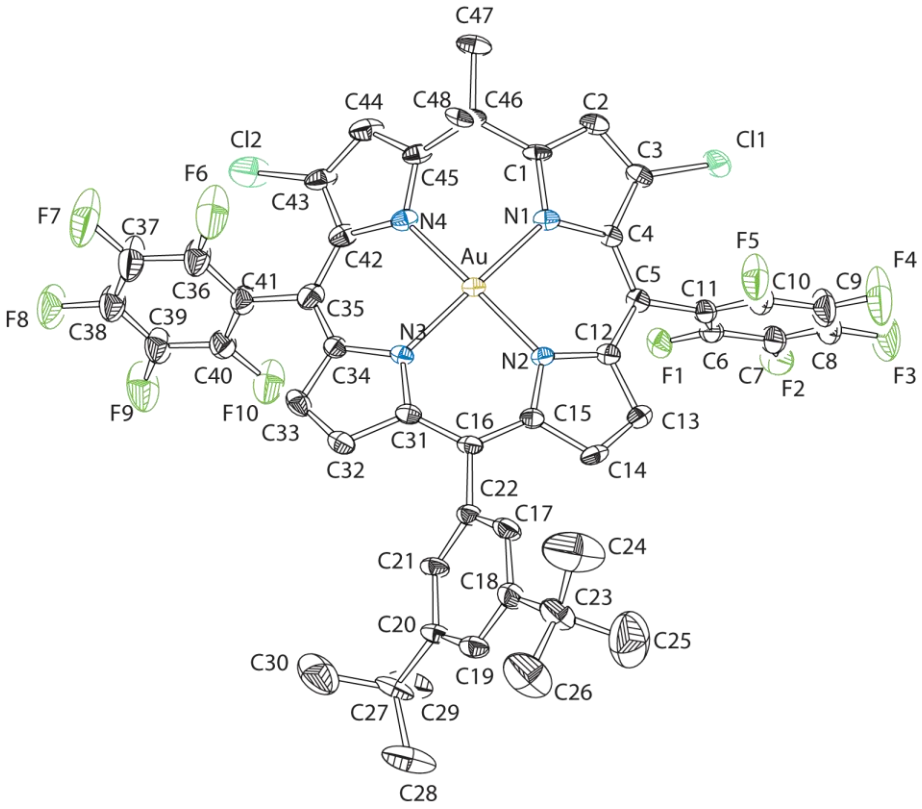

Figure 5.21 Numbered crystal structure of Au(Phl$^{3,5\text{-}tBu}$Cl$_2$) with all hydrogen atoms omitted for clarity and thermal ellipsoids shown at 50% probability.

Table 5.5 Selected bond lengths and angles for Au(Phl$^{3,5\text{-}tBu}$Cl$_2$).

Atoms	Bond Lengths (Å)	Atoms	Bond Angles (°)
Au(1)-N(1)	2.016(5)	**N(4)-Au-N(1)**	90.7(10)
Au(1)-N(2)	1.996(5)	**N(4)-Au-N(3)**	89.9(10)
Au(1)-N(3)	1.998(5)	**N(1)-Au-N(3)**	178.9(2)
Au(1)-N(4)	2.009(12)	**N(4)-Au-N(2)**	176.4(11)
Au(1)-N(4')	2.010(10)	**N(1)-Au-N(2)**	89.8(2)
C(3)-Cl(1)	1.721(7)	**N(3)-Au-N(2)**	89.5(2)
C(43)-Cl(2)	1.729(12)	**N(2)-Au-N(4')**	177.0(8)
		N(3)-Au-N(4')	89.2(8)
		N(4')-Au-N(1)	91.4(8)

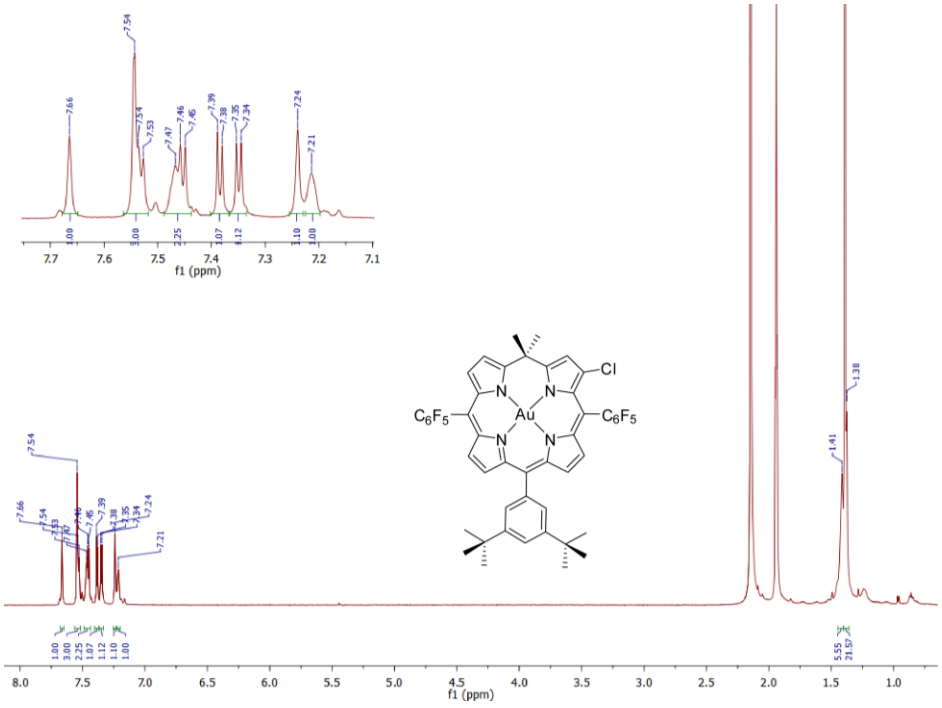

Figure 5.22 ^{1}H NMR of Au(Phl$^{3,5\text{-}tBu}$Cl) in CD_3CN displaying the binding of chloride to the β-positions of the pyrrole backbone of the phlorin macrocycle at the 2 position.

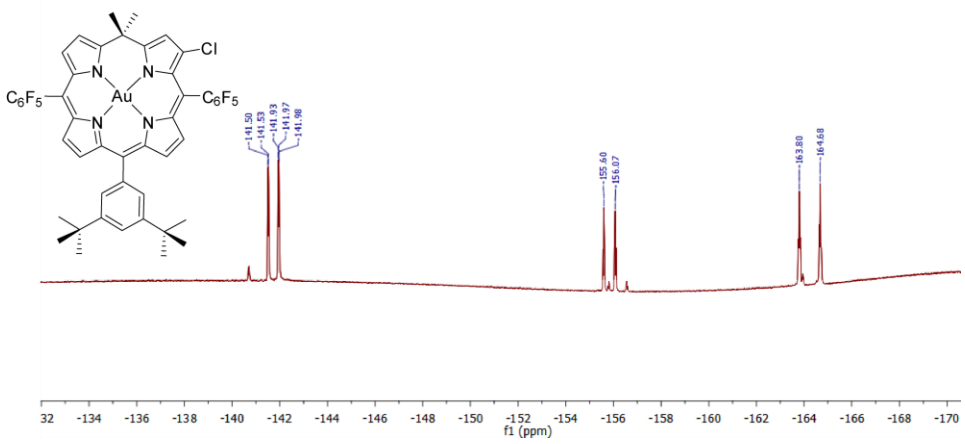

Figure 5.23 ^{19}F NMR of Au(Phl$^{3,5\text{-}tBu}$Cl) in CD_3CN shows that the pentafluorophenyl groups are no longer equivalent that is consistent with macrocycle lacking symmetry.

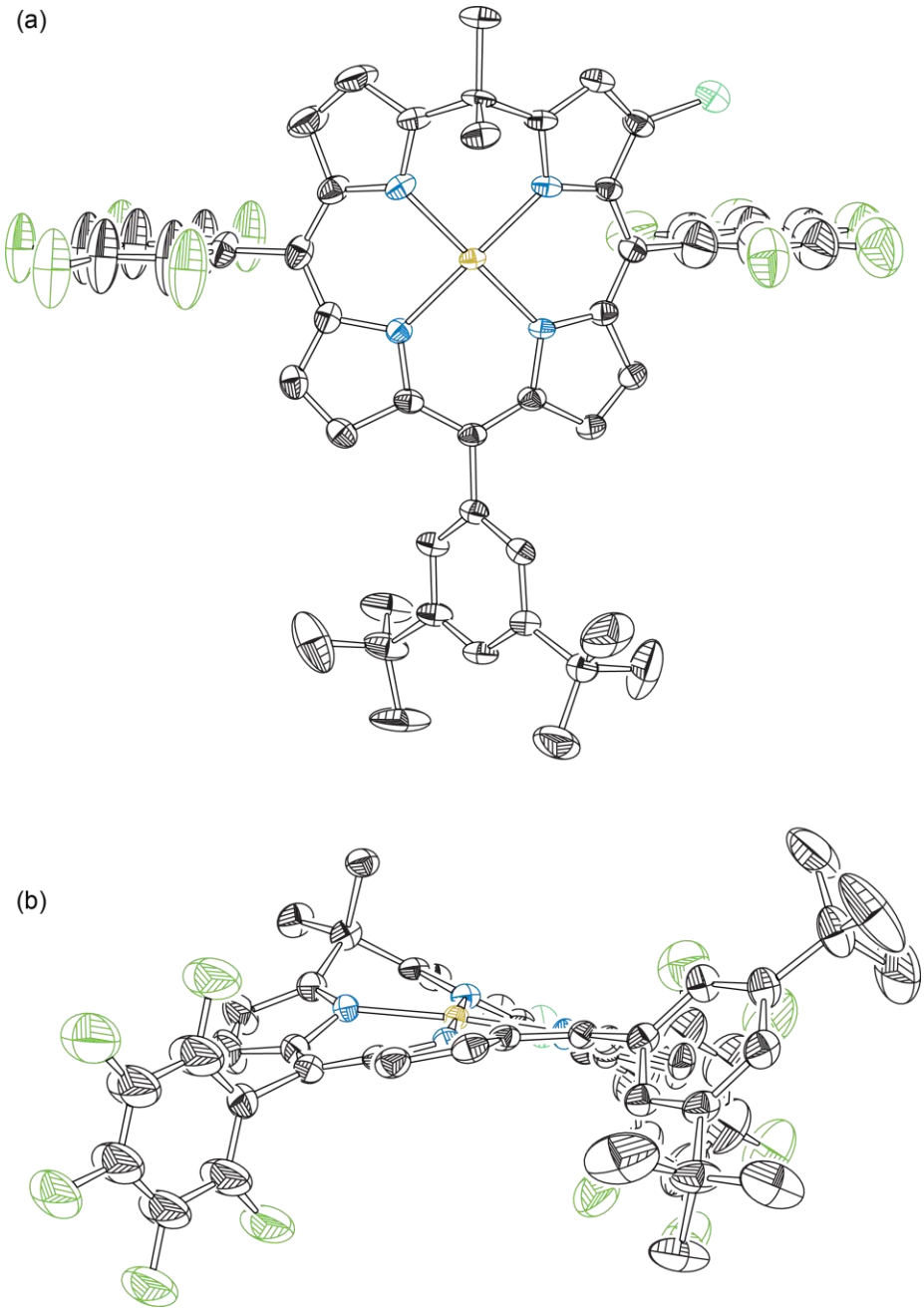

Figure 5.24 Crystal structure of Au(Phl$^{3,5\text{-}t\text{Bu}}$Cl) with view from (a) top and (b) side on. All hydrogen atoms were omitted for clarity and thermal ellipsoids are shown at 50% probability.

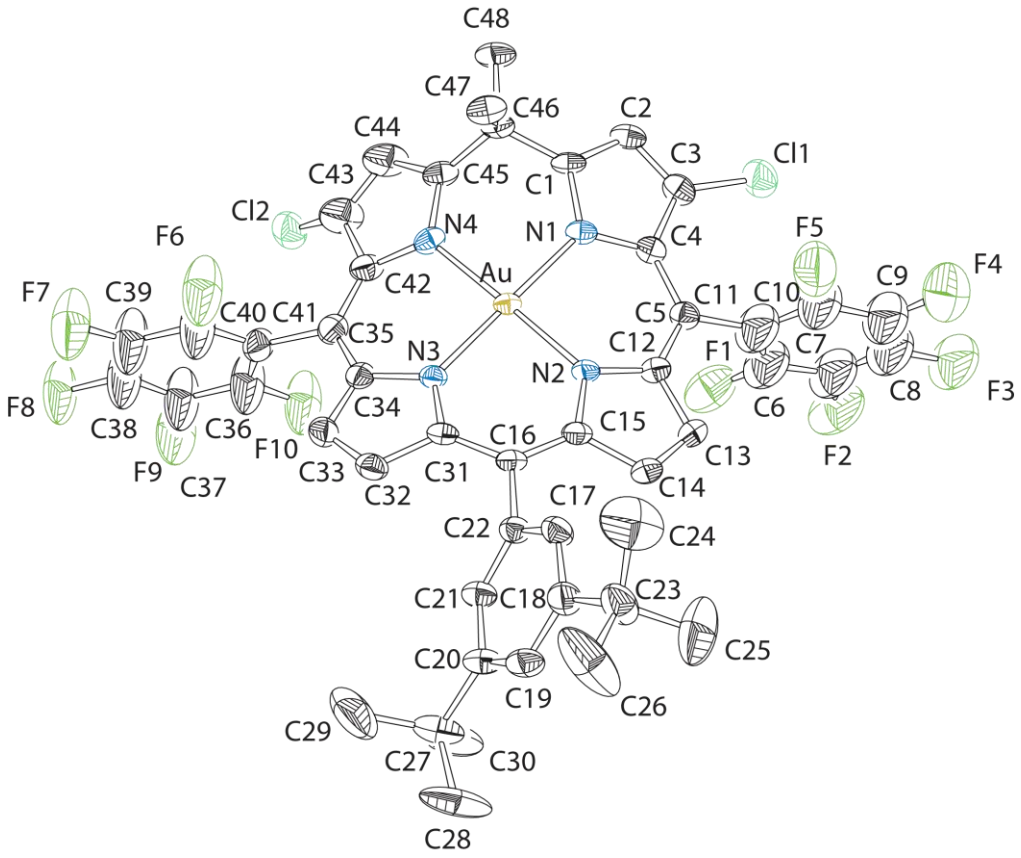

Figure 5.25 Numbered crystal structure of Au(Phl$^{3,5\text{-}tBu}$Cl) with all hydrogen atoms omitted for clarity and thermal ellipsoids shown at 50% probability. The structure contains two chlorine atoms as an average of the attachment at C43 and C3.

Table 5.6 Selected bond lengths and angles for Au(Phl$^{3,5\text{-}tBu}$Cl).

Atoms	Bond Lengths (Å)	Atoms	Bond Angles (°)
Au(1)-N(1)	2.006(5)	**N(4)-Au-N(1)**	90.2(2)
Au(1)-N(2)	1.989(5)	**N(4)-Au-N(3)**	90.1(2)
Au(1)-N(3)	1.996(5))	**N(1)-Au-N(3)**	179.4(2)
Au(1)-N(4)	2.005(5)	**N(4)-Au-N(2)**	176.4(2)
C(3)-Cl(1)	1.698(7)	**N(1)-Au-N(2)**	90.1(2)
C(43)-Cl(2)	1.692(11)	**N(3)-Au-N(2)**	89.56(19)

5.3.2 Reactivity of (Dichloroiodo)benzene with 3H(Phl$^{3,5\text{-}tBu}$)

With the reactivity of $PhICl_2$ and Au(Phl$^{3,5\text{-}tBu}$) as described, it was unknown if the central gold atom played a role in the chlorination of the pyrrole groups in the phlorin backbone. To investigate the influence of the central gold atom, the free base phlorin, 3H(Phl$^{3,5\text{-}tBu}$), was subjected to the same conditions as the gold derivative. 3H(Phl$^{3,5\text{-}tBu}$) was stirred with one equivalent of $PhICl_2$ at room temperature for 36 hours followed by purification using column chromatography. The resulting isolated products were determined to be the monochlorinated phlorin product, 3H(Phl$^{3,5\text{-}tBu}$Cl) and much of the free base phlorin that was unreacted. The purification of the products 3H(Phl$^{3,5\text{-}tBu}$Cl) and 3H(Phl$^{3,5\text{-}tBu}$) proved to quite difficult, with very little separation between the two compounds on the silica column. The monochloridnated product was the first green band isolated from the column, allowing for a portion of the material to be isolated cleanly from 3H(Phl$^{3,5\text{-}tBu}$). As can be seen from the NMR spectrum shown in Figure 5.26, there is a loss of symmetry within the phlorin macrocycle, similar to Au(Phl$^{3,5\text{-}tBu}$Cl). The ^{19}F NMR spectrum in Figure 5.27, displays six resonances for the pentafluorophenyl groups indicating the break in symmetry consistent with the addition of a single chloride to the phlorin scaffold. High-resolution mass spectrometry confirmed the formation of 3H(Phl$^{3,5\text{-}tBu}$Cl), showing that it is possible to chlorinate the ligand without a metal center.

The chlorination of 3H(Phl$^{3,5\text{-}tBu}$) without the presence of the gold atom suggests that the metal center is not directly involved in the chlorination of the ligand system. However, it is of note that the free base ligand reacts much slower than the gold derivative under the same conditions. The reaction of (dichloroiodo)benzene with 3H(Phl$^{3,5\text{-}tBu}$) yields only ~33 % of 3H(Phl$^{3,5\text{-}tBu}$Cl) along with unreacted starting material. In the case of Au(Phl$^{3,5\text{-}tBu}$) the only recovered phlorin based products are of

the mono and dichlorinated gold phlorin, with no recovery of unreacted starting material. Although the central gold atom may not have a direct role in the chlorination of the ligand, the change in the electronic structure from the coordination of gold may account for the difference in rate of reactivity, making the metalated derivative more reactive towards the (dichloroiodo)benzene. Similar results have been shown for copper(II) porphyrins, where chlorination at the β-position of the pyrrole using $PhICl_2$ was much faster and higher yielding than for the corresponding free base porphyrin.[184]

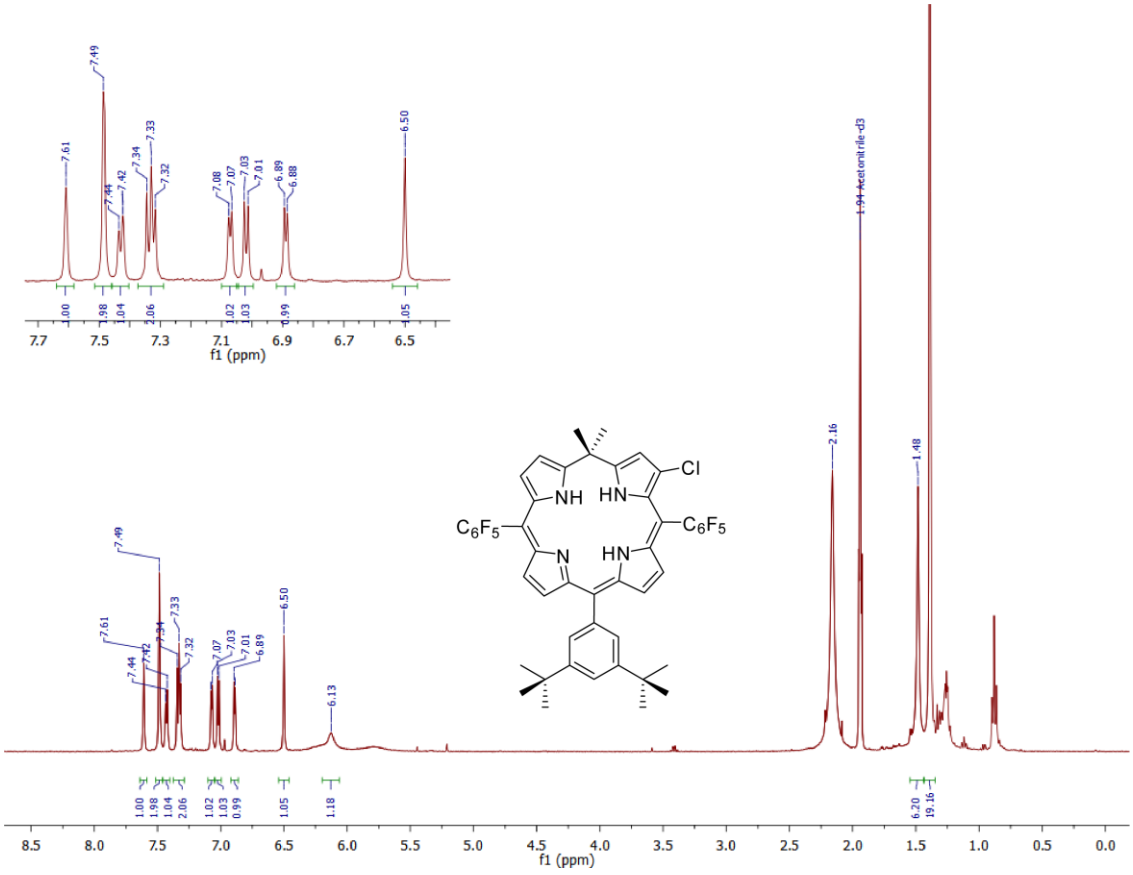

Figure 5.26 ^{1}H NMR of 3H(Phl$^{3,5\text{-}tBu}$Cl) in CD_3CN displaying the addition of chloride to the β-positions of the pyrrole backbone of the phlorin macrocycle at the 2 position.

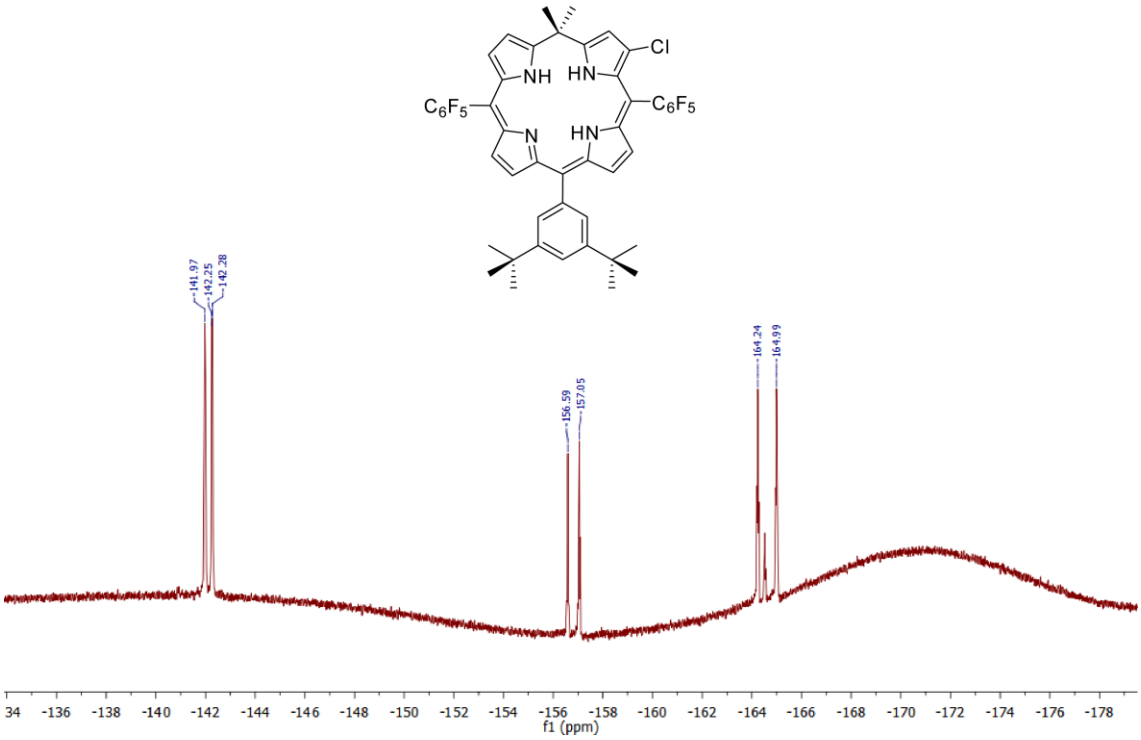

Figure 5.27 ^{19}F NMR of 3H(Phl$^{3,5\text{-}tBu}$Cl) in CD_3CN shows that the pentafluorophenyl groups are no longer equivalent that is consistent with macrocycle lacking symmetry.

5.4 Summary

The development of the phlorin macrocycle, in particular its use as a ligand, has been significantly underrepresented compared to other commonly studied porphyrinoids. This is due in part because of the limited synthetic routes for the preparation of a phlorin coordinated to a metal center. A different synthetic approach has been developed for the inclusion of a metal center beginning with the free base phlorin. After the study of several different conditions, a viable synthesis of the gold(III) phlorin has been shown. The first crystal structure of a gold(III) phlorin

containing geminal dimethyl substituents at the sp^3-hybridized *meso*-carbon has been reported. This was accomplished through the development of a novel free base phlorin macrocycle (3H($Phl^{3,5\text{-}tBu}$)) with the addition of the 3,5-*tert*-butylphenyl substituent at the 15-position providingthe necessary bulkiness to afford x-ray quality crystals.

The coordination of gold to the center of the macrocycle causes significant changes to the photophysical and redox properties of the phlorin. The absorption profile changes dramatically with the increase of the molar absorptivity in the Soret region and most notably with strong a absorption centered at ~775 nm. The heavy atom of gold also quenches the fluorescence that was observed for the free base macrocycle. The redox chemistry of the gold(III) phlorin is also substantially altered compared to that of the free base. The free base phlorin displayed three quasi-reversible oxidations at modest potentials, while the gold(III) phlorins display two fully reversible oxidations at similar potentials as the free base. The reductions of the gold(III) phlorins also occur at very similar potentials as the free base, however the gold derivatives display fully reversible reductions in the CVs, while the free base reductions are irreversible.

The Au(Phl) derivatives were investigated for use in energy storing catalysis. With the proposed cycle, the oxidation of the Au(Phl) along with the coordination of chloride was an essential intermediate for study of this chemistry. However, it was determined with the use of (dichloroiodo)benzene that the coordination of the chloride anions did not occur at the gold center, but rather the addition of chloride along the backbone of the phlorin was observed. The free base ligand also displayed the ability to add chloride along the backbone of the 2 or 8 pyrrole positions, although addition to the ligand occurred faster and in higher yield with the Au(Phl) derivative. Although

this may limit the use of Au(Phl) derivatives in the proposed energy storing catalytic reaction, the regioselectivity for the addition of chloride to the phlorin system creates another potential opportunity for the modification of the ligand system. This could enable further extension of the π-conjugation of the macrocycle, allowing for the attenuation of the absorption profile to reach longer wavelengths.

Chapter 6

THE DEVELOPMENT OF 10,10-DIMETHYLBILADIENE COMPLEXES FOR THE SENSITIZATION OF $^1O_2$

6.1 Introduction

Tetrapyrrole macrocycles such as porphyrins and corroles have been some of the most studied organic chromophores and redox cofactors.[1] Linear tetrapyrrole scaffolds like that of biladienes and biliverdins shown in Figure 6.1 have also been studied as organic chromophores and have displayed interesting absorption and photophysical properties,[185] although these compounds do not absorb light as well as the fully conjugated cyclic homologues.[186] Linear polypyrroles have also been shown to play a role in Nature, with their use as phytochrome photoreceptors that are

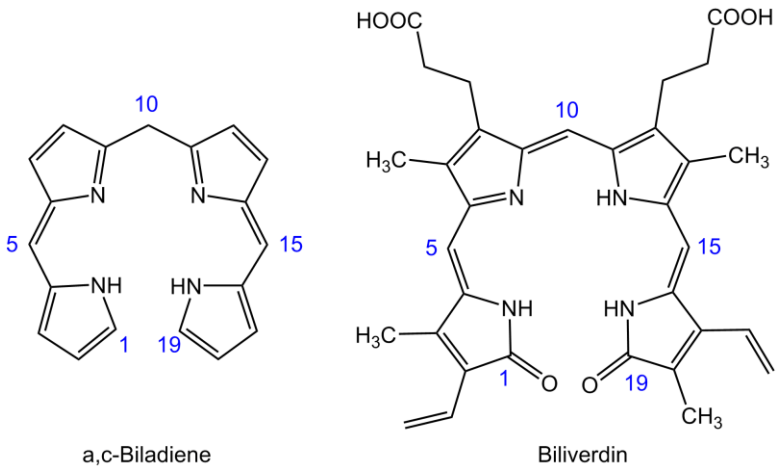

Figure 6.1 Numbered structures of a,c-biladiene and biliverdin.

responsible for the regulation of seed germination, flowering and stem growth in plants.[187] These linear scaffolds have also been shown the ability to coordinate both main group elements and transition metals,[188] including copper,[189,190] nickel,[191,192] cobalt,[193,194] and others.[195]

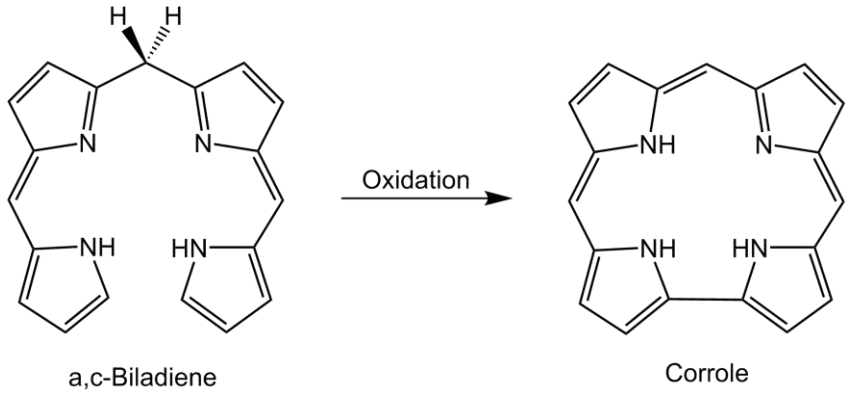

Scheme 6.1 Cyclization of a,c-biladienes to form corroles.

Although there have been some investigation in to linear tetrapyrrole scaffolds, they remain far less pursued than that of the cyclic homologues. The synthesis and inherent instability that has been observed for these linear scaffolds has hindered the investigation of the unique properties of these systems. Derivatives of a,c-biladienes that contain two protons on the sp^3-hybridized *meso*-carbon can rapidly decompose in the presence of light and air.[196] Additionally a,c-biladienes lacking substitution at the 1 and 19 terminal pyrrole positions can be oxidized leading to the cyclized corrole form shown in Scheme 6.1.[197-200] The inherent instability displayed by linear tetrapyrrole scaffolds such as bilirubin, can be demonstrated by the observation of several redox waves between 0.5-0.8 V versus SCE, leading to the oxidation of these systems at modest potentials.[201]

In order to increase the stability of these linear tetrapyrrole scaffolds the cyclization process in which the 10-position is deprotonated would need to be inhibited. The addition of alkyl groups at the 10-position would prevent the deprotonation from occurring,[202,203] increasing the stability of these systems.[204] With this in mind, 10,10-Dimethylbiladiene was considered a great scaffold to investigate the increase of stability through the addition of alkyl groups at the 10-position. The synthesis of 10,10-dimethylbiladiene was approached by adapting the methods used for the synthesis of porphyrinoids containing sp^3-hybridized centers[43,205-207] including the phlorin macrocycles described in previous chapters.[30,138,208,209] Like that of the phlorin macrocycle, strong electron withdrawing pentafluorophenyl groups were substituted at the 5 and 15 *meso*-carbons to potentially enhance the stability of the ligand.[208]

In this chapter a synthetic route for 10,10-dimethyl-5,15-dipentafluorophenylbiladiene (DMBil) that displays both synthetic availability and chemical stability will be shown. The use of DMBil as a ligand for transition metals including both Zn^{2+} and Cu^{2+} will be fully characterized. The solid-state structures, redox and photophysical properties of free base, zinc and copper derivatives will be comprehensively studied. The use of these systems as sensitizers for $^1O_2$ will also be investigated with the Zn^{2+} and free base displaying the ability to sensitize $^1O_2$ using visible light with modest efficiencies.

6.2 Synthesis of 10,10-Dimethyl-5,15-dipentafluorophenylbiladiene (DMBil)

The synthesis of DMBil began with the preparation of 5,5-Dimethyl-1,9-bis(pentafluorobenzoyly)-dipyrromethane as shown before in Chapter 3. The diacylated compound was reduced with $NaBH_4$ in a 3:1 ratio of THF and methanol.

After the reaction was quenched with water and extracted with CH_2Cl_2, the corresponding diol was stirred with $InCl_3$ and pyrrole at room temperature. Following the oxidation using DDQ and the addition of triethylamine the product was purified using chromatography to give the DMBil in 53% yield shown in Scheme 6.2.

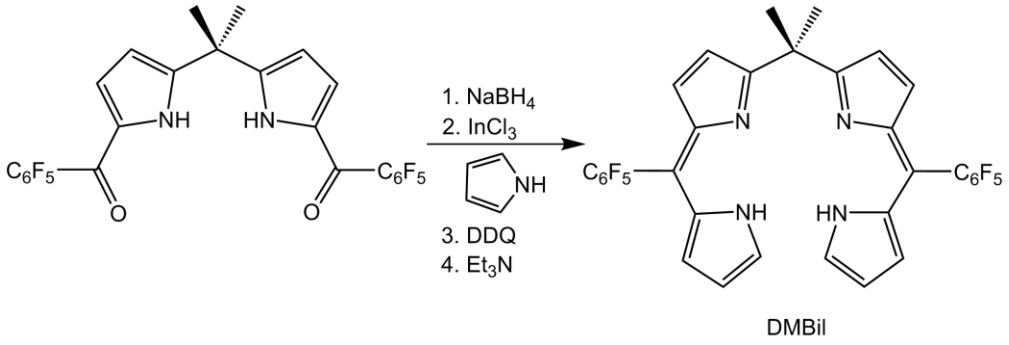

Scheme 6.2 Synthesis of 10,10-Dimethyl-5,15-pentafluophenylbiladiene (DMBil).

6.2.1 Solid-state structure of DMBil

The solid state structure of DMBil shown in Figure 6.2, shows that this scaffold is conformationally flexible and the two dipyrromethane units are distorted from coplanarity. This can be seen with the dihedral angle between the two dipyrromethanes bridged through the sp^3 carbon center being measured to be 66.08°. The pentafluorophenyl groups are also canted from being perpendicular to the dipyrromethane groups with dihedral angles of 67.57°. The bond lengths of the pyrrole groups are summarized in Table 6.1 and lead to the assignment of the protons being bound to each of the nitrogen atoms of the terminal pyrrole groups.

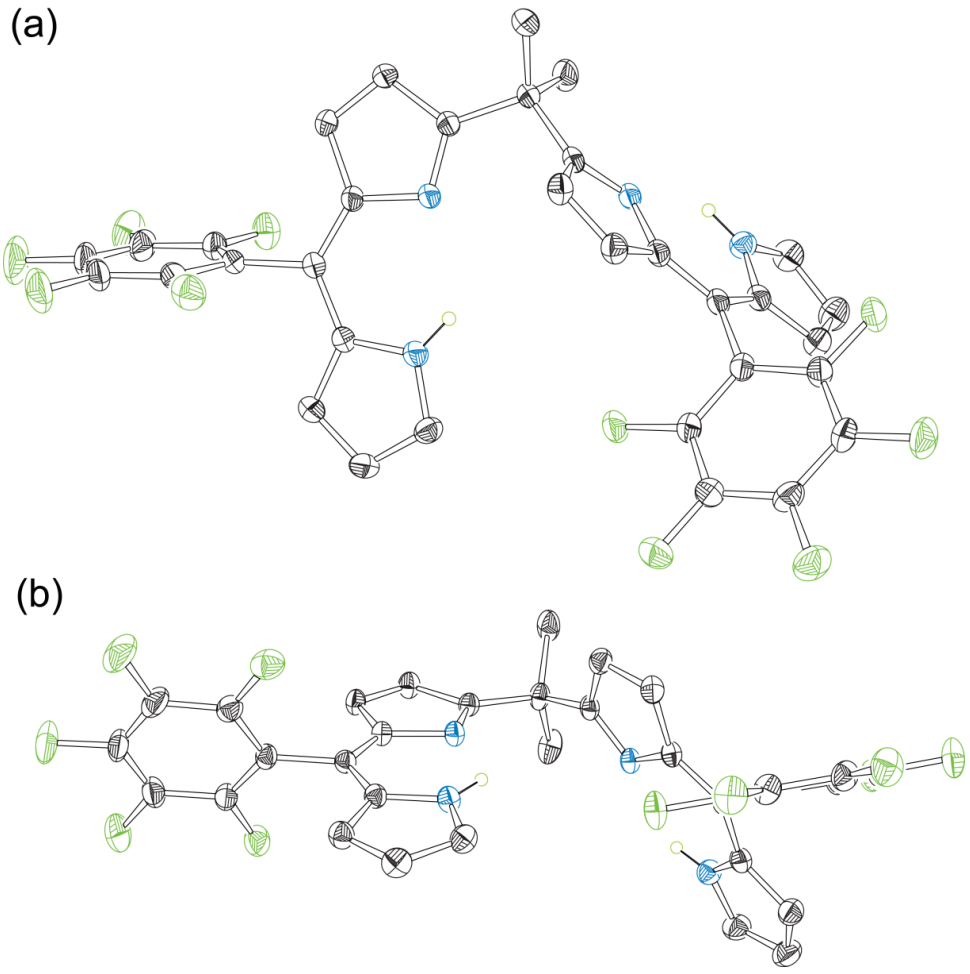

Figure 6.2 Crystal structure of DMBil (a) top and (b) plane view. Thermal ellipsoids are drawn at the 50% probability level. All non N-H hydrogens have been omitted for clarity.

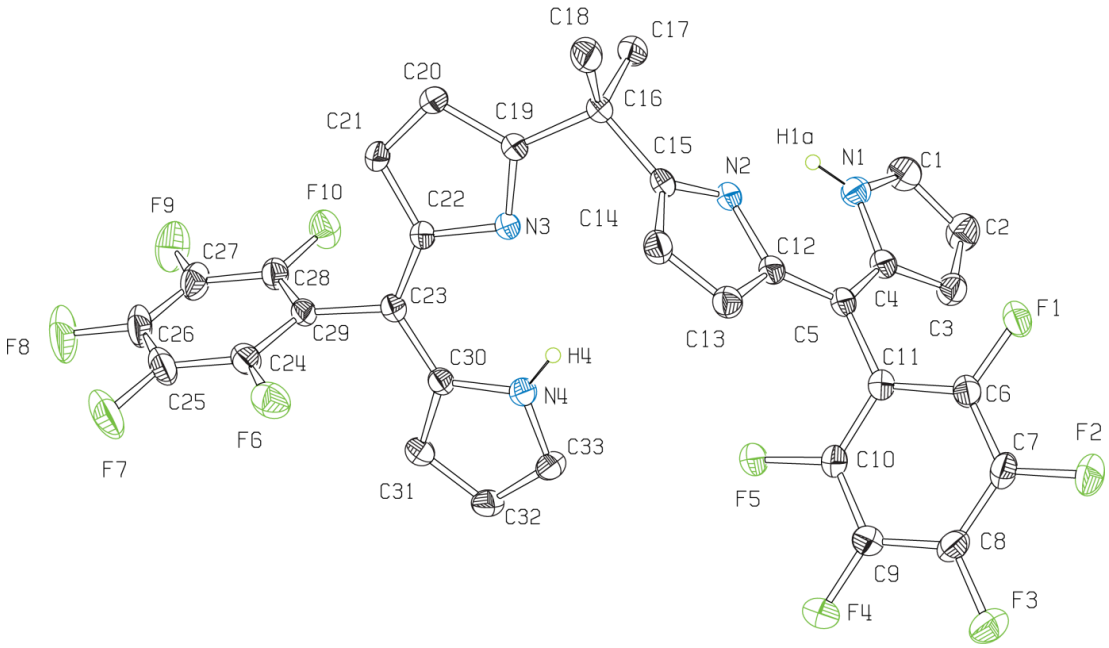

Figure 6.3 Fully labeled solid state structure of DMBil with thermal ellipsoids drawn at the 50% probability level. All non N-H hydrogens have been omitted for clarity.

Table 6.1 Selected bond lengths (Å) for DMBil.

Atoms	Bond Lengths (Å)
C(1)-N(1)	1.359(2)
C(4)-N(1)	1.376(2)
C(12)-N(2)	1.414(2)
C(15)-N(2)	1.311(2)
C(19)-N(3)	1.3086(19)
C(22)-N(3)	1.4123(19)
C(30)-N(4)	1.380(2)
C(33)-N(4)	1.351(2)

6.3 Synthesis of Zn(DMBil) and Cu(DMBil)

Zn(DMBil) was synthesized with the addition of excess $Zn(OAc)_2 \bullet 2H_2O$ to DMBil in DMF. The reaction was heated to 60 °C for four hours followed by the removal of solvent and subsequent brine washes, Zn(DMBil) was obtained in 70% yield. Although the product was obtained pure, it is of note that the Zn(DMBil) cannot be subject to the silica column chromatography as the Zn metal center will be removed.

The Cu(DMBil) was synthesized using a similar strategy as the Zn complex, with both shown in Scheme 6.3. $Cu(OAc)_2$ was added to DMBil that had been dissolved in MeCN and heated to 60 °C. The complex was purified with column chromatography and Cu(DMBil) was obtained in 92% yield.

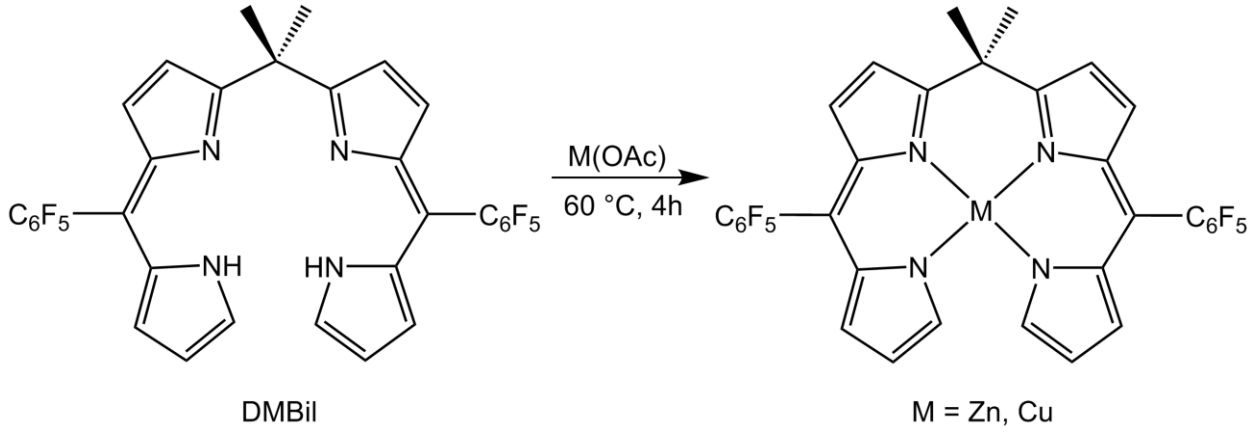

Scheme 6.3 Synthesis of Zn(DMBil) and Cu(DMBil).

6.3.1 Solid State Structures of Zn(DMBil) and Cu(DMBil)

Zn(DMBil) was crystallized from a 1:1 solution of $CHCl_3$ and MeOH with one equivalent of MeOH binding to the Zn metal center and displayed in Figure 6.4. The coordination geometry for the Zn(DMBil) is trigonal bipyramidal, which is different

from that of a Zn decamethyl-a,c-biladiene that did not crystalize with a solvato ligand.[210] The five coordinate Zn structure is reminiscent of Zn octaethylformylbiliverdinate with an aquao ligand bound to the Zn center however, the biliverdinate is conjugated making the coordination geometry square pyramidal.[211]

The coordination to Zn causes an interesting binding structure of the biladiene. The six membered ring made up of Zn(1), N(2), C(15), C(10), C(19) and N(3) adopts a boat type configuration, which causes C(18) to adopt an axial type positioning, while C(17) sits in a equatorial position. The two pyrrole groups that are connected through the sp^3 center have a compressed dihedral angle of 16.55°. This structure is highly distorted from planarity that is typical for corrole-like configurations, which can easily be seen from the in plane view shown in Figure 6.4. The terminal pyrroles are also canted by 48.40° with respect to each other.

The Cu(DMBil) is a four coordinate structure displayed in Figure 6.6 that, similarly to the Zn structure, is non-planar. This is unusual for most Cu^{2+} porphyrinoid complexes that typically adopt a planar geometry around the metal center. Like that of the Zn(DMBil) the terminal pyrroles of the Cu(DMBil) are canted by 50.59° with respect to each other and C(1) and C(19) of the pyrroles are separated by ~3.04 Å. The bond lengths of the nitrogen atoms to central copper atom range from 1.969 to 1.980 Å with the average bond length of 1.972 Å. The pentafluorophenyl groups are close to being orthogonal to the dipyrromethane groups with dihedral angles of 82.57°.

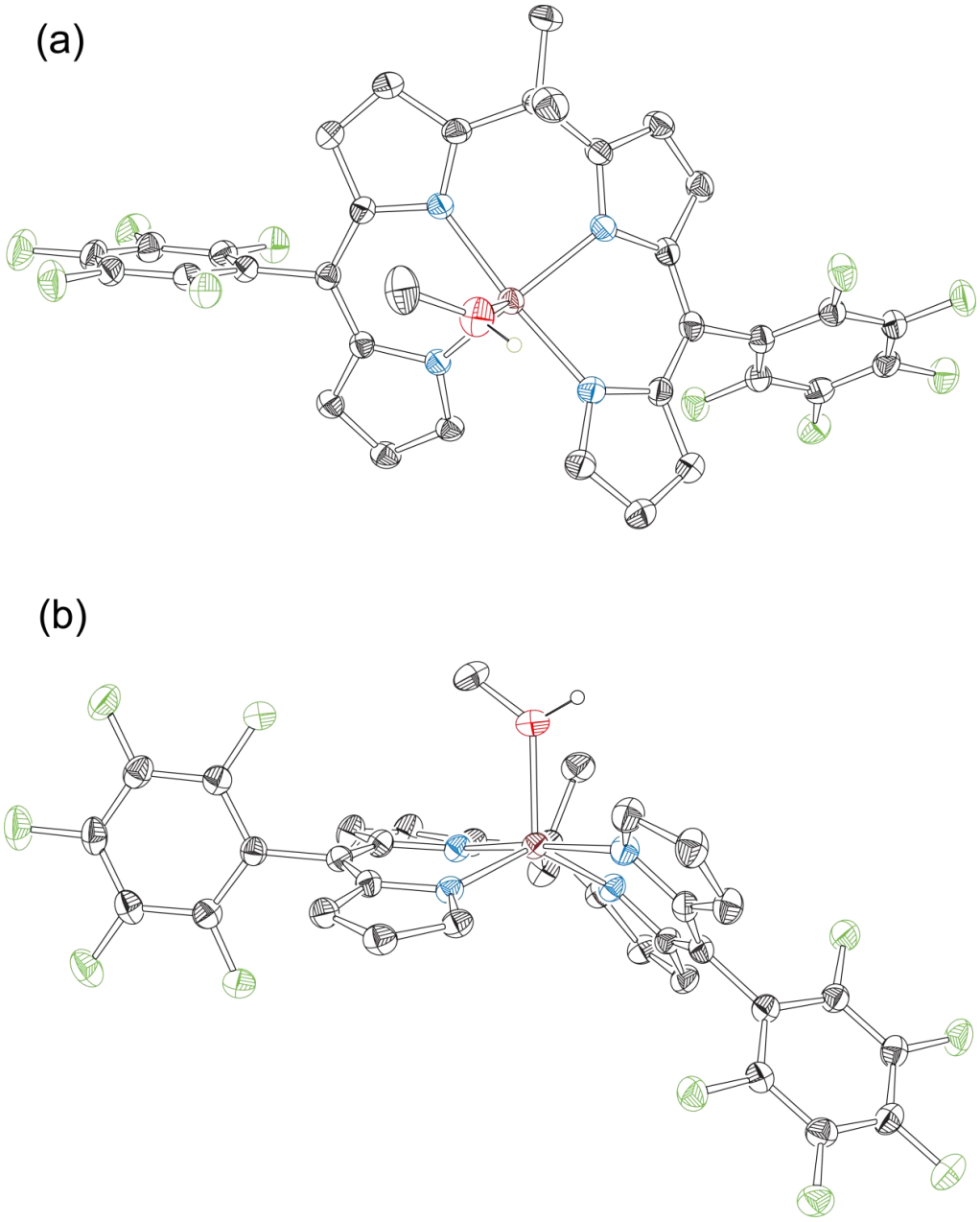

Figure 6.4 Crystal structure of Zn(DMBil) with (a) top and (b) plane view. Thermal ellipsoids are drawn at the 50% probability level. Hydrogen atoms (except those on the coordinated solvent molecule) are omitted for clarity.

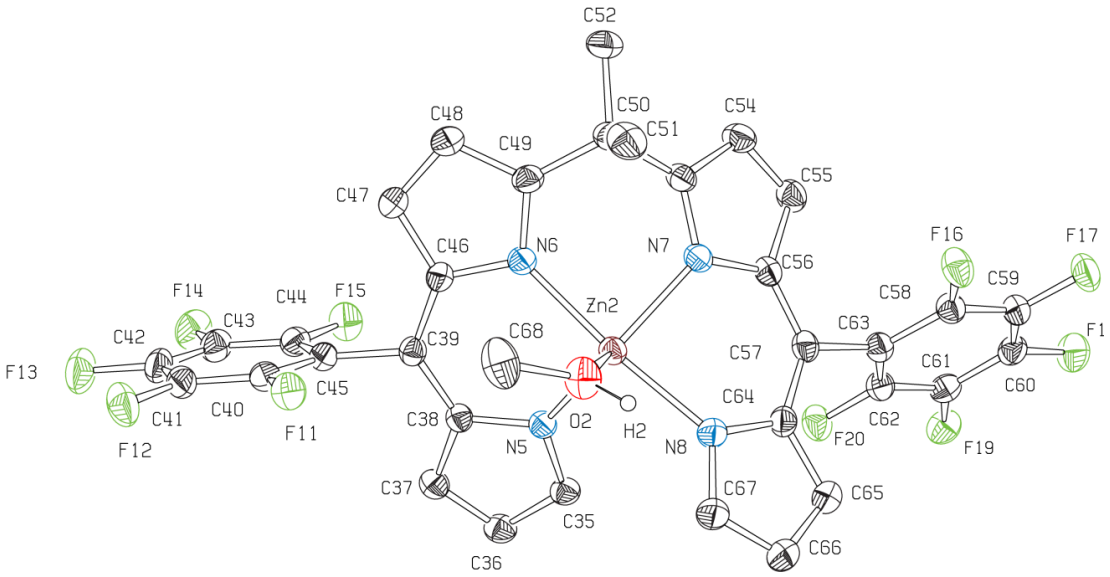

Figure 6.5 Fully labeled solid state structure of Zn(DMBil) with thermal ellipsoids drawn at the 50% probability level. Hydrogen atoms (except those on the coordinated solvent molecule) are omitted for clarity.

Table 6.2 Selected bond lengths (Å) for Zn(DMBil).

Atoms	Bond Lengths (Å)
Zn(1)-N(1)	2.070(2)
Zn(1)-N(2)	2.075(2)
Zn(1)-N(3)	2.046(2)
Zn(1)-N(4)	2.046(2)
Zn(1)-O(1)	2.1268(19)

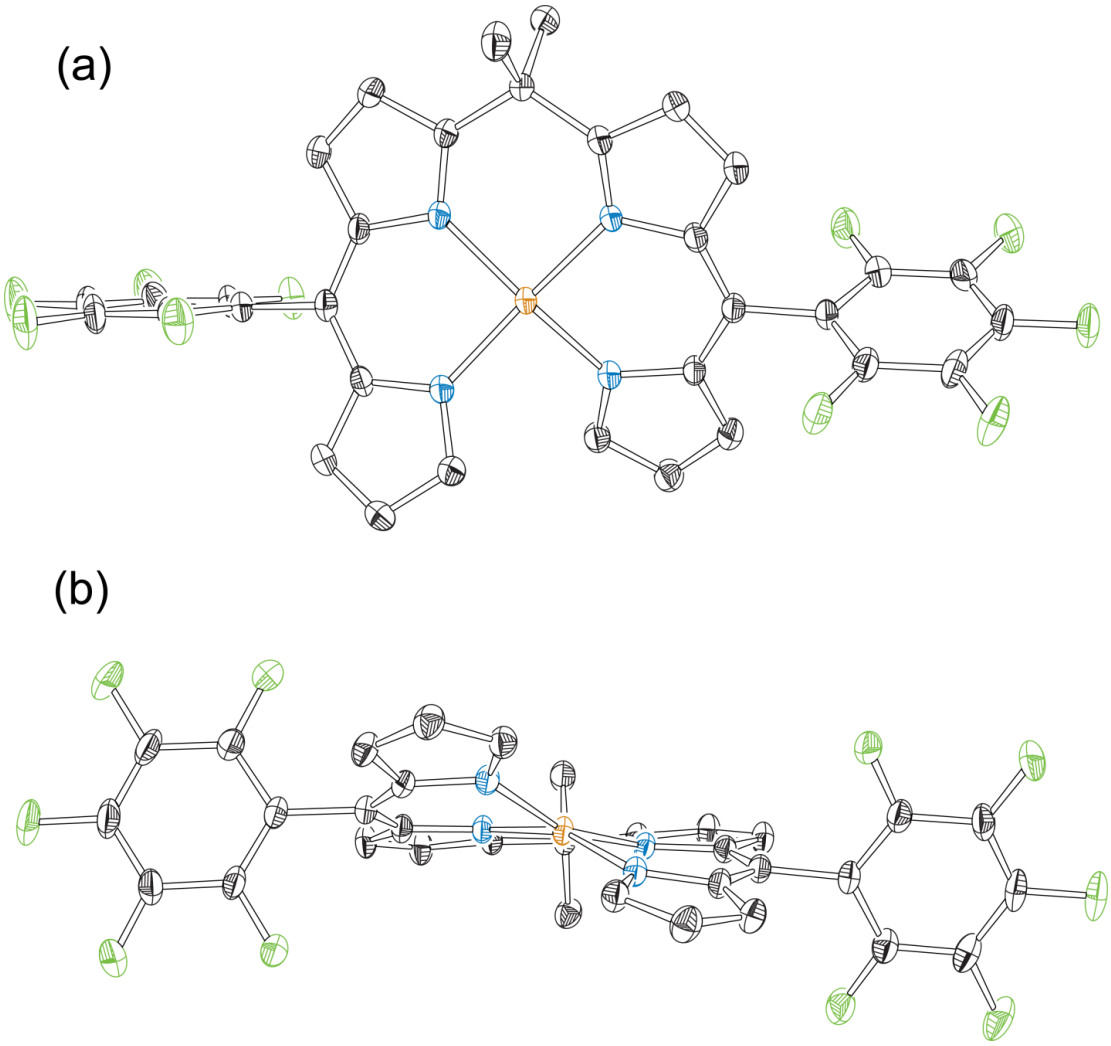

Figure 6.6. Solid state structure of Cu(DMBil) with (a) top and (b) plane view. Thermal ellipsoids are drawn at the 50% probability level. All hydrogen atoms have been omitted for clarity.

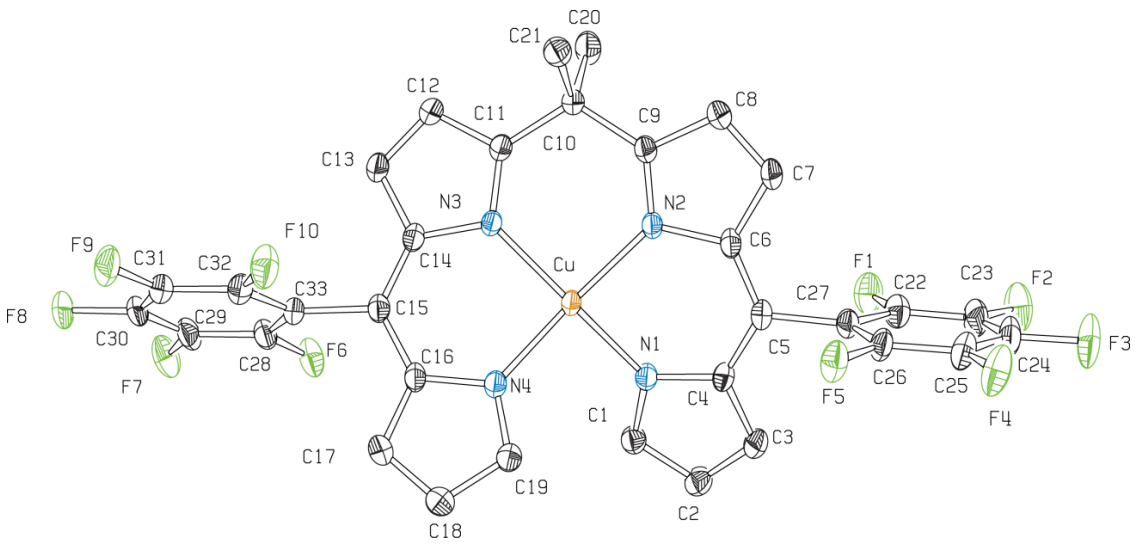

Figure 6.7 Fully labeled solid state structure of Cu(DMBil) with thermal ellipsoids are drawn at the 50% probability level. All hydrogen atoms have been omitted for clarity.

Table 6.3 Selected bond lengths (Å) for Cu(DMBil).

Atoms	Bond Lengths (Å)
Cu(1)-N(1)	1.980(2)
Cu(1)-N(2)	1.970(2)
Cu(1)-N(3)	1.970(2)
Cu(1)-N(4)	1.969(2)

6.4 Electrochemistry of DMBil, Zn(DMBil) and Cu(DMBil)

The biladiene displays rich redox chemistry, shown in CV traces of Figure 6.8, with 1.0 mM of analyte and 0.1 M $TBAPF_6$ in MeCN. A standard three electrode set up was used with a platinum disk electrode (2 mm) as the working electrode, a platinum wire as the counter electrode and a silver wire as a pseudo reference electrode. The DMBil displays two irreversible one electron oxidations at $E_{ox}(1)$ = 1.33 V and $E_{ox}(2)$ = 1.49 V as well as two irreversible one electron reductions at $E_{red}(1)$ = –1.05 V and $E_{red}(2)$ = –1.21 V.

The metalation of the DMBil scaffold causes significant changes in the redox properties. The Zn(DMBil) and Cu(DMBil) each have two one electron oxidations that are largely irreversible. The oxidations for Zn(DMBil) occur at $E_{ox}(1)$ = 1.04 V and $E_{ox}(2)$ = 1.33 V while the oxidations for Cu(DMBil) occur at $E_{ox}(1)$ = 0.92 V and $E_{ox}(2)$ = 1.24 V. The reductions of the Zn and Cu biladienes become reversible with binding of the metal center, with each displaying two reversible one electron reductions. The reductions for the Zn(DMBil) ($E_{red}(1)$ = –1.13 V and $E_{red}(2)$ = –1.31 V) occur at similar potentials as the free base DMBil, with each reduction varying by roughly 100 mV more negative. The reductions of the Cu(DMBil) are different from those displayed for both the DMBil and the Zn(DMBil). The potential of the first reduction is $E_{red}(1)$ = –0.88 V, which less negative than the zinc derivative by almost 250 mV. The second reduction at $E_{red}(2)$ = –1.34 V is similar to both the free base and Zn derivatives. The redox potentials for each of the biladiene derivatives are summarized in Table 6.4.

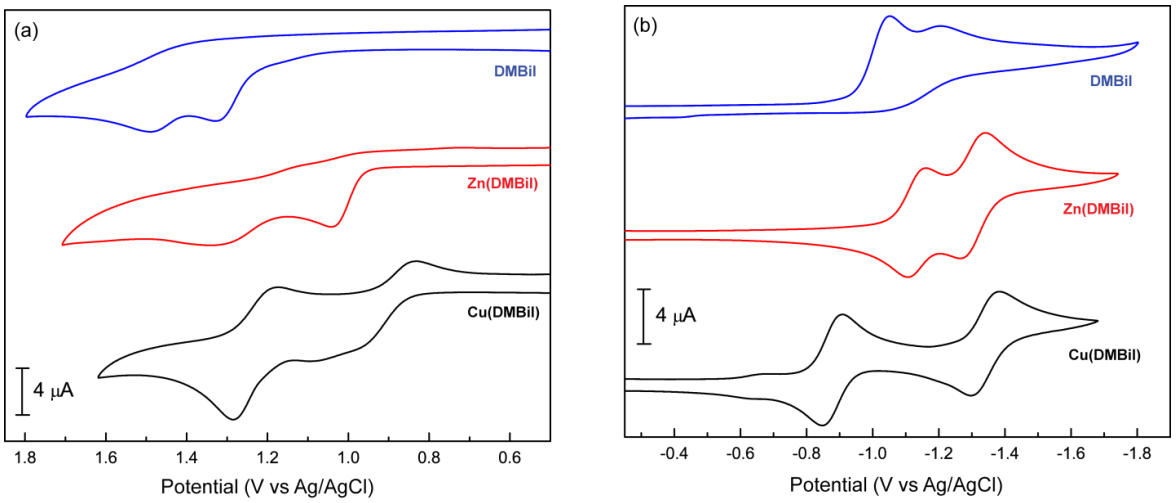

Figure 6.8 (a) Oxidative and (b) reductive cyclic voltammograms recorded for DMBil, Zn(DMBil) and Cu(DMBil) in MeCN containing 0.1 M $TBAPF_6$ and internal decamethylferrocene standard at a scan rate of 50 mV/s.

Table 6.4 Redox potentials for DMBil, Zn(DMBil) and Cu(DMBil).

	$E_{ox}(1)$, V	$E_{ox}(2)$, V	$E_{red}(1)$, V	$E_{red}(2)$, V
DMBil	1.33	1.49	–1.05	–1.21
Zn(DMBil)	1.04	1.33	–1.13	–1.31
Cu(DMBil)	0.92	0.24	–0.88	–1.34

6.4.1 UV-vis Spectroscopy

The absorption profile each of the biladienes studied was recorded in CH_2Cl_2 and shown in Figure 6.9. The free base biladiene, DMBil displayed wide absorption in the visible region from ~350 to 525 nm. This absorption is composed of two close absorption bands with the first having a maxima at 423 nm (ε = 41480) and the second with a maxima at 450 nm (ε = 43060). These resulting absorption bands were

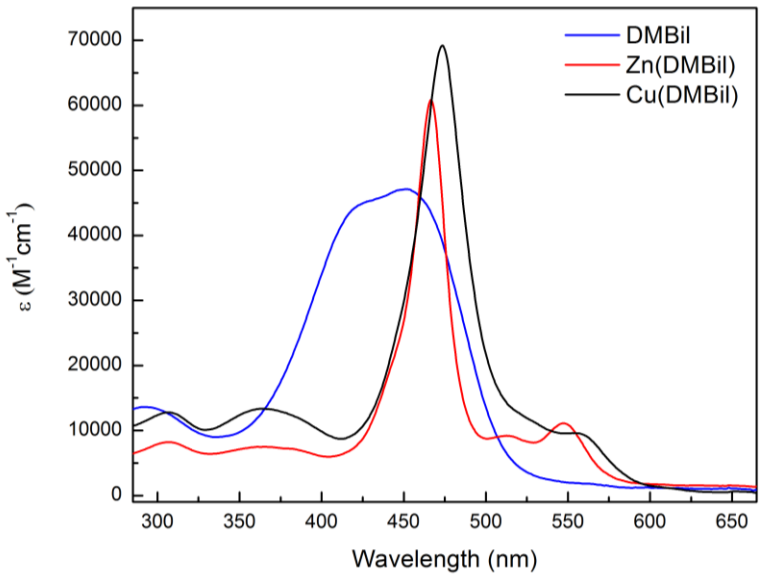

Figure 6.9 Overlay of the absorption profiles for each DMBil, Zn(DMBil) and Cu(DMBil).

investigated with the use of time-dependent density functional theory (TD-DFT) and found to be based in four molecular frontier orbitals. The π-π* transitions were found to involve the nearly degenerate HOMO and HOMO-1 levels along with the LUMO and LUMO+1 levels as shown in Figure 6.10. Absorption profiles of linear tetrapyrrole scaffolds such as 1,19-dideoxybiladiene-a,c have been shown to have similar shape to that of DMBil, with a strong single absorption.[202]

The addition of a metal to the center of the biladiene causes a significant shift in the absorption profile. The absorption profile for Zn(DMBil) shown in Figure 6.9, displays a single strong absorption at 467 nm (ε = 50790), which is not only shifted to longer wavelengths than that of the free base but is only comprised of a single absorption. The Zn(DMBil) also has weak absorptions at longer wave lengths of 513 nm (ε = 8180) and 548 nm (ε = 10170). TD-DFT suggests that the maximum

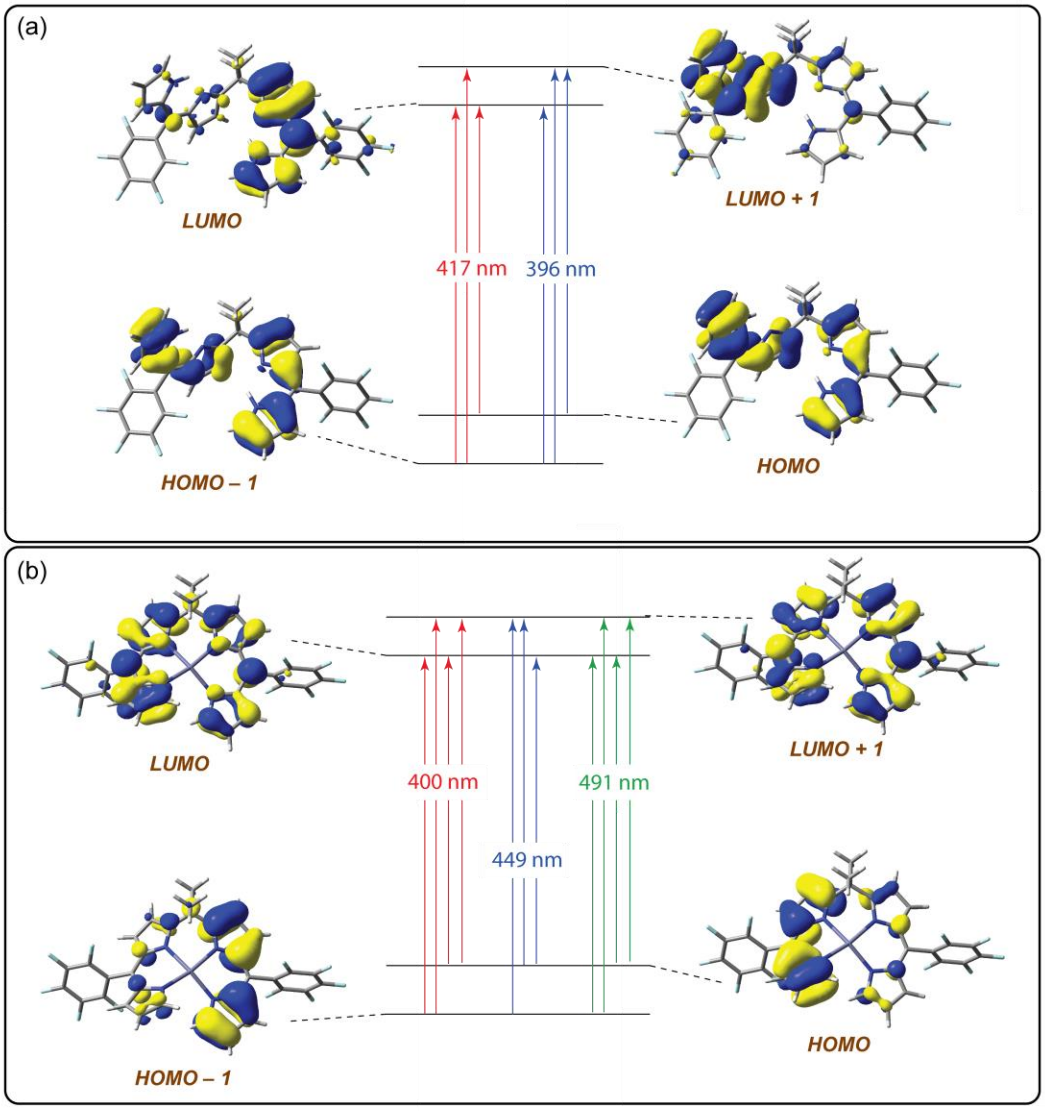

Figure 6.10 Representation of the molecular orbitals involved in the major electronic absorption transitions for (a) DMBil and (b) Zn(DMBil) in CH_2Cl_2.

absorption centered at 467 nm is based on four molecular frontier orbitals of HOMO-1, HOMO, LUMO and LUMO+1, similar to that of the π-π* transitions of the free base. The transitions at the longer wavelengths are primarily attributed to the same

four molecular orbitals between HOMO-1 and LUMO+1 as shown in Figure 6.10. The Cu(DMBil) absorption profile in Figure 6.9 is very similar to the Zn^{2+} derivative, with the maxima absorption at 477 nm (ε = 59400) as well as absorption at longer wavelengths centered at 558 nm (ε = 9100).

6.4.2 Fluorescence

DMBil was found to be strongly fluorescent, with the emission spectra shown in Figure 6.11. Upon photoexcitation at λ_{ex} = 450 nm a broad emission profile centered at 543 nm for DMBil was observed and ranging between 500-700 nm. Additional photophysics were studied and DMBil was found to have a fluorescence lifetime of τ_{fl} = 15.3 ps and fluorescence quantum yield of Φ_{fl} = 1.7 X 10^{-3} in deaerated CH_2Cl_2 at λ_{ex} = 450 nm. Zn(DMBil) was also found to be fluorescent, however the emission shifted to longer wavelengths compared to the free base with the emission maxima centered at 573 nm. The fluorescence lifetime was found to be τ_{fl} = 22.3 ps, which is significantly shorter than many typical porphyrinoids where lifetime are observed to be 2-15 ns at room temperature.[212] The fluorescence lifetimes observed for both the DMBil and Zn(DMBil) are similar to those of the phlorin derivatives studied in Chapter 3. The fluorescence quantum yield for Zn(DMBil) was found to be Φ_{fl} = 7.0 X 10^{-4}, which is less than half of that of the free base biladiene. Cu(DMBil) did not display any fluorescence, which is due to the open d shells of the Cu^{2+}, where the d-d states are lower in energy that the π-π^* states of the biladiene ligand. This is commonly seen with porphyrinoids complexes that support metals with open d shells. The photophysics for the free base, zinc and copper biladiene derivatives are summarized in Table 6.5.

Table 6.5 Photophysical data for DMBil, Zn(DMBil) and Cu(DMBil).

	λ_{abs}/nm (ε X 10^3 $M^{-1}cm^{-1}$)	λ_{em}/nm (Φ_{em})	τ_{fl} (ps)
DMBil	291(1.1), 423(41.4), 450(43.0)	543(1.7 X 10^{-3})	15.3
Zn(DMBil)	306(6.9), 368(6.6), 467(50.8), 513(8.2), 548(10.2)	573(7.0 X 10^{-4})	22.3
Cu(DMBil)	308(11.2), 364(13.0), 474(59.4), 558(9.1)		

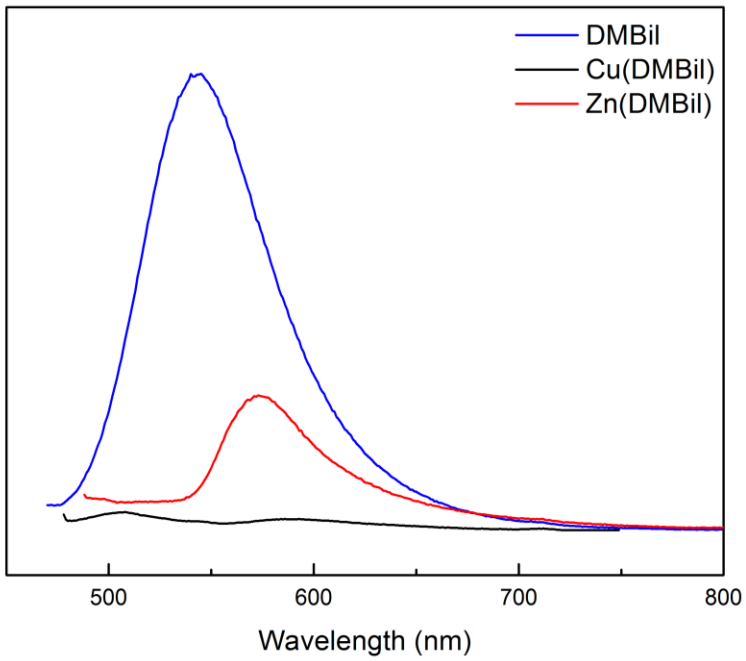

Figure 6.11 Emission spectra recorded in deaerated CH_2Cl_2 for DMBil, Zn(DMBil) and Cu(DMBil).

6.4.3 Sensitization of $^1O_2$

The ability of the biladiene scaffold to sensitize $^1O_2$ was investigated and the quantum yields for DMBil, Zn(DMBil) and Cu(DMBil) were measured. $[Ru(bpy)_3]^{2+}$ was used as the standard (Φ_{1O2} = 0.81 in MeOH)[213] and 1,3-diphenylisobenzofuran was used as the trapping agent.[214,215] The $^1O_2$ sensitization quantum yield for DMBil

was measure to be Φ_{1O2} = 1.5 X 10^{-2} in MeOH while irradiating at λ_{irr} = 500 nm. This clearly demonstrates that the DMBil is a platform that can support the sensitization of $^1O_2$ with a modest quantum yield, although it is of note that some porphyrinoids have shown the ability to sensitize $^1O_2$ with quantum yields nearing Φ_{1O2} = 0.80 in polar protic solvents.[216,217] Although the quantum yield for the sensitization of $^1O_2$ is lower than that of other previously studied systems, this discovery creates the opportunity for the development of the 10,10-dimetylbiladiene scaffold as a sensitizer of $^1O_2$.

The Zn(DMBil) derivative was also investigated for $^1O_2$ sensitization and was found to have a quantum yield of Φ_{1O2} = 2.6 X 10^{-2} in MeOH, while irradiating at λ_{irr} = 500 nm. The increase in the ability to sensitize $^1O_2$ is likely due to the coordination of Zn^{2+} in to the center of the dimethylbiladiene scaffold. The Zn^{2+} coordination enhances the ability of the biladiene scaffold to undergo intersystem crossing to the triplet state. The resulting intersystem crossing in consistent with the decrease in the Φ_{fl}, where Zn(DMBil) is less than half of the free base.

Cu(DMBil) was also investigated for the sensitization of $^1O_2$, but was found to largely ineffective. The $^1O_2$ sensitization was found to have a quantum yield of Φ_{1O2} = <0.2 X 10^{-2} in MeOH, while irradiating at λ_{irr} = 500 nm. This was not unexpected, with the excited states rapid relaxation to the low energy d-d states of the Cu^{2+}.

6.5 Summary

Linear tetrapyrrole scaffolds have remained underdeveloped compared to tetrapyrrole macrocycle systems such as porphyrins and corroles. A synthetic route has been described that allows for easy construction and isolation of the biladiene scaffold. The DMBil has shown good stability with the use of geminal dimethyl substitution at the 10-position as well as pentafluorophenyl groups at the 5 and 15

positions. DMBil has also shown interesting redox chemistry and use as a ligand system. The addition of both Zn^{2+} and Cu^{2+} to the center of the DMBil can be accomplished under mild conditions and is high yielding. Zn(DMBil) and Cu(DMBil) both support multielectron redox chemistry displaying the ability to be oxidized and reduced by two electrons. The photophysics for DMBil and Zn(DMBil) were measured and found to be fluorescent with relatively short lived fluorescent lifetimes. DMBil and Zn(DMBil) have shown the ability for the sensitization of $^1O_2$ with modest quantum yields. The biladiene represents a potential platform for the use in photodynamic therapy.

REFERENCES

[1] Milgrom, L. R. *The Colours of Life: An Introduction to the Chemistry of Porphyrins and Related Compounds*; Oxford University Press: New York, 1997.

[2] Gray, H. B.; Winkler, J. R. *Electron Transfer in Chemistry*; Wiley-VCH: Weinheim, Germany, 2001; Vol. 3.1.1.

[3] Riggs, A. F. *Cur. Opin. Struct. Biol*. **1991**, 1, 915−921.

[4] Sono, M.; Roach, M. P.; Coulter, E. D.; Dawson, J. H. *Chem. Rev*. **1996**, 96, 2841−2888.

[5] Dunford, H. B. *Heme Peroxidases*; John Wiley: Chichester, U.K., 1999.

[6] Winkler, J. R.; Gray, H. B. *Chem. Rev*. **1992**, 92, 369−379.

[7] Green, B. R.; Durnford, D. G. *Annu. Rev. Plant Physiol*. **1996**, 47, 685−714.

[8] Ben-Shem, A.; Frolow, F.; Nelson, N. *Photosynth. Res*. **2004**, 81, 239−250.

[9] Kerfeld, C. A.; Krogmann, D. W. *Annu. Rev. Plant Physiol*. **1998**, 49, 397−425.

[10] Kellett, R. M.; Spiro, T. G. *Inorg. Chem.* **1985**, 24, 2373-2377.

[11] Collman, J. P.; Wagenknecht, P. S.; Lewis, N. S. *J. Am. Chem. Soc.* **1992**, 114, 5665-5673.

[12] Bhugun, I.; Lexa, D.; Savéant, J.-M. *J. Am. Chem. Soc.* **1996**, 118, 3982-3983.

[13] Lee, C. H.; Dogutan, D. K.; Nocera, D. G. *J. Am. Chem. Soc.* **2011**, 133, 8775-8777.

[14] Wilson, A. D.; Newell, R. H.; McNevin, M. J.; Muckerman, J. T.; Dubois, M. R.; Dubois, D. L. *J. Am. Chem. Soc*. **2006**, 128, 358–366.

[15] Wilson, A. D.; Shoemaker, R. K.; Miedaner, A.; Muckerman, J. T.; Dubois, D. L.; Dubois, M. R. *Proc. Natl. Acad. Sci. U.S.A.* **2007**, 104, 6951–6956.

[16] Henry, R. M.; Shoemaker, R. K.; DuBois, D. L.; DuBois, M. R. *J. Am. Chem. Soc*. **2006**, 128, 3002–3010.

[17] Barton, B. E.; Rauchfuss, T. B. *J. Am. Chem. Soc*. **2010**, 132, 14877–14885.

[18] Nicolet, Y.; de Lacey, A. L.; Vérnede, X.; Fernandez, V. M.; Hatchikian, E. C.; Fontecilla-Camps, J. C. *J. Am. Chem. Soc*. **2001**, 123, 1596–1601.

[19] Chang, C. J.; Deng, Y.; Shi, C.; Chang, C. K.; Anson, F. C.; Nocera, D. G. *Chem. Commun.* **2000**, 1355-1356.

[20] Chang, C. J.; Loh, Z.-H.; Shi, C.; Anson, F. C.; Nocera, D. G. *J. Am. Chem. Soc.* **2004**, 126, 10013-10020.

[21] Rosenthal, J.; Nocera, D. G. *Acc. Chem. Res.* **2007**, 40, 543-553.

[22] Meunier, B. *Chem. Rev.* **1992**, 92, 1411-1456.

[23] Rose, E.; Andrioletti, B.; Zrig, S.; Quelquejeu-Ethéve, M. *Chem. Soc. Rev.* **2005**, 34, 573-583.

[24] Groves, J. T.; Myers, R. S. *J. Am. Chem. Soc.* **1983**, 105, 5791-5796.

[25] Stephenson, N. A.; Bell, A. T. *J. Mole. Catal. A: Chem.* **2007**, 275, 54-62.

[26] Hammouche, M.; Lexa, D.; Momenteau, M.; Savéant, J.-M. *J. Am. Chem. Soc.* **1991**, 113, 8455-8466.

[27] Bhugun.I.; Lexa, D.; Savéant, J.-M. *J. Am. Chem. Soc.* **1994**, 116, 5015-5016.

[28] Behar, D.; Dhanasekaran, T.; Neta, P.; Hosten, C. M.; Ejeh, D.; Hambright, P.; Fujita, E. *J. Phys. Chem. A* **1998**, 102, 2870−2877.

[29] Costentin, C.; Drouet, S.; Robert, M.; Savéant, J.-M. *Science*, **2012**, 338, 90-94.

[30] Pistner, A. J.; Yap, G. P. A.; Rosenthal, J. *J. Phys. Chem. C* **2012**, 116, 16918-16924.

[31] Ito, T.; Hamaguchi, T.; Nagino, H.; Yamaguchi, T.; Kido, H.; Zavarine, I. S.; Richmond, T.; Washington, J.; Kubiak, C. P. *J. Am. Chem. Soc.* **1999**, 121, 4625-4632.

[32] Ito, T.; Hamaguchi, T.; Nagino, H.; Yamaguchi, T.; Washington, J.; Kubiak, C. P. *Science* **1997**, 277, 660-663.

[33] Vahrenkamp, H.; Geiss, A.; Richardson, G. N. *J. Chem. Soc., Dalton Trans.* **1997**, 3643-3651.

[34] Balzani, V.; Juris, A.; Venturi, M.; Campagna, S.; Serroni, S. *Chem. Re*v. **1996**, 96, 759-833.

[35] Kunkely, H.; Pawlowski, V.; Vogler, A. *Inorg. Chim. Acta* **1994**, 225, 327-330.

[36] Vogler, A.; Osman, A. H.; Kunkely, H. *Coord. Chem. Rev.* **1985**, 64, 159-173.

[37] Heyduk, A. F.; Macintosh, A. M.; Nocera, D. G. *J. Am. Chem. Soc.* **1999**, 121, 5023-5032.

[38] Odom, A. L.; Heyduk, A. F.; Nocera, D. G. *Inorg. Chim. Acta* **2000**, 297, 330-337.

[39] Heyduk, A. F.; Nocera, D. G. *J. Am. Chem. Soc.* **2000**, 122, 9415-9426.

[40] Heyduk, A. F.; Nocera, D. G. *Science* **2001**, 293, 1639-1641.

[41] Manke, D. R.; Nocera, D. G. *Inorg. Chem*. **2003**, 42, 4431-4436.

[42] Hsu, T. L. C.; Helvoigt, S. A.; Partigianoni, C. M.; Turro´, C.; Nocera, D. G. *Inorg. Chem.* **1995**, 34, 6186-6190.

[43] Bachmann, J.; Nocera, D. G. *J. Am. Chem. Soc.* **2004**, 126, 2829-2837.

[44] Bachmann, J.; Nocera, D. G. *J. Am. Chem. Soc.* **2005**, 127, 4730-4743.

[45] Campbell, W. M.; Jolley, K. W.; Wagner, P.; Wagner, K.; Walsh, P. J.; Gordon, K. C.; Schmidt-Mende, L.; Nazeeruddin, M. K.; Wang, Q.; Grätzel, M.; Officer, D. L. *J. Phys. Chem. C* **2007**, 111, 11760-11762.

[46] Wang, Q.; Campbell, W. M.; Bonfantani, E. E.; Jolley, K. W.; Officer, D. L.; Walsh, P. J.; Gordon, K.; Humphry-Baker, R.; Nazeeruddin, M. K.; Gratzel, M. *J. Phys. Chem. B* **2005**, 109, 15397−15409.

[47] Papagiannakis, E.; Kennis, J. T. M.; van Stokkum, I. H. M.; Cogdell, R. J.; van Grondelle, R. *Proc. Natl. Acad. Sci. U.S.A.* **2002**, 99, 6017−6022.

[48] Cerullo, G.; Polli, D.; Lanzani, G.; De Silvestri, S.; Hashimoto, H.; Cogdell, R. J. *Science* **2002**, 298, 2395−2398.

[49] Frank, H. A.; Cogdell, R. *J. Photochem. Photobiol*. **1996**, 63, 257−264.

[50] Yella, A.; Lee, H.; Tsoa, H. N.; Yi, C.; Chandiran, A. K.; Nazeeruddin, M.; Diau, E. W.; Yeh, C.; Zakeeruddin, S. M.; Gratzel, M. *Science* **2011**, 334, 629-634.

[51] Simon, M.; Yella, A.; Gao, P.; Humphry-Baker, R.; Curchod, B. F. E.; Ashari-Astani, N.; Tavernelli, I.; Rothlisberger, U.; Nazeeruddin, Md. K.; Gratzel, M. *Nat. Chem.* **2014**, 6, 242-247.

[52] Nyokong, T. *Coord. Chem. Rev.* **2007**, 251, 1707-1722.

[53] Martín-Gomis, L.; Fernández-Lázaro, F.; Sastre-Santos, Á. *J. Mater. Chem. A* **2014**, 2, 15672-15682.

[54] Ikeuchi, T.; Nomoto, H.; Masaki, N.; Griffith, M. J.; Mori, S.; Kimura, M. *Chem. Commun*., **2014**, 50, 1941-1943.

[55] Ragoussi, M.-E.; Yum, J.-H.; Chandiran, A. K.; Ince, M.; de la Torre, G.; Grätzel, M.; Nazeeruddin, M. K.; Torres, T. *ChemPhysChem*, **2014**, 15, 1033-1036.

[56] Walker, D.; Chappel, S.; Mahammed, A.; Brunschwig, B. S.; Winkler, J. R.; Gray, H. B.; Zaban, A.; Gross, Z. *J. Porphyrins Phthalocyanines* **2006**, 10, 1259–1262.

[57] Pandey, R. K.; Zheng, G. In *The Porphyrin Handbook*, Kadish, K. M.; Smith, K. M.; Guilard, R. Eds.; Academic Press: San Diego, CA, 2000; Vol. 6, pp 157-230

[58] Dolmans, D. E. J. G. J.; Fukumura, D.; Jain, R. K. *Nat. Rev. Cancer* **2003**, 3, 380-387.

[59] Oleinick, N. L.; Antunez, A. R.; Clay, M. E.; Rihter, B. D.; Kenney, M. E. *Photochem. Photobiol*. **1993**, 57, 242-247.

[60] Detty, M. R.; Gibson, S. L.; Wagner, S. J. *J. Med. Chem*. **2004**, 47, 3897-3915.

[61] Pangborn, A. B.; Giardello, M. A.; Grubbs, R. H.; Rosen, R. K.; Timmers, F. J. *Organometallics* **1996**, 15, 1518-1520.

[62] Megiatto, J. D., Jr.; Schuster, D. I.; Abwandner, S.; de Miguel, G.; Guldi, D. M. *J. Am. Chem. Soc*. **2010**, 132, 3847-3861.

[63] Littler, B. J.; Miller, M. A.; Hung, C.-H.; Wagner, R. W.; O'Shea, D. F.; Boyle, P. D.; Lindsey, J. S. *J. Org. Chem.* **1999**, 64, 1391-1396.

[64] Borbas, K. E.; Chandrashaker, V.; Muthiah, C.; Kee, H. L.; Holten, D.; Lindsey, J. S. *J. Org. Chem*. **2008**, 73, 3145-3158.

[65] Brouwer, A. M. Standards for Photoluminescence Quantum Yield Measurements in Solution *Pure Appl. Chem*. **2011**, 83, 2213-2228.

[66] Brouwer, A. M. *Pure Appl. Chem.* **2011**, *83*, 2213.

[67] Calvert, J. M.; Caspar, J. V.; Binstead, R. A.; Westmoreland, T. D.; Meyer, T. J. *J. Am. Chem. Soc*. **1982**, 104, 6620-6627.

[68] Ma, Y.; Shaw, R.; Yu, X.; O'Neil, H. M.; Hong, K. *J. Phys. Chem. B* **2012**, 116, 14451-14460.

[69] Noviandri, I.; Brown, K. N.; Fleming, D. S.; Gulyas, P. T.; Lay, P. A.; Masters, A. F.; Philips, L. *J. Phys. Chem. B.* **1999**, 103, 6713-6722.

[70] Liu, Y.; Hammitt, R.; Lutterman, D. A.; Joyce, L. E.; Thummel, R. P.; Turro, C. *Inorg. Chem.*, **2009**, 48, 375-385.

[71] Bhattacharyya, K.; Das, P. K. *Chem. Phys. Lett*. **1985**, 116, 326−332.

[72] Frisch, M. J.; Trucks, G. W.; Schlegel, H. B.; Scuseria, G. E.; Robb, M. A.; Cheeseman, J. R.; Scalmani, G.; Barone, V.; Mennucci, B.; Petersson, G. A.; Nakatsuji, H.; Caricato, M.; et al. *Gaussian 09*, revision A.1; Gaussian, Inc., Wallingford, CT, 2009.

[73] Becke, A. D. *J. Chem. Phys.* **1993**, 98, 5648−5652.

[74] Becke, A. D. *Phys. Rev. A* **1988**, 38, 3098−3100.

[75] Lee, C.; Yang, W.; Parr, R. G. *Phys. Rev. B: Condens. Matter Mater. Phys*. **1988**, 7, 785−789.

[76] Cances, M. T.; Mennucci, B.; Tomasi, J. *J. Chem. Phys*. **1997**, 107, 3032−3041.

[77] Tomasi, J.; Persico, M. *Chem. Rev*. **1994**, 94, 2027−2094.

[78] Cossi, M.; Barone, V.; Mennucci, B.; Tomasi, J. *Chem. Phys. Lett*. **1998**, 286, 253−260.

[79] Mennucci, B.; Tomasi, J. *J. Chem. Phys*. **1997**, 106, 5151−5158.

[80] Cossi, M.; Scalmani, G.; Rega, N.; Barone, V. *J. Chem. Phys*. **2002**, 117, 43−54.

[81] Hay, P. J.; Wadt, W. R. *J. Chem. Phys*. **1985**, 82, 284−298.

[82] Marenich, A. V.; Cramer, C. J.; Truhlar, D. G. *J. Phys. Chem. B* **2009**, 113, 6378−6396.

[83] Hay, P. J.; Wadt, W. R. *J. Chem. Phys*. **1985**, 82, 284−298.

[84] Marenich, A. V.; Cramer, C. J.; Truhlar, D. G. *J. Phys. Chem. B* **2009**, 113, 6378−6396.

[85] Solladie´, N.; Walther, M. E.; Herschbach, H.; Leize, E.; Van Dorsselaer, A.; Figueira Duartec, T. M.; Nierengarten, J.-F. *Tetrahedron* **2006**, 62, 1979-1987.

[86] O'Brien, A. Y.; McGann, J. P.; Geier, G. R., III. *J. Org. Chem*. **2007**, 72, 4084-4094.

[87] Sheldrick, G.M. *Acta Cryst*. **2008**, A64, 112-122.

[88] Spek, A. L. *J. Appl. Cryst*. **2003**, 36, 7-13.

[89] Woodward, R B. *Ind. Chim. Belg.* **1962**, 27, 1293-1308.

[90] Jeandon, C.; Krattinger, B.; Ruppert, R.; Callot, H. J. *Inorg. Chem.* **2001**, 40, 3149-3153.

[91] Setsune, J.-i.; Ikeda, M.; Iida, T.; Kitao, T. *J, Am. Chem. Soc.* **1988**, 110, 6572-6574.

[92] Setsune, J.-i.; Ishimaru, Y.; Kitao, T. *Chem. Lett.* **1990**, 1351-1354.

[93] Setsune, J.-i.; Yamaji, H.; Kitao, T. *Tetrahedron Lett.* **1990**, 31, 5057-5060.

[94] Setsune, J.-i.; Wada, K.-i.; Higashino, H. *Chem. Lett.* **1994**, 213-215.

[95] Setsune, J.-i.; Kashihara, K.; Wada, K.-i. *Chem. Lett.* **2001**, 608-609.

[96] Krattinger, B.; Callot, H. J. *Chem. Commun.* **1996**, 1341-1342.

[97] Rupert, R.; Jeandon, C.; Sgambati, A.; Callot, H. J. *Chem. Commun.* **1999**, 2123-2124.

[98] Ishimaru, Y.; Sumida, S.; Iida, T. *Tetrahedron Lett.* **2001**, 42, 419-421.

[99] Krattinger, B.; Callot, H. J. *Eur. J. Chem.* **1999**, 1857-1867.

[100] LeSaulnier, T. D.; Graham, B. W.; Geier, G. R., III. *Tetrahedron Lett.* **2005**, 46, 5633-5637.

[101] O'Brien, A. Y.; McGann, J. P.; Geier, G. R., III. *J. Org. Chem.* **2007**, 72, 4084-4092.

[102] Krattinger, B.; Callot, H. J. *Tetrahedron Lett.* **1996**, 37, 7699-7702.

[103] Medforth, C. J. In *The Porphyrin Handbook;* Kadish, K. M.; Smith, K. M.; Guilard, R., Eds.; Academic: San Diego, CA, 2000; Chapt. 35, p 1.

[104] Pople, J. A.; Untch, K. G. *J. Am. Chem. Soc.* **1966**, 88, 4811-4815.

[105] Aihara, J.; Kimura, E.; Krygowski, T. M. *Bull. Chem. Soc. Jpn.* **2008**, 81, 826-835.

[106] Gomes, J. A. N. F.; Mallion, R. B. *Chem. Rev.* **2001**, 101, 1349-1384.

[107] Connelly, N. G.; Geiger, W. E. *Chem. Rev.* **1996**, 96, 877-910.

[108] Gale, P. A.; Sessler, J. L.; Král, V.; Lynch, V. *J. Am. Chem. Soc*. **1996**, 118, 5140−5141.

[109] Gale, P. A; Sessler, J. L; Král, V. *Chem. Commun*. **1998**, 1−8.

[110] Gale, P. A.; Anzenbacher, P., Jr.; Sessler, J. L. *Coord. Chem. Rev*. **2001**, 222, 57−102.

[111] Sessler, J. L.; Cyr, M.; Furuta, H.; Král, V.; Mody, T.; Morishima, T.; Shionoya, M.; Weghorn, S. *Pure Appl. Chem*. **1993**, 65, 393−398.

[112] Král, V.; Sessler, J. L.; Zimmerman, R. S.; Seidel, D.; Lynch, V.; Andrioletti, B. *Angew. Chem., Int. Ed*. **2000**, 39, 1055−1058.

[113] Sessler, J. L.; Zimmerman, R. S.; Bucher, C.; Král, V.; Andrioletti, B. *Pure Appl. Chem*. **2001**, 73, 1041−1057.

[114] Sessler, J. L.; Camiolo, S.; Gale, P. A. *Coord. Chem. Rev*. **2003**, 240, 17−55.

[115] Subbaiyan, N. K.; Hill, J. P.; Ariga, K.; Fukuzumi, S.; D'Souza, F. *Chem. Comm.* **2011**, 47, 6003-6005.

[116] Cogdell, R. J. *Philos. Trans. R. Soc. London, Ser. B* **1978**, 284, 569-579.

[117] Siefermann-Harms, D. *Physiol. Plant.* **1987**, 69, 561-568.

[118] Nieto-Pescador, J. S.; Abraham, B.; Pistner, A. J.; Rosenthal, J.; Gundlach, L. *Phys. Chem. Chem. Phys.* **2015**, Advance Article. **DOI:** 10.1039/C5CP00296F

[119] Wang, Q.; Campbell, W. M.; Bonfantani, E. E.; Jolley, K, W.; Officer, D. L.; Walsh, P. J.; Gordon, K.; Humphry-Baker, R.; Nazeeruddin, M. K.; Grätzel, M. *J. Phys. Chem. B*, **2005**, 109, 15397-15409.

[120] Gust, D.; Moore, T. A.; Moore, A. L. *Acc. Chem. Res.* **2001**, 34, 40-48.

[121] Campbell, W. M.; Burrel, A. K.; Officer, D. L.; Jolley, K, W. *Coord. Chem. Rev.* **2004**, 248, 1363-1379.

[122] Kay, A.; Grätzel, M. *J. Phys. Chem.* **1993**, 97, 6272-6277.

[123] Kay, A.; Humphry-Baker, R.; Grätzel, M. *J. Phys. Chem.* **1994**, 98, 952-959.

[124] Campbell, W. M.; Jolley, K. W.; Wangner, P.; Wangner, K.; Walsh, P. J.; Gordon, K. C.; Schmidt-Mende, L.; Nazeeruddin, M. K.; Wang, Q.; Grätzel, M.; Officer, D. L. *J. Phys. Chem. C* **2007**, 111, 11760-11762.

[125] Floriani, C.; Floriano-Moro, R. In *The Porphyrin Handbook;* Kadish, K. M., Smith, K. M., Guilard, R., Eds.; Academic Press: New York, 2000.

[126] Harel, Y.; Manassen, J. *J. Am. Chem. Soc.* **1977**, 99, 5817-5818.

[127] Kalyanasundaram, K.; Grätzel, M. *Helv. Chim. Acta.* **1980**, 63, 478-485.

[128] Bartocci, C.; Maldotti, A.; Varani, G.; Battioni, P.; Carassiti, V.; Mansuy, D. *Inorg. Chem.* **1991**, 30, 1255-1259.

[129] Rosenthal, J.; Pistorio, B. J.; Chng, L. L.; Nocera, D. G. *J. Org. Chem.* **2005**, 70, 1885-1888.

[130] Rosenthal, J.; Luckett, T. D.; Hodgkiss, J. M.; Nocera, D. G. *J. Am Chem. Soc.* **2006**, 128, 6546-6547.

[131] Gale, P. A.; Sessler, J. L.; Král, V.; Lynch, V. *J. Am. Chem. Soc.* **1996**, 118, 5140-5141.

[132] Gale, P. A.; Anzenbacker, P., Jr.; Sessler, J. L. *Coord. Chem. Rev.* **2001**, 222, 57-102.

[133] Pistner, A. J.; Lutterman, D. L.; Ghidiu, M. J.; Walker, E.; Yap, G. P. A.; Rosenthal, J. *J. Phys. Chem. C* **2014**, 118, 14124-14132.

[134] Gouterman, M. *J. Chem. Phys.* **1959**, 30, 1139-1161.

[135] Gouterman, M. *J. Mol. Spectrosc.* **1961**, 6, 138-163.

[136] Gouterman, M.; Wagnière, G. H. *J. Mol. Spectrosc.* **1963**, 11, 108-127.

[137] Spellane, P. J.; Gouterman, M. Antipas, A.; Kim, S.; Liu, Y. C. *Inorg. Chem.* **1980**, 19, 386-391.

[138] Pistner, A. J.; Lutterman, D. A.; Ghidiu, M. J.; Ma, Y.-Z.; Rosenthal, J. *J. Am. Chem. Soc.* **2013**, 135, 6601-6607.

[139] Sessler, J. L.; Cyr, M.; Furuta, H.; Král, V.; Mody, T.; Morishima, T.; Shinoya, M.; Weghorn, S. *Pure Appl. Chem.* **1993**, 65, 393-398.

[140] Sessler, J. L.; Hoehner, M. C.; Gebauer, A.; Andrievsky, A.; Lynch, V. *J. Org. Chem.* **1997**, 62, 9251-9260.

[141] Young, E. R.; Rosenthal, J.; Nocera, D. G. *Chem. Comm.* **2008**, 2322-2324.

[142] Jorgenson, W. L.; Pranata, J. *J. Am. Chem. Soc.* **1990**, 112, 2008-2010.

[143] Pranata, J.; Wierschke, S. G.; Jorgensen, W. L. *J. Am. Chem. Soc.* **1991**, 113, 2810-2819.

[144] Izutsu, K. *Acid-Base Dissociation Constants in Dipolar Aprotic Solvents*; Blackwell Scientific: Cambridge, MA, 1990.

[145] Bordwell, F. G. *Acc. Chem. Res.* **1988**, 21, 456-463.

[146] Smith, K. M. *Porphyrins and Metalloporphyrins*; Chapters 3 and 4; Elsevier Scientific Publishing Company: Amsterdam, 1975.

[147] Louche, L. M.-M.; Luro, F.; Gaydou, E. M.; Lesage, J.-C. *J. Agric. Food Chem.* **2000**, 48, 4728-4733.

[148] Arciero, D. M.; Hooper, A. B. *Biochem. Soc. Trans.* **1998**, 26, 385-389.

[149] Stolzenberg, A. M.; Stershic, M. T. *Inorg. Chem.* **1987**, 26, 3082-3083.

[150] Stolzenberg, A. M.; Stershic, M. T. *J. Am. Chem. Soc.* **1988**, 110, 6391-6402.

[151] Abou-Gamra, Z.; Harriman, A.; Neta, P. *J. Chem. Soc. Faraday Trans.* **1986**, 82, 2337-2350.

[152] Solis, B. H.; Maher, A. G.; Honda, T.; Powers, D. C.; Nocera, D. G.; Hammes-Schiffer, S. *ACS Catal.* **2014**, 4, 4516-4526.

[153] Closs, G. S.; Closs, L. E. *J. Am. Chem. Soc.* **1963**, 85, 818-819.

[154] Sugimoto, H. *J. Chem Soc Dalton Trans.* **1982**, 1169-1171.

[155] Jamin, M. E.; Iwamoto, R. T. *Inorg. Chim. Acta.* **1978**, 27, 135-143.

[156] Shimidzu, T.; Iyoda, T.; Honda, K. *Pure Appl. Chem.* **1988**, 60, 1025-1032.

[157] Segawa, H.; Azumi, R.; Shimidzu, T. *J. Am. Chem. Soc.* **1992**, 114, 7564-7565.

[158] Vestfrid, J.; Botoshansky, M.; Palmer, J. H.; Durrell, A. C.; Gray, H. B.; Gross, Z. *J. Am. Chem. Soc.* **2011**, 133, 12899-12901.

[159] Kowalska, D.; Liu, X.; Tripathy, U.; Mahammed, A.; Gross, Z.; Hirayama, S.; Steer, R. P. *Inorg. Chem.* **2009**, 48, 2670-2676.

[160] Paolesse, R.; Licoccia, S.; Boschi, T. *Inorganica Chimica Acta* **1990**, 178, 9-12.

[161] Kadish, K. M.; Will, S.; Adamian, V. A.; Walther, B.; Erben, C.; Ou, Z.; Guo, N.; Vogel, E. *Inorg. Chem.* **1998**, 37, 4573-4577.

[162] Simkhovich, L.; Mahammed, A.; Goldberg, I.; Gross, Z. *Chem. Eur. J.* **2001**, 7, 1041-1055.

[163] Reith, L. M.; Stiftinger, M.; Monkowius, U.; Knör, G.; Schoefberger, W. *Inorg. Chem.* **2011**, 50, 6788-6797.

[164] Kadish, K. M.; Erben, C.; Ou, Z.; Adamian, V. A.; Will, S.; Vogel, E. *Inorg. Chem.* **2000**, 39, 3312-3319.

[165] Meier-Callahan, A. E.; Gray, H. B.; Gross, Z. *Inorg. Chem.* **2000**, 39, 3605-3607.

[166] Meier-Callahan, A. E.; Di Bilio, A. J.; Simkhovich, L.; Mahammed, A.; Goldberg, I.; Gray, H. B.; Gross, Z. *Inorg. Chem.* **2001**, 40, 6788-6793.

[167] Liu, S.; Mase, K.; Bougher, C.; Hicks, S. D.; Abu-Omar, M. M.; Fukuzumi, S. *Inorg. Chem.* **2014**, 53, 7780-7788.

[168] Simkhovich, L.; Galili, N.; Saltsman, I.; Goldberg, I.; Gross, Z. *Inorg. Chem.* **2000**, 39, 2704-2705.

[169] Wasbotten, I. H.; Wondimagegn, T.; Ghosh, A. *J. Am. Chem. Soc.* **2002**, 124, 8104-8116.

[170] Luobeznova, I.; Simkhovich, L.; Goldberg, I.; Gross, Z. *Eur. J. Inorg. Chem.* **2004**, 1724-1732.

[171] Will, S.; Lex, J.; Vogel, E.; Schmickler, H.; Gisselbrecht, J.-P.; Haubtmann, C.; Bernard, M.; Gross, M. *Angew. Chem. Int. Ed. Engl.* **1997**, 36, 357-361.

[172] Ghosh, A.; Wondimagegn, T.; Parusel, A. B. J. *J. Am. Chem. Soc.* **2000**, 122, 5100-5104.

[173] Johnson, A. W.; Price, R. *J. Chem. Soc.* **1960**, 1649-1653.

[174] Broadhurst, M. J.; Grigg, R. *Chem. Commun.* **1970**, 807-809.

[175] Thomas, K. E.; Alemayehu, A. B.; Conradie, J.; Beavers, C.; Ghosh, A. *Inorg. Chem.* **2011**, 50, 12844-12851.

[176] Lai, S.-L.; Yang, C.; Chan, M.-Y.; Guan, X.; Kwok, C.-C.; Che, C.-M. *Adv. Funct. Mater.* **2014**, 24, 4655-4665.

[177] Teo, R. D.; Gray, H. B.; Lim, P.; Termini, J.; Domeshek, E.; Gross, Z. *Chem. Commun.* **2014**, 50, 13789-13792.

[178] Rabinovich, E.; Goldberg, I.; Gross, Z. *Chem. Eur. J.* **2011**, 17, 12294-12301.

[179] Esswein, A. J.; Nocera, D. G. *Chem. Rev.* **2007**, 107, 4022-4047.

[180] Heyduk, A. F.; Nocera, D. G. *Science*, **2001**, 293, 1639-1641.

[181] Esswein, A. J.; Dempsey, J. L.; Nocera, D. G. *Inorg. Chem.* **2007**, 46, 2362-2364.

[182] Cook, T. R.; Esswein, A. J.; Nocera, D. G. *J. Am. Chem. Soc.* **2007**, 129, 10094-10095.

[183] Fackler, J. P., Jr. *Inorg. Chem.* **2002**, 41, 6959-6972.

[184] Jin, L.-M.; Yin, J.-J.; Chen, L.; Guo, C.-C.; Chen, Q.-Y. *Synlett* **2005**, 19, 2893-2898.

[185] Braslavsky, S. E.; Holzwarth, A. R.; Schaffner, K. *Angew. Chem. Int. Ed.* **1983**, 22, 656-674.

[186] Gossauer, A.; Engel, J. Linear Polypyrrolic Compounds. In *The Porphyrins*, Part B; Dolphin, D., Ed.; Academic Press: New York, 1978.

[187] *Phytochrome and Photoregulation in Plants*; Furuya, M., Ed.; Academic Press: New York, 1987.

[188] Bonfiglio, J. V.; Bonnet, R.; Buckley, D. G.; Hamzetash, D.; Hursthouse, M. B.; Malik, K. M. A.; McDonagh, A. F.; Trotter, J. *Tetrahedron* **1983**, 39, 1865-1874.

[189] Balch, A. L.; Mazzanti, M.; Noll, B. C.; Olmstead, M. M. *J. Am. Chem. Soc.* **1993**, 115, 12206-12207.

[190] Koerner, R.; Olmstead, M. M.; Ozarowski, A.; Balch, A. L. *Inorg. Chem.* **1999**, 38, 3262-3263.

[191] Koerner, R.; Olmstead, M. M.; Ozarowski, A.; Phillips, S. L.; Van Calcar, P. M.; Winkler, K.; Balch, A. L. *J. Am. Chem. Soc.* **1998**, 120, 1274-1284.

[192] Lord, P. A.; Olmstead, M. M.; Balch, A. L. *Inorg. Chem.* **2000**, 39, 1128-1134.

[193] Attar, S.; Balch, A. L.; Van Calcar, P. M.; Winkler, K. *J. Am. Chem. Soc.* **1997**, 119, 3317-3323.

[194] Koerner, R.; Olmstead, M. M.; Van Calcar, P. M.; Winkler, K.; Balch, A. L. *Inorg. Chem.* **1998**, 37, 982-988.

[195] Lord, P. A.; Noll, B. C.; Olmstead, M. M.; Balch, A. L. *J. Am. Chem. Soc.* **2001**, 123, 10554-10559.

[196] Antina, E. V.; Gusev, G. B.; Rumyantsev, E. V.; Dudina, N. A. *Russ. J. Gen. Chem.* **2009**, 79, 1900-1909.

[197] Pandey, R. K.; Zhou, H.; Gerzevske, K.; Smith, K. M. *Chem. Comm.* **1992**, 183-185.

[198] Singh, J. P.; Xie, L. Y.; Dolphin, D. *Tetrahedron Lett.* **1995**, 36, 1567-1570.

[199] Neya, S.; Sato, T.; Hoshino, T. *Tetrahedron Lett.* **2008**, 49, 1613-1615.

[200] Paolesse, R.; Froiio, A.; Nardis, S.; Mastroianni, M.; Russo, M.; Nurco, D. J.; Smith, K. M. *J. Porphyrins Phthalocyanines* **2003**, 7, 585-592.

[201] Van Norman, J. D. *Anal Chem.* **1973**, 45, 173-175.

[202] Dolphin, D.; Johnson, A. W.; Leng, J.; van den Broek, P. *J. Chem. Soc. C* **1966**, 880-884.

[203] Genokhova, N. S.; Melent'eva, T. A.; Berezovskii, V. M. *Russ. Chem. Rev.* **1980**, 49, 1056-1067.

[204] Dolphin, D.; Harris, R. L. N.; Huppatz, J. L.; Johnson, A. W.; Kay, I. T.; Leng, J. *J. Chem. Soc. C* **1966**, 98-106.

[205] Harmjanz, M.; Gill, H. S.; Scott, M. J. *J. Am. Chem. Soc.* **2000**, 122, 10476-10477.

[206] Harmjanz, M.; Scott, M. J. *Inorg. Chem.* **2000**, 39, 5428-5429.

[207] Korobkov, I.; Gamarotta, S.; Yap, G. P. A. *Angew. Chem. Int. Ed.* **2002**, 41, 3433-3436.

[208] O'Brien, A. Y.; McGann, J. P.; Geier, G. R. III. *J. Org. Chem.* **2007**, 72, 4084-4092.

[209] Pistner, A. J.; Lutterman, D. A.; Ghidiu, M. J.; Walker, E.; Yap, G. P. A.; Rosenthal, J. *J. Phys. Chem. C.* **2014**, 118, 14124-14132.

[210] Sheldrick, W. S.; Engel, J. *Acta Crystallogr., Sect. B.* **1981**, 37, 250-252.

[211] Struckmeier, G.; Thewalt, U.; Fuhrhop, J. H. *J. Am. Chem. Soc.* **1976**, 98, 278-279.

[212] Whitten, D. *Rev. Chem. Intermed.* **1978**, 2, 107-138.

[213] Bhattacharyya, K.; Das, P. K. *Chem. Phys. Lett.* **1985**, 116, 326-332.

[214] Liu, Y.; Hammitt, R.; Lutterman, D. A.; Joyce, L. E.; Thummel, R. P.; Turro, C. *Inorg. Chem.* **2009**, 48, 375-385.

[215] Young, R. H.; Wehrly, K.; Martin, R. L. *J. Am. Chem. Soc.* **1971**, 93, 5774-5779.

[216] Zenkevich, E.; Sagun, E.; Knyukshto, V.; Shulga, A.; Mironov, A.; Efremova, O.; Bonnet, R.; Songca, S. P.; Kassem, M. *J. Photochem. Photobiol., B* **1996**, 33, 171-180.

[217] Kalyanasundaram, K. *Photochemistry of Polypyridine and Porphyrin Complexes;* Academic Press: London, 1992; p. 476.

Appendix A

BOND LENGTHS AND ANGLES FOR CRYSTAL STRUCTURES

Table A.1 Bond Lengths (Å) determined for 3H(Phl^F)

Bond	Length	Bond	Length
N(1)-C(1)	1.373(5)	C(19)-F(7)	1.338(7)
N(1)-C(4)	1.390(5)	C(19)-C(20)	1.369(8)
N(1)-H(1N)	0.9943	C(20)-F(8)	1.337(5)
C(1)-C(2)	1.384(5)	C(20)-C(21)	1.353(9)
C(1)-C(38)	1.502(5)	C(21)-F(9)	1.339(7)
C(2)-C(3)	1.399(6)	C(21)-C(22)	1.398(7)
C(2)-H(2)	0.95	C(22)-F(10)	1.334(6)
C(3)-C(4)	1.391(6)	C(23)-N(3)	1.335(5)
C(3)-H(3)	0.95	C(23)-C(24)	1.461(5)
C(4)-C(5)	1.423(6)	N(3)-C(26)	1.393(4)
C(5)-C(12)	1.374(6)	C(24)-C(25)	1.336(6)
C(5)-C(6)	1.496(5)	C(24)-H(24)	0.95
C(6)-C(7)	1.371(6)	C(25)-C(26)	1.453(5)
C(6)-C(11)	1.395(7)	C(25)-H(25)	0.9500
C(7)-F(1)	1.312(6)	C(26)-C(27)	1.381(5)
C(7)-C(8)	1.374(6)	C(27)-C(34)	1.423(5)
C(8)-F(2)	1.303(7)	C(27)-C(28)	1.496(5)
C(8)-C(9)	1.404(9)	C(28)-C(33)	1.375(6)
C(9)-F(3)	1.328(6)	C(28)-C(29)	1.389(6)
C(9)-C(10)	1.344(11)	C(29)-F(11)	1.332(5)
C(10)-F(4)	1.350(8)	C(29)-C(30)	1.382(6)
C(10)-C(11)	1.390(8)	C(30)-F(12)	1.337(5)
C(11)-F(5)	1.322(8)	C(30)-C(31)	1.364(8)
C(12)-N(2)	1.397(4)	C(31)-F(13)	1.345(5)
C(12)-C(13)	1.421(6)	C(31)-C(32)	1.380(7)
N(2)-C(15)	1.380(5)	C(32)-F(14)	1.317(6)
N(2)-H(2N)	0.989	C(32)-C(33)	1.382(6)
C(13)-C(14)	1.352(6)	C(33)-F(15)	1.341(5)
C(13)-H(13)	0.95	C(34)-N(4)	1.377(5)
C(14)-C(15)	1.430(5)	C(34)-C(35)	1.391(5)
C(14)-H(14)	0.95	N(4)-C(37)	1.355(5)

Bond	Length	Bond	Length
C(15)-C(16)	1.382(5)	N(4)-H(4N)	0.8634
C(16)-C(23)	1.429(5)	C(35)-C(36)	1.400(5)
C(16)-C(17)	1.493(5)	C(35)-H(35)	0.9500
C(17)-C(18)	1.373(7)	C(36)-C(37)	1.378(5)
C(17)-C(22)	1.393(6)	C(36)-H(36)	0.9500
C(18)-F(6)	1.327(6)	C(37)-C(38)	1.518(5)
C(18)-C(19)	1.397(6)	C(38)-C(40)	1.521(6)
C(38)-C(39)	1.527(5)	C(41)-Cl(1)	1.739(10)
C(39)-H(39A)	0.9800	C(41)-Cl(3)	1.743(10)
C(39)-H(39B)	0.9800	C(41)-H(41)	1.0000
C(39)-H(39C)	0.9800	C(42)-Cl(5)	1.719(12)
C(40)-H(40A)	0.9800	C(42)-Cl(4)	1.736(13)
C(40)-H(40B)	0.9800	C(42)-Cl(6)	1.764(12)
C(40)-H(40C)	0.9800	C(42)-H(42)	1.0000
C(41)-Cl(2)	1.716(10)		
C(41)-Cl(1)	1.739(10)		

Table A.2 Bond angles (°) determined for 3H(Phl^{F})

Bond	Angle	Bond	Angle
C(1)-N(1)-C(4)	109.6(3)	N(2)-C(12)-C(13)	105.5(3)
C(1)-N(1)-H(1N)	123.7	C(15)-N(2)-C(12)	110.3(3)
C(4)-N(1)-H(1N)	123.9	C(15)-N(2)-H(2N)	121.9
N(1)-C(1)-C(2)	107.9(3)	C(12)-N(2)-H(2N)	122.6
N(1)-C(1)-C(38)	121.3(3)	C(14)-C(13)-C(12)	109.4(4)
C(2)-C(1)-C(38)	130.5(3)	C(14)-C(13)-H(13)	125.3
C(1)-C(2)-C(3)	107.5(3)	C(12)-C(13)-H(13)	125.3
C(1)-C(2)-H(2)	126.3	C(13)-C(14)-C(15)	108.6(4)
C(3)-C(2)-H(2)	126.3	C(13)-C(14)-H(14)	125.7
C(4)-C(3)-C(2)	108.6(4)	C(15)-C(14)-H(14)	125.7
C(4)-C(3)-H(3)	125.7	N(2)-C(15)-C(16)	125.0(3)
C(2)-C(3)-H(3)	125.7	N(2)-C(15)-C(14)	105.9(3)
N(1)-C(4)-C(3)	106.3(4)	C(16)-C(15)-C(14)	128.9(3)
N(1)-C(4)-C(5)	122.3(3)	C(15)-C(16)-C(23)	124.7(3)
C(3)-C(4)-C(5)	131.3(4)	C(15)-C(16)-C(17)	117.4(3)
C(12)-C(5)-C(4)	125.7(3)	C(23)-C(16)-C(17)	117.3(3)
C(12)-C(5)-C(6)	119.1(4)	C(18)-C(17)-C(22)	117.0(4)
C(4)-C(5)-C(6)	115.1(3)	C(18)-C(17)-C(16)	123.0(4)
C(7)-C(6)-C(11)	116.8(4)	C(22)-C(17)-C(16)	119.9(4)

Bond	Angle	Bond	Angle
C(7)-C(6)-C(5)	120.8(4)	F(6)-C(18)-C(17)	120.5(4)
C(11)-C(6)-C(5)	122.1(4)	F(6)-C(18)-C(19)	117.6(5)
F(1)-C(7)-C(6)	118.5(4)	C(17)-C(18)-C(19)	121.8(5)
F(1)-C(7)-C(8)	117.0(4)	F(7)-C(19)-C(20)	121.1(4)
C(6)-C(7)-C(8)	124.4(5)	F(7)-C(19)-C(18)	119.5(5)
F(2)-C(8)-C(7)	122.3(5)	C(20)-C(19)-C(18)	119.3(5)
F(2)-C(8)-C(9)	120.1(5)	F(8)-C(20)-C(21)	119.9(5)
C(7)-C(8)-C(9)	117.2(5)	F(8)-C(20)-C(19)	119.3(5)
F(3)-C(9)-C(10)	122.8(6)	C(21)-C(20)-C(19)	120.8(4)
F(3)-C(9)-C(8)	117.7(6)	F(9)-C(21)-C(20)	121.5(5)
C(10)-C(9)-C(8)	119.5(5)	F(9)-C(21)-C(22)	119.0(6)
C(9)-C(10)-F(4)	119.3(6)	C(20)-C(21)-C(22)	119.5(5)
C(9)-C(10)-C(11)	122.5(6)	F(10)-C(22)-C(17)	119.7(4)
F(4)-C(10)-C(11)	118.3(7)	F(10)-C(22)-C(21)	118.8(5)
F(5)-C(11)-C(10)	120.1(6)	C(17)-C(22)-C(21)	121.5(5)
F(5)-C(11)-C(6)	120.5(5)	N(3)-C(23)-C(16)	125.9(3)
C(10)-C(11)-C(6)	119.3(6)	N(3)-C(23)-C(24)	111.6(3)
C(5)-C(12)-N(2)	126.2(4)	C(16)-C(23)-C(24)	122.3(3)
C(5)-C(12)-C(13)	128.3(4)	C(23)-N(3)-C(26)	105.5(3)
C(25)-C(24)-C(23)	106.2(3)	C(36)-C(35)-H(35)	126.3
C(25)-C(24)-H(24)	126.9	C(37)-C(36)-C(35)	108.2(3)
C(23)-C(24)-H(24)	126.9	C(37)-C(36)-H(36)	125.9
C(24)-C(25)-C(26)	107.2(3)	C(35)-C(36)-H(36)	125.9
C(24)-C(25)-H(25)	126.4	N(4)-C(37)-C(36)	107.3(3)
C(26)-C(25)-H(25)	126.4	N(4)-C(37)-C(38)	121.4(3)
C(27)-C(26)-N(3)	125.5(3)	C(36)-C(37)-C(38)	131.2(3)
C(27)-C(26)-C(25)	124.9(3)	C(1)-C(38)-C(37)	106.3(3)
N(3)-C(26)-C(25)	109.5(3)	C(1)-C(38)-C(40)	111.8(3)
C(26)-C(27)-C(34)	125.9(3)	C(37)-C(38)-C(40)	110.0(3)
C(26)-C(27)-C(28)	118.6(3)	C(1)-C(38)-C(39)	110.2(3)
C(34)-C(27)-C(28)	115.4(3)	C(37)-C(38)-C(39)	109.7(3)
C(33)-C(28)-C(29)	117.4(3)	C(40)-C(38)-C(39)	108.8(3)
C(33)-C(28)-C(27)	122.0(4)	C(38)-C(39)-H(39A)	109.5
C(29)-C(28)-C(27)	120.6(4)	C(38)-C(39)-H(39B)	109.5
F(11)-C(29)-C(30)	117.9(4)	H(39A)-C(39)-H(39B)	109.5
F(11)-C(29)-C(28)	120.7(3)	C(38)-C(39)-H(39C)	109.5
C(30)-C(29)-C(28)	121.3(4)	H(39A)-C(39)-H(39C)	109.5
F(12)-C(30)-C(31)	119.9(4)	H(39B)-C(39)-H(39C)	109.5
F(12)-C(30)-C(29)	120.4(5)	C(38)-C(40)-H(40A)	109.5
C(31)-C(30)-C(29)	119.6(4)	C(38)-C(40)-H(40B)	109.5
F(13)-C(31)-C(30)	120.1(5)	H(40A)-C(40)-H(40B)	109.5
F(13)-C(31)-C(32)	119.2(5)	C(38)-C(40)-H(40C)	109.5

Bond	Angle	Bond	Angle
C(30)-C(31)-C(32)	120.7(4)	H(40A)-C(40)-H(40C)	109.5
F(14)-C(32)-C(31)	120.5(4)	H(40B)-C(40)-H(40C)	109.5
F(14)-C(32)-C(33)	120.9(5)	Cl(2)-C(41)-Cl(1)	111.8(7)
C(31)-C(32)-C(33)	118.6(4)	Cl(2)-C(41)-Cl(3)	111.4(6)
F(15)-C(33)-C(28)	119.8(3)	Cl(1)-C(41)-Cl(3)	111.0(7)
F(15)-C(33)-C(32)	117.9(4)	Cl(2)-C(41)-H(41)	107.5
C(28)-C(33)-C(32)	122.3(4)	Cl(1)-C(41)-H(41)	107.5
N(4)-C(34)-C(35)	106.5(3)	Cl(3)-C(41)-H(41)	107.5
N(4)-C(34)-C(27)	122.9(3)	Cl(5)-C(42)-Cl(4)	110.0(10)
C(35)-C(34)-C(27)	130.6(3)	Cl(5)-C(42)-Cl(6)	109.7(9)
C(37)-N(4)-C(34)	110.6(3)	Cl(4)-C(42)-Cl(6)	109.9(9)
C(37)-N(4)-H(4N)	127.3	Cl(5)-C(42)-H(42)	109.1
C(34)-N(4)-H(4N)	121.8	Cl(4)-C(42)-H(42)	109.1
C(34)-C(35)-C(36)	107.4(3)	Cl(6)-C(42)-H(42)	109.1
C(34)-C(35)-H(35)	126.3	C(36)-C(35)-H(35)	126.3
C(36)-C(35)-H(35)	126.3	C(38)-C(40)-H(40A)	109.5
C(37)-C(36)-C(35)	108.2(3)	C(38)-C(40)-H(40B)	109.5
C(37)-C(36)-H(36)	125.9	H(40A)-C(40)-H(40B)	109.5
C(35)-C(36)-H(36)	125.9	C(38)-C(40)-H(40C)	109.5
N(4)-C(37)-C(36)	107.3(3)	H(40A)-C(40)-H(40C)	109.5
N(4)-C(37)-C(38)	121.4(3)	H(40B)-C(40)-H(40C)	109.5
C(36)-C(37)-C(38)	131.2(3)	Cl(2)-C(41)-Cl(1)	111.8(7)
C(1)-C(38)-C(37)	106.3(3)	Cl(2)-C(41)-Cl(3)	111.4(6)
C(1)-C(38)-C(40)	111.8(3)	Cl(1)-C(41)-Cl(3)	111.0(7)
C(37)-C(38)-C(40)	110.0(3)	Cl(2)-C(41)-H(41)	107.5
C(1)-C(38)-C(39)	110.2(3)	Cl(1)-C(41)-H(41)	107.5
C(37)-C(38)-C(39)	109.7(3)	Cl(3)-C(41)-H(41)	107.5
C(40)-C(38)-C(39)	108.8(3)	Cl(5)-C(42)-Cl(4)	110.0(10)
C(38)-C(39)-H(39A)	109.5	Cl(5)-C(42)-Cl(6)	109.7(9)
C(38)-C(39)-H(39B)	109.5	Cl(4)-C(42)-Cl(6)	109.9(9)
H(39A)-C(39)-H(39B)	109.5	Cl(5)-C(42)-H(42)	109.1
C(38)-C(39)-H(39C)	109.5	Cl(4)-C(42)-H(42)	109.1
H(39A)-C(39)-H(39C)	109.5	Cl(6)-C(42)-H(42)	109.1
H(39B)-C(39)-H(39C)	109.5		

Table A.3 Bond lengths (Å) determined for 3H(Phl^{CF3})

Bond	Length	Bond	Length
C(1)-F(1)	1.340(10)	C(23)-F(9)	1.344(11)
C(1)-C(6)	1.371(9)	C(23)-C(24)	1.408(10)
C(1)-C(2)	1.387(12)	C(24)-F(10)	1.356(9)
C(2)-F(2)	1.326(12)	C(24)-C(25)	1.356(9)
C(2)-C(3)	1.357(17)	C(26)-N(3)	1.391(6)
C(3)-C(4)	1.347(17)	C(26)-C(27)	1.443(7)
C(3)-F(3)	1.355(9)	C(27)-C(28)	1.343(7)
C(4)-F(4)	1.343(11)	C(28)-C(29)	1.447(7)
C(4)-C(5)	1.362(9)	C(29)-N(3)	1.350(6)
C(5)-F(5)	1.333(8)	C(29)-C(30)	1.421(7)
C(5)-C(6)	1.377(8)	C(30)-C(39)	1.394(7)
C(6)-C(7)	1.479(6)	C(30)-C(36)	1.493(6)
C(7)-C(42)	1.373(7)	C(31)-C(36)	1.349(9)
C(7)-C(8)	1.442(6)	C(31)-C(32)	1.391(8)
C(8)-C(9)	1.375(6)	C(32)-C(33)	1.377(16)
C(8)-N(1)	1.379(6)	C(32)-C(37)	1.501(17)
C(9)-C(10)	1.397(7)	C(33)-C(34)	1.353(16)
C(10)-C(11)	1.368(6)	C(34)-C(35)	1.362(9)
C(11)-N(1)	1.367(5)	C(34)-C(38)	1.503(17)
C(11)-C(12)	1.513(6)	C(35)-C(36)	1.381(9)
C(12)-C(15)	1.511(6)	C(37)-F(11')	0.99(3)
C(12)-C(13)	1.529(6)	C(37)-F(11)	1.249(13)
C(12)-C(14)	1.538(7)	C(37)-F(13)	1.271(18)
C(15)-N(2)	1.362(5)	C(37)-F(12)	1.341(14)
C(15)-C(16)	1.380(6)	C(37)-F(13')	1.37(4)
C(16)-C(17)	1.393(7)	C(37)-F(12')	1.39(3)
C(17)-C(18)	1.387(6)	C(38)-F(16)	1.266(19)
C(18)-N(2)	1.363(6)	C(38)-F(15)	1.291(10)
C(18)-C(19)	1.419(6)	C(38)-F(14)	1.349(14)
C(19)-C(26)	1.382(6)	C(39)-N(4)	1.375(6)
C(19)-C(25)	1.499(6)	C(39)-C(40)	1.441(7)
C(20)-F(6)	1.318(8)	C(40)-C(41)	1.356(7)
C(20)-C(21)	1.375(9)	C(41)-C(42)	1.429(7)
C(20)-C(25)	1.409(9)	C(42)-N(4)	1.388(6)
C(21)-F(7)	1.346(11)	C(23)-F(9)	1.344(11)
C(21)-C(22)	1.346(15)	C(23)-C(24)	1.408(10)
C(22)-F(8)	1.325(8)	C(24)-F(10)	1.356(9)
C(22)-C(23)	1.397(16)	C(24)-C(25)	1.356(9)

Table A.4 Bond angles (°) determined for 3H(Phl^{CF3})

Bond	Angle	Bond	Angle
F(1)-C(1)-C(6)	120.3(6)	C(15)-C(16)-C(17)	108.4(4)
F(1)-C(1)-C(2)	118.4(8)	C(18)-C(17)-C(16)	107.4(4)
C(6)-C(1)-C(2)	121.3(9)	N(2)-C(18)-C(17)	106.8(4)
F(2)-C(2)-C(3)	119.5(10)	N(2)-C(18)-C(19)	122.6(4)
F(2)-C(2)-C(1)	120.7(13)	C(17)-C(18)-C(19)	130.4(4)
C(3)-C(2)-C(1)	119.7(9)	C(26)-C(19)-C(18)	126.0(4)
C(4)-C(3)-F(3)	121.5(14)	C(26)-C(19)-C(25)	119.0(4)
C(4)-C(3)-C(2)	120.5(7)	C(18)-C(19)-C(25)	114.9(4)
F(3)-C(3)-C(2)	117.7(13)	F(6)-C(20)-C(21)	118.1(7)
F(4)-C(4)-C(3)	120.3(8)	F(6)-C(20)-C(25)	120.6(5)
F(4)-C(4)-C(5)	120.8(10)	C(21)-C(20)-C(25)	121.2(8)
C(3)-C(4)-C(5)	118.9(10)	F(7)-C(21)-C(22)	119.2(8)
F(5)-C(5)-C(4)	117.0(7)	F(7)-C(21)-C(20)	120.0(10)
F(5)-C(5)-C(6)	119.4(5)	C(22)-C(21)-C(20)	120.8(9)
C(4)-C(5)-C(6)	123.6(8)	F(8)-C(22)-C(21)	122.9(12)
C(1)-C(6)-C(5)	115.9(6)	F(8)-C(22)-C(23)	116.8(11)
C(1)-C(6)-C(7)	122.3(6)	C(21)-C(22)-C(23)	120.3(7)
C(5)-C(6)-C(7)	121.8(5)	F(9)-C(23)-C(22)	123.2(8)
C(42)-C(7)-C(8)	124.6(4)	F(9)-C(23)-C(24)	118.7(10)
C(42)-C(7)-C(6)	120.0(4)	C(22)-C(23)-C(24)	118.0(8)
C(8)-C(7)-C(6)	115.3(4)	F(10)-C(24)-C(25)	119.5(6)
C(9)-C(8)-N(1)	106.7(4)	F(10)-C(24)-C(23)	117.9(7)
C(9)-C(8)-C(7)	130.7(4)	C(25)-C(24)-C(23)	122.6(8)
N(1)-C(8)-C(7)	122.6(4)	C(24)-C(25)-C(20)	117.1(6)
C(8)-C(9)-C(10)	107.8(4)	C(24)-C(25)-C(19)	122.8(6)
C(11)-C(10)-C(9)	108.3(4)	C(20)-C(25)-C(19)	120.1(5)
N(1)-C(11)-C(10)	107.1(4)	C(19)-C(26)-N(3)	125.3(4)
N(1)-C(11)-C(12)	121.3(4)	C(19)-C(26)-C(27)	125.3(4)
C(10)-C(11)-C(12)	131.3(4)	N(3)-C(26)-C(27)	109.4(4)
C(15)-C(12)-C(11)	105.6(3)	C(28)-C(27)-C(26)	107.1(4)
C(15)-C(12)-C(13)	110.0(4)	C(27)-C(28)-C(29)	107.0(4)
C(11)-C(12)-C(13)	109.9(4)	N(3)-C(29)-C(30)	125.3(4)
C(15)-C(12)-C(14)	110.4(4)	N(3)-C(29)-C(28)	110.5(4)
C(11)-C(12)-C(14)	111.6(4)	C(30)-C(29)-C(28)	124.0(4)
C(13)-C(12)-C(14)	109.1(4)	C(39)-C(30)-C(29)	124.0(4)
N(2)-C(15)-C(16)	106.5(4)	C(39)-C(30)-C(36)	119.0(4)
N(2)-C(15)-C(12)	122.2(4)	C(29)-C(30)-C(36)	117.0(4)
C(16)-C(15)-C(12)	131.2(4)	C(36)-C(31)-C(32)	122.4(8)
C(33)-C(32)-C(31)	119.8(10)	F(13')-C(37)-F(12')	97(2)
C(33)-C(32)-C(37)	120.6(8)	F(11')-C(37)-C(32)	111.0(17)

Bond	Angle	Bond	Angle
C(31)-C(32)-C(37)	119.6(10)	F(11)-C(37)-C(32)	112.1(11)
C(34)-C(33)-C(32)	119.5(7)	F(13)-C(37)-C(32)	113.6(8)
C(33)-C(34)-C(35)	118.2(9)	F(12)-C(37)-C(32)	107.7(13)
C(33)-C(34)-C(38)	123.3(10)	F(13')-C(37)-C(32)	107(2)
C(35)-C(34)-C(38)	118.5(12)	F(12')-C(37)-C(32)	100.5(11)
C(34)-C(35)-C(36)	125.2(8)	F(16)-C(38)-F(15)	108.8(16)
C(31)-C(36)-C(35)	114.9(5)	F(16)-C(38)-F(14)	102.2(9)
C(31)-C(36)-C(30)	123.5(5)	F(15)-C(38)-F(14)	102.2(9)
C(35)-C(36)-C(30)	121.6(6)	F(16)-C(38)-C(34)	119.5(10)
F(11')-C(37)-F(11)	137(2)	F(15)-C(38)-C(34)	112.6(9)
F(11')-C(37)-F(13)	46(3)	F(14)-C(38)-C(34)	109.6(14)
F(11)-C(37)-F(13)	111.5(16)	N(4)-C(39)-C(30)	125.0(4)
F(11')-C(37)-F(12)	62(4)	N(4)-C(39)-C(40)	105.9(4)
F(11)-C(37)-F(12)	106.0(8)	C(30)-C(39)-C(40)	129.0(4)
F(13)-C(37)-F(12)	105.4(12)	C(41)-C(40)-C(39)	108.3(4)
F(11')-C(37)-F(13')	121(2)	C(40)-C(41)-C(42)	109.0(4)
F(11)-C(37)-F(13')	46(3)	C(7)-C(42)-N(4)	126.3(4)
F(13)-C(37)-F(13')	139(3)	C(7)-C(42)-C(41)	127.9(4)
F(12)-C(37)-F(13')	64(3)	N(4)-C(42)-C(41)	105.8(4)
F(11')-C(37)-F(12')	118(3)	C(11)-N(1)-C(8)	109.9(4)
F(11)-C(37)-F(12')	51(3)	C(18)-N(2)-C(15)	110.8(3)
F(13)-C(37)-F(12')	73(3)	C(29)-N(3)-C(26)	106.0(3)
F(12)-C(37)-F(12')	149.5(16)	C(39)-N(4)-C(42)	110.8(4)

Table A.5 Bond lengths (Å) determined for Au(Phl$^{3,5\text{-}tBu}$)

Bond	Length	Bond	Length
Au(1)-N(4)	2.006(6)	C(9)-C(10)	1.404(12)
Au(1)-N(3)	2.011(7)	C(10)-C(11)	1.504(12)
Au(1)-N(1)	2.011(6)	C(11)-C(14)	1.502(11)
Au(1)-N(2)	2.011(6)	C(11)-C(12)	1.539(13)
N(1)-C(22)	1.363(9)	C(11)-C(13)	1.544(12)
N(1)-C(19)	1.401(9)	C(14)-C(15)	1.400(11)
N(2)-C(2)	1.368(10)	C(15)-C(16)	1.390(11)
N(2)-C(5)	1.389(10)	C(16)-C(17)	1.410(10)
N(3)-C(10)	1.348(10)	C(17)-C(18)	1.413(11)
N(3)-C(7)	1.378(10)	C(18)-C(19)	1.376(10)
N(4)-C(14)	1.370(9)	C(18)-C(48)	1.490(10)

Bond	Length	Bond	Length
N(4)-C(17)	1.391(10)	C(19)-C(20)	1.428(10)
C(1)-C(2)	1.394(10)	C(20)-C(21)	1.356(10)
C(1)-C(22)	1.416(10)	C(21)-C(22)	1.429(10)
C(1)-C(28)	1.489(10)	C(23)-C(24)	1.397(11)
C(2)-C(3)	1.440(10)	C(23)-C(28)	1.393(11)
C(3)-C(4)	1.352(12)	C(24)-C(25)	1.388(11)
C(4)-C(5)	1.453(11)	C(24)-C(29)	1.538(11)
C(5)-C(6)	1.376(12)	C(25)-C(26)	1.401(11)
C(6)-C(7)	1.417(11)	C(26)-C(27)	1.399(10)
C(6)-C(42)	1.499(11)	C(26)-C(33)	1.522(11)
C(7)-C(8)	1.417(12)	C(27)-C(28)	1.399(10)
C(8)-C(9)	1.382(13)	C(29)-C(31)	1.489(15)
C(29)-C(30)	1.527(14)	C(46)-F(9)	1.335(10)
C(29)-C(32)	1.546(14)	C(46)-C(47)	1.387(11)
C(33)-C(36)	1.504(11)	C(47)-F(10)	1.344(10)
C(33)-C(34)	1.516(13)	C(47)-C(48)	1.385(12)
C(33)-C(35)	1.548(12)	Au(2)-N(5)	1.998(6)
C(37)-F(1)	1.323(13)	Au(2)-N(8)	2.002(6)
C(37)-C(42)	1.383(14)	Au(2)-N(7)	2.012(6)
C(37)-C(38)	1.387(13)	Au(2)-N(6)	2.019(6)
C(38)-C(39)	1.333(18)	N(5)-C(50)	1.376(9)
C(38)-F(2)	1.360(14)	N(5)-C(53)	1.395(9)
C(39)-F(3)	1.354(12)	N(6)-C(55)	1.384(10)
C(39)-C(40)	1.348(19)	N(6)-C(58)	1.378(9)
C(40)-F(4)	1.324(15)	N(7)-C(62)	1.375(9)
C(40)-C(41)	1.414(14)	N(7)-C(65)	1.383(10)
C(41)-F(5)	1.345(14)	N(8)-C(67)	1.384(9)
C(41)-C(42)	1.352(15)	N(8)-C(70)	1.386(9)
C(43)-F(6)	1.324(10)	C(49)-C(50)	1.396(10)
C(43)-C(44)	1.375(12)	C(49)-C(70)	1.412(10)
C(43)-C(48)	1.406(11)	C(49)-C(76)	1.502(10)
C(44)-F(7)	1.337(10)	C(50)-C(51)	1.440(11)
C(44)-C(45)	1.388(14)	C(51)-C(52)	1.361(11)
C(45)-F(8)	1.332(10)	C(52)-C(53)	1.436(10)
C(45)-C(46)	1.371(13)	C(53)-C(54)	1.381(10)
C(54)-C(55)	1.418(11)	C(74)-C(75)	1.416(11)
C(54)-C(90)	1.500(10)	C(74)-C(81)	1.547(13)
C(55)-C(56)	1.404(10)	C(75)-C(76)	1.386(11)
C(56)-C(57)	1.387(12)	C(77)-C(80)	1.521(12)
C(57)-C(58)	1.396(11)	C(77)-C(78)	1.519(14)
C(58)-C(59)	1.493(11)	C(77)-C(79)	1.568(14)
C(59)-C(62)	1.501(11)	C(81)-C(83)	1.429(18)

Bond	Length	Bond	Length
C(59)-C(61)	1.549(10)	C(81)-C(82)	1.444(18)
C(59)-C(60)	1.561(12)	C(81)-C(84)	1.53(2)
C(62)-C(63)	1.390(11)	C(85)-F(11)	1.336(9)
C(63)-C(64)	1.395(11)	C(85)-C(90)	1.376(10)
C(64)-C(65)	1.389(11)	C(85)-C(86)	1.375(10)
C(65)-C(66)	1.415(10)	C(86)-F(12)	1.337(10)
C(66)-C(67)	1.387(11)	C(86)-C(87)	1.371(13)
C(66)-C(96)	1.489(11)	C(87)-C(88)	1.335(13)
C(67)-C(68)	1.431(10)	C(87)-F(13)	1.370(10)
C(68)-C(69)	1.335(11)	C(88)-F(14)	1.363(10)
C(69)-C(70)	1.418(10)	C(88)-C(89)	1.381(11)
C(71)-C(76)	1.387(10)	C(89)-F(15)	1.340(9)
C(71)-C(72)	1.389(10)	C(89)-C(90)	1.398(10)
C(72)-C(73)	1.389(11)	C(91)-F(16)	1.337(12)
C(72)-C(77)	1.525(11)	C(91)-C(92)	1.372(13)
C(73)-C(74)	1.394(12)	C(91)-C(96)	1.371(13)
C(92)-F(17)	1.337(15)	C(94)-C(95)	1.348(14)
C(92)-C(93)	1.364(17)	C(94)-F(19)	1.365(15)
C(93)-C(94)	1.333(17)	C(95)-F(20)	1.334(13)
C(93)-F(18)	1.368(12)	C(95)-C(96)	1.407(13)

Table A.6 Bond angles (°) determined for Au(Phl$^{3,5\text{-}tBu}$)

Bond	Angle	Bond	Angle
N(4)-Au(1)-N(3)	89.9(3)	C(10)-C(11)-C(14)	107.4(7)
N(4)-Au(1)-N(1)	90.2(2)	C(10)-C(11)-C(12)	110.1(7)
N(3)-Au(1)-N(1)	178.3(3)	C(14)-C(11)-C(12)	109.7(7)
N(4)-Au(1)-N(2)	178.9(3)	C(10)-C(11)-C(13)	110.9(7)
N(3)-Au(1)-N(2)	90.1(3)	C(14)-C(11)-C(13)	110.7(7)
N(1)-Au(1)-N(2)	89.7(2)	C(12)-C(11)-C(13)	108.0(7)
C(22)-N(1)-C(19)	109.4(6)	N(4)-C(14)-C(15)	109.3(7)
C(22)-N(1)-Au(1)	126.4(5)	N(4)-C(14)-C(11)	121.1(7)
C(19)-N(1)-Au(1)	124.2(5)	C(15)-C(14)-C(11)	129.0(7)
C(2)-N(2)-C(5)	109.8(6)	C(16)-C(15)-C(14)	107.4(7)
C(2)-N(2)-Au(1)	125.8(5)	C(15)-C(16)-C(17)	107.3(7)
C(5)-N(2)-Au(1)	124.3(5)	N(4)-C(17)-C(18)	123.0(6)

Bond	Angle	Bond	Angle
C(10)-N(3)-C(7)	109.1(7)	N(4)-C(17)-C(16)	108.3(7)
C(10)-N(3)-Au(1)	125.6(5)	C(18)-C(17)-C(16)	127.8(7)
C(7)-N(3)-Au(1)	123.7(5)	C(19)-C(18)-C(17)	124.9(7)
C(14)-N(4)-C(17)	107.7(6)	C(19)-C(18)-C(48)	117.8(7)
C(14)-N(4)-Au(1)	125.4(5)	C(17)-C(18)-C(48)	117.2(7)
C(17)-N(4)-Au(1)	125.1(5)	C(18)-C(19)-N(1)	126.7(7)
C(2)-C(1)-C(22)	122.8(7)	C(18)-C(19)-C(20)	127.4(7)
C(2)-C(1)-C(28)	117.8(6)	N(1)-C(19)-C(20)	105.9(6)
C(22)-C(1)-C(28)	118.9(6)	C(21)-C(20)-C(19)	109.1(7)
N(2)-C(2)-C(1)	126.7(7)	C(20)-C(21)-C(22)	107.6(7)
N(2)-C(2)-C(3)	107.2(6)	N(1)-C(22)-C(1)	125.7(7)
C(1)-C(2)-C(3)	125.7(7)	N(1)-C(22)-C(21)	107.8(6)
C(4)-C(3)-C(2)	108.6(7)	C(1)-C(22)-C(21)	126.2(7)
C(3)-C(4)-C(5)	107.8(7)	C(24)-C(23)-C(28)	121.5(7)
C(6)-C(5)-N(2)	127.2(7)	C(23)-C(24)-C(25)	117.4(7)
C(6)-C(5)-C(4)	126.3(7)	C(23)-C(24)-C(29)	122.5(7)
N(2)-C(5)-C(4)	106.5(7)	C(25)-C(24)-C(29)	120.1(7)
C(5)-C(6)-C(7)	123.2(7)	C(24)-C(25)-C(26)	124.0(7)
C(5)-C(6)-C(42)	119.2(7)	C(25)-C(26)-C(27)	116.1(7)
C(7)-C(6)-C(42)	117.4(8)	C(25)-C(26)-C(33)	124.0(7)
N(3)-C(7)-C(6)	125.1(7)	C(27)-C(26)-C(33)	120.0(7)
N(3)-C(7)-C(8)	107.3(7)	C(26)-C(27)-C(28)	122.3(7)
C(6)-C(7)-C(8)	127.0(8)	C(23)-C(28)-C(27)	118.7(7)
C(9)-C(8)-C(7)	107.4(8)	C(23)-C(28)-C(1)	121.5(7)
C(8)-C(9)-C(10)	107.2(8)	C(27)-C(28)-C(1)	119.8(7)
N(3)-C(10)-C(9)	109.0(7)	C(31)-C(29)-C(30)	110.0(9)
N(3)-C(10)-C(11)	122.0(7)	C(31)-C(29)-C(24)	108.3(8)
C(9)-C(10)-C(11)	128.9(7)	C(30)-C(29)-C(24)	113.7(8)
C(31)-C(29)-C(32)	109.6(10)	F(10)-C(47)-C(46)	117.4(8)
C(30)-C(29)-C(32)	106.3(9)	C(48)-C(47)-C(46)	122.7(8)
C(24)-C(29)-C(32)	108.8(7)	C(47)-C(48)-C(43)	116.2(7)
C(36)-C(33)-C(34)	106.2(7)	C(47)-C(48)-C(18)	122.0(7)
C(36)-C(33)-C(26)	109.6(7)	C(43)-C(48)-C(18)	121.8(8)
C(34)-C(33)-C(26)	109.3(7)	N(5)-Au(2)-N(8)	89.6(2)
C(36)-C(33)-C(35)	110.3(7)	N(5)-Au(2)-N(7)	178.3(3)
C(34)-C(33)-C(35)	110.4(8)	N(8)-Au(2)-N(7)	89.9(2)
C(26)-C(33)-C(35)	110.9(7)	N(5)-Au(2)-N(6)	89.9(2)
F(1)-C(37)-C(42)	119.7(9)	N(8)-Au(2)-N(6)	178.4(3)
F(1)-C(37)-C(38)	118.7(10)	N(7)-Au(2)-N(6)	90.5(2)
C(42)-C(37)-C(38)	121.6(12)	C(50)-N(5)-C(53)	108.5(6)
C(39)-C(38)-F(2)	120.0(10)	C(50)-N(5)-Au(2)	126.3(5)
C(39)-C(38)-C(37)	120.1(12)	C(53)-N(5)-Au(2)	125.1(5)

Bond	Angle	Bond	Angle
F(2)-C(38)-C(37)	119.9(12)	C(55)-N(6)-C(58)	108.2(6)
C(38)-C(39)-F(3)	120.3(12)	C(55)-N(6)-Au(2)	124.4(5)
C(38)-C(39)-C(40)	121.4(10)	C(58)-N(6)-Au(2)	125.1(5)
F(3)-C(39)-C(40)	118.1(13)	C(62)-N(7)-C(65)	108.2(6)
F(4)-C(40)-C(39)	122.5(10)	C(62)-N(7)-Au(2)	125.2(5)
F(4)-C(40)-C(41)	119.6(13)	C(65)-N(7)-Au(2)	125.5(5)
C(39)-C(40)-C(41)	117.7(13)	C(67)-N(8)-C(70)	107.9(6)
F(5)-C(41)-C(42)	119.5(9)	C(67)-N(8)-Au(2)	125.6(5)
F(5)-C(41)-C(40)	117.5(11)	C(70)-N(8)-Au(2)	126.5(5)
C(42)-C(41)-C(40)	123.0(12)	C(50)-C(49)-C(70)	122.9(7)
C(41)-C(42)-C(37)	116.0(9)	C(50)-C(49)-C(76)	119.4(7)
C(41)-C(42)-C(6)	123.5(9)	C(70)-C(49)-C(76)	117.3(6)
C(37)-C(42)-C(6)	120.4(9)	N(5)-C(50)-C(49)	126.4(7)
F(6)-C(43)-C(44)	119.4(8)	N(5)-C(50)-C(51)	108.6(6)
F(6)-C(43)-C(48)	119.0(7)	C(49)-C(50)-C(51)	124.8(7)
C(44)-C(43)-C(48)	121.6(8)	C(52)-C(51)-C(50)	106.9(7)
F(7)-C(44)-C(43)	120.9(9)	C(51)-C(52)-C(53)	109.0(7)
F(7)-C(44)-C(45)	118.7(8)	C(54)-C(53)-N(5)	125.7(7)
C(43)-C(44)-C(45)	120.4(9)	C(54)-C(53)-C(52)	127.4(7)
F(8)-C(45)-C(46)	120.4(9)	N(5)-C(53)-C(52)	107.0(6)
F(8)-C(45)-C(44)	120.2(9)	C(53)-C(54)-C(55)	125.3(7)
C(46)-C(45)-C(44)	119.3(8)	C(53)-C(54)-C(90)	117.3(7)
F(9)-C(46)-C(45)	120.1(8)	C(55)-C(54)-C(90)	117.3(6)
F(9)-C(46)-C(47)	120.2(8)	N(6)-C(55)-C(56)	108.2(7)
C(45)-C(46)-C(47)	119.7(8)	N(6)-C(55)-C(54)	122.7(6)
F(10)-C(47)-C(48)	119.9(7)	C(56)-C(55)-C(54)	128.3(7)
C(57)-C(56)-C(55)	107.2(7)	C(75)-C(76)-C(49)	120.3(7)
C(56)-C(57)-C(58)	108.1(7)	C(71)-C(76)-C(49)	120.3(7)
N(6)-C(58)-C(57)	108.2(7)	C(80)-C(77)-C(78)	109.6(8)
N(6)-C(58)-C(59)	121.6(7)	C(80)-C(77)-C(72)	112.7(8)
C(57)-C(58)-C(59)	130.0(7)	C(78)-C(77)-C(72)	109.4(7)
C(58)-C(59)-C(62)	108.8(6)	C(80)-C(77)-C(79)	105.8(8)
C(58)-C(59)-C(61)	110.5(7)	C(78)-C(77)-C(79)	110.8(9)
C(62)-C(59)-C(61)	110.3(7)	C(72)-C(77)-C(79)	108.5(8)
C(58)-C(59)-C(60)	109.3(7)	C(83)-C(81)-C(82)	112.0(13)
C(62)-C(59)-C(60)	110.1(7)	C(83)-C(81)-C(84)	108.4(13)
C(61)-C(59)-C(60)	107.8(7)	C(82)-C(81)-C(84)	100.7(15)
N(7)-C(62)-C(63)	108.2(7)	C(83)-C(81)-C(74)	113.6(10)
N(7)-C(62)-C(59)	122.3(7)	C(82)-C(81)-C(74)	113.2(9)
C(63)-C(62)-C(59)	129.1(7)	C(84)-C(81)-C(74)	108.1(11)
C(64)-C(63)-C(62)	107.9(7)	F(11)-C(85)-C(90)	120.0(7)
C(63)-C(64)-C(65)	107.2(7)	F(11)-C(85)-C(86)	117.2(7)

Bond	Angle	Bond	Angle
N(7)-C(65)-C(64)	108.5(7)	C(90)-C(85)-C(86)	122.8(8)
N(7)-C(65)-C(66)	123.1(7)	F(12)-C(86)-C(87)	120.3(8)
C(64)-C(65)-C(66)	127.7(7)	F(12)-C(86)-C(85)	121.4(8)
C(67)-C(66)-C(65)	124.7(7)	C(87)-C(86)-C(85)	118.2(8)
C(67)-C(66)-C(96)	118.7(7)	C(88)-C(87)-C(86)	121.5(8)
C(65)-C(66)-C(96)	116.5(7)	C(88)-C(87)-F(13)	120.5(9)
N(8)-C(67)-C(66)	125.8(7)	C(86)-C(87)-F(13)	118.0(9)
N(8)-C(67)-C(68)	107.8(7)	C(87)-C(88)-F(14)	121.2(8)
C(66)-C(67)-C(68)	126.4(7)	C(87)-C(88)-C(89)	120.1(9)
C(69)-C(68)-C(67)	107.5(7)	F(14)-C(88)-C(89)	118.6(9)
C(68)-C(69)-C(70)	109.5(7)	F(15)-C(89)-C(88)	119.5(7)
N(8)-C(70)-C(49)	124.9(6)	F(15)-C(89)-C(90)	119.6(7)
N(8)-C(70)-C(69)	107.2(6)	C(88)-C(89)-C(90)	120.9(8)
C(49)-C(70)-C(69)	127.5(7)	C(85)-C(90)-C(89)	116.4(7)
C(76)-C(71)-C(72)	122.3(7)	C(85)-C(90)-C(54)	121.4(7)
C(71)-C(72)-C(73)	117.0(7)	C(89)-C(90)-C(54)	122.1(7)
C(71)-C(72)-C(77)	120.2(7)	F(16)-C(91)-C(92)	118.1(11)
C(73)-C(72)-C(77)	122.8(7)	F(16)-C(91)-C(96)	120.3(9)
C(74)-C(73)-C(72)	123.3(7)	C(92)-C(91)-C(96)	121.6(12)
C(73)-C(74)-C(75)	117.4(7)	F(17)-C(92)-C(93)	120.1(11)
C(73)-C(74)-C(81)	121.5(8)	F(17)-C(92)-C(91)	120.4(13)
C(75)-C(74)-C(81)	121.1(8)	C(93)-C(92)-C(91)	119.3(13)
C(76)-C(75)-C(74)	120.6(7)	C(94)-C(93)-C(92)	120.2(11)
C(75)-C(76)-C(71)	119.3(7)	C(94)-C(93)-F(18)	118.9(14)
C(92)-C(93)-F(18)	120.9(14)	F(20)-C(95)-C(96)	119.3(9)
C(93)-C(94)-C(95)	121.5(13)	C(94)-C(95)-C(96)	120.5(13)
C(93)-C(94)-F(19)	119.5(12)	C(91)-C(96)-C(95)	116.7(9)
C(95)-C(94)-F(19)	119.0(14)	C(91)-C(96)-C(66)	121.6(9)
F(20)-C(95)-C(94)	120.2(12)	C(95)-C(96)-C(66)	121.6(9)

Table A.7 Bond lengths (Å) determined for Au(Phl$^{3,5\text{-}tBu}$Cl)

Bond	Length	Bond	Length
Au-N(2)	1.989(5)	C(10)-C(11)	1.391(18)
Au-N(3)	1.996(5)	C(12)-C(13)	1.427(8)
Au-N(1)	2.006(5)	C(13)-C(14)	1.353(10)
Au-N(4)	2.005(5)	C(13)-H(13)	0.95
Cl(1)-C(3)	1.698(7)	C(14)-C(15)	1.442(8)

Bond	Length	Bond	Length
Cl(2)-C(43)	1.692(11)	C(14)-H(14)	0.95
F(1)-C(6)	1.330(15)	C(15)-C(16)	1.393(9)
F(2)-C(7)	1.377(16)	C(16)-C(31)	1.406(8)
F(3)-C(8)	1.358(14)	C(16)-C(22)	1.501(8)
F(4)-C(9)	1.375(17)	C(17)-C(18)	1.388(9)
F(5)-C(10)	1.333(15)	C(17)-C(22)	1.401(9)
F(6)-C(40)	1.346(12)	C(17)-H(17)	0.95
F(7)-C(39)	1.353(13)	C(18)-C(19)	1.394(10)
F(8)-C(38)	1.346(10)	C(18)-C(23)	1.539(10)
F(9)-C(37)	1.350(11)	C(19)-C(20)	1.395(10)
F(10)-C(36)	1.349(12)	C(19)-H(19)	0.95
N(1)-C(1)	1.372(7)	C(20)-C(21)	1.388(8)
N(1)-C(4)	1.396(8)	C(20)-C(27)	1.541(10)
N(2)-C(15)	1.377(7)	C(21)-C(22)	1.388(9)
N(2)-C(12)	1.389(8)	C(21)-H(21)	0.95
N(3)-C(31)	1.373(7)	C(23)-C(26)	1.518(12)
N(3)-C(34)	1.402(7)	C(23)-C(25)	1.524(15)
N(4)-C(45)	1.364(8)	C(23)-C(24)	1.548(14)
N(4)-C(42)	1.398(8)	C(24)-H(24A)	0.98
C(1)-C(2)	1.390(9)	C(24)-H(24B)	0.98
C(1)-C(46)	1.517(9)	C(24)-H(24C)	0.98
C(2)-C(3)	1.383(9)	C(25)-H(25A)	0.98
C(2)-H(2)	0.95	C(25)-H(25B)	0.98
C(3)-C(4)	1.409(8)	C(25)-H(25C)	0.98
C(3)-H(3)	0.95	C(26)-H(26A)	0.98
C(4)-C(5)	1.410(8)	C(26)-H(26B)	0.98
C(5)-C(12)	1.381(9)	C(26)-H(26C)	0.98
C(5)-C(11)	1.487(12)	C(27)-C(28)	1.505(11)
C(6)-C(11)	1.381(19)	C(27)-C(30)	1.501(11)
C(6)-C(7)	1.395(16)	C(27)-C(29)	1.552(15)
C(7)-C(8)	1.31(2)	C(28)-H(28A)	0.98
C(8)-C(9)	1.31(2)	C(28)-H(28B)	0.98
C(9)-C(10)	1.373(16)	C(28)-H(28C)	0.98
C(29)-H(29A)	0.98	C(42)-C(43)	1.410(10)
C(29)-H(29B)	0.98	C(43)-C(44)	1.350(12)
C(29)-H(29C)	0.98	C(43)-H(43)	0.95
C(30)-H(30A)	0.98	C(44)-C(45)	1.399(10)
C(30)-H(30B)	0.98	C(44)-H(44)	0.95
C(30)-H(30C)	0.98	C(45)-C(46)	1.486(9)
C(31)-C(32)	1.435(9)	C(46)-C(47)	1.528(9)
C(32)-C(33)	1.356(10)	C(46)-C(48)	1.540(8)
C(32)-H(32)	0.95	C(47)-H(47A)	0.98

Bond	Length	Bond	Length
C(33)-C(34)	1.415(9)	C(47)-H(47B)	0.98
C(33)-H(33)	0.95	C(47)-H(47C)	0.98
C(34)-C(35)	1.387(9)	C(48)-H(48A)	0.98
C(41)-C(36)	1.350(12)	C(48)-H(48B)	0.98
C(41)-C(40)	1.370(13)	C(48)-H(48C)	0.98
C(41)-C(35)	1.509(9)	C(42)-C(43)	1.410(10)
C(40)-C(39)	1.378(13)	C(43)-C(44)	1.350(12)
C(39)-C(38)	1.325(15)	C(43)-H(43)	0.95
C(38)-C(37)	1.333(15)	C(44)-C(45)	1.399(10)
C(37)-C(36)	1.377(12)	C(44)-H(44)	0.95
C(35)-C(42)	1.399(10)	C(45)-C(46)	1.486(9)

Table A.8 Bond angles (°) determined for Au(Phl$^{3,5\text{-}tBu}$Cl)

Bond	Angle	Bond	Angle
N(2)-Au-N(3)	89.56(19)	C(8)-C(7)-F(2)	122.4(12)
N(2)-Au-N(1)	90.1(2)	C(8)-C(7)-C(6)	121.4(14)
N(3)-Au-N(1)	179.4(2)	F(2)-C(7)-C(6)	116.1(14)
N(2)-Au-N(4)	176.4(2)	C(9)-C(8)-C(7)	120.2(13)
N(3)-Au-N(4)	90.1(2)	C(9)-C(8)-F(3)	120.2(15)
N(1)-Au-N(4)	90.2(2)	C(7)-C(8)-F(3)	119.4(14)
C(1)-N(1)-C(4)	108.0(5)	C(8)-C(9)-C(10)	121.4(16)
C(1)-N(1)-Au	126.2(4)	C(8)-C(9)-F(4)	120.8(12)
C(4)-N(1)-Au	124.6(4)	C(10)-C(9)-F(4)	117.6(14)
C(15)-N(2)-C(12)	108.6(5)	F(5)-C(10)-C(9)	120.9(14)
C(15)-N(2)-Au	125.9(4)	F(5)-C(10)-C(11)	117.9(10)
C(12)-N(2)-Au	124.6(4)	C(9)-C(10)-C(11)	121.1(14)
C(31)-N(3)-C(34)	108.3(5)	C(6)-C(11)-C(10)	115.4(11)
C(31)-N(3)-Au	126.3(4)	C(6)-C(11)-C(5)	121.7(12)
C(34)-N(3)-Au	125.2(4)	C(10)-C(11)-C(5)	122.9(12)
C(45)-N(4)-C(42)	108.2(5)	C(5)-C(12)-N(2)	125.6(5)
C(45)-N(4)-Au	124.6(4)	C(5)-C(12)-C(13)	126.5(6)
C(42)-N(4)-Au	122.9(4)	N(2)-C(12)-C(13)	107.8(5)
N(1)-C(1)-C(2)	109.4(5)	C(14)-C(13)-C(12)	108.0(6)
N(1)-C(1)-C(46)	121.8(5)	C(14)-C(13)-H(13)	126
C(2)-C(1)-C(46)	128.8(5)	C(12)-C(13)-H(13)	126
C(3)-C(2)-C(1)	107.1(5)	C(13)-C(14)-C(15)	108.2(5)
C(3)-C(2)-H(2)	126.5	C(13)-C(14)-H(14)	125.9
C(1)-C(2)-H(2)	126.5	C(15)-C(14)-H(14)	125.9
C(2)-C(3)-C(4)	108.6(6)	N(2)-C(15)-C(16)	127.0(5)

Bond	Angle	Bond	Angle
C(2)-C(3)-Cl(1)	122.5(5)	N(2)-C(15)-C(14)	107.2(5)
C(4)-C(3)-Cl(1)	128.9(5)	C(16)-C(15)-C(14)	125.4(5)
C(2)-C(3)-H(3)	125.7	C(15)-C(16)-C(31)	121.9(5)
C(4)-C(3)-H(3)	125.7	C(15)-C(16)-C(22)	117.8(5)
N(1)-C(4)-C(5)	123.7(5)	C(31)-C(16)-C(22)	119.5(5)
N(1)-C(4)-C(3)	106.9(5)	C(18)-C(17)-C(22)	120.6(6)
C(5)-C(4)-C(3)	129.3(6)	C(18)-C(17)-H(17)	119.7
C(12)-C(5)-C(4)	125.1(6)	C(22)-C(17)-H(17)	119.7
C(12)-C(5)-C(11)	116.5(7)	C(17)-C(18)-C(19)	118.5(6)
C(4)-C(5)-C(11)	118.4(7)	C(17)-C(18)-C(23)	121.1(6)
F(1)-C(6)-C(11)	118.5(11)	C(19)-C(18)-C(23)	120.3(6)
F(1)-C(6)-C(7)	121.2(13)	C(20)-C(19)-C(18)	122.2(6)
C(11)-C(6)-C(7)	120.2(15)	C(20)-C(19)-H(19)	118.9
C(18)-C(19)-H(19)	118.9	C(30)-C(27)-C(29)	108.2(10)
C(21)-C(20)-C(19)	117.7(6)	C(20)-C(27)-C(29)	107.8(7)
C(21)-C(20)-C(27)	119.6(6)	C(27)-C(28)-H(28A)	109.5
C(19)-C(20)-C(27)	122.7(6)	C(27)-C(28)-H(28B)	109.5
C(20)-C(21)-C(22)	121.7(6)	H(28A)-C(28)-H(28B)	109.5
C(20)-C(21)-H(21)	119.1	C(27)-C(28)-H(28C)	109.5
C(22)-C(21)-H(21)	119.1	H(28A)-C(28)-H(28C)	109.5
C(21)-C(22)-C(17)	119.2(6)	H(28B)-C(28)-H(28C)	109.5
C(21)-C(22)-C(16)	120.6(6)	C(27)-C(29)-H(29A)	109.5
C(17)-C(22)-C(16)	120.2(5)	C(27)-C(29)-H(29B)	109.5
C(26)-C(23)-C(25)	109.9(10)	H(29A)-C(29)-H(29B)	109.5
C(26)-C(23)-C(18)	111.3(7)	C(27)-C(29)-H(29C)	109.5
C(25)-C(23)-C(18)	108.2(8)	H(29A)-C(29)-H(29C)	109.5
C(26)-C(23)-C(24)	108.3(10)	H(29B)-C(29)-H(29C)	109.5
C(25)-C(23)-C(24)	107.5(9)	C(27)-C(30)-H(30A)	109.5
C(18)-C(23)-C(24)	111.6(7)	C(27)-C(30)-H(30B)	109.5
C(23)-C(24)-H(24A)	109.5	H(30A)-C(30)-H(30B)	109.5
C(23)-C(24)-H(24B)	109.5	C(27)-C(30)-H(30C)	109.5
H(24A)-C(24)-H(24B)	109.5	H(30A)-C(30)-H(30C)	109.5
C(23)-C(24)-H(24C)	109.5	H(30B)-C(30)-H(30C)	109.5
H(24A)-C(24)-H(24C)	109.5	N(3)-C(31)-C(16)	125.3(5)
H(24B)-C(24)-H(24C)	109.5	N(3)-C(31)-C(32)	107.8(5)
C(23)-C(25)-H(25A)	109.5	C(16)-C(31)-C(32)	126.6(6)
C(23)-C(25)-H(25B)	109.5	C(33)-C(32)-C(31)	107.7(6)
H(25A)-C(25)-H(25B)	109.5	C(33)-C(32)-H(32)	126.1
C(23)-C(25)-H(25C)	109.5	C(31)-C(32)-H(32)	126.1
H(25A)-C(25)-H(25C)	109.5	C(32)-C(33)-C(34)	108.8(6)
H(25B)-C(25)-H(25C)	109.5	C(32)-C(33)-H(33)	125.6
C(23)-C(26)-H(26A)	109.5	C(34)-C(33)-H(33)	125.6

Bond	Angle	Bond	Angle
C(23)-C(26)-H(26B)	109.5	C(35)-C(34)-N(3)	124.5(6)
H(26A)-C(26)-H(26B)	109.5	C(35)-C(34)-C(33)	128.2(6)
C(23)-C(26)-H(26C)	109.5	N(3)-C(34)-C(33)	107.3(5)
H(26A)-C(26)-H(26C)	109.5	C(36)-C(41)-C(40)	114.9(8)
H(26B)-C(26)-H(26C)	109.5	C(36)-C(41)-C(35)	122.4(7)
C(28)-C(27)-C(30)	110.3(8)	C(40)-C(41)-C(35)	122.5(7)
C(28)-C(27)-C(20)	113.1(7)	F(6)-C(40)-C(41)	119.5(8)
C(30)-C(27)-C(20)	110.0(7)	F(6)-C(40)-C(39)	118.5(10)
C(28)-C(27)-C(29)	107.3(9)	C(41)-C(40)-C(39)	121.9(10)
C(38)-C(39)-F(7)	119.9(9)	C(43)-C(44)-H(44)	125.8
C(38)-C(39)-C(40)	120.6(11)	C(45)-C(44)-H(44)	125.8
F(7)-C(39)-C(40)	119.2(10)	N(4)-C(45)-C(44)	108.3(6)
C(39)-C(38)-C(37)	119.4(9)	N(4)-C(45)-C(46)	121.1(5)
C(39)-C(38)-F(8)	120.0(10)	C(44)-C(45)-C(46)	130.0(6)
C(37)-C(38)-F(8)	120.6(9)	C(45)-C(46)-C(1)	107.6(5)
C(38)-C(37)-F(9)	120.3(8)	C(45)-C(46)-C(47)	110.3(5)
C(38)-C(37)-C(36)	119.8(10)	C(1)-C(46)-C(47)	110.9(5)
F(9)-C(37)-C(36)	119.8(10)	C(45)-C(46)-C(48)	109.7(5)
C(41)-C(36)-F(10)	118.7(8)	C(1)-C(46)-C(48)	109.5(5)
C(41)-C(36)-C(37)	123.1(10)	C(47)-C(46)-C(48)	108.8(5)
F(10)-C(36)-C(37)	118.0(9)	C(46)-C(47)-H(47A)	109.5
C(34)-C(35)-C(42)	125.4(6)	C(46)-C(47)-H(47B)	109.5
C(34)-C(35)-C(41)	116.4(6)	H(47A)-C(47)-H(47B)	109.5
C(42)-C(35)-C(41)	118.0(6)	C(46)-C(47)-H(47C)	109.5
N(4)-C(42)-C(35)	122.1(6)	H(47A)-C(47)-H(47C)	109.5
N(4)-C(42)-C(43)	106.7(6)	H(47B)-C(47)-H(47C)	109.5
C(35)-C(42)-C(43)	129.9(7)	C(46)-C(48)-H(48A)	109.5
C(44)-C(43)-C(42)	108.5(7)	C(46)-C(48)-H(48B)	109.5
C(44)-C(43)-Cl(2)	121.1(7)	H(48A)-C(48)-H(48B)	109.5
C(42)-C(43)-Cl(2)	126.0(7)	C(46)-C(48)-H(48C)	109.5
C(44)-C(43)-H(43)	125.8	H(48A)-C(48)-H(48C)	109.5
C(42)-C(43)-H(43)	125.8	H(48B)-C(48)-H(48C)	109.5
C(43)-C(44)-C(45)	108.4(6)		

Table A.9 Bond Lengths (Å) determined for Au($Phl^{3,5\text{-}tBu}Cl_2$)

Bond	Length	Bond	Length
Au-N(2)	1.996(5)	N(4')-C(45')	1.379(11)
Au-N(3)	1.998(5)	N(4')-C(42')	1.403(12)
Au-N(4)	2.009(12)	C(42')-C(43')	1.409(12)
Au-N(4')	2.010(10)	C(42')-C(35)	1.424(13)
Au-N(1)	2.016(5)	C(43')-C(44')	1.40(3)
Cl(1)-C(3)	1.721(7)	C(43')-Cl(2')	1.730(11)
N(4)-C(45)	1.381(13)	C(44')-C(45')	1.388(13)
N(4)-C(42)	1.400(13)	C(45')-C(46)	1.495(12)
C(42)-C(43)	1.392(14)	F(1')-C(6')	1.323(9)
C(42)-C(35)	1.415(14)	F(2')-C(7')	1.344(10)
C(43)-C(44)	1.38(3)	F(3')-C(8')	1.329(9)
C(43)-Cl(2)	1.729(12)	F(4')-C(9')	1.322(10)
C(44)-C(45)	1.391(14)	F(5')-C(10')	1.336(11)
C(45)-C(46)	1.496(14)	C(6')-C(7')	1.39
F(1)-C(6)	1.321(11)	C(6')-C(11')	1.39
F(2)-C(7)	1.333(11)	C(7')-C(8')	1.39
F(3)-C(8)	1.323(10)	C(8')-C(9')	1.39
F(4)-C(9)	1.321(11)	C(9')-C(10')	1.39
F(5)-C(10)	1.324(11)	C(10')-C(11')	1.39
C(6)-C(7)	1.39	C(11')-C(5)	1.508(9)
C(6)-C(11)	1.39	F(6')-C(36')	1.309(8)
C(7)-C(8)	1.39	F(7')-C(37')	1.326(9)
C(8)-C(9)	1.39	F(8')-C(38')	1.344(8)
C(9)-C(10)	1.39	F(9')-C(39')	1.328(9)
C(10)-C(11)	1.39	F(10')-C(40')	1.314(8)
C(11)-C(5)	1.491(10)	C(36')-C(37')	1.39
F(6)-C(36)	1.322(12)	C(36')-C(41')	1.39
F(7)-C(37)	1.329(12)	C(37')-C(38')	1.39
F(8)-C(38)	1.332(13)	C(38')-C(39')	1.39
F(9)-C(39)	1.324(13)	C(39')-C(40')	1.39
F(10)-C(40)	1.323(13)	C(40')-C(41')	1.39
C(36)-C(37)	1.39	C(41')-C(35)	1.538(9)
C(36)-C(41)	1.39	N(1)-C(1)	1.367(7)
C(37)-C(38)	1.39	N(1)-C(4)	1.393(8)
C(38)-C(39)	1.39	N(2)-C(15)	1.367(7)
C(39)-C(40)	1.39	N(2)-C(12)	1.404(8)
C(40)-C(41)	1.39	N(3)-C(31)	1.384(8)
C(41)-C(35)	1.505(12)	N(3)-C(34)	1.395(8)
C(1)-C(2)	1.389(9)	C(19)-C(20)	1.385(10)
C(1)-C(46)	1.522(9)	C(20)-C(21)	1.399(8)

Bond	Length	Bond	Length
C(2)-C(3)	1.394(9)	C(20)-C(27)	1.545(10)
C(3)-C(4)	1.422(8)	C(21)-C(22)	1.399(9)
C(4)-C(5)	1.418(8)	C(23)-C(24)	1.507(14)
C(5)-C(12)	1.375(8)	C(23)-C(26)	1.526(12)
C(12)-C(13)	1.433(9)	C(23)-C(25)	1.574(17)
C(13)-C(14)	1.356(10)	C(27)-C(28)	1.516(12)
C(14)-C(15)	1.435(9)	C(27)-C(29)	1.554(12)
C(15)-C(16)	1.397(9)	C(27)-C(30)	1.552(15)
C(16)-C(31)	1.403(9)	C(31)-C(32)	1.453(9)
C(16)-C(22)	1.503(8)	C(32)-C(33)	1.337(10)
C(17)-C(18)	1.390(9)	C(33)-C(34)	1.446(9)
C(17)-C(22)	1.401(10)	C(34)-C(35)	1.380(10)
C(18)-C(19)	1.399(10)	C(46)-C(48)	1.543(8)
C(18)-C(23)	1.530(10)	C(46)-C(47)	1.546(8)

Table A.10 Bond angles (°) determined for $Au(PhI^{3,5\text{-}tBu}Cl_2)$

Bond	Angle	Bond	Angle
N(2)-Au-N(3)	89.5(2)	C(10)-C(11)-C(5)	118.8(11)
N(2)-Au-N(4)	176.4(11)	C(6)-C(11)-C(5)	121.2(11)
N(3)-Au-N(4)	89.9(10)	F(6)-C(36)-C(37)	116.1(16)
N(2)-Au-N(4')	177.0(8)	F(6)-C(36)-C(41)	123.9(16)
N(3)-Au-N(4')	89.2(8)	C(37)-C(36)-C(41)	120
N(2)-Au-N(1)	89.8(2)	F(7)-C(37)-C(36)	123.5(16)
N(3)-Au-N(1)	178.9(2)	F(7)-C(37)-C(38)	116.5(16)
N(4)-Au-N(1)	90.7(10)	C(36)-C(37)-C(38)	120
N(4')-Au-N(1)	91.4(8)	F(8)-C(38)-C(39)	117.6(18)
C(45)-N(4)-C(42)	107.7(11)	F(8)-C(38)-C(37)	122.4(18)
C(45)-N(4)-Au	124(2)	C(39)-C(38)-C(37)	120
C(42)-N(4)-Au	125(2)	F(9)-C(39)-C(38)	122.4(18)
C(43)-C(42)-N(4)	107.3(11)	F(9)-C(39)-C(40)	117.6(17)
C(43)-C(42)-C(35)	130(2)	C(38)-C(39)-C(40)	120
N(4)-C(42)-C(35)	122(2)	F(10)-C(40)-C(41)	116(2)
C(44)-C(43)-C(42)	108.7(11)	F(10)-C(40)-C(39)	124(2)
C(44)-C(43)-Cl(2)	124(2)	C(41)-C(40)-C(39)	120
C(42)-C(43)-Cl(2)	127(2)	C(40)-C(41)-C(36)	120
C(43)-C(44)-C(45)	107.6(13)	C(40)-C(41)-C(35)	126.1(13)
N(4)-C(45)-C(44)	108.6(12)	C(36)-C(41)-C(35)	113.7(13)

Bond	Angle	Bond	Angle
N(4)-C(45)-C(46)	120(3)	C(45')-N(4')-C(42')	109.0(10)
C(44)-C(45)-C(46)	130(3)	C(45')-N(4')-Au	122(2)
F(1)-C(6)-C(7)	120.0(12)	C(42')-N(4')-Au	120.5(16)
F(1)-C(6)-C(11)	120.0(12)	N(4')-C(42')-C(43')	106.2(10)
C(7)-C(6)-C(11)	120	N(4')-C(42')-C(35)	120(2)
F(2)-C(7)-C(8)	121.6(10)	C(43')-C(42')-C(35)	131.6(19)
F(2)-C(7)-C(6)	118.4(10)	C(44')-C(43')-C(42')	108.8(9)
C(8)-C(7)-C(6)	120	C(44')-C(43')-Cl(2')	122.8(15)
F(3)-C(8)-C(7)	117.6(11)	C(42')-C(43')-Cl(2')	128.4(17)
F(3)-C(8)-C(9)	122.4(11)	C(45')-C(44')-C(43')	107.1(11)
C(7)-C(8)-C(9)	120	N(4')-C(45')-C(44')	108.9(10)
F(4)-C(9)-C(10)	121.9(11)	N(4')-C(45')-C(46)	121(2)
F(4)-C(9)-C(8)	118.1(11)	C(44')-C(45')-C(46)	130(2)
C(10)-C(9)-C(8)	120	F(1')-C(6')-C(7')	117.6(10)
F(5)-C(10)-C(9)	119.9(12)	F(1')-C(6')-C(11')	122.4(10)
F(5)-C(10)-C(11)	120.1(12)	C(7')-C(6')-C(11')	120
C(9)-C(10)-C(11)	120	F(2')-C(7')-C(6')	122.0(9)
C(10)-C(11)-C(6)	120	F(2')-C(7')-C(8')	118.0(9)
C(6')-C(7')-C(8')	120	C(31)-N(3)-Au	125.3(4)
F(3')-C(8')-C(9')	118.5(10)	C(34)-N(3)-Au	125.0(4)
F(3')-C(8')-C(7')	121.5(10)	N(1)-C(1)-C(2)	109.9(6)
C(9')-C(8')-C(7')	120	N(1)-C(1)-C(46)	122.4(5)
F(4')-C(9')-C(10')	119.7(10)	C(2)-C(1)-C(46)	127.8(5)
F(4')-C(9')-C(8')	120.3(10)	C(1)-C(2)-C(3)	106.4(5)
C(10')-C(9')-C(8')	120	C(2)-C(3)-C(4)	108.8(6)
F(5')-C(10')-C(9')	119.4(10)	C(2)-C(3)-Cl(1)	123.1(5)
F(5')-C(10')-C(11')	120.6(10)	C(4)-C(3)-Cl(1)	128.1(5)
C(9')-C(10')-C(11')	120	N(1)-C(4)-C(5)	124.2(5)
C(10')-C(11')-C(6')	120	N(1)-C(4)-C(3)	106.0(5)
C(10')-C(11')-C(5)	124.2(9)	C(5)-C(4)-C(3)	129.7(6)
C(6')-C(11')-C(5)	115.5(9)	C(12)-C(5)-C(4)	124.2(6)
F(6')-C(36')-C(37')	120.5(8)	C(12)-C(5)-C(11)	116.9(11)
F(6')-C(36')-C(41')	119.5(8)	C(4)-C(5)-C(11)	118.7(11)
C(37')-C(36')-C(41')	120	C(12)-C(5)-C(11')	116.1(10)
F(7')-C(37')-C(36')	118.4(8)	C(4)-C(5)-C(11')	119.6(10)
F(7')-C(37')-C(38')	121.6(8)	C(5)-C(12)-N(2)	126.2(6)
C(36')-C(37')-C(38')	120	C(5)-C(12)-C(13)	126.3(6)
F(8')-C(38')-C(37')	119.2(8)	N(2)-C(12)-C(13)	107.3(5)
F(8')-C(38')-C(39')	120.8(8)	C(14)-C(13)-C(12)	107.6(6)
C(37')-C(38')-C(39')	120	C(13)-C(14)-C(15)	108.7(6)
F(9')-C(39')-C(40')	121.6(8)	N(2)-C(15)-C(16)	126.6(6)
F(9')-C(39')-C(38')	118.4(8)	N(2)-C(15)-C(14)	107.6(5)

Bond	Angle	Bond	Angle
C(40')-C(39')-C(38')	120	C(16)-C(15)-C(14)	125.5(6)
F(10')-C(40')-C(39')	115.6(10)	C(15)-C(16)-C(31)	122.2(6)
F(10')-C(40')-C(41')	124.4(10)	C(15)-C(16)-C(22)	117.8(6)
C(39')-C(40')-C(41')	120	C(31)-C(16)-C(22)	119.2(5)
C(40')-C(41')-C(36')	120	C(18)-C(17)-C(22)	121.7(6)
C(40')-C(41')-C(35)	116.1(7)	C(17)-C(18)-C(19)	117.2(7)
C(36')-C(41')-C(35)	123.8(7)	C(17)-C(18)-C(23)	121.9(7)
C(1)-N(1)-C(4)	108.9(5)	C(19)-C(18)-C(23)	120.9(6)
C(1)-N(1)-Au	125.3(4)	C(20)-C(19)-C(18)	123.3(6)
C(4)-N(1)-Au	124.5(4)	C(19)-C(20)-C(21)	118.0(6)
C(15)-N(2)-C(12)	108.6(5)	C(19)-C(20)-C(27)	123.6(6)
C(15)-N(2)-Au	126.5(4)	C(21)-C(20)-C(27)	118.4(7)
C(12)-N(2)-Au	124.1(4)	C(20)-C(21)-C(22)	120.8(7)
C(31)-N(3)-C(34)	109.3(5)	C(21)-C(22)-C(17)	119.0(6)
C(21)-C(22)-C(16)	120.5(6)	C(35)-C(34)-N(3)	126.1(6)
C(17)-C(22)-C(16)	120.5(6)	C(35)-C(34)-C(33)	127.3(6)
C(24)-C(23)-C(26)	110.1(9)	N(3)-C(34)-C(33)	106.6(6)
C(24)-C(23)-C(18)	113.6(8)	C(34)-C(35)-C(42)	124.1(13)
C(26)-C(23)-C(18)	112.0(7)	C(34)-C(35)-C(42')	123.1(11)
C(24)-C(23)-C(25)	106.8(10)	C(34)-C(35)-C(41)	121.5(11)
C(26)-C(23)-C(25)	107.1(9)	C(42)-C(35)-C(41)	114.0(15)
C(18)-C(23)-C(25)	106.7(8)	C(34)-C(35)-C(41')	114.4(7)
C(28)-C(27)-C(20)	112.0(7)	C(42')-C(35)-C(41')	122.5(11)
C(28)-C(27)-C(29)	109.6(8)	C(45')-C(46)-C(1)	105.7(19)
C(20)-C(27)-C(29)	111.0(6)	C(45)-C(46)-C(1)	108(2)
C(28)-C(27)-C(30)	107.3(8)	C(45')-C(46)-C(48)	111(2)
C(20)-C(27)-C(30)	108.0(7)	C(45)-C(46)-C(48)	109(2)
C(29)-C(27)-C(30)	108.9(9)	C(1)-C(46)-C(48)	112.5(5)
N(3)-C(31)-C(16)	125.5(6)	C(45')-C(46)-C(47)	109.9(11)
N(3)-C(31)-C(32)	106.6(6)	C(45)-C(46)-C(47)	108.9(14)
C(16)-C(31)-C(32)	127.2(6)	C(1)-C(46)-C(47)	109.9(5)
C(33)-C(32)-C(31)	108.7(6)	C(48)-C(46)-C(47)	108.1(5)
C(32)-C(33)-C(34)	108.8(6)		

Table A.11 Bond Lengths (Å) determined for DMBil

Bond	Length	Bond	Length
C(1)-N(1)	1.359(2)	C(17)-H(17C)	0.98
C(1)-C(2)	1.371(3)	C(18)-H(18A)	0.98
C(1)-H(1)	0.95	C(18)-H(18B)	0.98
C(2)-C(3)	1.392(3)	C(18)-H(18C)	0.98
C(2)-H(2)	0.95	C(19)-N(3)	1.3086(19)
C(3)-C(4)	1.391(2)	C(19)-C(20)	1.459(2)
C(3)-H(3)	0.95	C(20)-C(21)	1.346(2)
C(4)-N(1)	1.376(2)	C(20)-H(20)	0.95
C(4)-C(5)	1.440(2)	C(21)-C(22)	1.444(2)
C(5)-C(12)	1.366(2)	C(21)-H(21)	0.95
C(5)-C(11)	1.492(2)	C(22)-C(23)	1.367(2)
C(6)-F(1)	1.3394(19)	C(22)-N(3)	1.4123(19)
C(6)-C(7)	1.375(2)	C(23)-C(30)	1.427(2)
C(6)-C(11)	1.392(2)	C(23)-C(29)	1.499(2)
C(7)-F(2)	1.3454(19)	C(24)-F(6)	1.346(2)
C(7)-C(8)	1.372(3)	C(24)-C(29)	1.382(2)
C(8)-F(3)	1.3406(19)	C(24)-C(25)	1.383(3)
C(8)-C(9)	1.377(2)	C(25)-F(7)	1.338(2)
C(9)-F(4)	1.3349(19)	C(25)-C(26)	1.367(3)
C(9)-C(10)	1.375(2)	C(26)-F(8)	1.335(2)
C(10)-F(5)	1.3495(18)	C(26)-C(27)	1.362(3)
C(10)-C(11)	1.389(2)	C(27)-F(9)	1.344(2)
C(12)-N(2)	1.414(2)	C(27)-C(28)	1.387(2)
C(12)-C(13)	1.450(2)	C(28)-F(10)	1.342(2)
C(13)-C(14)	1.348(2)	C(28)-C(29)	1.377(2)
C(13)-H(13)	0.95	C(30)-N(4)	1.380(2)
C(14)-C(15)	1.452(2)	C(30)-C(31)	1.392(2)
C(14)-H(14)	0.95	C(31)-C(32)	1.392(2)
C(15)-N(2)	1.311(2)	C(31)-H(31)	0.95
C(15)-C(16)	1.512(2)	C(32)-C(33)	1.378(2)
C(16)-C(19)	1.511(2)	C(32)-H(32)	0.95
C(16)-C(17)	1.535(2)	C(33)-N(4)	1.351(2)
C(16)-C(18)	1.545(3)	C(33)-H(33)	0.95
C(17)-H(17A)	0.98	N(1)-H(1A)	0.88
C(17)-H(17B)	0.98	N(4)-H(4)	0.88

Table A.12 Bond angles (°) determined for DMBil

Bond	Angle	Bond	Angle
N(1)-C(1)-C(2)	108.30(16)	C(14)-C(15)-C(16)	125.00(14)
N(1)-C(1)-H(1)	125.8	C(19)-C(16)-C(15)	108.87(12)
C(2)-C(1)-H(1)	125.8	C(19)-C(16)-C(17)	108.61(14)
C(1)-C(2)-C(3)	107.56(17)	C(15)-C(16)-C(17)	110.86(14)
C(1)-C(2)-H(2)	126.2	C(19)-C(16)-C(18)	109.52(13)
C(3)-C(2)-H(2)	126.2	C(15)-C(16)-C(18)	108.91(14)
C(4)-C(3)-C(2)	107.96(16)	C(17)-C(16)-C(18)	110.06(15)
C(4)-C(3)-H(3)	126	C(16)-C(17)-H(17A)	109.5
C(2)-C(3)-H(3)	126	C(16)-C(17)-H(17B)	109.5
N(1)-C(4)-C(3)	106.59(15)	H(17A)-C(17)-H(17B)	109.5
N(1)-C(4)-C(5)	122.84(14)	C(16)-C(17)-H(17C)	109.5
C(3)-C(4)-C(5)	130.57(16)	H(17A)-C(17)-H(17C)	109.5
C(12)-C(5)-C(4)	125.28(15)	H(17B)-C(17)-H(17C)	109.5
C(12)-C(5)-C(11)	118.15(14)	C(16)-C(18)-H(18A)	109.5
C(4)-C(5)-C(11)	116.57(14)	C(16)-C(18)-H(18B)	109.5
F(1)-C(6)-C(7)	118.13(14)	H(18A)-C(18)-H(18B)	109.5
F(1)-C(6)-C(11)	119.73(14)	C(16)-C(18)-H(18C)	109.5
C(7)-C(6)-C(11)	122.13(15)	H(18A)-C(18)-H(18C)	109.5
F(2)-C(7)-C(8)	119.96(15)	H(18B)-C(18)-H(18C)	109.5
F(2)-C(7)-C(6)	120.27(16)	N(3)-C(19)-C(20)	112.00(13)
C(8)-C(7)-C(6)	119.77(15)	N(3)-C(19)-C(16)	122.48(14)
F(3)-C(8)-C(7)	120.18(15)	C(20)-C(19)-C(16)	125.50(14)
F(3)-C(8)-C(9)	119.71(16)	C(21)-C(20)-C(19)	106.33(14)
C(7)-C(8)-C(9)	120.10(15)	C(21)-C(20)-H(20)	126.8
F(4)-C(9)-C(10)	121.04(15)	C(19)-C(20)-H(20)	126.8
F(4)-C(9)-C(8)	119.76(15)	C(20)-C(21)-C(22)	106.65(14)
C(10)-C(9)-C(8)	119.20(16)	C(20)-C(21)-H(21)	126.7
F(5)-C(10)-C(9)	117.65(15)	C(22)-C(21)-H(21)	126.7
F(5)-C(10)-C(11)	119.67(14)	C(23)-C(22)-N(3)	122.14(14)
C(9)-C(10)-C(11)	122.67(15)	C(23)-C(22)-C(21)	128.61(14)
C(10)-C(11)-C(6)	116.12(15)	N(3)-C(22)-C(21)	109.25(13)
C(10)-C(11)-C(5)	121.45(14)	C(22)-C(23)-C(30)	125.84(14)
C(6)-C(11)-C(5)	122.42(14)	C(22)-C(23)-C(29)	118.38(13)
C(5)-C(12)-N(2)	122.37(14)	C(30)-C(23)-C(29)	115.76(13)
C(5)-C(12)-C(13)	128.51(15)	F(6)-C(24)-C(29)	119.10(15)
N(2)-C(12)-C(13)	109.11(13)	F(6)-C(24)-C(25)	118.29(17)
C(14)-C(13)-C(12)	106.49(15)	C(29)-C(24)-C(25)	122.61(18)
C(14)-C(13)-H(13)	126.8	F(7)-C(25)-C(26)	121.14(18)
C(12)-C(13)-H(13)	126.8	F(7)-C(25)-C(24)	120.1(2)
C(13)-C(14)-C(15)	106.50(15)	C(26)-C(25)-C(24)	118.78(18)

Bond	Angle	Bond	Angle
C(13)-C(14)-H(14)	126.8	F(8)-C(26)-C(27)	119.4(2)
C(15)-C(14)-H(14)	126.8	F(8)-C(26)-C(25)	120.1(2)
N(2)-C(15)-C(14)	112.27(14)	C(27)-C(26)-C(25)	120.53(17)
N(2)-C(15)-C(16)	122.73(14)	F(9)-C(27)-C(26)	119.99(17)
F(9)-C(27)-C(28)	120.17(19)	C(33)-C(32)-C(31)	107.49(15)
C(26)-C(27)-C(28)	119.83(19)	C(33)-C(32)-H(32)	126.3
F(10)-C(28)-C(29)	120.03(14)	C(31)-C(32)-H(32)	126.3
F(10)-C(28)-C(27)	118.38(17)	N(4)-C(33)-C(32)	108.28(15)
C(29)-C(28)-C(27)	121.59(17)	N(4)-C(33)-H(33)	125.9
C(28)-C(29)-C(24)	116.65(15)	C(32)-C(33)-H(33)	125.9
C(28)-C(29)-C(23)	123.33(15)	C(1)-N(1)-C(4)	109.59(15)
C(24)-C(29)-C(23)	120.02(15)	C(1)-N(1)-H(1A)	125.2
N(4)-C(30)-C(31)	106.42(14)	C(4)-N(1)-H(1A)	125.2
N(4)-C(30)-C(23)	123.62(14)	C(15)-N(2)-C(12)	105.63(13)
C(31)-C(30)-C(23)	129.93(14)	C(19)-N(3)-C(22)	105.76(12)
C(30)-C(31)-C(32)	107.94(15)	C(33)-N(4)-C(30)	109.86(14)
C(30)-C(31)-H(31)	126	C(33)-N(4)-H(4)	125.1
C(32)-C(31)-H(31)	126	C(30)-N(4)-H(4)	125.1

Table A.13 Bond Lengths (Å) determined for Zn(DMBil)

Bond	Length	Bond	Length
Zn(1)-N(4)	2.046(2)	N(8)-C(67)	1.343(3)
Zn(1)-N(3)	2.065(2)	N(8)-C(64)	1.393(3)
Zn(1)-N(1)	2.070(2)	O(1)-C(34)	1.425(4)
Zn(1)-N(2)	2.075(2)	O(1)-H(1O)	0.95
Zn(1)-O(1)	2.1268(19)	O(2)-C(68)	1.419(4)
Zn(2)-N(5)	2.041(2)	O(2)-H(2O)	0.95
Zn(2)-N(7)	2.061(2)	C(1)-C(2)	1.392(4)
Zn(2)-N(8)	2.071(2)	C(1)-H(1)	0.95
Zn(2)-N(6)	2.073(2)	C(2)-C(3)	1.373(4)
Zn(2)-O(2)	2.1147(18)	C(2)-H(2)	0.95
F(1)-C(6)	1.352(3)	C(3)-C(4)	1.416(4)
F(2)-C(7)	1.342(3)	C(3)-H(3A)	0.95
F(3)-C(8)	1.340(3)	C(4)-C(5)	1.416(4)
F(4)-C(9)	1.346(3)	C(5)-C(12)	1.380(4)
F(5)-C(10)	1.348(3)	C(5)-C(11)	1.495(4)
F(6)-C(24)	1.343(3)	C(6)-C(7)	1.377(4)

Bond	Length	Bond	Length
F(7)-C(25)	1.340(3)	C(6)-C(11)	1.385(4)
F(8)-C(26)	1.336(3)	C(7)-C(8)	1.369(5)
F(9)-C(27)	1.337(3)	C(8)-C(9)	1.372(4)
F(10)-C(28)	1.340(3)	C(9)-C(10)	1.370(4)
F(11)-C(40)	1.348(3)	C(10)-C(11)	1.389(4)
F(12)-C(41)	1.336(3)	C(12)-C(13)	1.431(4)
F(13)-C(42)	1.338(3)	C(13)-C(14)	1.356(4)
F(14)-C(43)	1.339(3)	C(13)-H(13)	0.95
F(15)-C(44)	1.345(3)	C(14)-C(15)	1.430(4)
F(16)-C(58)	1.339(3)	C(14)-H(14)	0.95
F(17)-C(59)	1.345(3)	C(15)-C(16)	1.510(4)
F(18)-C(60)	1.334(3)	C(16)-C(19)	1.514(4)
F(19)-C(61)	1.340(3)	C(16)-C(18)	1.538(4)
F(20)-C(62)	1.342(3)	C(16)-C(17)	1.545(4)
N(1)-C(1)	1.341(3)	C(17)-H(17A)	0.98
N(1)-C(4)	1.386(3)	C(17)-H(17B)	0.98
N(2)-C(15)	1.336(3)	C(17)-H(17C)	0.98
N(2)-C(12)	1.402(3)	C(18)-H(18A)	0.98
N(3)-C(19)	1.336(3)	C(18)-H(18B)	0.98
N(3)-C(22)	1.389(3)	C(18)-H(18C)	0.98
N(4)-C(33)	1.337(3)	C(19)-C(20)	1.422(4)
N(4)-C(30)	1.392(3)	C(20)-C(21)	1.366(4)
N(5)-C(35)	1.339(3)	C(20)-H(20)	0.95
N(5)-C(38)	1.400(3)	C(21)-C(22)	1.421(3)
N(6)-C(49)	1.337(3)	C(21)-H(21)	0.95
N(6)-C(46)	1.385(3)	C(22)-C(23)	1.391(4)
N(7)-C(53)	1.332(3)	C(23)-C(30)	1.395(4)
N(7)-C(56)	1.400(3)	C(23)-C(29)	1.504(3)
C(24)-C(25)	1.379(4)	C(48)-H(48)	0.95
C(24)-C(29)	1.383(4)	C(49)-C(50)	1.510(4)
C(25)-C(26)	1.368(4)	C(50)-C(53)	1.517(4)
C(26)-C(27)	1.378(4)	C(50)-C(52)	1.535(4)
C(27)-C(28)	1.380(4)	C(50)-C(51)	1.542(4)
C(28)-C(29)	1.379(4)	C(51)-H(51A)	0.98
C(30)-C(31)	1.428(3)	C(51)-H(51B)	0.98
C(31)-C(32)	1.363(4)	C(51)-H(51C)	0.98
C(31)-H(31)	0.95	C(52)-H(52A)	0.98
C(32)-C(33)	1.408(4)	C(52)-H(52B)	0.98
C(32)-H(32)	0.95	C(52)-H(52C)	0.98
C(33)-H(33)	0.95	C(53)-C(54)	1.422(4)
C(34)-H(34A)	0.98	C(54)-C(55)	1.359(4)
C(34)-H(34B)	0.98	C(54)-H(54)	0.95

Bond	Length	Bond	Length
C(34)-H(34C)	0.98	C(55)-C(56)	1.422(4)
C(35)-C(36)	1.403(4)	C(55)-H(55)	0.95
C(35)-H(35)	0.95	C(56)-C(57)	1.386(4)
C(36)-C(37)	1.365(4)	C(57)-C(64)	1.398(4)
C(36)-H(36)	0.95	C(57)-C(63)	1.510(3)
C(37)-C(38)	1.421(3)	C(58)-C(59)	1.379(4)
C(37)-H(37)	0.95	C(58)-C(63)	1.389(4)
C(38)-C(39)	1.392(4)	C(59)-C(60)	1.368(4)
C(39)-C(46)	1.394(3)	C(60)-C(61)	1.371(4)
C(39)-C(45)	1.501(3)	C(61)-C(62)	1.381(4)
C(40)-C(41)	1.380(4)	C(62)-C(63)	1.383(4)
C(40)-C(45)	1.382(4)	C(64)-C(65)	1.422(4)
C(41)-C(42)	1.368(4)	C(65)-C(66)	1.371(4)
C(42)-C(43)	1.375(4)	C(65)-H(65)	0.95
C(43)-C(44)	1.377(4)	C(66)-C(67)	1.396(4)
C(44)-C(45)	1.377(4)	C(66)-H(66)	0.95
C(46)-C(47)	1.425(4)	C(67)-H(67)	0.95
C(47)-C(48)	1.364(4)	C(68)-H(68A)	0.98
C(47)-H(47)	0.95	C(68)-H(68B)	0.98
C(48)-C(49)	1.424(4)	C(68)-H(68C)	0.98

Table A.14 Bond angles (°) determined for Zn(DMBil)

Bond	Angle	Bond	Angle
N(4)-Zn(1)-N(3)	89.15(8)	C(34)-O(1)-Zn(1)	126.7(2)
N(4)-Zn(1)-N(1)	94.37(8)	C(34)-O(1)-H(1O)	116.6
N(3)-Zn(1)-N(1)	173.67(9)	Zn(1)-O(1)-H(1O)	116.6
N(4)-Zn(1)-N(2)	137.09(8)	C(68)-O(2)-Zn(2)	125.5(2)
N(3)-Zn(1)-N(2)	86.86(8)	C(68)-O(2)-H(2O)	117.2
N(1)-Zn(1)-N(2)	86.98(8)	Zn(2)-O(2)-H(2O)	117.2
N(4)-Zn(1)-O(1)	105.38(8)	N(1)-C(1)-C(2)	111.2(3)
N(3)-Zn(1)-O(1)	92.99(8)	N(1)-C(1)-H(1)	124.4
N(1)-Zn(1)-O(1)	91.15(8)	C(2)-C(1)-H(1)	124.4
N(2)-Zn(1)-O(1)	117.49(8)	C(3)-C(2)-C(1)	106.6(3)
N(5)-Zn(2)-N(7)	137.17(8)	C(3)-C(2)-H(2)	126.7
N(5)-Zn(2)-N(8)	94.62(9)	C(1)-C(2)-H(2)	126.7
N(7)-Zn(2)-N(8)	87.32(9)	C(2)-C(3)-C(4)	107.2(3)
N(5)-Zn(2)-N(6)	88.24(8)	C(2)-C(3)-H(3A)	126.4

Bond	Angle	Bond	Angle
N(7)-Zn(2)-N(6)	87.33(8)	C(4)-C(3)-H(3A)	126.4
N(8)-Zn(2)-N(6)	174.43(8)	N(1)-C(4)-C(5)	123.8(2)
N(5)-Zn(2)-O(2)	107.83(8)	N(1)-C(4)-C(3)	108.2(2)
N(7)-Zn(2)-O(2)	114.95(8)	C(5)-C(4)-C(3)	127.9(3)
N(8)-Zn(2)-O(2)	89.92(9)	C(12)-C(5)-C(4)	127.3(2)
N(6)-Zn(2)-O(2)	93.75(8)	C(12)-C(5)-C(11)	116.8(2)
C(1)-N(1)-C(4)	106.8(2)	C(4)-C(5)-C(11)	115.8(2)
C(1)-N(1)-Zn(1)	127.23(19)	F(1)-C(6)-C(7)	118.2(3)
C(4)-N(1)-Zn(1)	125.17(17)	F(1)-C(6)-C(11)	119.4(3)
C(15)-N(2)-C(12)	106.4(2)	C(7)-C(6)-C(11)	122.4(3)
C(15)-N(2)-Zn(1)	125.31(17)	F(2)-C(7)-C(8)	119.9(3)
C(12)-N(2)-Zn(1)	123.24(16)	F(2)-C(7)-C(6)	120.3(3)
C(19)-N(3)-C(22)	107.2(2)	C(8)-C(7)-C(6)	119.8(3)
C(19)-N(3)-Zn(1)	127.89(17)	F(3)-C(8)-C(7)	120.1(3)
C(22)-N(3)-Zn(1)	124.54(16)	F(3)-C(8)-C(9)	120.0(3)
C(33)-N(4)-C(30)	105.9(2)	C(7)-C(8)-C(9)	119.9(3)
C(33)-N(4)-Zn(1)	128.20(18)	F(4)-C(9)-C(10)	120.2(3)
C(30)-N(4)-Zn(1)	125.12(16)	F(4)-C(9)-C(8)	120.4(3)
C(35)-N(5)-C(38)	105.8(2)	C(10)-C(9)-C(8)	119.3(3)
C(35)-N(5)-Zn(2)	128.01(18)	F(5)-C(10)-C(9)	117.4(3)
C(38)-N(5)-Zn(2)	125.70(16)	F(5)-C(10)-C(11)	119.6(2)
C(49)-N(6)-C(46)	107.2(2)	C(9)-C(10)-C(11)	123.0(3)
C(49)-N(6)-Zn(2)	127.31(18)	C(6)-C(11)-C(10)	115.7(3)
C(46)-N(6)-Zn(2)	124.58(16)	C(6)-C(11)-C(5)	122.7(3)
C(53)-N(7)-C(56)	107.0(2)	C(10)-C(11)-C(5)	121.6(2)
C(53)-N(7)-Zn(2)	125.28(18)	C(5)-C(12)-N(2)	122.8(2)
C(56)-N(7)-Zn(2)	122.33(16)	C(5)-C(12)-C(13)	128.5(2)
C(67)-N(8)-C(64)	106.0(2)	N(2)-C(12)-C(13)	108.6(2)
C(67)-N(8)-Zn(2)	128.06(19)	C(14)-C(13)-C(12)	107.2(2)
C(64)-N(8)-Zn(2)	123.97(17)	C(14)-C(13)-H(13)	126.4
C(12)-C(13)-H(13)	126.4	F(7)-C(25)-C(24)	120.5(3)
C(13)-C(14)-C(15)	106.9(2)	C(26)-C(25)-C(24)	119.3(3)
C(13)-C(14)-H(14)	126.6	F(8)-C(26)-C(25)	120.1(3)
C(15)-C(14)-H(14)	126.6	F(8)-C(26)-C(27)	119.9(3)
N(2)-C(15)-C(14)	110.9(2)	C(25)-C(26)-C(27)	120.0(3)
N(2)-C(15)-C(16)	121.2(2)	F(9)-C(27)-C(26)	120.0(3)
C(14)-C(15)-C(16)	127.6(2)	F(9)-C(27)-C(28)	120.5(3)
C(15)-C(16)-C(19)	111.4(2)	C(26)-C(27)-C(28)	119.5(3)
C(15)-C(16)-C(18)	108.3(2)	F(10)-C(28)-C(29)	119.6(2)
C(19)-C(16)-C(18)	108.8(2)	F(10)-C(28)-C(27)	118.4(3)
C(15)-C(16)-C(17)	109.4(2)	C(29)-C(28)-C(27)	121.9(3)
C(19)-C(16)-C(17)	109.7(2)	C(28)-C(29)-C(24)	116.8(2)

Bond	Angle	Bond	Angle
C(18)-C(16)-C(17)	109.2(2)	C(28)-C(29)-C(23)	122.6(2)
C(16)-C(17)-H(17A)	109.5	C(24)-C(29)-C(23)	120.6(2)
C(16)-C(17)-H(17B)	109.5	N(4)-C(30)-C(23)	123.3(2)
H(17A)-C(17)-H(17B)	109.5	N(4)-C(30)-C(31)	108.8(2)
C(16)-C(17)-H(17C)	109.5	C(23)-C(30)-C(31)	127.8(2)
H(17A)-C(17)-H(17C)	109.5	C(32)-C(31)-C(30)	106.9(2)
H(17B)-C(17)-H(17C)	109.5	C(32)-C(31)-H(31)	126.5
C(16)-C(18)-H(18A)	109.5	C(30)-C(31)-H(31)	126.5
C(16)-C(18)-H(18B)	109.5	C(31)-C(32)-C(33)	106.5(2)
H(18A)-C(18)-H(18B)	109.5	C(31)-C(32)-H(32)	126.7
C(16)-C(18)-H(18C)	109.5	C(33)-C(32)-H(32)	126.7
H(18A)-C(18)-H(18C)	109.5	N(4)-C(33)-C(32)	111.8(2)
H(18B)-C(18)-H(18C)	109.5	N(4)-C(33)-H(33)	124.1
N(3)-C(19)-C(20)	110.3(2)	C(32)-C(33)-H(33)	124.1
N(3)-C(19)-C(16)	122.4(2)	O(1)-C(34)-H(34A)	109.5
C(20)-C(19)-C(16)	127.3(2)	O(1)-C(34)-H(34B)	109.5
C(21)-C(20)-C(19)	106.9(2)	H(34A)-C(34)-H(34B)	109.5
C(21)-C(20)-H(20)	126.6	O(1)-C(34)-H(34C)	109.5
C(19)-C(20)-H(20)	126.6	H(34A)-C(34)-H(34C)	109.5
C(20)-C(21)-C(22)	106.9(2)	H(34B)-C(34)-H(34C)	109.5
C(20)-C(21)-H(21)	126.5	N(5)-C(35)-C(36)	111.7(2)
C(22)-C(21)-H(21)	126.5	N(5)-C(35)-H(35)	124.1
N(3)-C(22)-C(23)	123.5(2)	C(36)-C(35)-H(35)	124.1
N(3)-C(22)-C(21)	108.7(2)	C(37)-C(36)-C(35)	106.7(2)
C(23)-C(22)-C(21)	127.4(2)	C(37)-C(36)-H(36)	126.6
C(22)-C(23)-C(30)	128.6(2)	C(35)-C(36)-H(36)	126.6
C(22)-C(23)-C(29)	115.8(2)	C(36)-C(37)-C(38)	107.1(2)
C(30)-C(23)-C(29)	115.5(2)	C(36)-C(37)-H(37)	126.5
F(6)-C(24)-C(25)	117.6(2)	C(38)-C(37)-H(37)	126.5
F(6)-C(24)-C(29)	120.1(2)	C(39)-C(38)-N(5)	123.6(2)
C(25)-C(24)-C(29)	122.3(3)	C(39)-C(38)-C(37)	127.6(2)
F(7)-C(25)-C(26)	120.2(3)	N(5)-C(38)-C(37)	108.6(2)
C(38)-C(39)-C(46)	127.6(2)	H(51B)-C(51)-H(51C)	109.5
C(38)-C(39)-C(45)	116.5(2)	C(50)-C(52)-H(52A)	109.5
C(46)-C(39)-C(45)	115.8(2)	C(50)-C(52)-H(52B)	109.5
F(11)-C(40)-C(41)	118.2(2)	H(52A)-C(52)-H(52B)	109.5
F(11)-C(40)-C(45)	119.5(2)	C(50)-C(52)-H(52C)	109.5
C(41)-C(40)-C(45)	122.3(3)	H(52A)-C(52)-H(52C)	109.5
F(12)-C(41)-C(42)	120.4(3)	H(52B)-C(52)-H(52C)	109.5
F(12)-C(41)-C(40)	120.4(3)	N(7)-C(53)-C(54)	110.6(2)
C(42)-C(41)-C(40)	119.2(3)	N(7)-C(53)-C(50)	122.4(2)
F(13)-C(42)-C(41)	119.1(3)	C(54)-C(53)-C(50)	126.9(2)

Bond	Angle	Bond	Angle
F(13)-C(42)-C(43)	120.7(3)	C(55)-C(54)-C(53)	106.8(2)
C(41)-C(42)-C(43)	120.2(3)	C(55)-C(54)-H(54)	126.6
F(14)-C(43)-C(42)	119.7(3)	C(53)-C(54)-H(54)	126.6
F(14)-C(43)-C(44)	120.9(3)	C(54)-C(55)-C(56)	107.5(2)
C(42)-C(43)-C(44)	119.4(3)	C(54)-C(55)-H(55)	126.3
F(15)-C(44)-C(43)	117.9(2)	C(56)-C(55)-H(55)	126.3
F(15)-C(44)-C(45)	119.9(2)	C(57)-C(56)-N(7)	123.1(2)
C(43)-C(44)-C(45)	122.2(3)	C(57)-C(56)-C(55)	128.7(2)
C(44)-C(45)-C(40)	116.7(2)	N(7)-C(56)-C(55)	108.1(2)
C(44)-C(45)-C(39)	122.0(2)	C(56)-C(57)-C(64)	128.3(2)
C(40)-C(45)-C(39)	121.3(2)	C(56)-C(57)-C(63)	116.1(2)
N(6)-C(46)-C(39)	123.6(2)	C(64)-C(57)-C(63)	115.5(2)
N(6)-C(46)-C(47)	108.8(2)	F(16)-C(58)-C(59)	117.3(2)
C(39)-C(46)-C(47)	127.1(2)	F(16)-C(58)-C(63)	120.5(2)
C(48)-C(47)-C(46)	106.8(3)	C(59)-C(58)-C(63)	122.2(3)
C(48)-C(47)-H(47)	126.6	F(17)-C(59)-C(60)	120.4(2)
C(46)-C(47)-H(47)	126.6	F(17)-C(59)-C(58)	119.7(3)
C(47)-C(48)-C(49)	107.0(3)	C(60)-C(59)-C(58)	119.9(3)
C(47)-C(48)-H(48)	126.5	F(18)-C(60)-C(59)	120.5(3)
C(49)-C(48)-H(48)	126.5	F(18)-C(60)-C(61)	119.8(3)
N(6)-C(49)-C(48)	110.2(2)	C(59)-C(60)-C(61)	119.7(2)
N(6)-C(49)-C(50)	122.8(2)	F(19)-C(61)-C(60)	119.7(3)
C(48)-C(49)-C(50)	126.9(2)	F(19)-C(61)-C(62)	120.5(3)
C(49)-C(50)-C(53)	112.3(2)	C(60)-C(61)-C(62)	119.8(3)
C(49)-C(50)-C(52)	109.5(2)	F(20)-C(62)-C(61)	117.7(2)
C(53)-C(50)-C(52)	109.5(2)	F(20)-C(62)-C(63)	120.1(2)
C(49)-C(50)-C(51)	107.7(2)	C(61)-C(62)-C(63)	122.2(2)
C(53)-C(50)-C(51)	109.0(2)	C(62)-C(63)-C(58)	116.3(2)
C(52)-C(50)-C(51)	108.9(2)	C(62)-C(63)-C(57)	122.1(2)
C(50)-C(51)-H(51A)	109.5	C(58)-C(63)-C(57)	121.7(2)
C(50)-C(51)-H(51B)	109.5	N(8)-C(64)-C(57)	122.8(2)
H(51A)-C(51)-H(51B)	109.5	N(8)-C(64)-C(65)	108.5(2)
C(50)-C(51)-H(51C)	109.5	C(57)-C(64)-C(65)	128.7(2)
H(51A)-C(51)-H(51C)	109.5	C(66)-C(65)-C(64)	107.3(3)
C(66)-C(65)-H(65)	126.4	C(66)-C(67)-H(67)	124
C(64)-C(65)-H(65)	126.4	O(2)-C(68)-H(68A)	109.5
C(65)-C(66)-C(67)	106.3(3)	O(2)-C(68)-H(68B)	109.5
C(65)-C(66)-H(66)	126.9	H(68A)-C(68)-H(68B)	109.5
C(67)-C(66)-H(66)	126.9	O(2)-C(68)-H(68C)	109.5
N(8)-C(67)-C(66)	112.0(3)	H(68A)-C(68)-H(68C)	109.5
N(8)-C(67)-H(67)	124	H(68B)-C(68)-H(68C)	109.5

Table A.15 Bond Lengths (Å) determined for Cu(DMBil)

Bond	Length	Bond	Length
Cu-N(4)	1.9690(18)	C(6)-C(7)	1.421(3)
Cu-N(2)	1.9699(16)	C(7)-C(8)	1.354(3)
Cu-N(3)	1.9703(16)	C(8)-C(9)	1.428(3)
Cu-N(1)	1.9799(18)	C(9)-C(10)	1.516(3)
N(1)-C(1)	1.342(3)	C(10)-C(11)	1.517(3)
N(1)-C(4)	1.385(3)	C(10)-C(20)	1.541(3)
N(2)-C(9)	1.335(3)	C(10)-C(21)	1.547(3)
N(2)-C(6)	1.405(2)	C(11)-C(12)	1.423(3)
N(3)-C(11)	1.333(3)	C(12)-C(13)	1.363(3)
N(3)-C(14)	1.403(2)	C(13)-C(14)	1.418(3)
N(4)-C(19)	1.326(3)	C(14)-C(15)	1.390(3)
N(4)-C(16)	1.400(2)	C(15)-C(16)	1.391(3)
F(1)-C(22)	1.342(3)	C(15)-C(33)	1.503(3)
F(2)-C(23)	1.343(3)	C(16)-C(17)	1.418(3)
F(3)-C(24)	1.336(3)	C(17)-C(18)	1.373(3)
F(4)-C(25)	1.335(3)	C(18)-C(19)	1.408(3)
F(5)-C(26)	1.340(3)	C(22)-C(23)	1.381(3)
F(6)-C(28)	1.336(3)	C(22)-C(27)	1.397(3)
F(7)-C(29)	1.335(3)	C(23)-C(24)	1.373(4)
F(8)-C(30)	1.341(3)	C(24)-C(25)	1.370(4)
F(9)-C(31)	1.340(3)	C(25)-C(26)	1.386(3)
F(10)-C(32)	1.333(3)	C(26)-C(27)	1.377(3)
C(1)-C(2)	1.395(3)	C(28)-C(33)	1.380(3)
C(2)-C(3)	1.364(4)	C(28)-C(29)	1.391(3)
C(3)-C(4)	1.421(3)	C(29)-C(30)	1.360(4)
C(4)-C(5)	1.392(3)	C(30)-C(31)	1.379(4)
C(5)-C(6)	1.382(3)	C(31)-C(32)	1.381(3)
C(5)-C(27)	1.506(3)	C(32)-C(33)	1.389(3)

Table A.16 Bond angles (°) determined for Cu(DMBil)

Bond	Angle	Bond	Angle
N(4)-Cu-N(2)	160.26(7)	C(13)-C(12)-C(11)	106.5(2)
N(4)-Cu-N(3)	91.39(7)	C(12)-C(13)-C(14)	107.38(18)
N(2)-Cu-N(3)	90.97(7)	C(15)-C(14)-N(3)	123.86(18)
N(4)-Cu-N(1)	92.50(7)	C(15)-C(14)-C(13)	127.20(18)
N(2)-Cu-N(1)	91.06(7)	N(3)-C(14)-C(13)	108.62(18)
N(3)-Cu-N(1)	162.63(7)	C(14)-C(15)-C(16)	126.41(19)

Bond	Angle	Bond	Angle
C(1)-N(1)-C(4)	105.41(17)	C(14)-C(15)-C(33)	116.64(18)
C(1)-N(1)-Cu	128.75(15)	C(16)-C(15)-C(33)	116.93(19)
C(4)-N(1)-Cu	125.30(14)	C(15)-C(16)-N(4)	122.98(19)
C(9)-N(2)-C(6)	106.33(17)	C(15)-C(16)-C(17)	128.2(2)
C(9)-N(2)-Cu	129.12(13)	N(4)-C(16)-C(17)	108.74(19)
C(6)-N(2)-Cu	123.70(14)	C(18)-C(17)-C(16)	107.2(2)
C(11)-N(3)-C(14)	106.37(16)	C(17)-C(18)-C(19)	105.8(2)
C(11)-N(3)-Cu	127.65(13)	N(4)-C(19)-C(18)	112.42(19)
C(14)-N(3)-Cu	124.11(14)	F(1)-C(22)-C(23)	119.1(2)
C(19)-N(4)-C(16)	105.85(17)	F(1)-C(22)-C(27)	119.7(2)
C(19)-N(4)-Cu	127.40(14)	C(23)-C(22)-C(27)	121.3(2)
C(16)-N(4)-Cu	126.74(14)	F(2)-C(23)-C(24)	120.6(2)
N(1)-C(1)-C(2)	112.0(2)	F(2)-C(23)-C(22)	119.4(3)
C(3)-C(2)-C(1)	106.7(2)	C(24)-C(23)-C(22)	120.0(2)
C(2)-C(3)-C(4)	106.57(19)	F(3)-C(24)-C(25)	119.3(3)
N(1)-C(4)-C(5)	122.61(19)	F(3)-C(24)-C(23)	120.3(3)
N(1)-C(4)-C(3)	109.36(19)	C(25)-C(24)-C(23)	120.3(2)
C(5)-C(4)-C(3)	127.73(19)	F(4)-C(25)-C(24)	121.4(2)
C(6)-C(5)-C(4)	127.14(19)	F(4)-C(25)-C(26)	119.6(2)
C(6)-C(5)-C(27)	116.24(18)	C(24)-C(25)-C(26)	119.0(2)
C(4)-C(5)-C(27)	116.54(18)	F(5)-C(26)-C(27)	119.55(19)
C(5)-C(6)-N(2)	123.91(19)	F(5)-C(26)-C(25)	117.9(2)
C(5)-C(6)-C(7)	127.31(18)	C(27)-C(26)-C(25)	122.5(2)
N(2)-C(6)-C(7)	108.50(19)	C(26)-C(27)-C(22)	116.85(19)
C(8)-C(7)-C(6)	107.59(18)	C(26)-C(27)-C(5)	121.85(19)
C(7)-C(8)-C(9)	106.6(2)	C(22)-C(27)-C(5)	121.3(2)
N(2)-C(9)-C(8)	110.92(18)	F(6)-C(28)-C(33)	120.00(19)
N(2)-C(9)-C(10)	126.03(18)	F(6)-C(28)-C(29)	118.1(2)
C(8)-C(9)-C(10)	122.92(19)	C(33)-C(28)-C(29)	121.9(2)
C(9)-C(10)-C(11)	116.02(17)	F(7)-C(29)-C(30)	120.3(2)
C(9)-C(10)-C(20)	107.79(17)	F(7)-C(29)-C(28)	120.3(2)
C(11)-C(10)-C(20)	109.11(18)	C(30)-C(29)-C(28)	119.4(2)
C(9)-C(10)-C(21)	108.12(18)	F(8)-C(30)-C(29)	119.6(3)
C(11)-C(10)-C(21)	107.21(17)	F(8)-C(30)-C(31)	120.0(3)
C(20)-C(10)-C(21)	108.4(2)	C(29)-C(30)-C(31)	120.4(2)
N(3)-C(11)-C(12)	111.08(18)	F(9)-C(31)-C(30)	120.3(2)
N(3)-C(11)-C(10)	126.32(17)	F(9)-C(31)-C(32)	120.2(3)
C(12)-C(11)-C(10)	122.25(19)	C(30)-C(31)-C(32)	119.5(3)
F(10)-C(32)-C(31)	118.5(2)	C(28)-C(33)-C(32)	117.1(2)
F(10)-C(32)-C(33)	119.91(19)	C(28)-C(33)-C(15)	121.3(2)
C(31)-C(32)-C(33)	121.6(3)	C(32)-C(33)-C(15)	121.6(2)

Appendix B

PERMISSION LETTERS

Title: Factors Controlling the Spectroscopic Properties and Supramolecular Chemistry of an Electron Deficient 5,5-Dimethylphlorin Architecture

Author: Allen J. Pistner, Daniel A. Lutterman, Michael J. Ghidiu, et al

Publication: The Journal of Physical Chemistry C

Publisher: American Chemical Society

Date: Jul 1, 2014

PERMISSION/LICENSE IS GRANTED FOR YOUR ORDER AT NO CHARGE

This type of permission/license, instead of the standard Terms & Conditions, is sent to you because no fee is being charged for your order. Please note the following:

- Permission is granted for your request in both print and electronic formats, and translations.
- If figures and/or tables were requested, they may be adapted or used in part.
- Please print this page for your records and send a copy of it to your publisher/graduate school.
- Appropriate credit for the requested material should be given as follows: "Reprinted (adapted) with permission from (COMPLETE REFERENCE CITATION). Copyright (YEAR) American Chemical Society." Insert appropriate information in place of the capitalized words.
- One-time permission is granted only for the use specified in your request. No additional uses are granted (such as derivative works or other editions). For any other uses, please submit a new request.

BACK | CLOSE WINDOW